



**Preparation and Properties of Poly(lactic acid) Foam Containing Rubber Wood
Sawdust and Chitosan**

Pasuta Sungsee

**A Thesis Submitted in Fulfillment of the Requirements for the Degree of
Doctor of Philosophy in Polymer Science and Technology**

Prince of Songkla University

2019

Copyright of Prince of Songkla University



**Preparation and Properties of Poly(lactic acid) Foam Containing Rubber Wood
Sawdust and Chitosan**

Pasuta Sungsee

**A Thesis Submitted in Fulfillment of the Requirements for the Degree of
Doctor of Philosophy in Polymer Science and Technology**

Prince of Songkla University

2019

Copyright of Prince of Songkla University

Thesis Title Preparation and Properties of Poly(lactic acid) Foam Containing
Rubber Wood Sawdust and Chitosan

Author Miss Pasuta Sungsee

Major Program Polymer Science and Technology

Major Advisor

Varaporn Tanrattanakul
.....

(Assoc. Prof. Dr. Varaporn Tanrattanakul)

Examining Committee:

[Signature]
.....

Chairperson

(Prof. Dr. Sarawut Rimdusit)

Varaporn Tanrattanakul
..... Committee

(Assoc. Prof. Dr. Varaporn Tanrattanakul)

Asira Fuongfuchat
..... Committee

(Dr. Asira Fuongfuchat)

Chiraphon Chaibundit
..... Committee


(Asst. Prof. Dr. Chiraphon Chaibundit)


The Graduate School, Prince of Songkla University, has approved this thesis as fulfillment of the requirements for the Degree of Doctor of Philosophy Polymer Science and Technology.

.....
(Prof. Dr. Damrongsak Faroongsarng)


Dean of Graduate School

This is to certify that the work here submitted is the result of the candidate's own investigations. Due acknowledgement has been made of any assistance received.


..... Signature
(Assoc. Prof. Dr. Varaporn Tanrattanakul)
Major Advisor


..... Signature
(Miss Pasuta Sungsee)
Candidate

I here certify that this work has not been accepted in substance for any degree, and is not being currently submitted in candidature for any degree.

.....Signature

(Miss Pasuta Sungsee)

Candidate

Thesis Title	Preparation and Properties of Poly(lactic acid) Foam Containing Rubber Wood Sawdust and Chitosan
Author	Miss Pasuta Sungsee
Major Program	Polymer Science and Technology
Academic Year	2018

ABSTRACT

The objectives of the present work were to prepare porous polymeric from poly(lactic acid) compounded with rubber wood sawdust (RWS) and chitosan (CH) by typical compression molding using chemical blowing agent for studying physical, mechanical and thermal properties, and to preliminarily investigate suitability of the obtained foams for bone scaffold application. Azodicarbonamide and zinc oxide was used as a chemical blowing agent and an accelerator, respectively. Poly(ethylene glycol) (PEG) was used as a plasticizer. Surface treatment of RWS was applied. Foam samples were classified into 3 types: (1) PLA/RWS foams, (2) PLA/PEG/CH foams and (3) PLA/CH/RWS foams. It was found that all the foams were closed-cell. Factors affecting foam morphology and physical properties (average pore size, void fraction (% VF) and density) were particle size and surface treatment of RWS and concentration of CH and PEG. These factors also affected the mechanical properties and thermal degradation of the foams. Foams contained smaller average pore size/% VF and higher density showed higher mechanical properties. The thermal degradation temperature determined from TGA technique of all three foams was lower than that of PLA foam. *In-vitro* degradation and cytotoxicity tests were applied to Foam 1 and 2. The *in-vitro* degradation was reported as % weight loss of the samples which tested for 2 months. Noticeably, average pore size, % VF and density affected % weight loss of both foams. The % weight loss of Foam 1 depended on its formulation. The % weight loss of all formulae of Foam 2 was significantly lower than that of PLA foam. Cytotoxicity was evaluated by cell proliferation obtained from cell culturing of MG63 (osteoblast-liked cell) for 7 days. All of Foam 1 and 2 showed non-cytotoxicity confirmed by the increment of cell proliferation throughout the cell culture.

Keywords: Poly(lactic acid), chitosan, sawdust, scaffold, PLA foam, cytotoxicity

ชื่อวิทยานิพนธ์	การเตรียมและสมบัติของโฟมพอลิแลคติกแอซิดประกอบด้วยผงซีลี้อย และไคโตซาน
ผู้เขียน	นางสาวปสุตา สังข์ศรี
สาขาวิชา	วิทยาศาสตร์และเทคโนโลยีพอลิเมอร์
ปีการศึกษา	2561

บทคัดย่อ

จุดประสงค์ของงานวิจัยนี้ เพื่อเตรียมโฟมพอลิเมอร์ที่มีรูพรุนจากพอลิแลคติกแอซิดผสมกับอนุภาคซีลี้อยไม่ยางพาราและไคโตซานโดยใช้การอัดขึ้นรูปแบบร้อนทั่วไปและสารฟูทางเคมี เพื่อศึกษาสมบัติทางกายภาพ สมบัติเชิงกลและสมบัติทางความร้อน และเพื่อการตรวจสอบเบื้องต้นถึงความเหมาะสมของโฟมที่เตรียมได้ในงานโครงเลี้ยงเซลล์กระดูก มีการใช้เอโซไดคาร์โบนาไมด์เป็นสารฟู ซึ่งค็อกซ์ไฮด์เป็นตัวกระตุ้น และพอลิเอทิลีนไกลคอลเป็นพลาสติกไซเซอร์ มีการปรับสภาพผิวของอนุภาคซีลี้อย ทำการเตรียมโฟมสามชนิดคือ (1) โฟมพอลิแลคติกแอซิดผสมอนุภาคซีลี้อย (2) โฟมพอลิแลคติกแอซิดผสมพอลิเอทิลีนไกลคอลและไคโตซาน และ (3) โฟมพอลิแลคติกแอซิดผสมไคโตซานและอนุภาคซีลี้อย ผลการทดลองพบว่าโฟมมีลักษณะเป็นเซลล์ปิด ปัจจัยที่มีผลต่อลักษณะพื้นฐานวิทยาและสมบัติทางกายภาพของโฟม (ค่าเฉลี่ยขนาดเซลล์ ปริมาตรรูพรุน และความหนาแน่น) คือขนาดอนุภาคซีลี้อย วิธีการปรับสภาพผิวอนุภาคซีลี้อย และปริมาณของพอลิเอทิลีนไกลคอลและไคโตซาน ปัจจัยดังกล่าวนี้มีผลต่อเนื่องถึงสมบัติเชิงกลและการสลายตัวทางความร้อนของโฟม โฟมที่มีค่าเฉลี่ยขนาดเซลล์และปริมาตรรูพรุนต่ำกว่าและมีค่าความหนาแน่นที่สูงกว่าจะแสดงสมบัติเชิงกลที่ดีกว่า อุณหภูมิการสลายตัวทางความร้อนที่ได้จากการทดสอบด้วยเทคนิคเทอร์โมกราวิเมตริกของโฟมทั้งสามชนิดมีค่าต่ำกว่าโฟมพอลิแลคติกแอซิด นำโฟมชนิดที่ 1 และ 2 มาทดสอบการย่อยสลายในสภาวะจำลองและความเป็นพิษต่อเซลล์ การศึกษาการย่อยสลายในสภาวะจำลองของโฟมรายงานผลด้วยค่า %weight loss ทำการทดสอบเป็นเวลา 2 เดือน พบว่าค่าเฉลี่ยขนาดเซลล์ ปริมาตรรูพรุนและความหนาแน่นมีอิทธิพลต่อ %weight loss ของโฟมทั้งสองชนิด โฟมชนิดที่ 1 มี %weight loss ที่แตกต่างกับโฟมพอลิแลคติกแอซิด โดยขึ้นอยู่กับสูตรผสม นอกจากนี้โฟมชนิดที่ 2 ทุกสูตรยังมี %weight loss ต่ำกว่าโฟมพอลิแลคติกแอซิดอย่างมีนัยสำคัญ ความเป็นพิษต่อเซลล์รายงานด้วยค่าการเพิ่มจำนวนเซลล์ที่ได้จากการเพาะเลี้ยงเซลล์ชนิด MG63 (เซลล์คล้ายเซลล์สร้างกระดูก) เป็นเวลา 7 วัน พบว่าโฟมชนิดที่ 1 และ 2 แสดงสมบัติไม่เป็นพิษต่อเซลล์ซึ่งยืนยันได้จากการเพิ่มขึ้นของค่าการเพิ่มจำนวนเซลล์ตลอดการเพาะเลี้ยงเซลล์

คำสำคัญ: พอลิแลคติกแอซิด ไคโตซาน ผงซีลี้อย โครงสร้างเลี้ยงเซลล์ โฟมพีแอลเอ ความเป็นพิษต่อเซลล์

ACKNOWLEDGEMENTS

First and foremost I would like to offer my sincerest gratitude to Associate Professor Dr. Varaporn Tanrattanakul who has been my wonderful advisor for providing me an opportunity to study in Ph.D. program and supporting me throughout my Ph.D. study with her patience, knowledge and professional guidance. Associate Professor Dr. Varaporn Tanrattanakul always besides me and gives me a good suggestion whenever I had problems and questions about my experimental, research and thesis writing. I would like to thank you her for the countless hours that she has been spending, reading, discussing and correcting with me, my manuscript and my thesis. Her hard working and work discipline are very good examples for me to practice and improve myself to be the best as well as I can do.

I am sincerely grateful to Graduate School and Research and Development Office, the grant number SCI590146, Prince of Songkla University and Nakhon Si Thammarat Rajabhat University for financial support. This thesis work would be not comfortably succeed if I was not supported by all of the scholarships.

I would like to express my gratitude to my thesis committee, Professor Dr. Sarawut Rimdusit, Dr. Asira fuongfuchat and Assistant Professor Dr. Chiraphon Chaibundit, for valuable and beneficial comments on this thesis.

I would like to thank you Miss Khanitta Panjapheree for her support and knowledge in *in-vitro* degradation and cytotoxicity testing. I am also grateful to all lecturers, technicians, officers and all my friends at the Department of Materials Science and Technology, Faculty of Science, Prince of Songkla University, especially for VT group members for their friendship, encouragement and unlimited help throughout my study duration.

I would like to thank you all my teachers of all my study levels and also my advisors of my study in bachelor degree and master degree. My studying in Ph.D degree would be not succeed if I did not obtain their knowledge, advice and cultivation in the pass.

Finally, I am very profound gratitude to my family, especially my parents, for their education, cultivation, support with all aspects and endless

encouragement since I was born, all steps of my life and also in my studying in Ph.D degree. I dedicate this thesis to my family and all the teachers who have taught me, most importantly, the people who I met and who helped me to create, develop and complete this thesis.

To this end, I fully take all responsibility for any mistakes that may have occurred in this work.

Pasuta Sungsee

CONTENTS

	Page
ABSTRACT	v
ACKNOWLEDGEMENT	vii
CONTENTS	ix
LIST OF TABLES	xvi
LIST OF FIGURES	xviii
LIST OF ABBREVIATIONS	xxvii
CHEAPTER 1 GENERAL INTRODUCTION	
1.1 Background	1
1.2 Objectives	3
1.3 References	4
CHEAPTER 2 LISTERATURE REVIEW	
2.1 Tissue engineering	7
2.1.1 General information	7
2.1.2 Scaffold for bone tissue engineering	7
2.1.3 Biomaterial used for scaffold preparation	9
2.1.4 Synthetic polymers for bone scaffold preparation	10
2.2 Poly(lactic acid) foams	11
2.2.1 Poly(lactic acid)	11
2.2.1.1 General information	11
2.2.1.2 Synthesis of poly(lactic acid)	13
2.2.2 Poly(lactic acid) in medical and tissue engineering	15
2.2.3 Preparation methods of poly(lactic acid) based scaffold	15
2.2.3.1 Thermal induced phase separation	15
2.2.3.2 Solvent casting and porogen leaching	16
2.2.3.3 Solid freeform fabrication technique	16
2.2.3.4 Microsphere sintering method	17
2.2.3.5 Electrospinning	17
2.2.3.6 Coating method	18

CONTENTS (continued)

	Page
2.2.3.7 Supercritical gas foaming	18
2.2.3.8 Melting process	19
2.2.4 Foaming of PLA using blowing agents	20
2.2.4.1 General polymer foaming process	20
2.2.4.2 Blowing agent	21
2.2.4.3 Foaming of PLA using physical blowing agents	22
2.2.4.4 Foaming of PLA using chemical blowing agents	22
2.3 Rubber wood sawdust	23
2.3.1 General information	23
2.3.2 Composites of PLA/wood sawdust	25
2.4 Chitosan	27
2.4.1 General information	27
2.4.2 Biocomposites of PLA/chitosan	27
2.5 Poly(ethylene glycol)	29
2.5.1 General information	29
2.5.2 Poly(lactic acid)/poly(ethylene glycol) blending	30
2.6 Azodicarbonamide	31
2.7 Silane coupling agents	32
2.8 Biodegradation of polymer based biomaterials	33
2.8.1 Biodegradation mechanism	33
2.8.1.1 Hydrolytic mechanism	34
2.8.1.2 Oxidative mechanism	35
2.8.1.3 Enzymatic mechanism	35
2.8.2 Degradation-observing techniques	35
2.8.2.1 Water absorption and weight loss	35
2.8.2.2 Molecular weight	36
2.8.2.3 Crystallinity	36
2.8.2.4 Morphology	36

CONTENTS (continued)

	Page
2.8.2.5 Surface chemistry	37
2.8.2.6 Mechanical properties	37
2.8.3 Degradation of poly(lactic acid)	37
2.8.4 Degradation of chitosan	38
2.8.5 Degradation of poly(ethylene glycol)	39
2.9 Polymer characterizations	40
2.9.1 Mechanical properties	40
2.9.1.1 Impact strength	40
2.9.1.2 Tensile properties	41
2.9.1.3 Flexural properties	44
2.9.2 Thermal properties	46
2.9.2.1 Differential scanning calorimeter	46
2.9.2.2 Dynamic thermal gravimetric analysis	47
2.9.2.3 Thermal gravimetric analysis	49
2.9.3 Fourier transforms infrared spectroscopy	50
2.9.4 Scanning electron microscope	51
2.9.5 X-Ray diffraction	52
2.9.6 <i>In-vitro</i> cytotoxicity properties	54
2.9.6.1 Cell proliferation testing	54
2.9.6.2 Cell cytotoxicity assays	55
2.10 References	57
CHEAPTER 3 MATERIALS AND METHODOLOGY	
3.1 Materials	69
3.1.1 Materials for surface treatment of rubber wood sawdust	69
3.1.2 Materials for preparation of unfoamed and foamed PLA compounds	69
3.1.3 Materials for <i>in-vitro</i> degradation and cytotoxicity characterization of foam samples	70

CONTENTS (continued)

	Page
3.2 Instruments	71
3.3 Methodology	72
3.3.1 Preparation of various sizes of rubber wood sawdust	72
3.3.2 Alkaline treatment of rubber wood sawdust (NaOH-treated RWS)	72
3.3.3 Silane treatment of rubber wood sawdust	72
3.3.3.1 Method A	73
3.3.3.2 Method B	74
3.3.3.3 Method C	74
3.3.4 Preparation of unfoamed PLA/RWS compounds	74
3.3.5 Preparation of unfoamed PLA/PEG/chitosan compounds	76
3.3.6 Preparation of PLA compounded foams	76
3.3.7 Preparation of sample sheet by compression molding	77
3.3.7.1 Preparation of unfoamed sheet	77
3.3.7.2 Preparation of foamed sheet	77
3.3.8 Characterizations	79
3.3.8.1 Fourier transforms infrared spectroscopy (FTIR)	79
3.3.8.2 X-Ray diffraction spectroscopy (XRD)	79
3.3.8.3 Surface morphology	79
3.3.9 Physical and mechanical properties	79
3.3.9.1 Density and void fraction (VF)	79
3.3.9.2 Pore morphology	80
3.3.9.3 Impact strength	81
3.3.9.4 Tensile properties	81
3.3.9.5 Flexural properties	81
3.3.10 Thermal properties	81
3.3.10.1 Differential scanning calorimeter	81
3.3.10.2 Dynamic mechanical thermal analysis	82

CONTENTS (continued)

	Page
3.3.10.3 Thermogravimetric analysis	82
3.3.11 <i>In-vitro</i> degradation testing	82
3.3.11.1 <i>In-vitro</i> degradation according to Rakmea <i>et al.</i> [7]	82
3.3.11.2 <i>In-vitro</i> degradation according to Zhang and Cui, [8]	83
3.3.12 Cell cytotoxicity assay	83
3.3.13 Statistical analysis of data	84
3.4 References	84
CHEAPTER 4 RESULTS AND DISCUSSIONS	
4.1 Preparation and properties of unfoamed PLA/RWS compounds	86
4.1.1 Suitable RWS particle sizes and RWS content	86
4.1.1.1 Impact strength	86
4.1.1.2 Tensile properties	93
4.1.2 Characterizations of treated-RWS	95
4.1.2.1 Chemical structures of RWS	95
4.1.2.2 Surface morphology of RWS	103
4.1.2.3 Crystallinity Index and thermal degradation of RWS	104
4.1.3 Effect of surface treatment on unfoamed PLA/RWS properties	107
4.1.3.1 Impact strength	107
4.1.3.2 Tensile properties	111
4.1.4 Effect of silane type on unfoamed PLA/RWS properties	114
4.1.4.1 Impact strength	115
4.1.4.2 Tensile properties	116
4.1.4.3 Thermal properties	117
4.2 Properties and characterization of PLA foams	120

CONTENTS (continued)

	Page
4.2.1 Morphology and physical properties	121
4.2.2 Mechanical properties	123
4.2.3 Thermal degradation properties	124
4.2.4 FTIR analysis	126
4.2.5 <i>In-vitro</i> degradation properties	127
4.3 Properties and characterization of PLA/RWS compounded foams	128
4.3.1 Morphology and physical properties	128
4.3.2 Mechanical properties	131
4.3.3 Characterizations of PLA compounded foams	135
4.3.3.1 DMTA analysis	135
4.3.3.2 TGA analysis	137
4.3.4 <i>In-vitro</i> degradation properties	138
4.3.5 Cytotoxicity properties	139
4.4 Properties and characterization of unfoamed and foamed PLA compounds	142
4.4.1 Properties of unfoamed PLA/PEG/chitosan	142
4.4.1.1 Mechanical properties	142
4.4.1.2 Thermal properties	145
4.4.2 Properties of PLA/PEG/chitosan foams	147
4.4.2.1 Morphology and physical properties	147
4.4.2.2 Thermal properties	149
4.4.2.3 Mechanical properties	153
4.4.2.4 <i>In-vitro</i> degradation properties	156
4.4.2.5 Cytotoxicity properties	157
4.5 Properties and characterization of PLA/chitosan/RWS foams	159
4.5.1 Morphology and physical properties	159
4.5.2 Mechanical properties	160
4.5.3 Thermal degradation properties	163

CONTENTS (continued)

	Page
4.6 References	164
CHEAPTER 5 CONCLUSIONS	
5.1 Preparation and characterization of RWS and PLA/RWS compounds	169
5.2 Preparation and characterization of PLA foams and PLA/RWS foams	170
5.3 Preparation and characterization of PLA/PEG/CH compounds, PLA/PEG/CH foams and PLA/CH/RWS foams	171
5.4 Perspectives	172
APPENDICES	173
APPENDIX A:	
SEM images demonstrating pore morphology of nine zones of the foam specimens	174
APPENDIX B:	
Abstract published in the 11 th SPSJ International Polymer Conference 2016	183
APPENDIX C:	
Full proceeding published in Pure and Applied Chemistry International Conference 2018	185
APPENDIX D:	
Abstract published in the 47 th World Polymer Congress (MACRO 2018)	192
APPENDIX E:	
Research paper submitted in Journal of Applied Polymer Science	194
APPENDIX F:	
Research paper submitted in Songklanakarin Journal of Science and Technology	223
VITAE	247

LIST OF TABLES

		Page
Table 2.1	Mechanical properties of polymers used for scaffold preparation	11
Table 2.2	Properties of chemical blowing agents	21
Table 3.1	Materials used for surface treatment of rubber wood sawdust	69
Table 3.2	Materials used for preparation of unfoamed and foamed PLA compounds	69
Table 3.3	Materials used for <i>in-vitro</i> degradation and cytotoxicity characterization of foam samples	69
Table 3.4	Instruments	70
Table 3.5	Surface treatment conditions of RWS in the method A-C	73
Table 3.6	Composition of unfoamed PLA/nontreated-RWS compounds	75
Table 3.7	Composition of unfoamed PLA/treated-RWS compounds	75
Table 3.8	Composition of unfoamed PLA/PEG/CH compounds	76
Table 3.9	Composition for preparation of PLA compounded foams	78
Table 4.1	Mechanical properties of PLA compounds containing 5 wt% and 10 wt% of RWS with various particle size	95
Table 4.2	FTIR assignment of nontreated RWS and GPMS	98
Table 4.3	Thermal degradation temperature and crystallinity index of nontreated RWS and RWS treated with NaOH and GPMS using method A	104
Table 4.4	Mechanical properties of PLA composites containing 5 wt% of RWS with particle size of $\leq 75 \mu\text{m}$ and 212-600 μm	114
Table 4.5	Composition of unfoamed PLA/treated-RWS compounds to observe effect of silane type on mechanical properties of PLA compounds	115
Table 4.6	Thermal properties determined from first heating and cooling scan of DSC thermograms	119
Table 4.7	Thermal properties determined from second heating scan of DSC thermograms	120

LIST OF TABLES (continued)

		Page
Table 4.8	Average pore size and physical properties of PLA foams with different ZnO contents	122
Table 4.9	Thermal degradation temperatures of PLA and foamed PLA with different ZnO contents	126
Table 4.10	Average pore size and physical properties of PLA/RWS compounded foams	130
Table 4.11	Izod impact strength, tensile properties and flexural properties of PLA/RWS foams	132
Table 4.12	Thermal degradation temperatures of PLA foam and PLA/RWS foams	138
Table 4.13	Thermal properties determined from the first heating and cooling scan of DSC thermograms	146
Table 4.14	Thermal and crystallinity properties determined from the second heating scan of DSC thermograms	146
Table 4.15	Physical properties and average pore diameters of PLA foam samples	148
Table 4.16	Thermal and crystallinity properties determined from the first heating and cooling scan of DSC thermograms of PLA compounded foams	150
Table 4.17	Thermal and crystallinity properties determined from the second heating scan of DSC thermograms of PLA compounded foams	151
Table 4.18	Thermal degradation properties of the foams	153
Table 4.19	Impact strength and tensile properties of foam samples	154
Table 4.20	Physical properties of foam samples	159
Table 4.21	Mechanical and thermal degradation properties of foam samples	163

LIST OF FIGURES

		Page
Figure 2.1	Basic principle of tissue engineering	7
Figure 2.2	Schematic diagram demonstrating the objectivities of scaffold in tissue engineering	9
Figure 2.3	Stereoisomers of (a) lactic acids, and (b) lactides	12
Figure 2.4	Synthesis methods of poly(lactic acid)	14
Figure 2.5	SEM images of porous polymer foams fabricated by (a) TIPS method, (b) solvent casting and particle leaching, (c) SFFT and (d) microsphere sintering	17
Figure 2.6	Typical polymer foaming process using blowing agents	21
Figure 2.7	Chemical structure of (a) cellulose, (b) hemicellulose, and (c) lignin	24
Figure 2.8.	Chemical structure of (a) poly(<i>N</i> -acetyl- β -D-glucosamine) or chitin and (b) chitosan repeat units and (c) partially acetylated chitosan	27
Figure 2.9	Living anionic polymerization of EO	30
Figure 2.10	The decomposition reaction of azodicarbonamide (AZDC)	31
Figure 2.11	General structure of organosilanes	32
Figure 2.12	Interaction mechanism of silane coupling agent with wood flour and PLA	33
Figure 2.13	Mechanism of hydrolytic degradation in polymers	34
Figure 2.14	Polymerization-degradation rout ways of poly(lactic acid)	38
Figure 2.15	Probable degradation mechanism of chitosan	39
Figure 2.16	Oxidative degradation mechanism of PEG backbone	40
Figure 2.17	(a) Cantilever beam (Izod-type) impact machine, (b) Notched impact specimen according to ASTM D256 and (c) Izod and Charpy pendulum	41
Figure 2.18	Tensile specimen demonstrating length, reduced gauge section and enlarged width according to ASTM D412 type C	42
Figure 2.19	Stress-strain curve of polymer film	43

LIST OF FIGURES (continued)

		Page
Figure 2.20	(a) Universal testing machine equipped with bending fixture accessories and (b) fixture used to set loading nose and support spacing and alignment	44
Figure 2.21	Typical curve of flexural stress and flexural strain	45
Figure 2.22	Diagram of DSC instrument connected with computer and output data	46
Figure 2.23	Diagrams of (a) heat flux DSC and (b) power-compensation DSC	47
Figure 2.24	DSC thermogram exhibiting the interest transitions	47
Figure 2.25	(a) A one kind of DMTA instrument showing important composition and (b) the different modes for sample holding	48
Figure 2.26	DMTA thermogram of storage modulus, loss modulus and tan delta as a function of temperature of the material	48
Figure 2.27	Diagram of thermogravometric analyzer	49
Figure 2.28	TGA and DTG curves of bulk PS- <i>b</i> -PMMA	50
Figure 2.29	Stretching and bending vibrations in molecules	50
Figure 2.30	Schematic diagram of typical FTIR analysis process	51
Figure 2.31	Schematic diagram of the basic SEM instruments	52
Figure 2.32	Schematic representing (a) diagrams of the basic XRD analysis and (b) the Bragg's law equation	53
Figure 2.33	The XRD diffractogram of a count rate versus degree 2-theta (2θ)	53
Figure 2.34	Mechanism of the WST-1 reduction in the presence of intermediate electron acceptor (mPMs)	55
Figure 2.35	SEM images demonstrating various types' cells adhesion on the difference material surfaces: (a) osteoblast cells on surface-modified zirconia, (b) FOST cells on titanium anodic films, and (c) Saos-2 cells on electrospun PLA	56

LIST OF FIGURES (continued)

		Page
Figure 2.36	SEM images of MG63 osteoblast-like cells adhesion on different material surface and culture time: (a) e-PTFE membrane/1 days, (b) nHA/PA66 membrane/5 days, and (c) 3D printed PLA scaffold/2 days	57
Figure 3.1	The foam sheet showing the specimen zones used to observe pore morphology by using SEM	80
Figure 4.1	Effect of nontreated-RWS contents on Charpy impact strength of PLA (particle size: 212-600 μm)	87
Figure 4.2	Effect of nontreated-RWS contents on Izod impact strength of PLA (particle size: 212-600 μm)	87
Figure 4.3	Effect of nontreated-RWS contents on unnotched impact strength of PLA (particle size: 212-600 μm)	88
Figure 4.4	Effect of nontreated-RWS contents on notched impact strength of PLA (particle size: 212-600 μm)	88
Figure 4.5	Effect of nontreated-RWS contents on Charpy impact strength of PLA (particle size: $\leq 212 \mu\text{m}$)	89
Figure 4.6	Effect of nontreated-RWS contents on Izod impact strength of PLA (particle size: $\leq 212 \mu\text{m}$)	89
Figure 4.7	Effect of impact testing method on unnotched impact strength of PLA (particle size: $\leq 212 \mu\text{m}$)	90
Figure 4.8	Effect of impact testing method on notched impact strength of PLA (particle size: $\leq 212 \mu\text{m}$)	90
Figure 4.9	Effect of nontreated-RWS contents on Izod impact strength of PLA (particle size: 75-150 μm)	91
Figure 4.10	Effect of nontreated-RWS contents on Izod impact strength of PLA (particle size: $\leq 75 \mu\text{m}$)	92
Figure 4.11	Effect of particle size on Izod impact strength of PLA compounds containing 5 wt% of RWS	92

LIST OF FIGURES (continued)

		Page
Figure 4.12	Effect of particle size on Izod impact strength of PLA compounds containing 10 wt% of RWS	92
Figure 4.13	Effect of particle size and contents on tensile properties of PLA compounds: (a) modulus, (b) stress at break and (c) strain at break	94
Figure 4.14	FTIR spectra of GPMS and RWS (212-600 μm) before and after surface treatment with NaOH and GPMS using method A	97
Figure 4.15	Proposed interaction mechanism of GPMS with RWS and PLA	98
Figure 4.16	FTIR spectra of RWS (212-600 μm) treated with various GPMS content using method A	99
Figure 4.17	FTIR spectra of APMS and treated RWS (212-600 μm) before and after surface treatment with APMS using method A and method A without pH adjusting	100
Figure 4.18	FTIR spectra of GPMS and RWS (212-600 μm) before and after surface treatment with various GPMS content using method B	101
Figure 4.19	FTIR spectra of GPMS and RWS (≤ 75 μm) before and after surface treatment with NaOH and GPMS using method A	102
Figure 4.20	FTIR spectra of GPMS and RWS (≤ 75 μm) before and after surface treatment with GPMS using method B and C	102
Figure 4.21	SEM images at 175X and 1000X of RWS with particle size of 212-600 μm : (a, d) nontreated-RWS, (b, e) NaOH-treated RWS and (c, f) 1%GPMS-A	103
Figure 4.22	XRD patterns of nontreated-RWS, NaOH-treated RWS and 1%GPMS-A with different particle size: (a) ≤ 75 μm and (b) 212-600 μm	105
Figure 4.23	TGA and DTG graph of RWS before and after treatment with different particle size: (a) ≤ 75 μm and (b) 212-600 μm	106

LIST OF FIGURES (continued)

		Page
Figure 4.24	Effect of alkaline treatment and GPMS treatment using method A on Izod impact strength of PLA compounds (particle size: $\leq 75 \mu\text{m}$)	107
Figure 4.25	Effect of alkaline treatment and GPMS treatment using method B on Izod impact strength of PLA compounds (particle size: $\leq 75 \mu\text{m}$)	108
Figure 4.26	Effect of surface treatment method on (a) unnotched Izod impact strength and (b) notched Izod impact strength of PLA compounds (particle size: $\leq 75 \mu\text{m}$)	108
Figure 4.27	Effect of alkaline treatment and GPMS treatment using method A on Izod impact strength of PLA compounds (particle size: 212-600 μm)	109
Figure 4.28	Effect of NaOH treatment and GPMS treatment using method B on Izod impact strength of PLA compounds (particle size: 212-600 μm)	109
Figure 4.29	Effect of surface treatment method on (a) unnotched Izod impact strength and (b) notched Izod impact strength of PLA compounds (particle size: 212-600 μm)	110
Figure 4.30	Effect of RWS particle size on: (a) unnotched impact strength and (b) notched impact strength of PLA compounds (method A)	110
Figure 4.31	Effect of RWS particle size on: (a) unnotched impact strength and (b) notched impact strength of PLA compounds (method B)	111
Figure 4.32	Effect of surface treatment method on tensile properties of PLA compounds: (a) modulus, (b) stress at break and (c) strain at break (particle size: $\leq 75 \mu\text{m}$)	112
Figure 4.33	Effect of surface treatment method on tensile properties of PLA compounds: (a) modulus, (b) stress at break, and (c) strain at break (particle size: 212-600 μm)	113

LIST OF FIGURES (continued)

		Page
Figure 4.34	Effect of silane type on Izod impact strength of PLA compounds	115
Figure 4.35	Effect of silane coupling agent type on tensile properties of PLA compounds: (a) modulus, (b) stress at break and (c) strain at break	117
Figure 4.36	DSC thermograms of PLA and PLA compound pellets containing 5 wt% RWS (particle size: $\leq 75\mu\text{m}$)	118
Figure 4.37	DSC thermograms of PLA and unfoamed PLA composite with 5 wt% of RWS (particle size: 212-600 μm)	119
Figure 4.38	SEM image of PLA foams with different AZDC/ZnO ratios: (a) 3/0.3, (b) 3/0.5 and (c) 3/1.0	121
Figure 4.39	Effect of ZnO content on average pore size of PLA foams	122
Figure 4.40	Effect of ZnO content on the relation of average pore size and density of PLA foams	123
Figure 4.41	Effect of ZnO contents on notched Izod impact strength and density of PLA foams	123
Figure 4.42	Effect of ZnO contents on tensile properties of PLA foams: (a) modulus and (b) stress at break and strain at break	124
Figure 4.43	Effect of ZnO contents on flexural properties of PLA foams: (a) flexural modulus and density and (b) flexural stress	124
Figure 4.44	TGA and DTG curves of AZDC	125
Figure 4.45	(a) TGA and (b) DTG curves of PLA and PLA foams with different AZDC/ZnO ratios	125
Figure 4.46	FTIR spectra of PLA pellet, AZDC/ZnO (3/0.1 wt/wt) and PLA1.0 foam	126
Figure 4.47	Effect of ZnO contents on <i>in-vitro</i> degradation of PLA foams	127
Figure 4.48	Effect of particle size and surface treatment of RWS on pore morphology of the foams: (a) PLA0.1, (b) T1S, (c) T2S, (d) T0L and (e) T2L	129

LIST OF FIGURES (continued)

		Page
Figure 4.49	Effect of particle size and surface treatment of RWS on Izod impact strength of the foams: (a) unnotched specimens and (b) notched specimens	133
Figure 4.50	Effect of particle size and surface treatment of RWS on tensile properties of the foams: (a) modulus, (b) stress at break and (c) strain at break	134
Figure 4.51	Effect of particle size and surface treatment of RWS on flexural properties of the foams: (a) flexural modulus and (b) flexural stress	135
Figure 4.52	(a) Storage modulus and (b) tan delta as a function of temperature of PLA foam and PLA/RWS foams	136
Figure 4.53	(a) TGA and (b) DTG curves of PLA foam and PLA/RWS foams	137
Figure 4.54	Weight loss (%) as a function of incubation time of foam specimens	139
Figure 4.55	Cell proliferation on the polished surface of foam specimens at 1, 3, 5 and 7 days	140
Figure 4.56	SEM images of freeze-fractured surfaces of foam specimens demonstrating cell adhesion after 7 days: (a) blank, (b) PLA0.1, (c) T0L, (d) T1S, (e) T2S and (f) T2L	141
Figure 4.57	Effect of chitosan and PEG on Izod impact strength of unfoamed PLA (a) unnotched specimens and (b) notched specimens	143
Figure 4.58	Effect of chitosan and PEG on Izod impact strength of unfoamed PLA: (a) modulus, (b) stress at break and (c) strain at break	144
Figure 4.59	DSC thermograms of unfoamed PLA compounds	147
Figure 4.60	SEM images of foam samples: (a) PLA0.1, (b) 1C0P, (c) 3C0P, (d) 0C5P, (e) 1C5P and (f) 3C5P	149
Figure 4.61	DSC thermograms of PLA compounded foams	152

LIST OF FIGURES (continued)

		Page
Figure 4.62	(a) TGA and (b) DTG curves of PLA foam and PLA compounded foams	153
Figure 4.63	Tensile properties of foam samples: (a) tensile modulus and (b) tensile strength	155
Figure 4.64	Flexural properties of foam samples: (a) flexural modulus and (b) flexural strength	156
Figure 4.65	Weight loss as a function of incubation time of PLA compounded foams	157
Figure 4.66	MG-63 cell proliferation on the polished surface of samples at 1, 3, 5 and 7 days	158
Figure 4.67	SEM images of cell adhesion on the polished surface of foam samples after 7 days of cell culture: (a) PLA, (b) 1C0P, (c) 3C0P, (d) 0C5P, (e) 1C5P and (f) 3C5P	158
Figure 4.68	Cell morphology of PLA compounded foams: (a) PLA0.1, (b) 1C0P, (c) 1C0PR1 and 1C0PR3 foam	160
Figure 4.69	Izod impact strength of foam samples: (a) unnotched and (b) notched specimens	161
Figure 4.70	Tensile properties of foam samples: (a) tensile modulus and (b) stress at break	162
Figure 4.71	Flexural properties of foam samples: (a) flexural modulus and (b) flexural stress	162
Figure 4.72	(a) TGA and (b) DTG curves of PLA foam and PLA/CH/RWS foams	164
Figure A1	Pore morphology of PLA0.1 foam	175
Figure A2	Pore morphology of PLA0.3 foam	175
Figure A3	Pore morphology of PLA0.5 foam	176
Figure A4	Pore morphology of PLA1.0 foam	176
Figure A5	Pore morphology of T1S foam	177

LIST OF FIGURES (continued)

		Page
Figure A6	Pore morphology of T2S foam	177
Figure A7	Pore morphology of T0L foam	178
Figure A8	Pore morphology of T2L foam	178
Figure A9	Pore morphology of 1C0P foam	179
Figure A10	Pore morphology of 3C0P foam	179
Figure A11	Pore morphology of 0C5P foam	180
Figure A12	Pore morphology of 1C5P foam	180
Figure A13	Pore morphology of 3C5P foam	181
Figure A14	Pore morphology of 1C0PR1 foam	181
Figure A15	Pore morphology of 1C0PR3 foam	182

LIST OF ABBREVIATIONS

APMS	3-aminopropyl trimethoxy silane
ASTM	American Society for Testing and Materials
AZDC	Azodicarbonamide
CH	Chitosan
CI	Crystallinity index
DMTA	Dynamic mechanical thermal analysis
DSC	Differential scanning calorimetry
DTG	Derivative thermo gravimetric analysis
E	Young's modulus
E'	Storage modulus
FTIR	Fourier transforms infrared spectroscopy
GPMS	3-glycidoxypopyl trimethoxy silane
MG-63	MG-63 cell line human
NaOH	Sodium hydroxide
PBS	Phosphated-buffered solution
PEG	Poly(ethylene glycol)
PLA	Poly(lactic acid)
PP	Polypropylene
PS	Polystyrene
RWS	Rubber wood sawdust
SEM	Scanning electron microscope
Tan δ	Damping factor
TGA	Thermal gravimetric analysis
T _m	Melting temperature
T _{d onset}	Onset temperature of degradation
T _{d end}	End-set temperature of degradation
T _d	Degradation temperature
T _g	Glass transition temperature
T _{cc}	Cold crystallization temperature

LIST OF ABBREVIATIONS (continued)

VF	Void fraction
X_{c1}	Degree of crystallinity by considering ΔH_{cc}
X_{c2}	Degree of crystallinity by excluding ΔH_{cc}
XRD	X-ray diffraction spectroscopy
ZnO	Zinc oxide
ΔH_m	Heat of melting
ΔH_{cc}	Heat of cold crystallization
α -MEM	Alpha-Minimum essential medium
σ_b	Stress at break
ε_b	Strain at break

CHAPTER 1

GENERAL INTRODUCTION

1.1 Background

Nowadays, utilization of biomaterials as porous scaffold to allow physical support and suitable environment for tissue development in the damaged tissue plays an important role in bone tissue engineering. Scaffold is defined as artificial solid biomaterials used for supporting three-dimensional tissue formation and for performing some, or all, of functions as following: 1) to support cell-scaffold interaction, 2) to provide transport of nutrient, gases and metabolic waste for allowing cell bioactivities and 3) to mechanically support defective tissue which prevent a deformation of the growing tissue during tissue regeneration [1]. Scaffold can be seeded with various kinds of cells such as stem cells, mature differentiated cells and progenitor cells in order to induce tissue formation *in-vitro* or *in-vivo*. Furthermore, scaffold can be directly implanted *in-vivo* in order to act as a guiding artificial material in defective tissue regeneration. The characteristics required for ideal scaffold are opened-cell structure or closed-cell with interconnected cell structure, biocompatibility, biodegradability, appropriate surface chemistry, matching of its mechanical properties with the infective tissue and low-cost production with controlled properties [2].

The biomaterials used in scaffold fabrication are divided into the following three main categories. The first one is ceramic such as hydroxyapatite (HA) and tricalcium phosphate (TCP). The second one is natural polymer such as collagen, gelatin, and silk. The third category is synthetic polymer which is very useful in bone scaffold application because of its processability. The properties required for scaffold application such as porosity, pore size, biodegradation rate and mechanical properties can be tailored by using synthetic polymers. Poly(lactic acid) (PLA), polyglycolide (PGA), poly(lactic-co-glycolic acid) (PLGA) are synthesis polymers widely used in tissue engineering application [1].

Poly(lactic acid), a well-known biodegradable thermoplastic polyester, is a biomaterial commonly used in medical application such as drugs delivery, suture,

bone fixation materials, and PLA has been preliminary used in bone scaffold application. Scaffolds have been prepared by various techniques including 3D printing [3], thermally induced phase separation (TIPS) [4], solid freeform fabrication technique (SFFT) [5], solvent casting with particle leaching [6] and melting process, etc. [7]. Scaffolds containing microcellular structure were prepared by melting process using supercritical gases (CO_2 or N_2) as a physical blow agent through microcellular injection molding [8] or microcellular extrusion [9-10]. However, it requires expensive special equipment. The alternative technique to produce PLA foam is melting process and use of a conventional chemical blowing agent due to its easy operation, simple equipment and low costs.

PLA has been blended with bioactive compounds which are compounds influencing on a tissue or cell living in order to improve biocompatibility of PLA. The examples of bioactive compounds blended with PLA were tricalcium phosphate (TCP) [11-12], calcium phosphate (CaP) [13-14], hydroxyapatite (HA) [15], bioactive glass [16], silk worm fibres [17-18] and chitosan (CH) [19]. Chitosan (CH) is a cationic polysaccharide obtained from deacetylation of chitin in the alkaline system, and it is used in scaffold application because of its non-toxicity, biodegradability, and biocompatibility [20]. Reactive amino and hydroxyl groups of chitosan provided various bioactive properties such as antimicrobial activity, bone regeneration and anti-inflammatory, etc. [21]. In addition, the biological testing through human osteosarcoma cell culturing on the PLA/CH composites indicated a good cell viability and cell proliferation properties [22].

Normally, plasticizers are used to improve flexibility of PLA because PLA is a brittle polymer. Poly(1,3-butanediol) (PBOH), dibutyl sebacate (DBS), oligomeric lactic acid (OLA), acetyl tri-n-butyl citrate (ATBC) and poly(ethylene glycol) (PEG) have been used as a plasticizer for PLA [23]. PEG is normally used in the medical field so that it is interesting to use for scaffold preparation. PEG with various molecular weight was used as a plasticizer for PLA. For example, PEG with molecular weight of 400 g/mol (PEG400) improved processability of PLA-based scaffolds prepared by the 3D printing method and changed the surface geometry and the degradation rate of the 3D printed scaffolds [24]. The addition of PEG with molecular weight of 6000 g/mol (PEG6000) improved pore morphology of the PLA-

based scaffold prepared by supercritical CO₂ foaming and particle leaching method [25].

In Thailand, Para rubber (*Hevea brasiliensis*) wood is usually used as a raw material in the wooden furniture industry. The manufacturing of wooden furniture produces large amount of rubber wood sawdust (RWS) as industrial waste. Wood sawdust added in PLA/triclosan blend acted as an antibacterial promoter. It increased hydrophilicity of the PLA/triclosan blend and supported triclosan (antibacterial agent) migration onto the surface of the composite by diffusion process to kill bacteria [26]. PLA/wood sawdust composite film impregnated with pediocin PA-1/AcH (Ped), antimicrobial agent, was used as antimicrobial packaging for raw slice pork in order to decrease the quantity of listeria [27]. RWS has been used as a reinforcing agent in rubber/RWS composites. The mechanical performances of these composites were appropriate to use in anti-stab body armour application [28]. The activated carbon obtained from RWS acted as a reinforcing agent in polyurethane composites to utilize as a microwave absorber [29]. Surface treatment of RWS is required. Alkaline and silane surface treatment using sodium hydroxide [26] and N-2(aminoethyl)-3-aminopropyl trimethoxysialne, [27], respectively, have been applied to decrease hydrophilicity of wood sawdust before blending with hydrophobic PLA in order to improve its interfacial adhesion.

To the best of our knowledge, there has been no previous report on the preparation of PLA compounded foams containing RWS, chitosan and PEG by using typical compression foam molding and a typical chemical blowing agent. The present study investigated the influence of RWS, treated RWS, PEG and chitosan on physical, mechanical and thermal properties of unfoamed and foamed PLA. The cytotoxicity and *in-vitro* degradation were carried out for preliminary investigation suitability of these PLA compounded foams for bone scaffold application.

1.2 Objectives

To prepare porous polymeric from poly(lactic acid) compounded with RWS and chitosan by typical compression molding using chemical blowing agent for studying physical, mechanical and thermal properties, and to preliminarily investigate suitability of the obtained foams for bone scaffold application.

1.3 References

1. Dhandayuthapani, B., Yoshida, Y., Maekawa, T. and Kumar, D. S. 2011 Polymeric scaffolds in tissue engineering application: A review. *International Journal of Polymer Science*. 1-19.
2. Kramschuster, A. and Turng, L.-S. 2013. Fabrication of tissue engineering scaffolds. *Handbook of Biopolymers and Biodegradable Plastics*. <http://dx.doi.org/10.1016/B978-1-4557-2834-3.00017-3>. (accessed 10/8/2018).
3. Serra, T., Planell, J. A. and Navarro, M. 2013 High-resolution PLA-based composite scaffolds via 3-D printing technology. *Acta Biomaterialia*. 9: 5521-5530.
4. La Carrubba, V., Carfi Pavia, F., Brucato, V. and Piccarolo, S. 2008 PLLA/PLA scaffolds prepared via Thermally Induced Phase Separation (TIPS): tuning of properties and biodegradability. *International Journal of Material Forming*. 1-5.
5. Tanodekaew, S., Channasanon, S., Kaewkong, P. and Uppanan, P. 2013 PLA-HA scaffolds: preparation and bioactivity. *Procedia Engineering*. 59: 144-149.
6. Huang, R., Zhu, X., Zhao, T. and Wan, A. 2014 Preparation of tissue engineering porous scaffold with poly(lactic acid) and polyethylene glycol solution blend by solvent-casting/particulate-leaching. *Materials Research Express*. 1: 1-10.
7. Rezwani, K., Chen, Q. Z., Blaker, J. J. and Boccaccini, A. R. 2006 Biodegradable and bioactive porous polymer/inorganic composite scaffolds for bone tissue engineering. *Biomaterials*. 27: 3413-3431.
8. Ameli, A., Jahani, D., Nofar, M., Jung, P. U. and Park, C. B. 2014 Development of high void fraction polylactide composite foams using injection molding: Mechanical and thermal insulation properties. *Composites Science and Technology*. 90: 88-95.
9. Pilla, S., Kim, S. G., Auer, G. K., Gong, S. and Park, C. B. 2009 Microcellular extrusion-foaming of polylactide with chain-extender. *Polymer Engineering and Science*. 1653-1660.
10. Wang, J., Zhu, W., Zhang, H. and Park, C. B. 2012 Continuous processing of low-density, microcellular poly(lactic acid) foams with controlled cell morphology and crystallinity. *Chemical Engineering Science*. 75: 390-399.

11. Montjovent, M.-O., Mark, S., Mathieu, L., Scaletta, C., Scherberich, A., Delabrade, C., Zambelli, P.-Y., Bourban, P.-E., Applegate, L. A. and Pioletti, D. P. 2008 Human fetal bone cells associated with ceramic reinforced PLA scaffolds for tissue engineering. *Bone*. 42: 554-564.
12. Rakovsky, A., Gotman, I., Rabkin, E. and Gutmanas, E. Y. 2014 β -TCP-poly lactide composite scaffolds with high strength and enhanced permeability prepared by a modified salt leaching method. *Journal of the Mechanical Behavior of Biomedical Material*. 32: 89-98.
13. Guarino, V. and Ambrosio, L. 2008 The synergic effect of polylactide fiber and calcium phosphate particle reinforcement in poly ϵ -caprolactone-based composite scaffolds. *Acta Biomaterialia*. 4: 1778-1787.
14. Zhou, H., Lawrence, J. G. and Bhaduri, S. B. 2012 Fabrication aspects of PLA-CaP/PLGA-CaP composites for orthopedic application: A review. *Acta Biomaterialia*. 8: 1999-2016.
15. Zhang, P., Hong, Z., Yu, T., Chen, X. and Jing, X. 2009 In vivo mineralization and osteogenesis of nanocomposite scaffold of poly(lactide-co-glycolide) and hydroxyapatite surface-grafted with poly(L-lactide). *Biomaterials*. 30: 58-70.
16. Blaker, J. J., Maquet, V., Jérôme. R., Boccaccini, A. R. and Nazhat, S. N. 2005 Mechanical properties of highly porous PDLA/Bioglass[®] composite foams as scaffolds for bone tissue engineering. *Acta Biomaterialia*. 1: 643-652.
17. Cheung, H.-Y., Lau, K.-T., Tao, X.-M. and Hui, D. 2008 A potential material for tissue engineering: Silkworm silk/PLA biocomposite. *Composites Part B*. 39: 1026-1033.
18. Cheung, H.-Y., Lau, K.-T., Pow, Y.-F., Zhao, Y.-Q. and Hui, D. 2010 Biodegradation of a silkworm silk/PLA composite. *Composites Part B*. 41: 223-228.
19. Niu, X., Li, X., Liu, H., Zhou, G., Feng, Q., Cui, F. and Fan, Y. 2012 Homogenous chitosan/poly(L-Lactide) composite scaffolds prepared by emulsion freeze drying. *Journal of Biomaterials Science*. 23: 391-404.
20. Bonilla, J., Fortunati, E., Vargas, M., Chiralt, A. and Kenny, J. M. 2013 Effects of chitosan on the physicochemical and antimicrobial properties of PLA films. *Journal of Food Engineering*. 119: 236-243.

21. Montilla, A., Ruiz-Matute, A. I. and Corzo, N. 2013. Biological effects and extraction processes for marine chitosan. digital.csic.es/bitstream/10261/126740/4/MARINE%20CHITOSAN.pdf. (accessed 25/8/2018).
22. Tanase, C. E. and Spiridon, I. 2014 PLA/chitosan/keratin composites for biomedical applications. *Material Science and Engineering C*. 40: 242-247.
23. Pillin, I., Montrelay, N. and Grohens, Y. 2006 Thermo-mechanical characterization of plasticized PLA: Is the miscibility the only significant factor?. *Polymer*. 47: 4676-4682.
24. Serra, T., Ortiz-Hernandez, M., Engel, E., Planell, J. A. and Navarro, M. 2014 Relevance of PEG in PLA-based blends for tissue engineering 3D-printed scaffolds. *Materials Science and Engineering C*. 38: 55-62.
25. Chen, B.-Y., Jing, X., Mi, H.-Y., Zhao, H., Zhang, W.-H., Peng, X.-F. and Turng, L.-S. 2015 Fabrication of polylactic acid/polyethylene glycol (PLA/PEG) porous scaffold by supercritical CO₂ foaming and particle leaching. *Polymer Engineering and Science*: 1339-1348.
26. Praprudivongs, C. and Sombatsompop, N. 2012 Roles and evidence of wood flour as an antibacterial promoter for triclosan-filled poly(lactic acid). *Composites Part B*. 43: 2730-2737.
27. Woraprayote, W., Kingcha, Y., Amonphanpokin, P., Kruenate, J., Zendo, T., Sonomoto, K., Benjakul, S. and Visessanguan, W. 2013 Anti-listeria activity of poly(lactic acid)/sawdust particle biocomposite film impregnated with pediocin PA-1/AcH and its use in raw sliced pork. *International Journal of Food Microbiology*. 167: 229-235.
28. Yong, K. C. 2014 Rubber wood fibre based flexible composites: Their preparation, physical strength reinforcing and stab resistance behavior. *Polymers & Polymer Composites*. 22 (4): 375-380.
29. Shaaban, A., Se, S.-M., Ibrahim, I. M. and Ahsan, Q. 2015 Preparation of rubber wood sawdust-based activated carbon and its use as a filler of polyurethane matrix composites for microwave absorption. *New Carbon Materials*. 30 (2): 167-175.

CHAPTER 2

LITERATURE REVIEW

2.1 Tissue engineering

2.1.1 General information

Tissue engineering is utilization of a principle of engineering and life science to develop biological substitutes for restoring, maintaining or improving the tissue function [1]. Four main components of tissue engineering are scaffold, living cell or tissue, controlling of growth factor, and cell culturing. Tissue engineering is processed by applying these components through 5 steps: 1) isolation of cells during biopsy, 2) cultivation and proliferation of isolated cells, 3) culturing the cells into scaffold, 4) developing the cultured cells to be a tissue in scaffold, and 5) implanting cell cultured scaffold into a live body (Figure 2.1) [2].

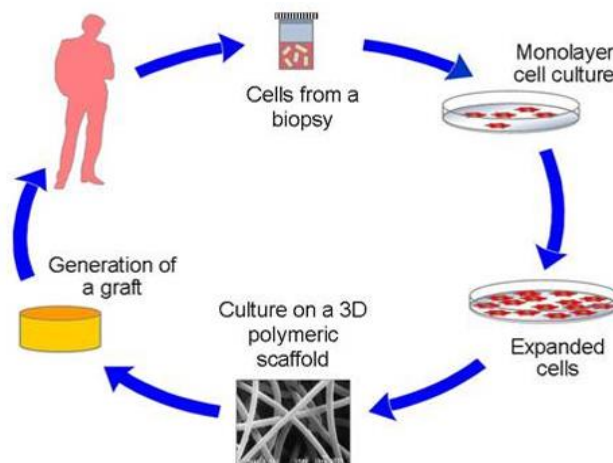


Figure 2.1 Basic principle of tissue engineering [2].

2.1.2 Scaffold for bone tissue engineering

Scaffold is an artificial structure which is able to support three-dimensional tissue formation in order to generate cell adhesion, cell division and cell

proliferation and to provide transportation of nutrient and metabolic waste. The characteristics required for ideal scaffold are as following: 1) opened-cell structure or closed-cell with interconnected cell structure, 2) biocompatibility and biodegradation, 3) suitable surface chemistry, 4) mechanical properties, and 5) ability of production with low cost and high quality [3]. interconnected cell structure are required for cell infiltration and cell adhesion to scaffold which are considered by porosity and pore size. The optimum porosity and pore size of scaffold should be close to those of the target tissue. Based on porosity, human bone is divided into cortical bone and cancellous bone with porosity of 5 to 13% and 30 to 90%, respectively [4]. The pore size suggested for bone regeneration and collateral bone growth are in the range of 50 to 710 μm [3] and 10 to 1000 μm [5], respectively. Good biocompatibility or non-cytotoxicity is an important characteristic of material used as scaffold to allow cell bioactivities. Suitable biodegradation rate is necessary because defective tissue requires a mechanical supporting of a scaffold during tissue repairing. The chemistry on scaffold surface influences the capability of cells adhesion to the surface, cell differentiation, and cell proliferation. Thus, surface chemistry is important characteristic of ideal scaffold. The mechanical properties of scaffold should be designed closely to those of the target tissue because scaffold has to support the damage tissue during the tissue growth in order to prevent growing tissue deformation. Furthermore, scaffold preparation should be developed to be a mass production, without toxic solvent use and low cost, because it is regularly used in tissue engineering.

There are four main objectivities to use scaffold in tissue engineering as following: 1) pre-made porous scaffold, 2) decellularized extracellular matrix (EMC), 3) cell sheets with secreted EMC, and 4) cell encapsulated in self-assembled hydrogel (Figure 2.2) [6]. Pre-made porous scaffold is normally used in bone tissue engineering and it can be prepared by many fabrication methods. The function of bone scaffold is being a porous material that allow cell grow directly in the infective tissue. The other function is being a porous material for cell seeding to obtain cell-seeded scaffolds for implanting into defective tissues.

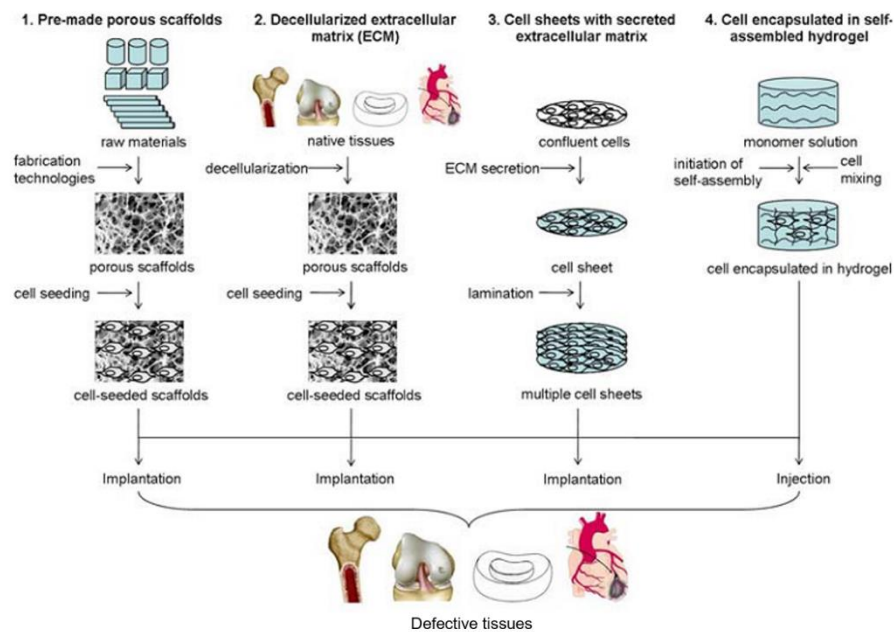


Figure 2.2 Schematic diagram demonstrating the objectivities of scaffold in tissue engineering [6].

2.1.3 Biomaterial used for scaffold preparation

Biomaterials used for pre-made porous scaffold preparation is consisted of ceramics, natural polymers and synthetic polymers. Hydroxyapatite (HA) and tricalcium phosphate (TCP) are ceramics commonly used for scaffold fabrication in bone tissue engineering due to their very good biocompatibility. The chemical structure of HA and TCP are partially similar to a native bone. However, ceramic scaffolds are difficult to control decomposition rate, brittleness and low elasticity. Natural polymers can be divided into 3 main categories: 1) protein, such as collagen, silk, elastin, gelatin and fibrinogen, 2) polysaccharides such as chitin, cellulose and amylose, and 3) polynucleotide such as RNA and DNA. Scaffold made from natural polymers is high bioactivity because it exhibit a good cell interaction but low mechanical properties.

Synthetic polymers are very valuable in medical filed and tissue engineering due to their proceesability. Although synthetic polymers exhibit low bioactivity, the necessary properties such as porosity, biodegradation rate and mechanical properties of scaffold prepared from synthetic polymer can be tailored to

match with the target tissue. Moreover, it is cheaper than other biomaterials because it can be produced in large quantities and low cost [7].

2.1.4 Synthetic polymers for bone scaffold preparation

Polymer materials for scaffold manufacturing can be divided into 4 types which are polypropylene fumarate (PPF), polyhydroxyalkanoate (PHA), surface bioeroding polymer, and saturated aliphatic polyesters. Polypropylene fumarate (PPF) is an unsaturated polyester. Degradation products of PPF such as fumaric acid and propylene glycol are biocompatible products which can be immediately eliminated from the body. Development of PPF as a composite scaffold is not widely investigated as compared with poly(lactic acid) (PLA) or poly(lactide-co-glycoside) (PLGA).

Polyhydroxyalkanoate (PHA) including poly-3-hydroxybutyrate (PHB), copolymer of 3-hydroxybutyrate and 3-hydroxyvalerate (PHBV), copolymer of 3-hydroxybutyrate and 3-hydroxyhexanoate (PHBHHx) and poly-3-hydroxy octanoate (PHO), are aliphatic polyesters produced by microorganisms and can be decomposed by hydrolysis process. They are interesting thermo-processable polymers to use in medical devices and tissue engineering applications. Nevertheless, time-consuming to extract PHA from bacterial culture make it not availability.

Surface bioeroding polymer is a polymer passed heterogeneous hydrolysis process to show a surface eroding behavior. Polymers shown this property are poly (anhydrides), poly(ortho-ester), and polyphosphazene. Surface bioeroding polymer is more potential to use as scaffold than polymer with bulk degrading property because of three advantages: 1) retaining of mechanical integrity throughout the lifetime of degradation of scaffold, 2) lowering toxic affectation and 3) enhancing of tissue ingrowth into the scaffold due to increasing of pore size during erosion process.

The most of saturated aliphatic polyesters which are often used as a 3D scaffold in tissue engineering are poly(lactic acid) (PLA), poly(glycolic acid) (PGA), and poly(lactic-co-glycolide) (PLGA). These polymers have chemical properties providing hydrolytic degradation via de-esterification. The monomeric components of each polymer such as lactic acid and glycolic acid can be completely eliminated by natural mechanism in the human body. Physical, mechanical and biodegradation properties of PLA and PGA can be designed by varying molecular weight and using

them as a copolymer. PLA and PGA have been approved by the US Food and Drug Administration (FDA) which are normally used in medical products. Mechanical properties of polymers used for scaffold manufacturing are listed in Table 2.1 [8].

Table 2.1 Mechanical properties of polymers used for scaffold preparation [8]

Polymer	T _m (°C)	T _g (°C)	Biodegradable time (months)	Tensile strength (MPa)	Modulus (GPa)
Bulk degradable polymer					
Poly(D,L-lactic acid)	-	55-60	12-16	Film or Disk: 29-35	Film or Disk: 1.9-2.4
Poly(L-lactic acid)	173-178	60-65	24	Film or Disk: 28-50 Fibre: 870-2300	Film or Disk: 1.2-3.0 Fibre : 10-16
PGA	225-230	35-40	6-12	Fibre: 340-920	Fibre : 10-16
PLGA	-	45-55	1-12	41.1-55.2	1.4-2.8
PPF	-	-	Bulk	-	-
Polycaprolactone	58	-72	>24	-	-
PHA and blends	120-177	-2-4	Bulk	20-43	-
Surface erodative polymer					
Poly(anhydrides)	150-200	-	Surface	25-27	0.14-1.4
Poly(ortho-esters)	30-100	-	Surface	-	2.5-4.4
Polyphosphazene	-66-50	242	Surface	-	-

2.2 Poly(lactic acid) foams

2.2.1 Poly(lactic acid)

2.2.1.1 General information

Poly(lactic acid) or polylactide is a biodegradable polymer derived from lactic acid or cyclic lactide. It is a highly versatile material made from 100% renewable resources such as corn, sugar beets, wheat, and other starch product [9]. Lactic acid or 2-hydroxypropionic acid is produced by fermentation of engineered microbes of lactobacillus genus and by chemical synthesis which is hydrolysis of lactronitrile using a strong acid [10-11]. Lactic acid has ‘‘D’’ and ‘‘L’’ stereoisomers which are referred

to R and S configuration, respectively (Figure 2.3 (a)) [12]. Polymerization of lactic acid produces PLA with racemic mixture (50% D and 50% L). Cyclic lactide dimer have 3 forms including D,D-lactide, L,L-lactide, and L,D -or D,L- lactide or meso lactide (Figure 2.3 (b)) [13]. The polymerization of cyclic lactide produces poly-D-lactide (PDLA), poly-L-lactide (PLLA), and poly-DL-lactide (PDLLA).

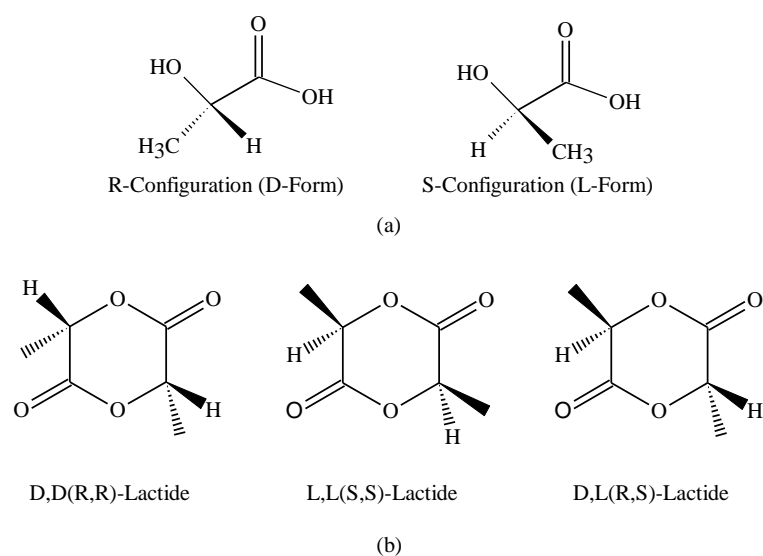


Figure 2.3 Stereoisomers of (a) lactic acids, and (b) lactides [12].

PLA has been developed for more than 50 years. Nowadays, PLA has been approved by European regulatory authorities and FDA making PLA widely used in many applications including packaging, food applications, drug delivery and medical devices [11]. PLLA has been reported to be an orthorhombic crystal structure (α -form) containing left-handed helix conformation by Lasprilla *et al.* [11]. The stereoisomers of lactic acid or lactide monomers, D-form/L-form ratios of lactic acid or D-lactide/L-lactide ratios and thermal history have direct effect on PLA crystallinity. In addition, properties of PLA depend on molecular weight, processing temperature, and annealing time. PLA containing more than 90% of PLLA has a tendency to be semicrystalline whereas PLA containing less than 90% of PLLA has a tendency to be amorphous. The PLLA content has the influence on the transition temperature. As PLLA content decreases the melting temperature (T_m) and glass transition temperature (T_g) decrease. The change of transition temperatures consequently affects physical characteristics of

PLA including heat capacity, density, rheological and mechanical properties. Poly(lactic acid) or polylactide exhibits amorphous polymer with a clearness and colorless when it is quenched from the melt. Glass transition temperature is the most important factor for amorphous PLA because its chain mobility is dramatically changed at above T_g . The melting temperature and glass transition temperature are the important factors to predict PLA properties [14]. The melt enthalpy estimated for 100% crystallinity PLA (ΔH°_m) is 93 J/g. The glass transition temperature of semicrystalline PLA is around 60 °C and the melting temperature is around 170 °C. Based on viscosity difference, semicrystalline PLA has higher shear viscosity than that of amorphous PLA and its shear viscosity decreases as increases temperature [15].

2.2.1.2 Synthesis of poly(lactic acid)

The well-known route ways to obtain high molecular weight PLA are direct polycondensation, azeotropic dehydration condensation, and ring opening polymerization (Figure 2.4). The direct polycondensation is normally consisted of 3 steps: removal of water by condensation, polycondensation of oligomer, and melt polycondensation. Solvents and catalysts under high pressure and high temperature environment are used. The melt polycondensation can be processed without using of any organic solvent and the reaction temperature should higher than T_m of the polymer, it is called solid-state polycondensation. This method is simple and low costs but the reaction condition is very sensitive [16]. The chain extension reaction is effective route way to overcome high molecular weight PLA by direct polycondensation. In this method, lactic acid is polycondensated in the presence of difunctional monomer (e.g. diols or diacids) to obtain prepolymer. Then, a chain coupling agent such as diisocyanate or bis (amino-ether) is used to connect between low molecular weight prepolymers to obtain high molar mass polymer [17]. The Mitsui Toatsu Chemical Company developed a new process based on direct polycondensation. Poly-DL-lactic acid (PDLLA) was successfully prepared using the mixing of lactic acid, high boiling point organic solvent, and catalysts. PDLLA shows a molecular weight of about 300,000 (MW) [11].

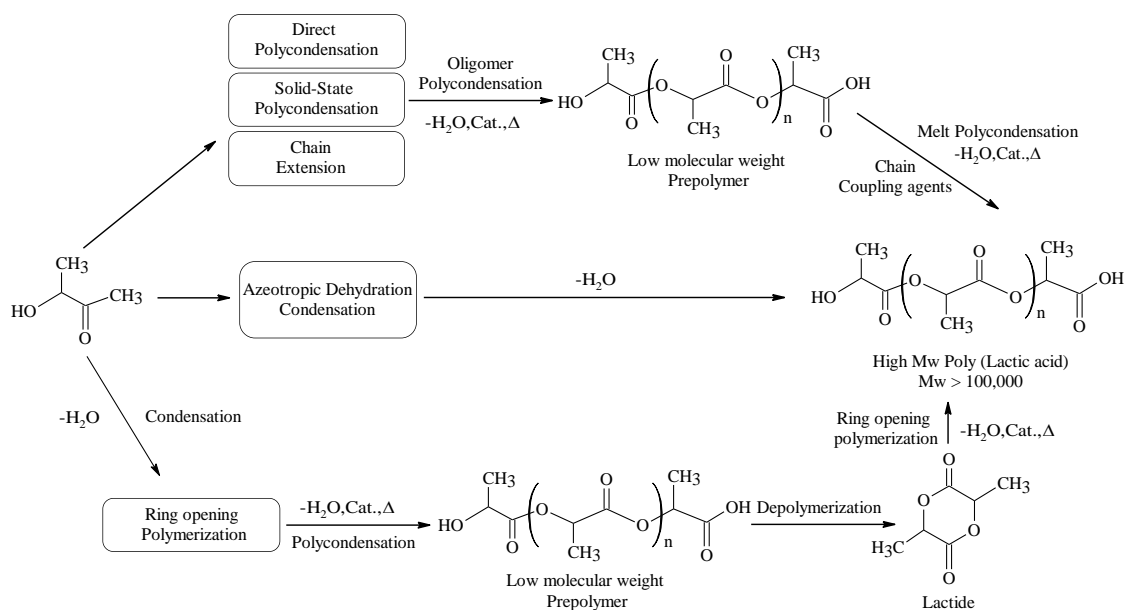


Figure 2.4 Synthesis methods of poly(lactic acid) [11, 18].

The azeotropic dehydration condensation is a direct polymerization method to produce high molecular weight PLA without using chain extender. A general procedure contains as the following steps. Firstly, pressure reduction of distillation of lactic acid is carried out at 130 °C for 2-3 h to eliminate the condensing water. Secondly, catalyst and diphenyl ether are added, and then, the tube packed with molecular sieves is attached to the reaction vessel. Thirdly, the refluxing solvent is returned to the vessel by the way of the molecular sieves at 130 °C for 30-40 h. Finally, the polymer is isolated and precipitated for purification to obtain high molecular weight PLA [18].

Ring opening polymerization (ROP) is conducted by ring opening of the lactide in the presence of catalysts through three steps: polycondensation depolymerization and ring-opening polymerization. ROP can be carried out in melt, bulk, or solution state and it can be carried out by anionic, cationic, and coordination insertion mechanism depending on the catalyst. Many kinds of catalysts have been used in ROP including metal catalysts, organic catalysts, cationic catalysts and single site catalysts composed of various multivalent ligands. The metal catalyst group widely used in ROP of lactide is tin (II) 2-ethylhexanoate (Sn(Oct)₂) due to high reaction rate, high conversion and high molecular weight of obtained products [11]. Because metal catalyst in ROP generates a pollution, the efforts to develop biocompatible ROP method

with organic catalysts have been done. The example of organic catalyst used in this reaction is N-heterocyclic carbenes (NHC). Trifluoromethanesulfonic acid (HOTf) and methyl trifluoromethanesulfonate (MeOTf) are the examples of cationic catalysts used in ROP. Single site catalysts composed of various multivalent ligands, for example, [MeBDI_{DIPP}] SnOMe is used in ROP of PLA via stereo-controlled polymerization [16].

2.2.2 Poly(lactic acid) in medical and tissue engineering applications

PLA is biodegradable polymer widely used in medical applications such as sutures, bone fixation, and drug delivery materials, etc. PLA has been applied as ecological materials and surgical implant materials and it also has been preliminary used as scaffold in tissue engineering. Fibers made from PLA can be constructed in to vary shapes and can be used as a surgical implant devices such as sutures. Nowadays, PLA is one of the most desirable polymer matrixes in tissue engineering. PLA is not only biodegradability and made from renewable resources but it also works very well and gives the excellent properties with low costs for medical and tissue engineering applications. 3D porous PLA scaffold is utilized for cell culturing to use in gene therapy for tissue regeneration such as muscle tissues, bone and cartilage, and other treatments in orthopedic, cardiovascular and neurological system. PLA may take time for 10 months to 4 years to degrade depending on microstructure factors, such as porosity, chemical composition and crystallization which affect its tensile strength [14].

2.2.3 Preparation methods of poly(lactic acid) based scaffold

There are many methods to produce three dimensional scaffold with high porous structure as following [8].

2.2.3.1 Thermal induced phase separation

High porous scaffold can be produced by thermal induced phase separation (TIPS) method which can control porous size for each type of tissue, e.g. nerves, muscles, bones and teeth. Scaffold obtained from this method is high porosity with anisotropic tubular and interconnected pore morphology (Figure 2.5 (a)) [8]. Pore feature, mechanical properties, bioactivity and degradation rates of the scaffold made

by TIPS method can be controlled by polymer concentration in the solution, volume fraction of secondary phase, quenching temperature, and polymer and solvent use.

2.2.3.2 Solvent casting and porogen leaching.

Solvent casting is carried out by dissolution of polymer into organic solvent and mixing with porogen particles. The mixture is then casted on the mold. After that, the solvent is evaporated and then particles were leached out to generate porous morphology in the polymer sheet/film (Figure 2.5 (b)) [8]. Porogen particle is a substance used in scaffold preparation to generate porous structure. Sodium chloride is normally used as porogen. This technique is a simple method without using any special equipment. However, disadvantages of this technique are limitation of product shapes, toxicity of used solvents that may remain in the sample and low mechanical properties of the sample.

2.2.3.3 Solid freeform fabrication technique

Solid freeform fabrication technique (SFFT) has been used to produce high interconnected pore scaffolds. The digital data produced from image source such as computer tomography were applied to design pore structure so that scaffold can be prepared with precisely controlled structure. The example morphology of scaffold prepared by this technique is displayed in Figure 2.5 (c) [8]. PLA/TCP composite scaffold with high porosity (up to 90%) has been produced by SFFT, using low-temperature deposition based on a layer-by-layer manufacturing method, computer-driven by 3D digital model. A parallel layers formed macropores (400 μm of diameter) and sublimation of the solvent during freeze-drying generated micropores (5 μm of diameter). The mechanical properties of PLA/TCP scaffold were close to human cancellous bone. Although SFFT can produce controlled pore structure scaffold, this route takes more time as compared with other technique because a temporary mold has to be firstly prepared.

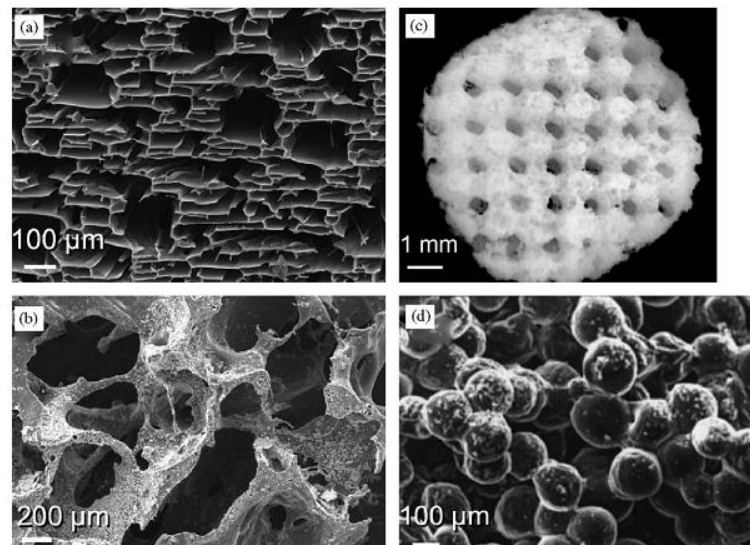


Figure 2.5 SEM images of porous polymer foams fabricated by (a) TIPS method, (b) solvent casting and particle leaching, (c) SFFT and (d) microsphere sintering [8].

2.2.3.4 Microsphere sintering method

PLA/ceramic scaffold prepared by microsphere sintering technique consisting of two steps: 1) synthesis of PLA/ceramic microspheres by emulsion/solvent evaporation and 2) sintering the composite microspheres to obtain a 3D porous scaffold. This method has been utilized to produce porous composites of biodegradable polymer/bioactive glasses. For example, composite microspheres of PLGA/Bioglass[®] have been produced by a water-oil-water emulsion technique followed by sintering to obtain cylindrical shape samples. The composite microspheres showed a good interconnected porous structure, approximately 40% porosity and 90 μm porous size. The mechanical properties were closed to those of the cancellous bone. Moreover, reinforcement with Bioglass[®] is able to increase compressive strength of PLGA. A typical structure of scaffold prepared by microsphere sintering method is displayed in Figure 2.5 (d) [8].

2.2.3.5 Electrospinning

Electrospinning is a simple and versatile method to obtain non-woven fibers from many polymers and composites. Usability of scaffold prepared by this

method in medical field is increased because of many important aspects including large surface areas, high porosities and easy to be incorporated with functional components such as drugs, genes and enzymes. However, a toxic solvent used in this method may effect to cells if it is not completely eliminated, and there are several factors which have to be controlled to obtain desired fiber features. Thus, electrospinning is difficult and time-consuming as compared to other methods [4].

2.2.3.6 Coating method

Bioceramic-coated porous scaffolds have been produced in a foam, fibers and mesh forms by slurry dipping or eletrophoretic deposition (EPD). Development of micro-porous foam composite coated with Bioglass[®] particles has been prepared by using slurry dipping. Because of the small particle size of Bioglass[®] (less than 5 μm), it generates the stability and homogeneous coatings on the foam surface and the infiltration of Bioglass[®] particles through the porous networks was completely done. EPD is an alternative technique to prepare bioceramic-coated scaffold. In this method, the foam sample is oriented vertically to the larger dimension of the electrodes. Bioglass[®] particles are charged in aqueous suspension. The aqueous suspension containing bioglass[®] particles is infiltrated into the foam or scaffold sample. Slurry dipping technique is more suitable than EPD technique because EPD technique frequently reduce interconnected pores of the scaffold sample [8].

2.2.3.7 Supercritical gas foaming

Supercritical gas foaming is a technique to fabricate foam or scaffold without a toxic solvent. This technique can control foam structure and its properties. The process is carried out through nucleation and growth of gas bubbles which were dispersed throughout a continuous phase of polymer by sudden depressurization. Porous structure is generated when the dispersed gas phase is removed from the continuous phase of polymer. For example, the procedure to prepare PLA-CaP/PLGA-CaP composite scaffold is as following. A homogeneous mixture of PLA/PLGA and CaP particles was firstly prepared by melt-extrusion and it was located in a pressure chamber. Then, CO₂ gas is diffused into the molten mixture to form a melt-gas solution under a saturation pressure at a temperature above T_m of the polymer. After that, the

foam expansion was carried out through gas sudden releasing and cooling. This step increased polymer viscosity and the permanent foam was obtained by the solidification and recrystallization. Three key advantages making the scaffold made by this technique better than the scaffold made by solvent casting have been reported. These key advantages were 1) non-using toxic solvent, 2) super enhancing mechanical properties, and 3) good HA particles exposing on the scaffold surface which support bone regeneration [4].

2.2.3.8 Melting process

There are many kinds of melting processes used to prepare a dense medical products including forging, pressing, sintering, extrusion, and microwave irradiation. For a porous products, Gomes *et al.* [19] have developed a new method for manufacturing biodegradable scaffolds through injection molding. Corn starch-based polymer blends, hydroxyl apatite and blowing agent were used. The corn starch was blended with either ethylene vinyl alcohol (SEVA-C) or cellulose acetate (SCA), and the blowing agent was Hostalon[®]P9947. Hostalon[®]P9947 mainly composed of carboxylic acids which was reacted by heating. CO₂ and water would be released after heating. The obtained foam sample showed a compact skin and a porous core.

Mi *et al.* [20] have prepared thermoplastic polyurethane (TPU)/PLA scaffold through microcellular injection molding. The injection machine was equipped with supercritical carbon dioxide supply system which can be precisely controlled the injected gas weight by adjusting gas flow rate and gas valve opening time. It was found that the tensile strength and compression strength of the foam were suitable to be used as an artificial scaffold. The elongation at break was increased with increasing TPU contents. This technique is easy, reproducible and interesting to develop from laboratory scale to industrial scale. However, it requires expensive special equipment to generate supercritical CO₂.

2.2.4 Foaming of PLA using blowing agents

2.2.4.1 General polymer foaming process

A general polymer foaming process using blowing agent contains 3 main steps: polymer/gas solution formation, bubbles nucleation and growth, and solidification (Figure 2.6). In polymer/gas solution formation, a gas blowing agent is dissolved into the molten polymer under a high pressure to form a homogeneous phase saturated solution. A key factor in this steps is pressure, and a lesser factor is temperature.

In bubbles nucleation, small bubbles were formed in the polymer melt by pressure releasing and temperature controlling. Bubble nucleation is classified into heterogeneous and homogenous nucleation. Heterogeneous nucleation is more preferable than homogenous nucleation. Many kinds of additives can be used as nucleation sites to generate heterogeneous nucleation in foaming processes such as nano-calcium carbonate [21], nano-silica [22] and chitosan [23], etc. In theory, the critical nucleus is defined as the minimum radius that bubble is able to grow. Nucleated bubbles showing the radius larger than that of the critical nucleus will survive and grow, whereas nucleated bubbles showing the radius smaller than that of the critical nucleus will collapse. Surviving bubbles continuously expand by gas diffusion from polymer matrix into the bubbles.

A foam with cellular structure will be achieved by solidification. The factors controlling bubble growth and foam structure are time provided bubble growth before solidification, pressure, temperature and the presence of others bubbles in polymer matrix. The obtained foam properties depend on many factors. Gas loading, gas which remain dissolved in the molten polymer, gas lost to surrounding and rate of pressure reduction affect the foam density. The nucleation kinetics, bubbles growth process and bubbles coalescence during foaming process affect the pore size and pore size distribution [24].

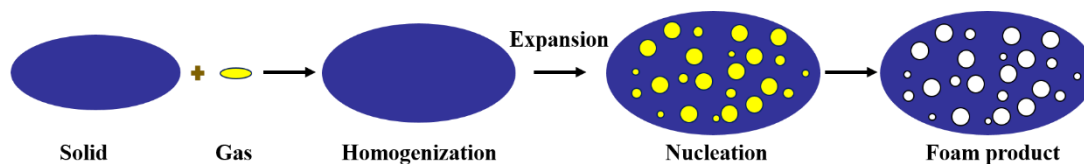


Figure 2.6 Typical polymer foaming process using blowing agents [25].

2.2.4.2 Blowing agent

Blowing agents used to generate gas dissolving into polymer matrix are divided into physical blowing agents (PBA) and chemical blowing agents (CBA). In foaming process using PBA, gases can be introduced and dissolved directly into a solid polymer in the solid state foaming process, and gases can be introduced into molten polymer for microcellular extrusion or microcellular injection molding process. CO₂ and N₂ gases are typically used as the physical blowing agent. Chlorofluorocarbons or argon has been used also in polypropylene, polyethylene and polystyrene foams.

In foaming process using CBA, gases can be released under a certain conditions through chemical reaction (endothermic or exothermic reaction) or thermal decomposition. Eight kinds of chemicals used as CBA are azodicarbonamide (AZDC or ADC), 4,4-oxybis benzene sulfonyl hydrazide (OBSH), p-toluene sulfonyl hydrazide (TSH), 5-phenyltetrazole (5-PT), p-toluene sulfonyl semicarbazide (PTSS), dinitroso pentamethylene tetramine (DNPT), sodium bicarbonate (SBC) and zinc carbonate (ZnCO₃) [26]. A major properties of some CBA are listed in Table 2.2.

Table 2.2 Properties of chemical blowing agents [25]

Products	Decomposition temp. range (°C)	Gas evolution (ml/g)	Main gases
AZDC	200-215	220	CO, CO ₂ , NH ₃
AZDC activated	140-215	130-220	N ₂ , CO, CO ₂ , NH ₃
OBSH	155-165	110-125	N ₂ , H ₂ O
TSH	105-110	115	N ₂ , H ₂ O
5-PT	240-250	190-210	N ₂
DNPT	190-200	190-200	N ₂ , NH ₃ , CH ₂ O

2.2.4.3 Foaming of PLA using physical blowing agents

The processing methods using the physical blowing agent that have been reported for PLA foam preparation were batch foaming process, microcellular injection molding and microcellular extrusion foaming. Corre *et al.* [27] have investigated the influence of rheological properties and process parameters on cellular structure of chain extended PLA foams prepared by melt blending followed by batch foaming process using supercritical CO₂. The addition of chain extender (CESA®-Extend OMAN698493) to PLA through reactive extrusion process has been done. It improved melt viscosity, elasticity and melt strength of PLA. The obtained PLA foams exhibited a cellular structure, and the cell sizes were ranging from macro scale to micro scale depending on the foaming parameters.

The PLA and PLA composites foams have been successfully prepared by Ameli *et al.* [28] and Ding *et al.* [29] via microcellular injection molding process. It is well known as Mucell® process. The special part was applied to generate physical blowing agent (N₂). Ameli *et al.* [28] found that the addition of talc and nanoclay could induce crystallinity during PLA foaming. The foam containing nanoclay showed stronger effect on cell morphology, average pore size, void fraction, flexural properties and impact resistance than those of the foam containing talc.

The influence of addition of cellulose fibers (northern bleached softwood kraft, NBSK) or black spruce medium density fiberboard (MDF) on crystallization of PLA/PEG foams prepared by microcellular injection molding process was observed by Ding *et al.* [29]. They found that the addition of NBSK and MDF influenced on cell nucleation and enhanced melt strength of PLA/PEG blends resulting in an increase of cell density, and a decrease of cell size and cell size distribution of PLA/PEG foam. The foaming process using physical blowing agents (supercritical CO₂ or N₂) is high productivity and short time process. However, it requires expensive special equipment to generate supercritical gases.

2.2.4.4 Foaming of PLA using chemical blowing agents

Chemical blowing agents (CBA) are divided into endothermic and exothermic blowing agents. The endothermic CBA that have been used in PLA foam preparation were BIH40 (it contains approximately 40% of the decomposition gas

(CO₂) and polyethylene as a carrier polymer) [30] and CBA containing of sodium bicarbonate and citric acid (1:1) [31]. Azodicarbonamide (AZDC) and commercial grade activated AZDC (Celogen 754-A) are exothermic CBA widely used in PLA foam preparation [31-33]. Zimmermann *et al.* [31] have studied effect of adding endothermic CBA (sodium bicarbonate and citric acid (1:1)) and exothermic CBA (AZDC, CS4M grade) on PLA foam properties. PLA foams were performed by compression molding followed by foam expanding in electric oven at 190 °C under ambient pressure. They found that PLA foam using exothermic CBA exhibited smaller cell size and higher cell concentration as compared with PLA foam containing endothermic CBA.

Zinc oxide (ZnO) has been used as an accelerator of AZDC to decrease foaming temperature by Luo *et al.* [32]. PLA foams were successfully prepared by using compression molding process. They found that the certain ZnO content could decrease decomposition temperature and enhance decomposition rate of AZDC. PLA foam density decreased with increasing AZDC/ZnO contents resulting in lowering foam tensile strength. In addition, the *in-vitro* cytotoxicity testing of ZnO has been reported. Saranya *et al.* [34] has been reported that ZnO nanopowder improved cell viability in pig kidney cell line and madin darby bovine kidney. PLA foaming using melting process and chemical blowing agent is easy operation, low costs and use of simple equipment, and PLA foams prepared through this route for preliminary investigation to use in scaffold application have not been reported.

2.3 Rubber wood sawdust

2.3.1 General information

Wood sawdust, one kind of lignocellulose materials, is industrial waste largely obtained from wooden furniture production. The main compositions of wood sawdust are cellulose, hemicellulose and lignin. The chemical structures are shown in Figure 2.7 [35]. Para rubber (*Hevea brasiliensis*) tree is an industrial crop in Thailand. The rubber latex obtained from Para rubber tree is used as a raw material in gloves or tire production industry. The Para rubber wood is typically utilized in furniture industry in Thailand and large amount of Para rubber wood sawdust (RWS) becomes the industrial waste. Thus, utilization of RWS is interesting. Yong [36] has been reported

that compositions of RWS were cellulose (39%), hemicellulose and cell wall (29%), lignin (28%) and ash (4%). The crystal structure and crystallinity of RWS have been reported by Kamphunthong *et al.* [37]. Crystal structure measured by X-ray diffractometer of RWS was a native cellulose I exhibiting characteristic peaks at 2θ of 22.7° and overlapping peaks at 2θ of 14° and 16° . Moreover, its crystallinity index calculated from XRD was 57.86%. The thermal properties of RWS were characterized by thermal gravimetric analysis. The $T_{d \text{ onset}}$ of RWS was 254°C , and three decomposition temperatures at approximately 265°C , 290°C and 440°C were found which correspond to the decomposition of hemicellulose, cellulose and lignin, respectively.

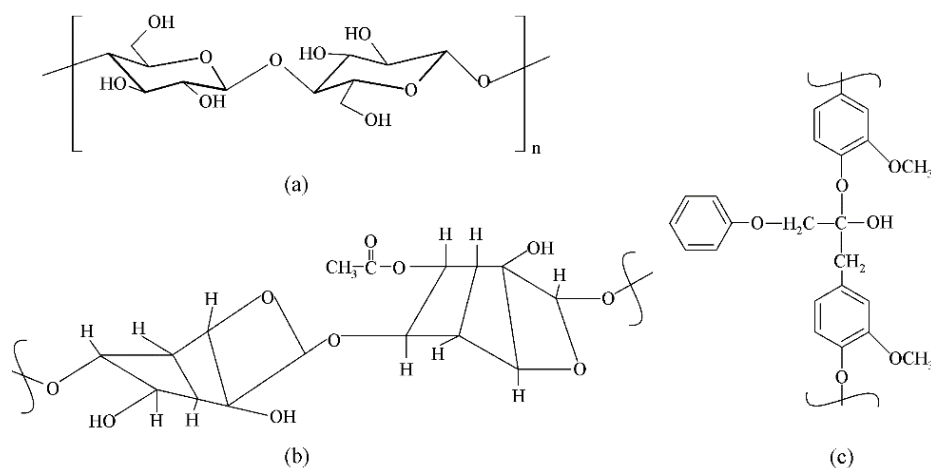


Figure 2.7 Chemical structure of (a) cellulose, (b) hemicellulose, and (c) lignin [35].

For cytotoxicity of cellulose and lignin, Alexandrescu *et al.* [38] have reported cytotoxicity of cellulose nanofibril-based structures, (1) dense and thin structure and (2) porous structure, made from *Eucalyptus* pulp. The results showed that the nanofibrils did not exert acute toxic phenomena on the tested 3T3 cells (fibroblast cells). In addition, Barapatre *et al.* [39] have found that lignin fractions extracted from the wood of *Acacia nilotica* depicted higher cytotoxic potential on breast cancer cell which seem to be a promising candidate as anti-cancer agent [39].

2.3.2 Composites of PLA/wood sawdust

Wood sawdust is widely used in wood plastic composite (WPC) production by blending with thermoplastic such as polyethylene (PE), polypropylene (PP), polyvinyl chloride (PVC). WPC containing biopolymers and wood sawdust has been also studied. Sykacek *et al.* [40] have determined the mechanical properties of WPC containing wood sawdust and 5 types of biopolymers including 1) poly(butylenes adipate-co-terephthalate), PBAT, 2) poly(lactic acid) or PLA, 3) PBAT/PLA compounded resin, 4) PLA-co-polyester blend and 5) tenite propionate. They found that an increase of wood sawdust content ranging from 20 to 70 wt% decreased flow ability in the injection molding process. Tensile strength and flexural strength were significantly improved in all types of biopolymer except WPC of PLA incorporated with more than 65 wt% of wood sawdust. WPC containing PLA as a thermoplastic matrix was difficult to process owing to incompatibility between hydrophobicity of PLA and hydrophilicity of wood sawdust. Therefore, surface treatment is normally applied to wood sawdust before using in PLA/wood sawdust composite preparation.

Wood sawdust has been impregnated in phenolic resin solution before using as a reinforce agent in PLA composites. The PLA composite reinforcing with wood particle impregnated with 1 wt% phenolic resin solution showed increasing of the composite strength and decreasing of the water adsorption as compared with PLA composite reinforcing with the untreated-one. The strength of the composite decreased as increased phenolic resin concentration owing to increase the coating thickness on the wood particle [41]. Faludi *et al.* [42] have improved an interfacial adhesion between PLA and wood sawdust by using N,N-(1,3-phenylene diamaleimide) (BMI) and 1,1-(methylenedi-4,-1-phenylene) bismaleimide (DBMI) as coupling agents. They found that wood sawdust modified with BMI and DBMI up to 5 wt% of sawdust content improved the strength and stiffness of PLA/wood sawdust composite. The mechanical properties results demonstrated that DBMI was more efficient to act as the coupling agent in PLA/ wood sawdust composite than BMI.

The utilization of wood sawdust as an antibacterial material in PLA/ wood sawdust composite has been reported. Praprudivongs and Sombatsompop [43] have investigated the mechanical and antibacterial performance of wood sawdust/PLA composite blended with triclosan. The wood sawdust was chemically treated using N-

2(aminoethyl)-3-aminopropyltrimethoxysilane (KBM 603) before blending. The addition of wood sawdust changed the mechanical properties of the composites. Young's modulus of the composite increased with increasing wood sawdust content whereas the tensile strength, elongation at break and impact strength decreased. In addition, wood sawdust acted as antibacterial promoter in PLA/triclosan/wood sawdust blends. Wood sawdust supported triclosan (antibacterial agent) to migrate onto the composite flat film surface to kill the bacteria. Woraprayote *et al.* [44] have fabricated PLA/wood sawdust composite films containing anti-listeria agent, pediocin PA-1/AcH (Ped). The composite films were processed through extrusion blown film process and Ped was added by using diffusion coating method. They found that wood sawdust played an important role in embedding Ped into hydrophobic PLA film. Dry-heat treatment of PLA composite film before coating with Ped improved anti-listeria activity, tensile strength, film transparency and its solubility in water. The composite film of PLA/wood sawdust incorporated with Ped could be used as a good anti-listeria biodegradable packaging for pork and other high-moisture foods.

Para rubber wood sawdust (RWS) is not widely used in biopolymer composite, especially for PLA composites to use in medical application. However, the researches studying in polymer/RWS composites have been reported. Laminated rubber/RWS composite was successfully prepared by using carboxylated nitrile latex based adhesive system. The composites showed good elasticity and stiffness. The strength-stab resistance testing demonstrated that this rubber/RWS composite could be utilized as anti-stab body armor [36]. RWS has been used as a raw material to prepare activated carbons via chemical activation using ZnCl_2 at 500 °C for 60 min. The activated carbon acted as a reinforcing agent in polyurethane composite to use as a microwave absorber in electromagnetic interference (EMI) shielding application [45]. Petchwattana and Covavisaruch [46] have prepared the toughened PLA by melt blending of PLA and acrylic core-shell rubber (CSR) in twin screw extruder before blending with RWS. They found that the tensile modulus and tensile strength of PLA/RWS composite increased with increasing rubber wood sawdust content (5-30 wt%) but the elongation at break and impact strength were decreased. The elongation at break and the impact strength of the composites were improved when toughened-PLA (PLA blended with 5 wt% CSR) was used instead the neat PLA.

2.4 Chitosan

2.4.1 General information

Chitin or poly (β -(1 \rightarrow 4)-N-acetyl-D-glucosamine) is a polysaccharide consisting of β -(1 \rightarrow 4)-linked 2-amino-2-deoxy- β -D-glucopyranose (GlcN) (Figure 2.8 (a)). It is found in the exoskeleton of arthropods or in the cell walls of fungi and yeast [47]. Chitosan is a derivative of chitin which contain high amount of 2-acetamido-2-deoxy- β -D-glucopyranose (GlcNAc). Chitosan is obtained from deacetylation reaction of chitin, N-Acetyl glucosamine group is changed to glucosamine group, and it contain at least 60% of degree of N-acetylation (DA). DA is assigned as the average number of GlcNAc units per 100 monomer showing as a percentage form [48]. The chemical structure of repeat units and partially acetylated chitosan are displayed in Figure 2.8 (b) and (c), respectively [47]. Deacetylation reaction of chitin to obtain chitosan is divided into 2 methods involving chemical and biological (microbial) methods. The reactions normally contain three steps: demineralisation, deproteinisation and decoloration [49]. The properties of chitosan such as solubility depend on variation of %DA, distribution of acetyl group along its main chain and its molecular weight.

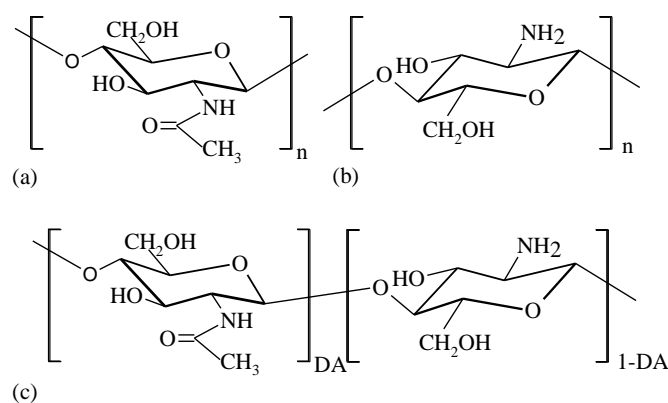


Figure 2.8 Chemical structure of (a) poly(*N*-acetyl- β -D-glucosamine) or chitin and (b) chitosan repeat units and (c) partially acetylated chitosan [47].

2.4.2 Biocomposites of PLA/chitosan

Chitosan (CH) has been used in many applications due to good oxygen barrier properties, biodegradability, biocompatibility, non-toxicity and antimicrobial

activity [50]. Chitosan has been processed by solution method in water, organic solvent, ionic liquids and the acid condition. For example, Xu *et al.* [51] have prepared micro and nano fibers of chitosan/PLA through electrospinning for using in tissue engineering application. Chitosan-poly lactide composites blended with montmorillonite (Cloisite 30B) have been prepared by solvent evaporation method to use in drug release devices [52].

Melt blending of chitosan with bioplastics such as poly(caprolactone), poly(vinyl alcohol) and PLA has been reported [53]. Bonilla *et al.* [54] have prepared PLA/CH films by melt blending in twin-screw extruder followed by film forming. The addition of chitosan to PLA increased crystallization temperature but it decreased mechanical properties. PLA/CH films exhibited high antimicrobial activity as compared with the neat PLA film. PLA/CH/keratin blends have been prepared by melt blending using internal mixer followed by compression molding. The osteosarcoma cell line culture on the blends indicated a good viability and cell proliferation [50].

Influence of chitosan on properties of PLA/chitosan biocomposite sheets has been observed by Răpă *et al.* [55]. These composites sheets were prepared via compression molding, and tributyl o-acetyl citrate (ATBC) was used as a plasticizer. They found that ATBC could decrease brittleness of PLA and the biocomposites exhibited non-toxic in radish and cucumber seed germination. Moreover, the addition of chitosan significantly reduced amount of *S. aureus* and *E. coli* on the contact surface of the PLA/CH sheet. It was suitable to use as packaging materials for non-fatty foods at refrigeration temperature with a pH above 4.5.

In scaffold preparation, PLA/chitosan scaffold has been prepared by many solution methods such as thermal induced phase separation (TIPS) [56], emulsion freeze-drying [57], and electrospinning [58], etc. Niu *et al.* [56] have prepared nano-hydroxyapatite (n-HAC)/PLLA/chitosan microsphere (CMs) scaffold by TIPS method. CMs contents were varied (10, 30 and 50 wt% of PLLA). It was found that incorporation less than 30 wt% of CMs insignificantly affected the morphology and porosity of n-HAC/PLLA/CMs scaffolds. However, its porosity rapidly decreased as increased CMs content. The compressive modulus and compressive strength of the biocomposite scaffold increased with increasing CMs contents.

Niu *et al.* [57] have successfully fabricated interconnected pore structure chitosan/PLLA scaffolds by emulsion freeze-drying method using oil-in-water emulsification system. The mechanical properties of the scaffolds increased with as increased PLLA content. The cell viability and cell proliferation evaluated from *in-vitro* cytotoxicity testing of the chitosan/PLLA scaffolds were comparable to those of the neat chitosan scaffold but it was lower than those of PLLA scaffold [57]. As mentioned above, PLA/chitosan biocomposite scaffolds prepared by solution have been reported. However, based on our knowledge, PLA/chitosan biocomposite scaffold prepared by melting techniques has not been reported.

2.5 Poly(ethylene glycol)

2.5.1 General information

Polymer of ethylene oxide is called in different name depending on its molecular weight. Polymer of ethylene oxide with molecular weight higher than 30,000 g/mol is typically called polyethylene oxide (PEO) or polyoxyethylene (POE), whereas polymer with molecular weight lower than 30,000 g/mol is referred as polyethylene glycol (PEG). PEG with a common chemical structure of $\text{H}-(\text{O}-\text{CH}_2-\text{CH}_2)_n-\text{OH}$ is a crystalline polyether exhibiting high water solubility and very low toxicity. PEG is a biocompatible polymer widely used in variety of applications including cosmetic, pharmaceutical and medical applications, etc. In medical field, monomethyl-ether terminated PEG (mPEG) containing single hydroxyl group is designed. Its terminal hydroxyl group can be covalently coupled with a larger molecule such as therapeutic protein or peptide and liposomes. This process is well known as “PEGylation”. The well-known trade name of PEG include Carbowax, for industrial use, and Carbowax Sentry, Fortrans, Polyox and Pogoxol for pharmaceutical, medical and cosmetic use.

PEG is prepared by the interaction between ethylene oxide (EO), water, and ethylene glycol or ethylene oligomer through cationic or anionic polymerization. Oxyanionic polymerization method is usually used to prepare PEG because it produce low polydispersity PEG. Low molecular weight PEG is synthesized by controlling the addition of EO to water or alcohols (initiators) in the presence of alkaline metal

compound (catalyst). High molecular weight PEG is synthesized by living oxyanionic polymerization of EO in high polar and aprotic solvents as shown in Figure 2.9 [59].

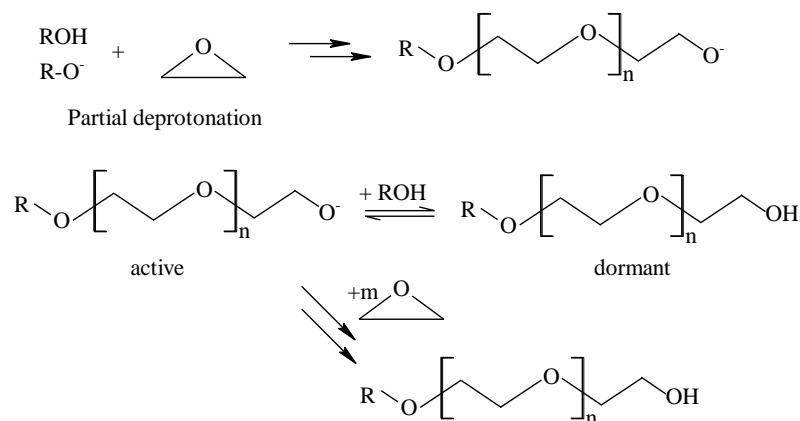


Figure 2.9 Living anionic polymerization of EO [59].

2.5.2 Poly(lactic acid)/poly(ethylene glycol) blending

The well-known limitations of PLA are low flexibility, plasticity and crystallinity which restrict application area of PLA. Blending PLA with variety of plasticizers has been used to enhance these limitation properties. Based on molecular characteristic, plasticizers used for PLA are divided into 1) low molecular weight plasticizers such as glycerol, lactides, acetyl tri-n-butyl citrate (ATBC) and 2) oligomer plasticizers such as oligomeric lactic acid (OLA), polyethylene glycol (PEG). PEG is widely used as a plasticizer for PLA in medical applications due to their water solubility and low toxicity [60-61]. Martin and Averouss [62] found that adding of 20 wt% PEG, molecular weight of 400 g/mol (PEG400), to PLA decreased T_g from 58 °C to 12 °C. Pillin *et al.* [61] reported that PLA blended with lower than 10 wt% of PEG400 and PEG1000 exhibited miscibility confirmed by demonstrating only one T_g of the blends.

For scaffold application, Zhang *et al.* [63] have prepared PLA/PEG6000 scaffolds by using supercritical CO₂ bath foaming process. They found that the impact strength of PLA increased as increased PEG600 content (5, 10, and 20 wt%), whereas the tensile properties decreased. The addition of PEG 6000 to PLA decreased T_g and T_{cc} and it changed closed-cell morphology of PLA scaffold to interconnected cell morphology. Moreover, the pore connectivity of PLA/PEG scaffolds increased with increasing PEG600 content. The widely used PEG in medical and pharmaceutical

application and its plasticization effect on PLA demonstrated that it is interesting to use PEG in PLA scaffold preparation.

2.6 Azodicarbonamide

Azodicarbonamide (AZDC) is utilized in three forms including powder form, formulated material in powder form and materials in master batch or pre-dispersed form. The decomposition of AZDC is proceeded through the competition of three exothermic reactions as shown in Figure 2.10 [64]. Decomposition of AZDC generates gas (32%), solid residues (41%), and sublimate (27%). The obtained gas contains nitrogen (65%), carbon monoxide (32%) and other gases (3%), ammonia (NH₃) and carbon dioxide (CO₂). The obtained solid contains urazol (57%), cyanic acid (38%), hydrazo-dicarbonamide (3%) and cyamelide (2%). AZDC particle size, processing temperature and time have effect on its decomposition. The processing temperature allowing the decomposition of AZDC is above 210 °C. According to AZDC decomposition reaction (Figure 2.10), the reaction rate of the reaction (3) increases as increases AZDC particle size because cyanic acid generated from the reaction (1) and (2) has longer time to contact to unreacted AZDC, it accelerates the decomposition process. In addition, AZDC has been reported to use as non toxic blowing agent in composite foam containing hydroxyapatite and poly(ethylene-co (vinyl acetate)) for tissue engineering by Sunny *et al.* [65].

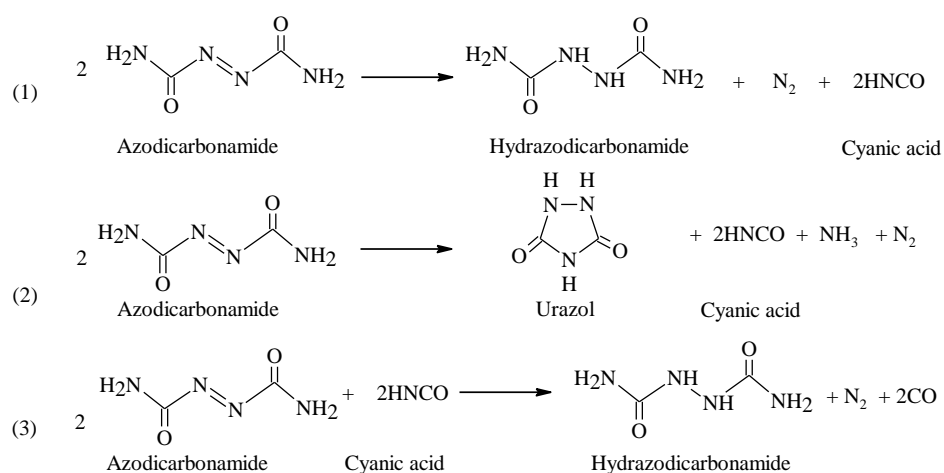


Figure 2.10 The decomposition reaction of azodicarbonamide (AZDC) [64].

2.7 Silane coupling agents

Silane is a coupling agent widely used to improve interfacial adhesion in polymer/filler composite through the reaction of silicon functional group (X) and organo-functional group (Y). General formula of silane is shown in Figure 2.11 [66]. X group is hydrolysable group reacting with the hydroxyl group of the filler. Y group is bonded with silicon functional group through a short chain carbon, and it is reacted with polymer by chemical reaction (grafting) or physicochemical interaction (hydrogen bonding, acid-base interaction or entanglement). The Y group can be a non-functional or functional group such as amino, epoxy, vinyl, methacrylate, and mercapto, etc.

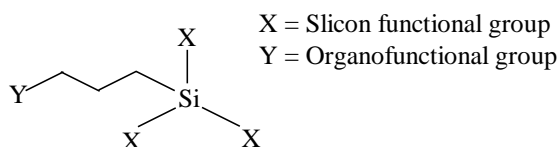


Figure 2.11 General structure of organosilanes [66].

The commercial silane coupling agents used to improve interfacial adhesion in PLA/filler composite are 3-aminopropyltriethoxysilane and 3-glycidoxypropyl trimethoxysilane containing amino- and epoxy organo functional group, respectively [64]. The interaction mechanism between wood flour, silane and PLA has been reported by Lv *et al.* [67] as shown in Figure 2.12. The OR groups in silane are hydrolyzed and transformed to silanols in the first step which is called hydrolysis process (Figure 2.12 (a)). The self-condensation is concomitantly proceeded during hydrolysis process to form -Si-O-Si- group (Figure 2.12 (b)). After wood flour was added into hydrolyzed silane solution, the active OH groups of wood flour can react with the reactive silanol groups to produce stable covalent (Si-O-wood flour) bond and the free silanol group can react to each other, forming a network structure of -Si-O-Si- (Figure 2.12 (c)). The coupling agents are finally grafted with PLA chains when treated wood flour is blended with PLA (Figure 2.12 (d)). The self-condensation reduces the chance of reactive silanol which accesses to hydroxyl group in the wood

flour surface. This reaction rate can be slowed down by adjusting the hydrolysis system to acidic pH environment [67].

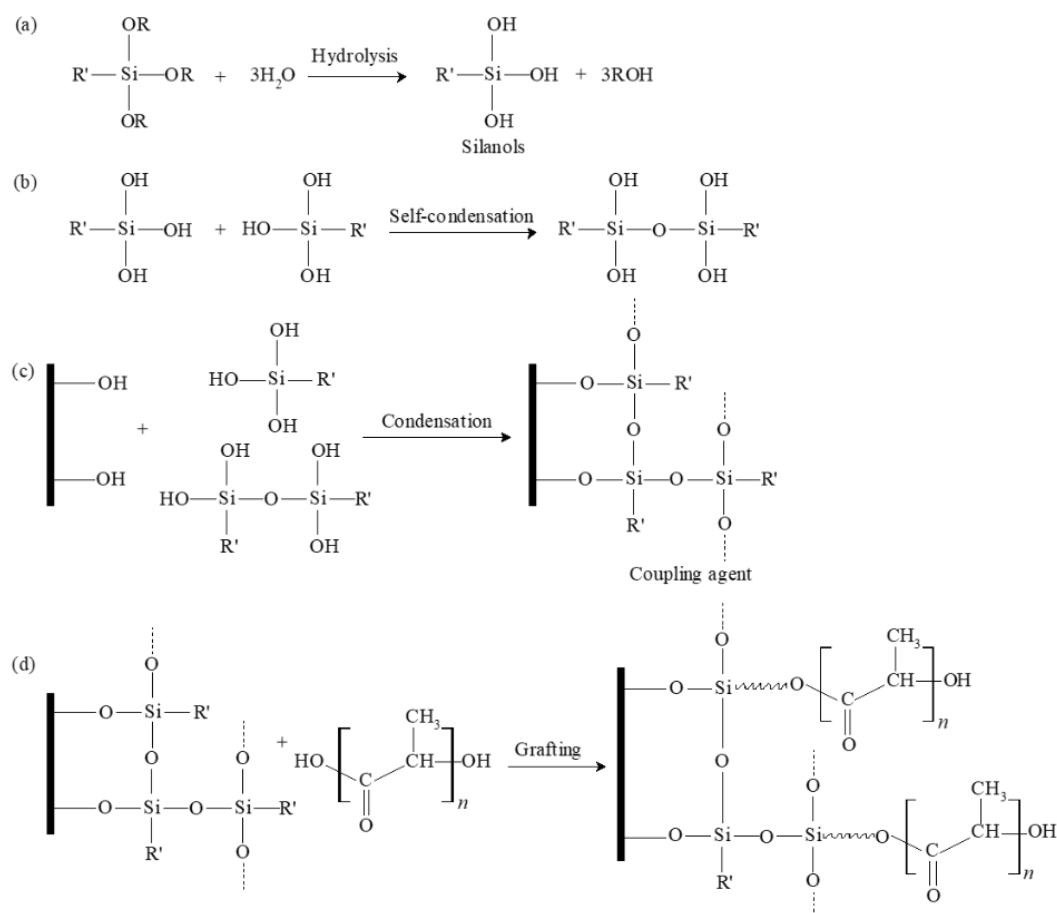


Figure 2.12 Interaction mechanism of silane coupling agent with wood flour and PLA [67].

2.8 Biodegradation of polymer based biomaterials

2.8.1 Biodegradation mechanism

In a biological environment such as an organism or human body, biodegradation process of polymer is occurred by physical, chemical and biological interaction between polymer and biological environment. The degradation of polymers used as biomedical devices is divided into 4 main steps: 1) hydrolysis with water in the tissue, 2) oxidation (oxidants are generated by tissue), 3) enzymatic degradation and 4)

physical degradation such as lowering of mechanical properties and water swelling [68]. The biodegradation rate depends on where biomaterials are implanted in the human body and the polymer characteristics such as crystallinity, molecular structure, hydrophobicity or hydrophilicity and surface area. The polymer materials can be degraded in the biological environment through at least three mechanisms: hydrolysis, oxidation and enzymatic mechanism.

2.8.1.1 Hydrolytic mechanism

Hydrolytic degradation of polymer is defined as a scission of hydrolysable bonds of polymer chain to obtain oligomers and monomers by attacking of water. The hydrolysable bonds include glycosides, esters, orthoesters, anhydrides, carbonates, amides, urethanes and ureas. The mechanism involves two main steps. The first step is the water contacting to hydrolysable bond of polymer at the polymer surface or polymer matrix following by bond scission. It results in initial reduction of polymer molecular weight. The second step, molecular weight of degrading polymer is significantly reduced by further hydrolysis [69]. There are two mechanisms normally occur in the hydrolytic degradation of solid polymer matrices including surface erosion or heterogeneous reaction and bulk or homogeneous erosion as shown in Figure 2.13 [69]. The degradation by surface erosion is normally faster than that of bulk erosion.

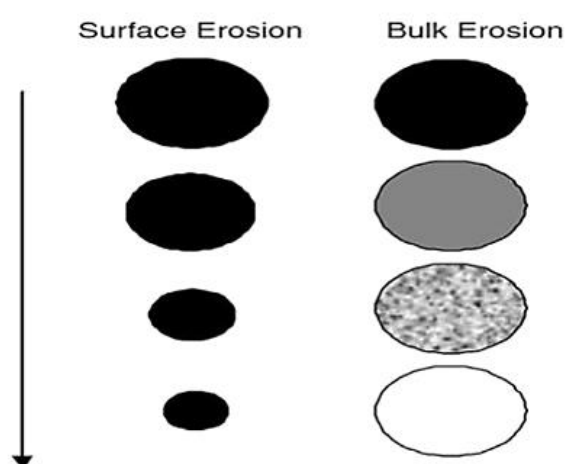


Figure 2.13 Mechanism of hydrolytic degradation in polymers [69].

2.8.1.2 Oxidative mechanism

Oxidative degradation of polymeric biomaterials is processed by inflammatory process. After implanting biomaterials into the body tissue, reactive oxygen species (ROS) are produced from macrophages, specific leukocytes and inflammatory cells and, then, inflammatory response is occurred. The example of ROS are hydrogen peroxide (H_2O_2), superoxide (O_2^-), hypochlorous acid (HOCl) and nitric oxide (NO). The oxidative effect generated by these ROS is the cause of chain scission of polymeric biomaterials and promote its degradation [69].

2.8.1.3 Enzymatic mechanism

Enzymes are biological catalysts to accelerate the reaction rate in the living body. In human body, hydrolysis reaction of polymeric biomaterials can be catalyzed by enzymes, it is called hydrolases. The examples of hydrolases are protease, esterases, phosphatases and glycosidases, etc. The enzyme-polymer chain interaction contains typically four steps: 1) enzyme diffusion from the bulk solution to the solid polymer surface, 2) enzyme adsorption on the polymer to form the enzyme-polymer complex, 3) acceleration of hydrolysis reaction rate and 4) diffusion of soluble degraded products from the solid polymer to the solution [69].

2.8.2 Degradation-observing techniques

The parameters used to observe degradation process are loss of mechanical strength of polymer matrix, reduction of molecular weight, changing of crystallinity and weight loss of a sample before and after degradation [70]. The selection of techniques to observe degradation of polymeric biomaterials should base on degradation stage and required specific property of the materials under investigation. The characterization techniques and properties used to observe degradation of polymeric biomaterials are as following [71].

2.8.2.1 Water absorption and weight loss

The water absorption of polymeric biomaterials is evaluated from water uptake values typically obtained after incubation of the materials in the solution. It indicates hydrophilicity or hydrophobicity and tendency of degradation through

hydrolysis process of polymer. The mass changes during degradation of polymer can be observed by comparison the weight before and after degradation testing period. The initial weight of dried samples should be precisely measured before testing. After degradation, the degraded sample should be washed using distilled water to eliminate remainder of enzyme, salts, or other impurities and then dried under vacuum stage until constant weight is obtained. The weight loss is a factor used for initial observation of biopolymer degradation. It is calculated and reported in term of percentage (% weight loss) [71].

2.8.2.2 Molecular weight

The chain scission normally occurs during degradation process resulting in a decrease of polymer molecular weight. Techniques to evaluate molecular weight are viscometry technique and gel permeation chromatography (GPC). The molecular weight in terms of number-average (M_n), weight-average (M_w) and the polydispersity index are parameters used to analyze degradation of biopolymers. The changing of polymer molecular weight affects crystallinity, weight loss, morphology and mechanical properties of polymer [71].

2.8.2.3 Crystallinity

Crystallinity of polymeric biomaterials after degradation can be monitored using differential scanning calorimetry (DSC) or wide-angle x-ray diffraction (WAXD). Crystallinity observed by DSC is based on changing of the glass transition temperature (T_g), crystallization temperature (T_c), melting temperature (T_m) and heat of fusion values. In WAXD analysis, the peak shifting, peak disappearance, appearance of new peaks and broader peak in the WAXD pattern are parameters indicating the crystallinity of polymeric biomaterials during degradation [71].

2.8.2.4 Morphology

During degradation, surface morphology changing and appearance of macro/micropores or cracks can be occurred. It is characterized by microscopy techniques such as scanning electron microscope (SEM), light microscopy, and atomic force microscopy (AFM). The freeze-fracturing in liquid nitrogen of the degraded

sample before testing is carried out to observe the change of cross section area of the degraded sample [71].

2.8.2.5 Surface chemistry

Characterization techniques to monitor surface chemistry of polymeric biomaterials during biodegradation are x-ray photoelectron spectroscopy (XPS), Fourier transformation infrared (FTIR) spectroscopy and contact angle measurement. Each technique is used based on required information and the depth of analyzed specimen. XPS technique provides element data and chemical groups at the first 10 nm depth of the surface specimen. FTIR with attenuated total reflectance (FTIR-ATR) gives chemical group information at the 5 μm depth of the surface specimen. Moreover, this technique can analyze chemical surface of the wet surface specimen which is useful to observe surface chemistry of the specimen during biodegradation process. Contact angle measurement is utilized to observe hydrophobicity at the surface of the specimen. High contact angle demonstrates high hydrophobic surface of the materials [71].

2.8.2.6 Mechanical properties

During degradation, mechanical properties are an important role to control and support a new tissue formation. Biomaterials used to repair defective tissue should be degraded to provide an area for a new tissue growth. At the same time, it should maintain a minimum mechanical strength of defective tissue in order to prevent new tissue deformation. Tensile, bending and compressive testing are commonly used to observe mechanical properties of polymeric biomaterials. The testing methods are described in the American Society for Testing and Materials (ASTM) standards [71].

2.8.3 Degradation of poly(lactic acid)

Biodegradable polymers including polycarbonates, polyanhydrides, polyamide, polyorthesters and polyester are mainly degraded through hydrolysis mechanism. In aqueous solution, polyester is very sensitive to degrade by hydrolysis via random scission of ester bonds. In hydrolysis in the presence of acid, the protonation of carbonyl group in polyester can catalyze the cleavage of carbon-oxygen bond along the polyester chain. This process is controlled by four basic factors: 1) rate constant, 2)

solubility of degraded products, 3) amount of absorbed water and 4) diffusion coefficient of chain fragment within the polymer. The polymerization-degradation of PLA (polyester) via hydrolysis is displayed in Figure 2.14 [69].

During *in-vitro* hydrolysis process, reaction of chain cleavage of PLA occurs specifically in amorphous region resulting in increment of crystallinity of polymer and, then, chain scission occurs. The carboxylic end groups occurred during chain scission act as catalyst to accelerate the hydrolytic degradation of PLA. It is called auto-acceleration or self-catalysis [70]. Similarly to *in-vivo* hydrolysis process, the degradation is slow at the first time that PLA sample is implanted in the human body, and low molecular weight of acid products can be removed by metabolism. After that, the rate of hydrolysis process is increased, and consequently acid products have not enough time to be eliminated by metabolism. This results in occurring of self-catalysis which accumulates and accelerates the degradation [72].

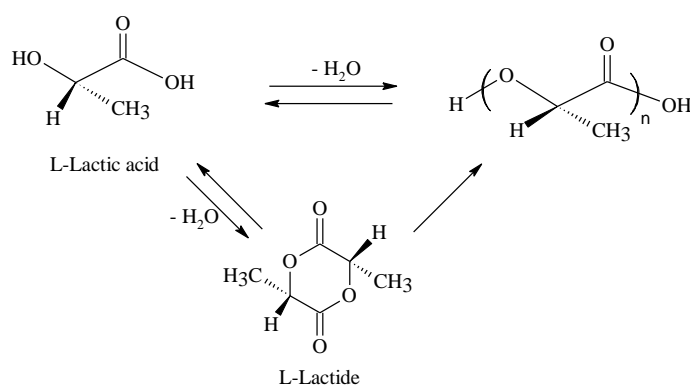


Figure 2.14 Polymerization-degradation rout ways of poly(lactic acid) [70].

2.8.4 Degradation of chitosan

Chitosan stability depends on internal factors including purity level, molecular weight, polydispersity index and degree of deacetylation and external factors including environment (humidity and temperature) and preparation methods. In *in-vivo* condition, chitosan can be degraded by enzymes, especially for lysozyme which normally appears in mammalian tissue. In *in-vitro* condition, chitosan can be degraded in via chemical, oxidation and enzymatic hydrolysis reaction. The internal factors mentioned above play an important role in degradation mechanism and degradation rate

of chitosan. The biodegradation of chitosan is begun by depolymerization process. It is a random cleavage of β -1,4-glycosidic bonds followed by deacetylation resulting in decreasing of its molecular weight as shown in Figure 2.15 [73]. Continuously, functional groups of chitosan such as amino, carbonyl and hydroxyl are destroyed. Furthermore, depolymerization of chitosan may generate a free radical to induce oxidation process. Interchain crosslinking can occur during degradation process resulting in changing of structure and physicochemical properties of polymer (Figure 2.15).

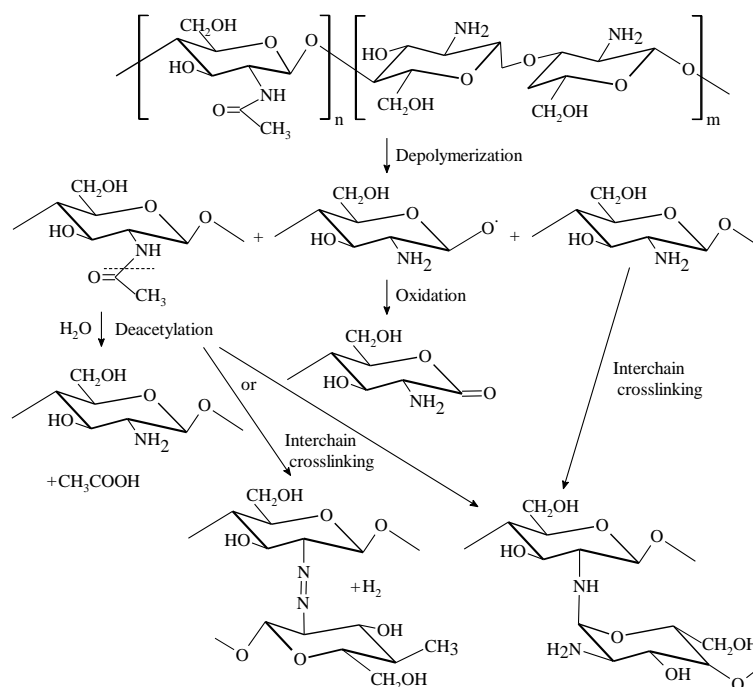


Figure 2.15 Probable degradation mechanism of chitosan [73].

2.8.5 Degradation of poly(ethylene glycol)

Poly(ethylene glycol) is synthesized by free radical polymerization, and it contains C-C in the main chains. Therefore, it is defined as a non-biodegradable polymer. However, the stability of PEG strongly depends on many factors such as temperature, pH, water content, an appearance of enzyme and oxidants such as reactive oxygen species (ROS). In *in-vivo* condition, PEG can be biodegraded through hydrolysis process and enzymatic oxidation. Reactive oxygen species are generated by

single electron transfer, and they are catalyzed by enzyme. ROS can react with the polymer chain by oxidation resulting in polymer biodegradation. The degradation mechanism of PEG is started from hydrogen abstraction followed by addition of another oxygen or radical to generate bond scission as shown in Figure 2.16 [74].

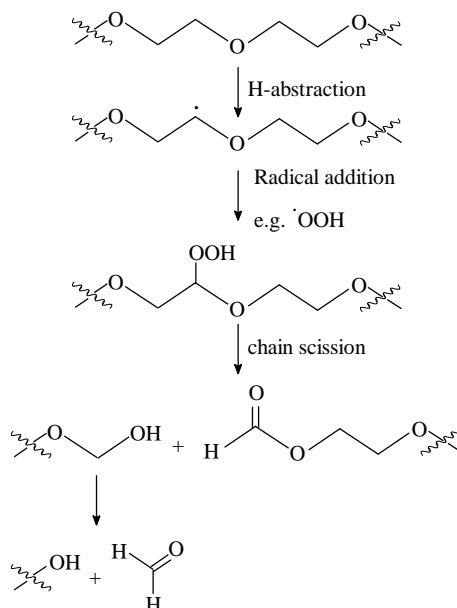


Figure 2.16 Oxidative degradation mechanism of PEG backbone [74].

2.9 Polymer characterizations

2.9.1 Mechanical properties

2.9.1.1 Impact strength

The important objective of impact testing is reliable data to evaluate impact performance of the materials. There are several methods used to measure the impact strength of plastic such as Izod, Charpy, Gardner, and tensile impact testing. The Izod and Charpy methods are usually used to measure impact strength of plastics. The specimen is tested under rapid loading. The impact machine is installed with a different pendulum capacity, depending on the testing standard. The pendulum can rotate around the hinge which is located at the top of the machine (Figure 2.17 (a)) [75].

The specimens for impact testing are divided into two main types including unnotched- and notched-specimens. Figure 2.17 (b) [76] demonstrates notched specimen dimension according to ASTM D256. The difference of Izod and Charpy method depends on the direction of the specimen located in the holder and the direction of impact force as shown in Figure 2.17 (c) [77]. In Izod impact testing, the specimen is located vertically in the holder and it is broken by hitting of the pendulum at the notched side of the specimen. In Charpy impact testing, the specimen is located in the holder and the notched section is in the middle of the holder. The specimen is broken by hitting of pendulum at the opposite of the notched side of the specimen. The fracture energy with the unit of Joule (J) is determined from the swing-up angle and swing-down angle of the pendulum. The impact strength is calculated from fracture energy divided by cross-section area. The unit is J/m or kJ/m^2 [78].

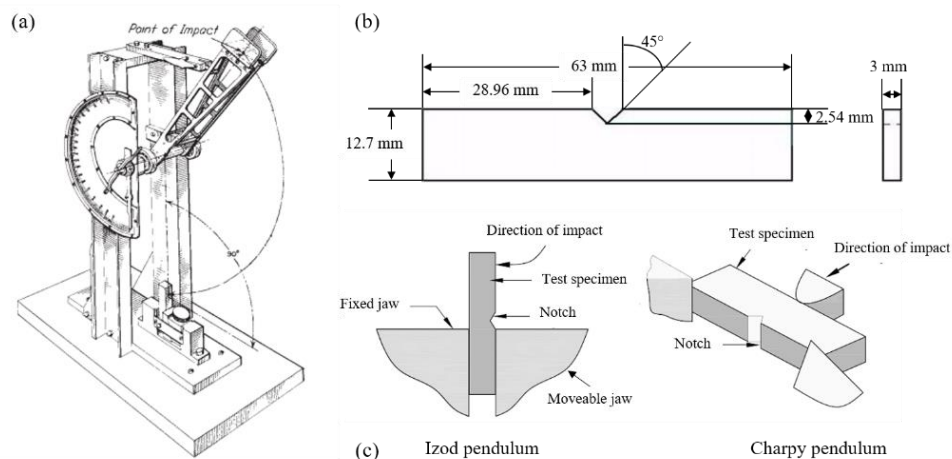


Figure 2.17 (a) Cantilever beam (Izod-type) impact machine, (b) Notched impact specimen according to ASTM D256 and (c) Izod and Charpy pendulum; modified from [75-77].

2.9.1.2 Tensile properties

Tensile testing is normally used to evaluate mechanical properties of materials. The elastic deformation, strength, ductility and strain-hardening are mechanical properties obtained from tensile testing. The examples of tensile parameters are Young's modulus, yield strength, ultimate tensile strength, % elongation and % area

of reduction. The tension test is proceeded by applying tension force at a specific extension rate to the specimen until the specimen is broken. Force-extension data are observed and recorded during testing process. The dimension containing gauge length and cross section area of tensile tested specimens depends on testing standard as shown in Figure 2.18 [79].

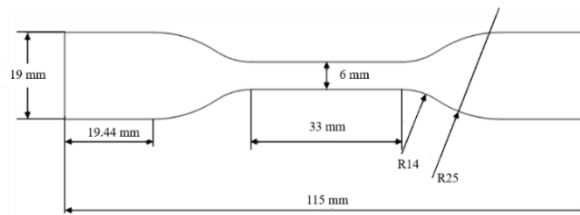


Figure 2.18 Tensile specimen demonstrating length, reduced gauge section and enlarged width according to ASTM D412 type C [79]

The tensile loading and extension obtained from tensile testing are used to calculate tensile stress (σ) and tensile strain (ε) as defined in the equation 1 and 2, respectively, where F is the tension force and A_0 is the original cross-sectional area at the gauge of the specimen. L_0 and L_f are original length and final length of the specimen, respectively:

$$\sigma = \frac{F}{A_0} \quad (1)$$

$$\varepsilon = \frac{L_f - L_0}{L_0} = \frac{\Delta L}{L_0} \quad (2).$$

Stress-strain relationship will be observed from stress-strain curve (Figure 2.19) [78]. Regions of A-B, B-C, and C-D demonstrate elastic deformation, plastic strain-hardening deformation and necking regions, respectively. The B, C and D points is yield point, ultimate strength and fracture point, respectively. During the tensile loading, the specimen will initially undergo the elastic deformation followed by plastic deformation. During elastic deformation, the specimen loaded by the tension

force is stretched, and the specimen dimension is temporarily changed. It can return to the original shape after the tension force is removed [79].

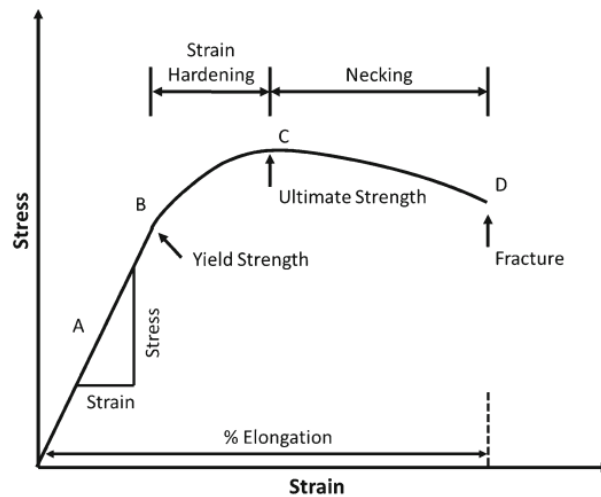


Figure 2.19 Stress-strain curve of polymer film [80].

The slope of the linear stress-strain curve (A-B region) is called Young's modulus (E) which is calculated by the equation 3:

$$E = \frac{\sigma}{\varepsilon} \quad (3).$$

The specimen dimension is then permanently changed after yield strength point in plastic deformation. Polymer typically exhibits three types of stress-strain behavior which are brittle, plastic and elastomeric stress-strain behavior. These behaviors depend on chemical structure. Brittle stress-strain behavior exhibits high strength but very low strain, and it is normally found in amorphous polymer. Plastic stress-strain behavior is normally found in semicrystalline polymer which shows moderate strength and relatively high strain. Elastomeric stress-strain behavior is generally observed in rubber material demonstrating extremely high elongation and very low stress at fracture point [81].

2.9.1.3 Flexural properties

Flexural testing is usually utilized to determine the bending force of material under three point loading condition. The universal testing machine equipped with accessories of flexural bending test is used as shown in Figure 2.20 (a) [82]. The rectangular specimen is placed on the support span with the length of L . The force is applied to the middle of the specimen at the $L/2$ position of the support span, and the loading nose creates three point bending at the specified rate (Figure 2.20 (b)) [83]. A variety of specimen shapes can be used. However, the specimen length should be long enough to allow overhanging on each end (at least 10 % longer than support span length) to prevent specimen slipping. The support span, speed of loading and the maximum deflection are parameters of flexural testing. ASTM D790 and ISO 178 are the standard testing methods typically used for flexural testing of plastics and polymers. The loading is stopped when the specimen is broken in the ISO 178 standard testing, and the loading is stopped when the specimen is reached to 5% deflection or the specimen is broken before 5% deflection for ASTM D790 [82].

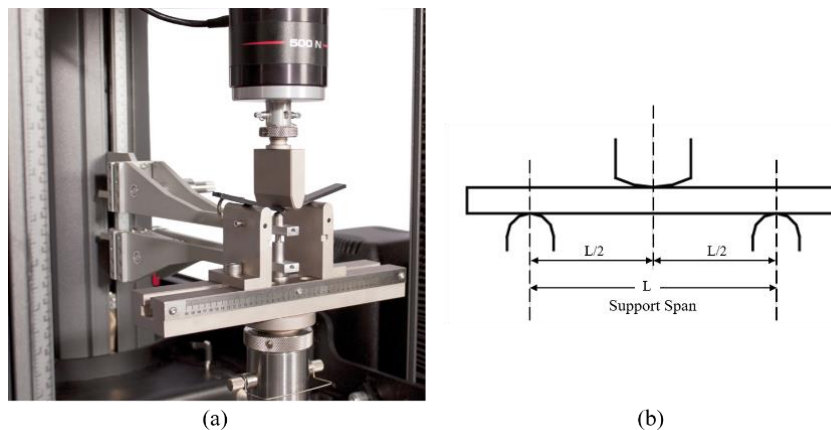


Figure 2.20 (a) Universal testing machine equipped with bending fixture accessories and (b) fixture used to set loading nose and support spacing and alignment [82-83].

A typical of flexural stress-strain curve is shown in Figure 2.21 [83]. It contains a, b, and c curves. The “a” curve is flexural stress-strain curve of the specimen that is broken before yielding. The “b” curve is found in the specimen that is reached

to yield point, and then, it is broken before 5% strain. The “c” curve can be observed in the specimen that is broken after 5% strain without yielding. The flexural stress (σ_f) (MPa), the flexural strain (ϵ_f) (mm/mm) and the flexural modulus of elasticity (E_f) (MPa) are calculated by the equation 4, 5, and 6, respectively:

$$\sigma_f = \frac{3PL}{2bLd^2} \quad (4)$$

$$\epsilon_f = \frac{6Dd}{L^2} \quad (5)$$

$$E_B = \frac{L^3 m}{4bd^3}$$

(6).

P is load at a given point on the load deflection curve (N). L is support span length (mm), b and d are width of tested beam (mm) and depth of tested beam, respectively. D is maximum deflection of the center of the beam (mm), and m is slope of the tangent to the initial straight (N/mm) [83].

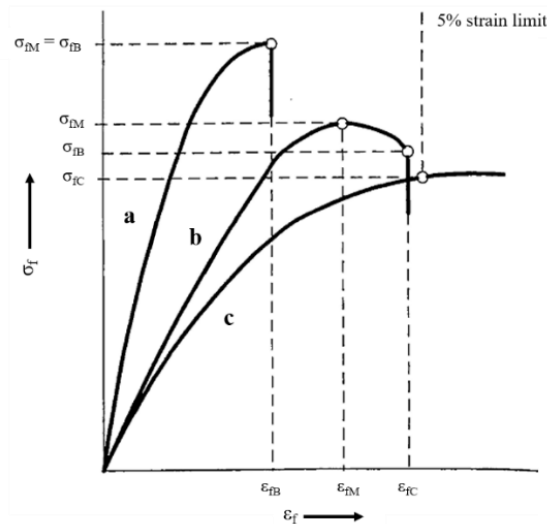


Figure 2.21 Typical curve of flexural stress and flexural strain [83].

2.9.2 Thermal properties

2.9.2.1 Differential scanning calorimeter

Differential scanning calorimeter (DSC) is thermal analysis technique widely used to determine amount of energy absorbed by the specimen to undergo the endothermic phase transition (or amount of energy released from the specimen in exothermic processes such as crystallization) as a function of time or temperature. The DSC instrument is shown in Figure 2.22 [84]. There are many kinds of DSC system including heat flux DSC, power compensated DSC, modulated DSC, hyper DSC and pressure DSC [85]. Heat flux DSC and power compensated DSC systems are commonly used (Figure 2.23) [86]. In the Heat flux DSC system, the specimen and reference are connected and controlled by a single furnace. In power compensated DSC system, the specimen and reference are separately connected and controlled by using different furnaces [85]. Figure 2.24 [87] displays typical DSC output showing DSC thermogram of heat flow versus temperature. The relation of heat flow and temperature in DSC thermogram can be evaluated to obtain various information including glass transition temperature, melting point, crystallization temperature and time, degree of crystallinity, rate and degree of curing, reaction kinetics, purity, oxidative stability and thermal stability [87].

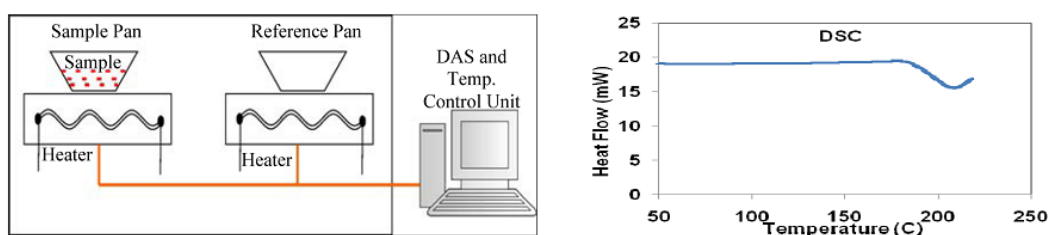


Figure 2.22 Diagram of DSC instrument connected with computer and output data [84].

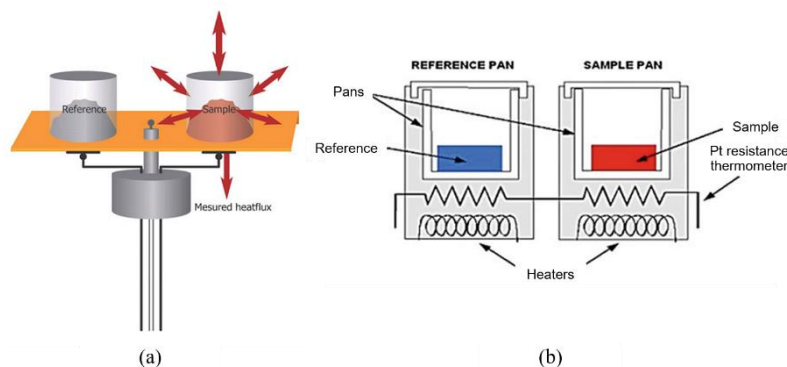


Figure 2.23 Diagrams of (a) heat flux DSC and (b) power-compensation DSC [87].

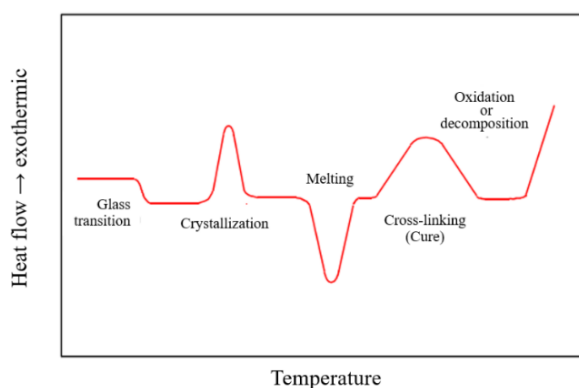


Figure 2.24 DSC thermogram exhibiting the interest transitions [87].

2.9.2.2 Dynamic thermal gravimetric analysis

Dynamic thermal gravimetric analysis (DMTA) is one kind of thermal analysis technique widely used to observe and to characterize mechanical and viscoelastic properties of materials including polymers, ceramics and metals. The specimen will be placed in the specimen holder in the DMTA instrument (Figure 2.25 (a)) [88]. The specimen can be held in the specimen holder with different direction (deformation modes) as shown in Figure 2.25 (b) [88]. The deformation mode used for testing depends on material type, degree of stiffness and specimen forms such as film, foam and fiber forms. The dynamic force with particular frequency is applied to the specimen and strain is measured as a function of temperature by linear variable differential transformer (LVDT) displacement sensor. As the specimen is dynamically

moved in the instrument, the storage modulus (E'), loss modulus (E'') and tan delta ($\tan \delta$) are determined. The storage modulus (E') is the elastic response (storage energy), it indicates stiffness of the specimen. The loss modulus (E'') is the viscous response or energy which is dispersed during one testing cycle of the specimen. Tan delta ($\tan \delta$) or damping or loss factor is the ratio of loss modulus to storage modulus ($\tan \delta = E''/ E'$) which is useful to observe energy absorbing of the specimen. In addition, the glass transition temperature can be determined at the temperature of the maximum $\tan \delta$ curve or the maximum loss modulus curve (Figure 2.26) [89].

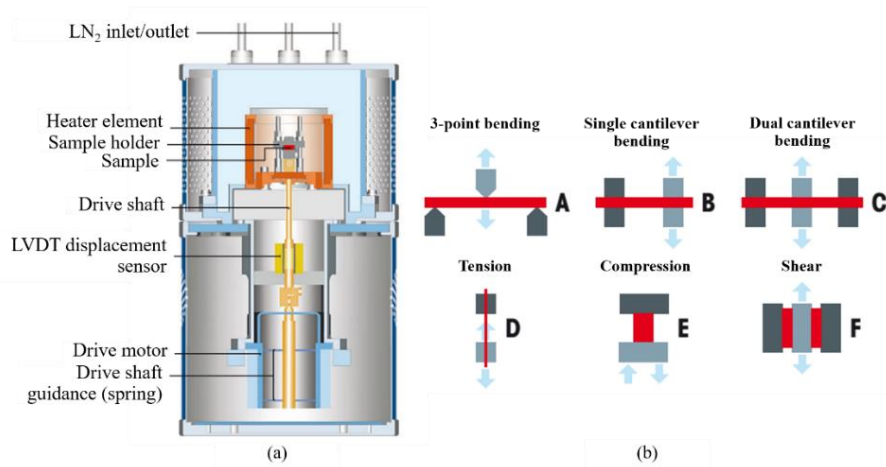


Figure 2.25 (a) A one kind of DMTA instrument showing important composition and (b) the different modes for sample holding [88].

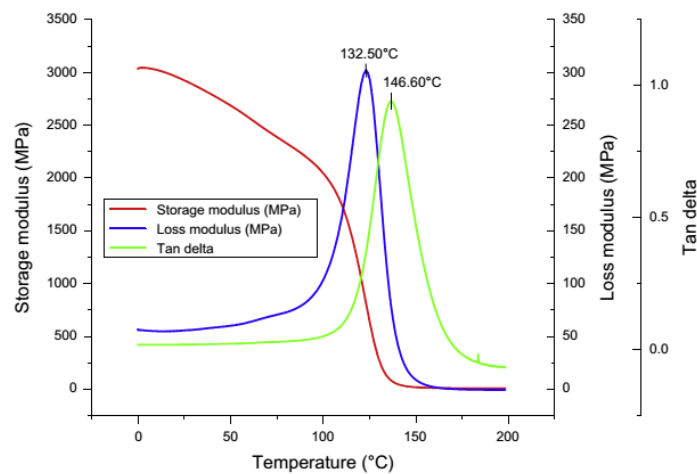


Figure 2.26 DMTA thermogram of storage modulus, loss modulus and tan delta as a function of temperature of the material [88].

2.9.2.3 Thermal gravimetric analysis

Thermal gravimetric analysis (TGA) is a technique to measure amount or rate of the weight change of materials such as polymer, composites and food as a function of time or temperature under controlled atmosphere. TGA is primarily utilized to determine thermal stability, oxidative stability and composition ratios of materials. Moreover, TGA can be used to estimate lifetime, decomposition kinetics, moisture content and volatile content of materials. The basic components of thermal gravimetric analyzer are balance, sample holder, furnace, programming unit (to control temperature), and recording unit (to record weight and temperature changes). The pan containing sample (about 5-20 mg) is placed in the sample holder which is supported by a precision balance. The sample is heated with a constant rate in a furnace and the sample weight is observed throughout the experiment. An inert gas such as nitrogen or oxidizing gas such as oxygen is used to control sample environment (Figure 2.27) [90]. During experiment, the sample weight change is automatically recorded as a function of temperature and time. The result is generally displayed as a thermogram showing the relation of weight remaining (%) as a function of temperature or the relation of first derivative of thermogravimetric analysis (DTG) as a function of temperature as shown in Figure 2.28 [91].

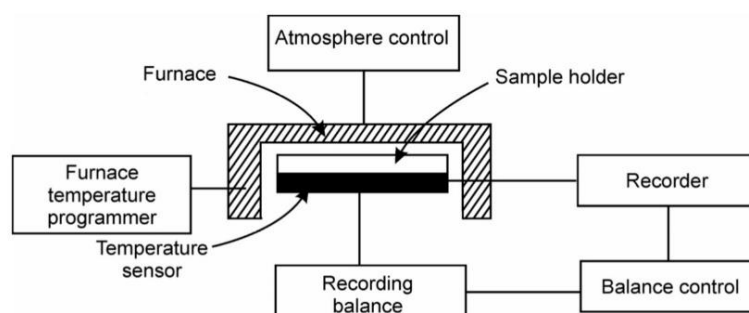


Figure 2.27 Diagram of thermogravimetric analyzer [90].

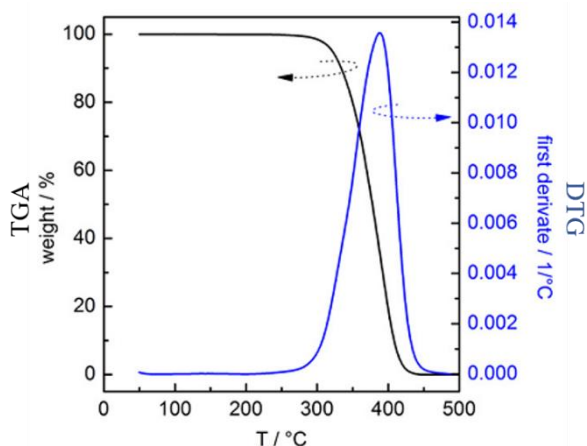


Figure 2.28 TGA and DTG curves of bulk PS-*b*-PMMA [91].

2.9.3 Fourier transforms infrared spectroscopy

Fourier transforms infrared spectroscopy (FTIR) is a preferred technique of infrared spectroscopy utilized to identify and determine molecular structure and quality and quantity of inorganic and organic components. FTIR analysis is based on the principle of combination of molecular vibrations of the sample. The examples of molecular vibrations are stretching, scission, rocking, twisting, and wagging (Figure 2.29) [92] which have specific frequencies or wavenumbers occurring in the infrared region. The typical FTIR analysis process is displayed in Figure 2.30 [93]. Firstly, the sample is tested in spectrometer, and the particular interferogram signal is obtained from the detector. Then, the signal is digitized and sent to FFT computer (the computer that the fourier transformation occur). Finally, the FTIR spectrum representing specific functional groups of the sample's molecule is obtained for analysis and interpretation.

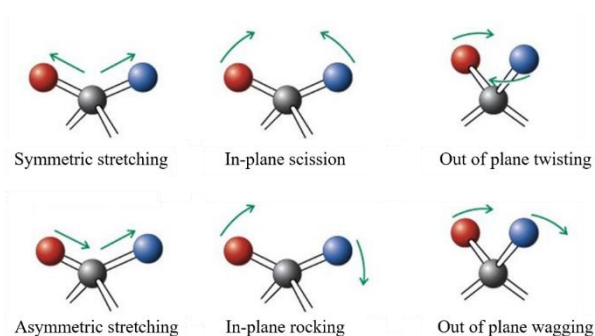


Figure 2.29 Stretching and bending vibrations in molecules [92].

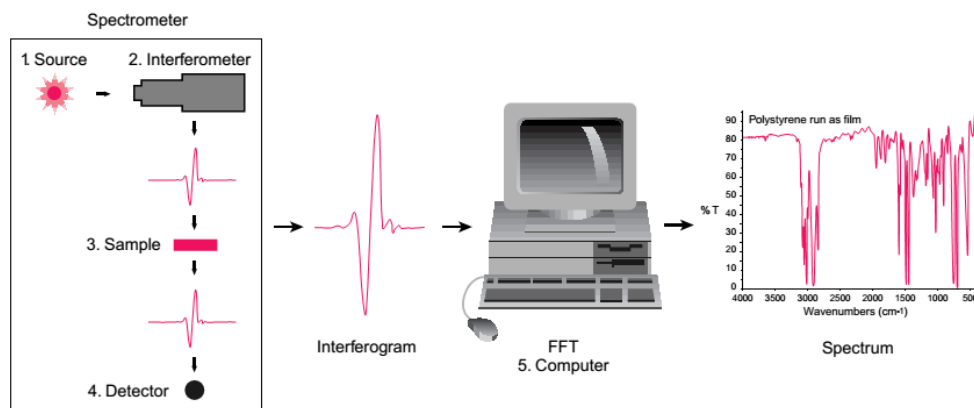


Figure 2.30 Schematic diagram of typical FTIR analysis process [93].

2.9.4. Scanning electron microscope

The scanning electron microscope (SEM) is a basic instrument of the electron microscopes commonly used to create high-resolution images to observe morphology on the surface of the solid specimen. SEM is very useful to semi-quantitatively or qualitatively determine chemical compositions, crystalline structure and crystal orientations of the specimen. The schematic diagram of SEM procedure is showed in Figure 2.31. The electron gun generates the electron beam which is focused by magnetic lenses, and it is introduced onto the specimen. The focused beam is dissipated as individuality of signals which is produced by electron-specimen interactions [94]. The obtained signals can be secondary electrons, backscattered electrons (BSE), diffracted backscattered electrons (EBSD), X-rays, visible light and heat. These signals are detected by specific detector. Secondary electrons and BSE signals are normally useful to produce SEM images. Secondary electron signals produce specimen morphology and topology. BSE signals produce a contrasts in composition of multiphase specimens. EBSD signals are utilized to observe crystal structures and orientations of minerals [94].

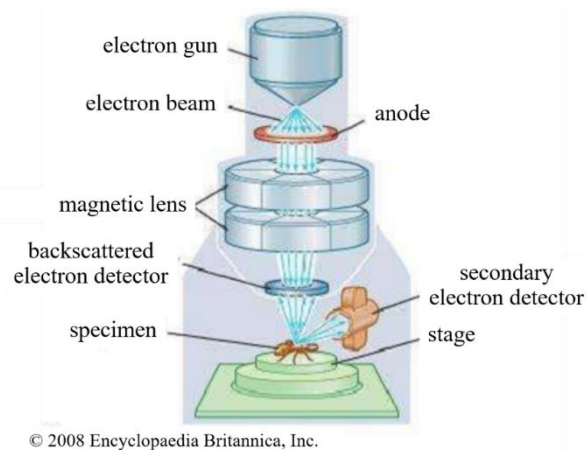


Figure 2.31 Schematic diagram of the basic SEM instruments [94].

2.9.5. X-Ray diffraction

X-Ray diffraction (XRD) is analytical technique commonly used to identify crystal structure and to evaluate atom spacing and unit cell dimension of materials. The procedure of XRD is shown in Figure 2.32 (a) [95]. The X-ray generated by cathode ray tube is filtered by the filter to obtain monochromatic radiation. Then, X-ray is collimated using collimator to the specimen. The interaction between the incident X-ray and the specimen generates diffracted X-ray with an angle of 2θ (Figure 2.32 (b)) [96]. The Bragg's equation is used (the equation 7), where n is the order of the reflection, it must be an integer, and λ is the wavelength of the incident X-ray beam, it is obtained from the experiment. The angle (θ) between incident X-ray beam and scattering plane of the specimen is measured, and the diffracted X-ray is given by $2d \sin \theta$. Therefore, the distance between the lattice planes or d-spacing (d) of the specimen is calculated from the Bragg's equation:

$$n\lambda = 2d \sin \theta \quad (7).$$

The d-spacing indicates crystal characteristic of the materials in term of a set of unique d-spacing [96]. After detector recording, the X-ray signal is converted to a count rate or X-ray intensity. A graph of X-ray intensity versus the angle between incident and diffracted X-ray beam (2θ) is obtained, it is called diffractogram (Figure

2.33) [97]. The XRD diffractogram is useful for qualitative and quantitative analysis, and it is utilized to determine a unit cell lattice parameters, crystallite size and degree of crystallinity of the materials.

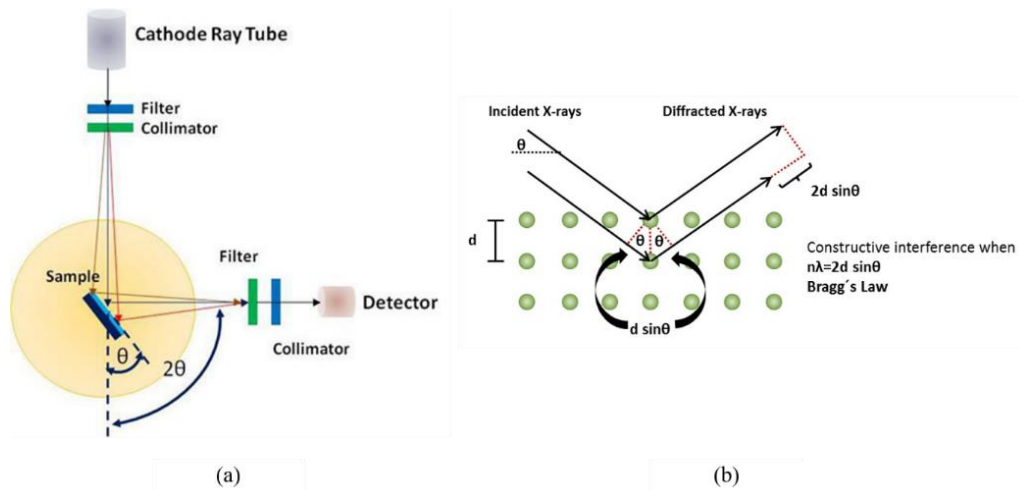


Figure 2.32 Schematic representing (a) diagrams of the basic XRD analysis and (b) the Bragg's law equation [95-96].

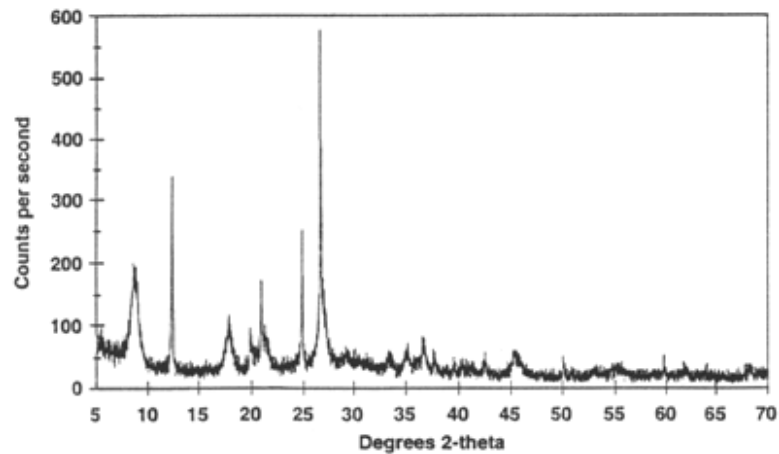


Figure 2.33 The XRD diffractogram of a count rate versus degree 2-theta (2θ) [97].

2.9.6 *In-vitro* cytotoxicity properties

2.9.6.1 Cell proliferation testing

The cytotoxicity and cell proliferation testing are necessary to evaluate the opportunity to utilize biopolymer materials in tissue engineering application. The important factors in cytotoxicity and cell proliferation testing are cells properties, types and concentration of compounds used in the experiment, duration of the testing and the medium or serum used in the cell culture. Three basic concepts used to evaluate cell proliferation or cytotoxicity are measurements of: 1) cell viability, 2) cell survival and 3) cell proliferation from cell metabolism. The methods widely used to measure cell viability are trypan blue exclusion dyes assay, fluorescent based live/dead staining assay, lactate dehydrogenase (LDH) leakage assay and neutral red assay. The clonogenic cell survival assay is the example method to measure cell survival. Cytotoxicity or cell proliferation is evaluated from cell proliferative ability and reproductive ability of clonogenic cell (the cells forming a bulky colony after receiving testing agent). A result is assigned as a curve showing the relation between amount of the agent and the fraction of survival cells (the cells that can retain its ability to procreate new cells). This curve is called cell survival curve [98]. The last concept is measuring cell proliferation by determining cell metabolic activities such as DNA/RNA/protein replication, ATP synthesis and dehydrogenase activity. The example assays of last concept are $^3\text{[H]}$ -thymidine incorporation assays, determining DNA replication assay, ATP assays and tetrazolium reduction assays.

Tetrazolium reduction assays is the method observing dehydrogenase activity during cell proliferation. Tetrazolium salt is used, and it will be transformed to formazan dye under the presence of metabolic active cells. The obtained formazan dye subsequently changes the color of the medium. The absorption of the medium appearing in dye solution can be detected by using microplate reader or spectrophotometer. MTT, MTS, XTT and WST-1 are tetrazolium compounds mostly used to detect a living cell. These compounds are divided into 2 basic types: 1) Positively charged compound such as MTT which is easily to filtrates into viable cells and 2) Negatively charged compounds which are water-soluble tetrazolium salts such as MTS, XTT and WST-1. Negatively charged compounds are not easily to filtrate into the cells. Therefore,

intermediate electron acceptor reagents containing cell penetration ability such as phenazine methyl sulfate (PMS) or phenazine ethyl sulfate (PES) have to be used [99]. The mechanism of the WST-1 reduction is shown in Figure 2.34 [100]. WST-1 can be reduced and changed by NADH or NADPH in the viable cell using mPMS (1-methoxy-5-methyl-phenazinium methyl sulfate) as an intermediate electron acceptor. Then, WST-1 becomes water-soluble colored formazan product which can be detected by microplate reader or spectrophotometer in the suitable wavelength. [99].

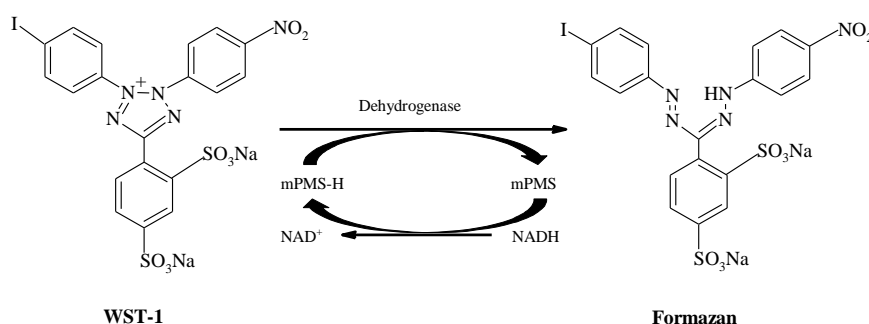


Figure 2.34 Mechanism of the WST-1 reduction in the presence of intermediate electron acceptor (mPMS) [100].

2.9.6.2 Cell cytotoxicity assays

Bone tissue engineering requires substitutable materials which can repair and maintain the function of bone tissue. The porous structure and biocompatibility of the selected materials which mimic the biological environment also play important role in bone tissue engineering [101]. The biocompatibility of materials is associated with cell adhesion and biological environment. Therefore, cytotoxicity testing using osteoblast cell culture to evaluate the biocompatibility of the materials is necessary in bone tissue engineering. Many kinds of osteoblast cells have been reported to use in cytotoxicity testing such as human primary osteoblast (hOB) cells [99], FOST cells [102], human osteoblast cell line (Saos-2) [103] and MG63 osteoblast-like cell [104]. The cell adhesion and cell spreading are firstly created by cell-biomaterial surface touching. Material surface has effect on cell adhesion and cell spreading, and it affects cell proliferation.

Figure 2.35 displays SEM images of osteoblast cell adhesion on different material surfaces. Figure 2.35 (a) [105] shows triangular or elongated shape of osteoblast cells adhering and spreading on the modified zirconia surface after 1 day incubation. Figure 2.35 (b) [102] shows adhesion of FOST cells on titanium anodic films after 4 hr incubation demonstrating cell spreading with irregular direction onto the film surface. Osteoblast cell adhesion on PLA substrate also has been reported by Liu *et al.* [103]. Figure 2.35 (c) shows adhesion of human osteoblast cell line (Saos-2) on the electrospun PLA after cell culture for 5 days. Liu *et al.* [103] found that the cell adhesion and spreading were improved when 15% nHA (nano-hydroxyapatite) was incorporated.

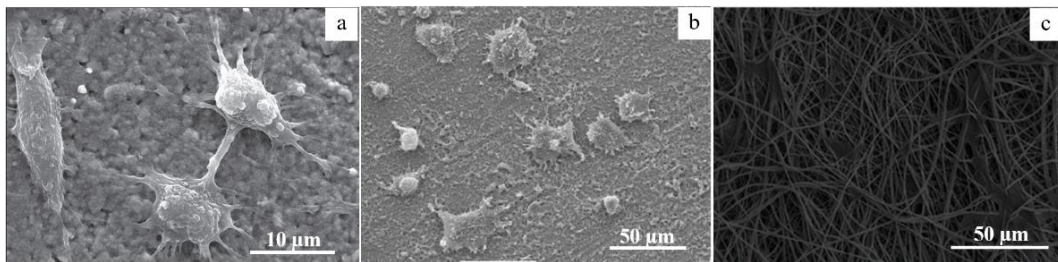


Figure 2.35 SEM images demonstrating various types' cells adhesion on the difference material surfaces: (a) osteoblast cells on surface-modified zirconia, (b) FOST cells on titanium anodic films, and (c) Saos-2 cells on electrospun PLA [102-103, 105].

MG63, osteoblast-like cell used in cytotoxicity testing of this research, also has been used to observe biocompatibility of many kinds of biomaterials for using in tissue engineering such as expanded poly(tetrafluoroethylene) (e-PTFE) membranes, nano-hydroxyapatite/polyamide-66 (nHA/PA-66) membrane [102] and PLA scaffold fabricated by 3D printing method [106]. The examples of MG63 cell adhesion and cell spreading on the material surface are displayed in Figure 2.36 (a)-(c). The MG63 cell exhibited various shape such as long spindle, triangle and square. Figure 2.36 (a) [104] shows MG63 cell with long spindle shape and pseudopods-like spreading on the e-PTFE membrane surface after 1 day incubation. An increase of cell culture time leads to cell growing up and higher cell spreading. Figure 2.36 (b) [104] demonstrates the

SEM image of MG63 cell spreading on nHA/PA66 membrane after 5 days incubation. The MG63 cell was long-spindle shape and it is adhered to the edging of or the middle of the membrane pores with fully pseudopods-like spreading. That demonstrates good biocompatibility of the nHA/PA66 membrane [104]. The MG63 cell adhesion on the smooth surface of 3D printed PLA scaffold after 2 day incubation shows in Figure 2.36 (c) [106]. The cells spread on the scaffold surface with resemble oval shaped to spindle-shaped morphology.

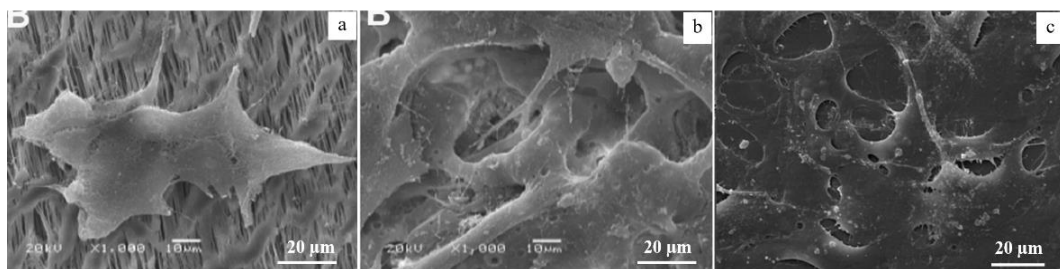


Figure 2.36 SEM images of MG63 osteoblast-like cells adhesion on different material surface and culture time: (a) e-PTFE membrane/1 days, (b) nHA/PA66 membrane/5 days, and (c) 3D printed PLA scaffold/2 days [104, 106].

2.10 References

1. Carvalho, J.L., Carvalho, P.H., Gomes, D.A. and Goes, A.M. 2013. Innovative strategies for tissue engineering. *Advance in biomaterial science and biomedical applications*. <http://dx.doi.org/10.5772/53337>. (accessed 10/8/ 2018).
2. Caruana, A. 2014. Tissue engineering principle. WikiLectures. https://www.wikilectures.eu/w/Tissue_engineering_principle. (accessed 10/8/2018).
3. Kramschuster, A. and Turng, L.-S. 2013. Fabrication of tissue engineering scaffolds. *Handbook of Biopolymers and Biodegradable Plastics*. <http://dx.doi.org/10.1016/B978-1-4557-2834-3.00017-3>. (accessed 10/8/2018).
4. Zhou, H., Lawrence, J. G. and Bhaduri, S. B. 2012 Fabrication aspects of PLA-CaP/PLGA-CaP composites for orthopedic application: A review. *Acta Biomaterialia*. 8: 1999-2016.

5. Dutta, R. C., Dey, M., Dutta, A. K. and Basu, B. 2017 Competent processing techniques for scaffolds in tissue engineering. *Biotechnology Advances*. 35: 240-250.
6. Chan, B. P. and Leong, K. W. 2008 Scaffolding in tissue engineering: General approaches and tissue-specific considerations. *European Spine Journal*. 17: S467-S479.
7. Dhandayuthapani, B., Yoshida, Y., Maekawa, T. and Kumar, D. S. 2011 Polymeric scaffolds in tissue tissue engineering application: A review. *International Journal of Polymer Science*. 1-19.
8. Rezwan, K., Chen, Q. Z., Blaker, J. J. and Boccaccini, A. R. 2006 Biodegradable and bioactive porous polymer/inorganic composite scaffolds for bone tissue engineering. *Biomaterials*. 27: 3413-3431.
9. Balkcom, M., Welt, B. and Berger, K. 2002. Notes from the packaging laboratory: Polylactic acid--An exciting new packaging material. <http://ufdcimages.uflib.ufl.edu/IR/00/00/15/27/00001/AE21000.pdf>. (accessed 11/8/2018).
10. Jacobsen, S. Fritz, H.-G. Degée, P., Dubois, P. and Jérôme, R. 2000 New developments on the ring opening polymerization of polylactide. *Industrial Crops and Products*. 11: 265-275.
11. Lasprilla, A. J. R., Martinez, G. A. R., Lunelli, B. H., Jardini, A. L. and Filho, R. M. 2012 Poly-lactic acid synthesis for application in biomedical devices: A review. *Biotechnology Advances*. 30: 321-328.
12. Gupta, A. P. and Kumar, V. 2007 New emerging trends in synthetic biodegradable polymers – Polylactide: A critique. *European Polymer Journal*. 43: 4053-4074.
13. Vink, E. T. H., Rábago, K. R., Glassner, D. A. and Gruber, P. R. 2003 Application of life cycle assessment to Nature WorksTM polylactide (PLA) production. *Polymer Degradation and Stability*. 80: 403-419.
14. Savioli Lopes, M., Jardini, A. L. and Maciel Filho, R. 2012 Poly(lactic acid) production for tissue engineering applications. *Procedia Engineering*. 42: 1402-1413.
15. Kawamoto, N., Sakai, A., Horikoshi, T., Urushihara, T. and Tobita, E. 2000 Physical and mechanical properties of poly(L-lactic acid) nucleated by

- dibenzoylhydrazide compound. *Journal of Applied Polymer Science*. 103: 244-250.
16. Lee, C. and Hong, S. 2014 An overview of the synthesis and synthetic mechanism of poly(lactic acid). *Modern Chemistry & Application*. 2 (4): 1-5.
 17. Södergård, A. and Stolt, M. 2002 Properties of lactic acid based polymer and their correlation with composition. *Progress in Polymer Science*. 27: 1123-1163.
 18. Kaplan, A.E. 1998. *Biopolymers from Renewable Resources*. Germany: Springer-Verlag Berlin Heidelberg.
 19. Gomes, M. E., Ribeiro, A. S., Malafaya, P. B., Reis, R. L. and Chuha, A. M. 2001 A new approach based on injection moulding to produce biodegradable starch-based polymeric scaffolds: morphology, mechanical and degradation behaviour. *Biomaterials*. 22: 883-889.
 20. Mi, H.-Y., Salick, M. R., Jing, X., Jacques, B. R., Crone, W. C., Peng, X.-F. and Turng, L.-S. 2013 Characterization of thermoplastic polyurethane/ polylactic acid (TPU/PLA) tissue engineering scaffolds fabricated by microcellular injection molding. *Material Science and Engineering C*. 33: 4767-4776.
 21. Abbasi, M., Khorasani, S. N., Bagheri, R. and Esfahani, J. M. 2011 Microcellular foaming of low-density polyethylene using Nano-CaCO₃ as a nucleating agent. *Polymer Composites*. 1718-1725.
 22. Zhai, W., Yu, J., Wu, L., Ma, W. and He, J. 2006 Heterogeneous nucleation uniformizing cell size distribution in microcellular nanocomposites foams. *Polymers*. 47: 7580-7589.
 23. Vázquez, M. O., Ramírez-Arreola, D. E., Bernache, J., Gómez, C., Robledo-Ortiz, J. R., Rodrigue, D. and González-Núñez, R. 2009 Using chitosan as a nucleation agent in thermoplastic foams for heavy metal adsorption. *Mecromolecular Symposia*. 283-284: 152-158.
 24. Ruiz, J. A. R., Vincent, M., Agassant, J.-F., Sadik, T., Pillon, C. and Carrot, C. 2015 Polymer foaming with chemical blowing agents: Experiment and modeling. *Polymer Engineering and Science*. 55: 2018-2029.
 25. Lee, S.-T. and Scholz, D. 2009 *Polymeric foams: Technology and developments in regulation, process, and products*. Taylor & Francis Group, LLC: NW Suite 300 USA.

26. Quinn, S. 2011 Chemical blowing agents: providing production, economic and physical improvements to a wide range of polymers. *Plastics Additives and Compounding*. 16-21.
27. Corre, Y.-M., Maazouz, A., Duchet, J. and Reignier, J. 2011 Batch foaming of chain extended PLA with supercritical CO₂: Influence of the rheological properties and the process parameters on the cellular structure. *Journal of Supercritical Fluids*. 58: 177-188.
28. Ameli, A., Jahani, D., Nofar, M., Jung, P. U. and Park, C. B. 2014 Development of high void fraction polylactide composite foams using injection molding: Mechanical and thermal insulation properties. *Composites Science and Technology*. 90: 88-95.
29. Ding, W., Chang, E., Jahani, D., Alemdar, A., Wang, Q., Park, C. B. and Sain, M. 2016 Development of PLA/cellulosic fibre composites foams using injection molding: Foaming and mechanical properties. *SPE ANTEC™ Indianapolis*. 1783-1787.
30. Matuana, L. M., Faruk, O. and Diaz, C. A. 2009 Cell morphology of extrusion foamed poly(lactic acid) using endothermic chemical foaming agent. *Bioresource Technology*. 100: 5947–5954.
31. Zimmermann, M. V. G., Brambilla, V. C., Brandalise, R. N. and Zattera, A. J. 2013 Observations of the effects of different chemical blowing agents on the degradation of poly(lactic Acid) foams in simulated soil. *Materials Research*. 16 (6): 1266-1273.
32. Luo, Y., Zhang, J., Qi, R., Lu, J., Hu, X. and Jiang, P. 2013 Polylactide foams prepared by a traditional chemical compression molding method. *Journal of Applied Polymer Science*. 330-337.
33. Najafi, N., Heuzey, M.-C., Carreau, P. J., Therriault, D. and Park, C. B. 2015 Mechanical and morphological properties of injection molded linear and branched-polylactide (PLA) nanocomposite foams. *European Polymer Journal*. 73: 455–465.
34. Saranya, S., Vijayanarai, K., Pavithra, S., Raihana, N. and Kumanan, K. 2017 In vitro cytotoxicity of zinc oxide, iron oxide and copper nanopowders prepared by green synthesis. *Toxicology Reports*. 4: 427-430.

35. Kabir, M. M., Wang, H., Lau, K. T. and Cardona, F. 2012 Chemical treatments on plant-based natural fibre reinforced polymer composites: An overview. *Composites Part B*. 43: 2883-2892.
36. Yong, K. C. 2014 Rubber wood fibre based flexible composites: Their preparation, physical strength reinforcing and stab resistance behaviour. *Polymers & Polymer Composites*. 22 (4): 375–380.
37. Kamphunthong, W., Hornsby, P. and Sirisinha, K. 2012 Isolation of cellulose nanofibers from Para rubberwood and their reinforcing effect in poly(vinyl alcohol) composites. *Journal of Applied Polymer Science*. 125: 1642–1651.
38. Alexandrescu, L., Syverud, K., Gatti, A. and Chinga-Carrasco, G. 2013 Cytotoxicity tests of cellulose nanafibril-based structures. *Cellulose*. 20: 1765-1775.
39. Barapatre, A., Meena, A. S., Mekala, S., Das, A. and Jha, H. 2016 In vitro evaluation of antioxidant and cytotoxic activities of lignin fractions extracted from *Acacia nilotica*. *International Journal of Biological Macromolecules*. 86: 443-453.
40. Sykacek, E., Hrabalova, M., Frech, H. and Mundigler, N. 2009 Extrusion of five biopolymers reinforced with increasing wood flour concentration on a production machine, injection moulding and mechanical performance. *Composites Part A*. 40: 1272–1282.
41. Csizmadia, R., Faludi, G., Renner, K., Móczó, J. and Pukánszky, B. 2013 PLA/wood biocomposites: Improving composite strength by chemical treatment of the fibers. *Composites Part A*. 53: 46–53.
42. Faludi, G., Dora, G., Renner, K., Móczó, J. and Pukánszky, B. 2013 Improving interfacial adhesion in pla/wood biocomposites. *Composites Science and Technology*. 89: 77–82.
43. Praprudivongs, C. and Sombatsompop, N. 2012 Roles and evidence of wood flour as antibacterial promoter for triclosal-filled poly(lactic acid). *Composites Part B*. 43: 2730–2737.
44. Woraprayote, W., Kingcha, Y., Amonphanpokin, P., Krueenate, J., Zendo, T., Sonomoto, K., Benjakul, S. and Visessanguan, W. 2013 Anti-listeria activity of poly(lactic acid)/sawdust particle biocomposite film impregnated with pediocin

- PA-1/AcH and its use in raw sliced pork. *International Journal of Food Microbiology*. 167: 229-235.
45. Shaaban, A., Se, S.-M., Ibrahim, I. M. and Ahsan, Q. 2015 Preparation of rubber wood sawdust-based activated carbon and its use as a filler of polyurethane matrix composites for microwave absorption. *New Carbon Materials*. 30 (2): 167-175.
 46. Petchwattana, N. and Covavisaruch, S. 2014 Mechanical and morphological properties of wood plastic biocomposites prepared from toughened poly(lactic acid) and rubber wood sawdust (*Hevea brasiliensis*). *Journal of Bionic Engineering*. 11: 630-637.
 47. Rinaudo, M. 2006 Chitin and chitosan: Properties and applications. *Progress in Polymer Science*. 31: 603-632.
 48. Kumirska, J., Weinhold, M. X., Thöming, J. and Stepnowski, P. 2011 Biomedical activity of chitin/chitosan based materials-Influence of physicochemical properties apart from molecular weight and degree of N-acetylation. *Polymers*. 3: 1875-1901.
 49. Hamed, I., Özogul, F. and Regenstein, J. M. 2016 Industrial applications of crustacean by products (chitin, chitosan, and chitooligosaccharides): A review. *Trend in Food Science & Technology*. 48: 40-50.
 50. Tanase, C. E. and Spiridon, I. 2014 PLA/chitosan/keratin composites for biomedical applications. *Materials Science and Engineering C*. 40: 242-247.
 51. Xu, J., Zhang, J., Gao, W., Liang, H., Wang, H. and Li, J., 2009 Preparation of chitosan/PLA blend micro/nanofibers by electrospinning. *Materials Letters*. 63: 658-660.
 52. Nanda, R., Sasmal, A. and Nayak, P. L. 2011 Preparation and characterization of chitosan–polylactide composites blended with Cloisite 30B for control release of the anticancer drug paclitaxel. *Carbohydrate Polymers*. 83: 988-994.
 53. Grande, R., Pessan, L. A. and Carvalho, A. J. F. 2015 Ternary melt blends of poly(lactic acid)/poly(vinyl alcohol)-chitosan. *Industrial Crops and Products*. 72: 159-165.

54. Bonilla, J., Fortunati, E., Vargas, M., Chiralt, A. and Kenny, J. M. 2013 Effects of chitosan on the physicochemical and antimicrobial properties of PLA films. *Journal of Food Engineering*. 119: 236-243.
55. Râpă, M., Mitelut, A. C., Tănase, E. E., Grosu, E., Popescu, P., Popa, M. E., Rosnes, J. T., Sivertsvik, M., Darie-Nită, R. N. and Vasile, C. 2016 Influence of chitosan on mechanical, thermal, barrier and antimicrobial properties of PLA-biocomposites for food packaging. *Composites Part B*. 102: 112-121.
56. Niu, X., Feng, Q., Wang, M., Guo, X. and Zheng, Q. 2009 In vitro degradation and release behavior of porous poly(lactic acid) scaffolds containing chitosan microspheres as a carrier for BMP-2-derived synthetic peptide. *Polymer Degradation and Stability*. 94: 176-182.
57. Niu, X., Li, X., Liu, H., Zhou, G., Feng, Q., Cui, F. and Fan, Y. 2012 Homogeneous chitosan/poly(L-lactide) composite scaffolds prepared by emulsion freeze-drying. *Journal of Biomaterials Science*. 23: 391-404.
58. Zhu, C., Ma, X., Xian, L., Zhou, Y. and Fan, D. 2014 Characterization of a co-electrospun scaffold of HLC/CS/PLA for vascular tissue engineering. *Bio-Medical Materials and Engineering*. 24: 1999-2005.
59. Herzberger, J., Niederer, K., Pohlit, H., Seiwert, J., Worm, M., Wurm, F. R. and Frey, H. 2016 Polymerization of ethylene oxide, propylene oxide, and other alkylene oxides: Synthesis, novel polymer architectures, and bioconjugation. *Chemical Reviews*. 116: 2170-2243.
60. Toncheva, A., Mincheva, R., Kancheva, M., Manolova, N., Rashkov, I., Dubois, P. and Markova, N. 2016 Antibacterial PLA/PEG electrospun fibers: Comparative study between grafting and blending PEG. *European Polymer Journal*. 75: 223-233.
61. Pillin, I., Montrelay, N. and Grohens, Y. 2006 Thermo-mechanical characterization of plasticized PLA: Is the miscibility the only significant factor?. *Polymer*. 47: 4676-4682.
62. Martin, O. and Avèrous, L. 2001 Poly(lactic acid): plasticization and properties of biodegradable multiphase systems. *Polymer*. 42: 6209-6219.
63. Zhang, W., Chen, B., Zhao, H., Yu, P., Fu, D., Wen, J. and Peng, X. 2013 Processing and characterization of supercritical CO₂ batch foamed poly(lactic

- acid)/poly(ethylene glycol) scaffold for tissue engineering application. *Journal of Applied Polymer Science*. 3066-3073.
64. Reyes-Labrata, J. A. and Marcilla, A. 2008 Kinetic study of the decomposition involved in the thermal degradation of commercial azodicarbonamide. *Journal of Applied Polymer Science*. 107: 339-346.
 65. Sunny, M. C., Vincy, P. V., Anil Kumar, P. R. and Ramesh, P. 2011 Porous composites of hydroxyapatite-filled poly[ethylene-co-(vinyl acetate)] for tissue engineering en synthesis. *Polymer International*. 60: 51-58.
 66. Sungkhsee, N. 2009. Overcoming PLA limitations by compounding with modified additive. Master of Science Thesis. The Petroleum and Petrochemical College, Chulalongkorn University, Bangkok, Thailand.
 67. Lv, S., Tan, H., Gu, J. and Zhang, Y. 2015 Silane modified wood flour blended with poly (lactic acid) and its effects on composite performance. *BioResources*. 10 (3): 5426-5439.
 68. Lyu, S. and Untereker, D. 2009 Degradability of polymers for implantable biomedical devices. *International Journal of Molecular Sciences*.10: 4033-4065.
 69. Tamariz, E. and Rois-Ramírez, A. 2013. Biodegradation of medical purpose polymeric materials and their impact on biocompatibility. *Biodegradation- Life of Science*. <http://dx.doi.org/10.5772/56220>. (accessed 21/11/2018).
 70. Elsayy, M. A., Kim, K.-H., Park, J.-W. and Deep, A. 2017 Hydrolytic degradation of polylactic acid (PLA) and its composites. *Renewable and Sustainable Energy Reviews*. 79: 1346-1352.
 71. Azevedo, H. and Reis, R.L. 2004. Understanding the enzymatic degradation of biodegradable polymers and strategies to control their degradation rate. *Biodegradable Systems in Tissue Engineering and Regenerative Medicine*. 177-201. <https://core.ac.uk/download/pdf/55614175.pdf> (accessed 21/11/ 2018).
 72. Li, L., Ding, S. and Zhou, C. 2004 Preparation and degradation of PLA/chitosan composite materials. *Journal of Applied Polymer Science*. 91: 274–277.
 73. Szymańska, E. and Winnicka, K. 2015 Stability of chitosan-A challenge for pharmaceutical and biomedical applications. *Marine Drugs*. 13: 1819-1846.

74. Ulbricht, J., Jordan, R. and Luxenhofer, R. 2014 On the biodegradability of polyethylene glycol, polypeptoids and poly (2-oxazoline)s. *Biomaterials*. 35: 4848-4861.
75. MatWeb materials properties data. 2018. Izod impact strength testing of Plastics. <http://www.matweb.com/reference/izod-impact.aspx>. (accessed 25/07/2018).
76. Sanjay, M. R., Arpitha, G. R., Laxmana Naik, L. L., Gopalakrishna, K. and Yogesha, B. 2016 Studies on mechanical properties of banana/e-glass fabrics reinforced polyester hybrid composites. *Journal of Material and Environment Science*. 7 (9): 3179-3192.
77. Pham, T.M. and Hao, H. 2016. Review of concrete structures strengthened with FRP against impact loading. <https://www.researchgate.net/publication/302630760>. (accessed 25/7/2018).
78. Mitsui Chemical Analysis & Consulting Service, INC. 2002. Charpy and Izod impact tests. <https://www.mcanac.co.jp/en/service/detail/6a002.html?c1n=by+Analytical+Instrument&c1s=machine&c2n=Mechanical+Properties+Test&c2s=10>. (accessed 25/07/2018).
79. Udomphol, T. 2005. Laboratory 3 tensile testing. Mechanical metallurgy laboratory 431303. https://www.academia.edu/26337396/Laboratory_3_Tensile_testing_Mechanical_metallurgy_laboratory_431303_1. (accessed 25/07/2018).
80. Lim, H. and Hoag, S. W. 2013 Plasticizer effects on physical–mechanical properties of solvent cast Soluplus[®] films. *AAPS PharmSciTech*. 14 (3): 903-911.
81. Tony, F. Background information. Operating instructions. Instron 5582 universal tester. faculty.olin.edu/Instron%20Universal%20Tester%20Operating%20Instructions.pdf. (accessed 25/07/2018).
82. Instrons[®]. 2018. ISO 178 flexure testing of plastics. <http://www.instron.us/en-us/testing-solutions/by-test-type/flexure/iso-178>. (accessed 31/7/2018).
83. ASTM international. 2002. ASTM D790-02. Standard test methods for flexural properties of unreinforced and reinforced plastics and electrical insulating materials. *Annual Book of ASTM Standards*. 146-154.

84. Khurana, D. and Agarwal, A.-K. 2011 Oxidation stability, engine performance and emissions investigations of Karanja, Neem and Jatropha biodiesel and blends. Article in SAE International Journal of Fuels and Lubricants. 1-10.
85. Bhadeshi, H.K.D.H. 2002. Differential scanning calorimetry: Introduction. <https://www.phase-trans.msm.cam.ac.uk/2002/Thermal2.pdf>. (accessed 1/8/2018).
86. Parlouër, P. L. 2013. Thermal analysis and calorimetry techniques for catalytic investigations. *Calorimetry and Thermal Methods in Catalysis*. Springer Series in Materials Science. 154: 51-101.
87. Dean, D. 2014. Differential scanning calorimetry. University of Alabama at Birmingham. https://www.uab.edu/engineering/home/images/downloads/DSC_UAB_TA_May_2014_Compatibility_Mode.pdf. (accessed 1/8/2018).
88. Mettler-Teledo. 2016. Dynamic mechanical analysis. Comprehensive materials characterization. https://www.mt.com/dam/Analytical/ThermalAnalysis/TA-PDF/DMA1_Brochure_en_30129289A_V02.16.pdf. (accessed 5/8/2018).
89. Hamerton, I., Tang, W., Anguita, J. V. and Silva, R. P. 2014 Towards the rational design of polymers using molecular simulation: Predicting the effect of cure schedule on thermo-mechanical properties for a cycloaliphatic amine-cured epoxy resin. *Reactive & Functional Polymers*. 74: 1-15.
90. Varun, L. 2013. What is thermogravimetric analysis. The savant club. <https://lalithvarun.blogspot.com/2013/02/what-is-thermogravimetric-analysis.html>. (accessed 2/8/2018).
91. Seguni, G., Gimmara, T. J., Lupi, F. F., Sparnacci, K., Antonioil, D., Gianotti, V., Vita, F., Placentino, I. F., Hilhorst, J, Ferrero, C., Francescangeli, O., Laus, M. and Perego, M. 2014 Thermally induced self-assembly of cylindrical nanodomains in low molecular weight PS-b-PMMA thin films. *Nanotechnology*. 25: 1-8.
92. Shadid, K.A. 2016. Infrared spectroscopy theory and interpretation of IR spectra – ppt video online download. <https://slideplayer.com/slide/8335494/> (accessed 4/8/2018).

93. Thermo Nicolet. 2001. Introduction to Fourier transformation infrared spectroscopy. <http://jimlund.org/blog/pics/IR200/FTIRintro.pdf> (accessed 4/8/2018).
94. Bradbury, S., Joy, D.C. and Ford, B.J., 2018. Scanning electron microscope. <https://www.britannica.com/technology/scanning-electron-microscope>. (accessed 1/8/2018).
95. Failure analysis and technologies private limited. 2015. XRD (X-ray Powder Diffraction). <https://www.indiamart.com/proddetail/xrd-x-ray-powder-diffrac-tion-16339163130.html>. (accessed 5/8/2018).
96. Anton Paar Wiki. 2018. X-Ray diffraction (XRD). https://wiki.anton-paar.com/fileadmin/wiki/images/X-ray_Diffraction/Schematic-representation-of-the-Bragg-equation.jpg. (accessed 5/8/2018).
97. Dutrow, B.L. and Clark, C.M. 2018. X-Ray powder diffraction (XRD). Geochemical instrumentation and analysis. https://serc.carleton.edu/research_education/geochemsheets/techniques/XRD.html. (accessed 5/8/2018).
98. Munshi, A., Hobbs, M. and Meyn, R.E. 2005 Clonogenic cell survival assay. In: Methods in molecular medicine. Chemosensitivity. Humana Press Inc., Totowa, NJ.
99. Riss, T.L., Moravec, R.A., Niles, A.L., Duellman, S., Benink, H.A., Worzella, T.J. and Minor, L. 2016 Cell viability assays. In: Assay guidance manual. Bethesda (MD): Eli Lilly & Company and the National Center for Advancing Translational Sciences.
100. Yin, L.-M., Wei, Y., Wang, Y., Xu, Y.-D. and Yang, Y.-Q. 2013 Long term and standard incubations of WST-1 reagent reflect the same inhibitory trend of cell viability in rat airway smooth muscle cells. International Journal of Medical Sciences. 10 (1): 68-72.
101. Balu, R., Kumar, T. S. S., Ramalingam, M. and Ramakrishna, S. 2011 Electrospun polycaprolactone/poly(1,4-butylene adipate-co-polycaprolactam) blends: Potential biodegradable scaffold for bone tissue regeneration. Journal of Biomaterials and Tissue Engineering. 1: 30-39.

102. Campos, D. M., Santos Jr., E., Kuromoto, N. K. and Soares, G. A. 2007 Preliminary results of osteoblast adhesion on titanium anodic films. *Revista Matéria*. 12 (1): 150-155.
103. Liu, C., Wong, H. M., Yeung, K. W. K. and Tjong, S. C. 2016 Novel electrospun polylactic acid nanocomposite fiber mats with hybrid graphene oxide and nanohydroxyapatite reinforcements having enhanced biocompatibility. *Polymer*. 8: 287-305.
104. Ye, J., Yao, Q., Mo, A., Nie, J., Liu, W., Ye, C. and Chen, X. 2011 Effect of an antibacterial membrane on osteoblast-like cells in vitro. *International Journal of Nanomedicine*. 6: 1853-1861.
105. Pae, A., Lee, H., Noh, K. and Woo, Y.-H. 2014 Cell attachment and proliferation of bone marrow-derived osteoblast on zirconia of various surface treatment. *Journal of Advance Prosthodont*. 6: 96-102.
106. Gregor, A., Filová, E., Novák, M., Kronek, J., Chlup, H., Buzgo, M., Blahnová, V., Lukášová, V., Bartoš, M., Nečas, A. and Hošek, J. 2017 Designing of PLA scaffolds for bone tissue replacement fabricated by ordinary commercial 3D printer. *Journal of Biological Engineering*. 11-33.

CHAPTER 3

MATERIALS AND METHODOLOGY

3.1 Materials

3.1.1 Materials for surface treatment of rubber wood sawdust

The materials used in this topic are listed in Table 3.1

Table 3.1 Materials used for surface treatment of rubber wood sawdust

Material name	Initials	Formula	Producer/Supplier
Rubber wood sawdust (size: $\leq 75 \mu\text{m}$ and $212\text{-}600 \mu\text{m}$)	RWS	-	Khaomahachai Parawood Co, Ltd., Thailand.
3-glycidoxypropyl trimethoxy silane	GPMS	$\text{C}_9\text{H}_{20}\text{O}_5\text{Si}$	Sigma-Aldrich Co., Ltd, Thailand.
3-aminopropyl trimethoxy silane	APMS	$\text{C}_6\text{H}_{17}\text{NO}_3\text{Si}$	Sigma-Aldrich Co., Ltd, Thailand.
Acetic acid	-	CH_3COOH	Sigma-Aldrich Co., Ltd, Thailand.
Ethanol	-	$\text{CH}_3\text{CH}_2\text{OH}$	RCI Labscan Asia Co., Ltd, Thailand.
Sodium hydroxide	-	NaOH	RCI Labscan Asia Co., Ltd, Thailand.

3.1.2 Materials for preparation of unfoamed and foamed PLA compounds

The materials used in this topic are listed in Table 3.2

Table 3.2 Materials used for preparation of unfoamed and foamed PLA compounds

Materials name	Initials	Formula	Producer/Supplier
Poly(lactic acid), 4042D	PLA	$\text{H}(\text{CO}_2\text{CH}_3)_n\text{OH}$	NatureWorks LLC. USA.
Rubber wood sawdust	RWS	-	Khaomahachai Para wood Co, Ltd., Thailand.
Chitosan	CH	-	Thai Food and Chemical Co., Ltd, Thailand.

Table 3.2 Materials used for preparation of unfoamed and foamed PLA compounds
(continued)

Material name	Initials	Formula	Producer/Supplier
Polyethylene glycol (Molecular weight 6000 g/mol)	PEG	$H(OCH_2CH_2)_n$ OH	Sigma-Aldrich Co., Ltd, Thailand.
Azodicarbonamide	AZDC	$C_2H_4O_2 N_4$	Greatchem and Supply Pty., Ltd., China.
Zine Oxide	ZnO	ZnO	Kit Phaibun Chemistry Ltd., Thailand.

3.1.3 Materials for *in-vitro* degradation and cytotoxicity characterization of foam samples

The materials used in this topic are listed in Table 3.3

Table 3.3 Materials used for *in-vitro* degradation and cytotoxicity characterization of foam samples

Material name	Initials	Formula	Producer/Supplier
Alpha-Minimum essential medium	α -MEM medium	-	Gibco™, Invitrogen, Carlsbad, CA, USA.
Di-sodium hydrogen phosphate dehydrate	-	$Na_2HPO_4 \cdot 2H_2O$	RCI Labscan Asia Co., Ltd, Thailand.
Lysozyme enzyme	-	-	Sigma-Aldrich Co., Ltd, Thailand.
MG-63 cell line human	MG63	-	Sigma-Aldrich Co., Ltd, Thailand.
Sodium hydrogen phosphate dehydrate	-	$NaH_2PO_4 \cdot 2H_2O$	RCI Labscan Asia Co., Ltd, Thailand.
Penicillin-streptomycin	-	-	Sigma-Aldrich Co., Ltd, Thailand.
Fungizone	-	-	Sigma-Aldrich Co., Ltd, Thailand.

Table 3.3 Materials used for *in-vitro* degradation and cytotoxicity characterization of foam samples (continued)

Material name	Initials	Formula	Producer/Supplier
Fetal bovine serum	-	-	Gibco™, Invitrogen, Carlsbad, CA, USA.
Osteogenic medium	OS	-	Sigma-Aldrich Co., Ltd, Thailand.

3.2 Instruments

The instruments used in this works are listed in Table 3.4

Table 3.4 Instruments

Instruments	Model	Country
Analytical balance	METTLER Toledo® ML204/01	Switzerland
Dynamic mechanical thermal analyzer (DMTA)	METTLER Toledo® STARe system DMA1 Module.	Switzerland
Differential scanning calorimeter (DSC)	NETZSCH® DSC 200 F3	USA
Evaporator	BUCHI® Rotavapor	Switzerland
Fourier transform infrared spectrometer (FTIR)	BRUKER® TENSOR 27 spectrophotometer	Germany
High speed grinder	NanoTech® NT-500D	Thailand
Hot air oven	UM 400, MEMMERT Co., Ltd.	Germany
Impact testing machine	ZWICK® 5102.202	USA
Simultaneous thermal analyzer (STA)	NETZSCH® STA 449 F3-Jupiter	Germany
Scanning electron microscope (SEM)	Quanta 400® FEI, JEOL	Japan
Twin screw extruder (L:D ratio of 15:1)	PRISM® TSE16TC	USA
Universal testing machine	(1) INSTRON® 5569	USA
	(2) INSTRON® 3365	USA

Table 3.4 Instruments (continued)

Instruments	Model	Country
Vacuum Oven	Thermo Fisher [®] Model 29	China
X-ray diffractometer (XRD)	X' Pert MPD [®] PHILIPS	Netherlands

3.3 Methodology

3.3.1 Preparation of various sizes of rubber wood sawdust

Rubber wood sawdust (RWS) obtained from Khaomahachai Parawood Co, Ltd. were dried in a hot air oven at 105 °C for 24 h to remove moisture before separating into four range of RWS particle sizes using a series of sieves. The RWS particle sizes of $\leq 212 \mu\text{m}$ and 212-600 μm were directly obtained from sieving (mesh no. 70 and 30). The particle sizes of $\leq 75 \mu\text{m}$ and 75-150 μm were obtained by two steps, grinding using high speed grinder followed by sieving (mesh no. 200 and 100). All four ranges of RWS particles were used to prepare unfoamed PLA/RWS compounds. The particle sizes of $\leq 75 \mu\text{m}$ and 212-600 μm were used for surface treatment and for preparing foamed PLA/RWS compounds.

3.3.2 Alkaline treatment of rubber wood sawdust (NaOH-treated RWS)

The alkaline treatment was applied to RWS by using 5% (w/v) NaOH solution [1]. The first step was the addition of RWS in NaOH solution under continuous stirring for 1 h at room temperature and then washed with water until the pH was neutral. The second step, RWS was dried by using an evaporator at 80 °C for 1 h followed by using a vacuum oven at 70 °C for 15 h. The final step was done by drying in a hot air oven at 70 °C until the constant weight was reached. The obtained RWS were called NaOH-treated RWS 75 and NaOH-treated RWS 212-600, respectively.

3.3.3 Silane treatment of rubber wood sawdust

The silane treatment was carried out using 3 methods: A, B and C. The preparation conditions are displayed in Table 3.5.

Table 3.5 Surface treatment conditions of RWS in the method A-C

Sample	Method	NaOH treatment	Silane content (%)	RWS size (μm)	pH solution = 5	Bath temp. ($^{\circ}\text{C}$)
GPMS-A	A	✓	1, 3, 5 0.5, 1, 3, 5	≤ 75 212-600	✓	70
APMS-A	A	✓	1, 5	212-600	✓	70
APMS-WA	A	✓	5	212-600	x	70
GPMS-B	B	x	5 1, 3, 5	≤ 75 212-600	x	70
GPMS-C	C	x	5	≤ 75	✓	70

Footnotes: *The silane content unit was wt% of RWS.

3.3.3.1 Method A

GPMS was applied to the NaOH-treated RWS. Firstly, GPMS was hydrolyzed in 60% (v/v) ethanol solution under continuous stirring for 1 h at room temperature and, then, the solution was adjusted to pH 5 with acetic acid. Secondly, the NaOH-treated RWS (7.5 % w/v of ethanol solution) was added in the hydrolyzed GPMS solution with continuous stirring followed by heating up to 70 $^{\circ}\text{C}$. After the solution temperature reached to 70 $^{\circ}\text{C}$, the solution was then continuously stirred for 1 h. The obtained product (GPMS-A) was washed with water until pH was neutral and dried. The smaller particle size ($\leq 75 \mu\text{m}$) was dried by using an evaporator at 70 $^{\circ}\text{C}$ for 1 h and the larger particle (212-600 μm) was dried by using a vacuum filter at room temperature. Finally, GPMS-A was dried at 105 $^{\circ}\text{C}$ for 2 h in a vacuum oven and, then, drying in an oven at 70 $^{\circ}\text{C}$ until the constant weight was obtained [1].

APMS was applied to the NaOH-treated RWS by using a similar procedure to GPMS treatment as described above. The larger particle RWS (212-600 μm) was used. The obtained product was referred to APMS-A. There was another condition for APMS treatment which was the method A without pH adjusting of the hydrolyzed APMS with acetic acid in the first step. This condition was used to determine effect of pH. The obtained product was referred to APMS-WA.

3.3.3.2 Method B

This method was similar to method A, except the virgin RWS (non-treated RWS) was used and the hydrolyzed GPMS solution was not adjusted to pH 5 with acetic acid.

3.3.3.3 Method C

The procedure of method C was done similar to method A, except the virgin RWS (non-treated RWS) was used.

The treated-RWS obtained from silane treatment were named as “a%B-X xxx”, where “a” was silane content (%), B was silane type, “X” was a treatment method and “xxx” was RWS particle size, respectively. For example, “1%GPMS-A 75” was the NaOH-treated RWS with RWS particle size of $\leq 75 \mu\text{m}$ treated with 1%GPMS using method A, and “5%APMS-WA 212-600” was the NaOH-treated RWS with RWS particle size of 212-600 μm treated with 5%APMS using method A without pH adjusting.

3.3.4 Preparation of unfoamed PLA/RWS compounds

The RWS with various particle size ($\leq 75 \mu\text{m}$, 75-150 μm , $\leq 212 \mu\text{m}$ and 212-600 μm) were prepared as mentioned in topic 3.3.1. The compositions of unfoamed PLA/RWS compounds are listed in Table 3.6 and Table 3.7. PLA pellets and RWS were dried at 105°C in a hot air oven over night to remove moisture then kept in desiccator. Because of a short length of the screws of the twin screw extruder, PLA pellets and RWS were blended in a twin screw extruder for two times to obtain homogeneous blending. The first extrusion was performed at a temperature profile of 120, 165 and 165 °C for a feed, middle and die zone, respectively. The screw speed was 100 rpm. The extrudates were pelletized and extruded again at the same temperature and the screw speed was 150 rpm. After that, extrudates were pelletized to obtain the compounded pellets.

Table 3.6 Composition of unfoamed PLA/nontreated-RWS compounds

Composition No.	1	2	3	4	5	6	7	8	9	10	11	12
PLA	95	95	95	95	90	90	90	90	85	85	85	85
RWS (212-600 μm)	5	-	-	-	10	-	-	-	15	-	-	-
RWS (≤ 212 μm)	-	5	-	-	-	10	-	-	-	15	-	-
RWS (75-150 μm)	-	-	5	-	-	-	10	-	-	-	15	-
RWS (≤ 75 μm)	-	-	-	5	-	-	-	10	-	-	-	15

Footnotes: PLA and RWS contents were used in wt% unit.

Table 3.7 Composition of unfoamed PLA/treated-RWS compounds

Composition No.	1	2	3	4	5	6	7	8	9	10	11	12	13	14	15	16	17
RWS size	≤ 75 μm								212-600 μm								
PLA	95	95	95	95	95	95	95	95	95	95	95	95	95	95	95	95	95
NaOH-treated	5	-	-	-	-	-	-	-	5	-	-	-	-	-	-	-	-
0.5% GPMS-A	-	-	-	-	-	-	-	-	-	5	-	-	-	-	-	-	-
1% GPMS-A	-	5	-	-	-	-	-	-	-	-	5	-	-	-	-	-	-
3% GPMS-A	-	-	5	-	-	-	-	-	-	-	-	5	-	-	-	-	-
5% GPMS-A	-	-	-	5	-	-	-	-	-	-	-	-	5	-	-	-	-
1% APMS-A	-	-	-	-	5	-	-	-	-	-	-	-	-	5	-	-	-
1% GPMS-B	-	-	-	-	-	5	-	-	-	-	-	-	-	-	5	-	-
3% GPMS-B	-	-	-	-	-	-	5	-	-	-	-	-	-	-	-	5	-
5% GPMS-B	-	-	-	-	-	-	-	5	-	-	-	-	-	-	-	-	5

Footnotes: PLA and RWS contents were used in wt% unit.

3.3.5 Preparation of unfoamed PLA/PEG/chitosan compounds

The compositions of unfoamed PLA/PEG/chitosan (CH) compounds are listed in Table 3.8. PLA pellets and chitosan were dried at 105°C and 50°C, respectively, over night in a hot air oven to remove moisture then kept in a desiccator. PLA/PEG/CH compounds were prepared by using a twin screw extruder. The first extrusion was carried out at a temperature profile of 140, 165 and 165 °C for a feed, middle and die zone, respectively and the screw speed was 80 rpm. Then, the extrudates were pelletized and extruded again at a temperature of 130, 150 and 150 °C for a feed, middle and die zone, respectively, and the screw speed was 150 rpm.

Table 3.8 Composition of unfoamed PLA/PEG/CH compounds

Sample name	Contents (wt%)		
	PLA	PEG	Chitosan
PLA	100.0	0.0	0.0
PLA-CH1	100.0	0.0	1.0
PLA-CH3	100.0	0.0	3.0
PLA-PEG-CH0	95.0	5.0	0.0
PLA-PEG-CH1	94.1	4.9	1.0
PLA-PEG-CH3	92.2	4.8	3.0
PLA-PEG-CH5	90.3	4.7	5.0

3.3.6 Preparation of PLA compounded foams

The first extrusion was performed without AZDC and ZnO at a temperature profile of 140, 165 and 165°C for a feed, middle and die zone, respectively. The screw speed was 100 rpm. The extrudates were then pelletized and melt blended again with AZDC and ZnO at a lower temperature profile (130, 150 and 150°C for a feed, middle and die zone, respectively) to avoid AZDC decomposition in the extruder. The higher screw speed of 150 rpm was used in order to reduce residence time in the extruder. AZDC and ZnO were used as chemical blowing agent and accelerator, respectively. The compositions for foam preparation are listed in Table 3.9. The content of PLA compounded pellets obtained from the first extrusion was 98 wt% and the content of the compound of AZDC and ZnO was 2 wt%. The AZDC/ZnO weight ratios

were varied to prepare PLA foams (foam no. 1-5). The RWS type and RWS particle size used to prepare the PLA/RWS foams (foam no. 6-9) were different depending on the foam name, and the RWS added in PLA/RWS/chitosan foams (foam no. 15-16) was the 1%GPMS-A 212-600 RWS.

3.3.7 Preparation of sample sheet by compression molding

3.3.7.1 Preparation of unfoamed sheet

A 2 mm-thick sheet of unfoamed sample was obtained by compression molding at 150°C. The compounded pellets were pre-heated at a pressure of 100 kg/cm² for 5 min and then heated at a pressure of 150 kg/cm² for 12 min. After that, the sample was cooled under this pressure for 10 min. The unfoamed PLA/nontreated-RWS compounds were prepared in order to determine the effect of RWS particle size and RWS content by considering the mechanical properties of the molded samples. The appropriate compositions were used to prepare the unfoamed PLA/treated-RWS compounds which were blended in the twin screw extruder as described above.

3.3.7.2 Preparation of foamed sheet

The compression molding was carried out in a close mold to obtain a foamed sheet. Three mold dimension were used: (1) 130 x 130 x 2 mm, (2) 100 x 100 x 25.4 mm and (3) 130 x 130 x 3 mm by using the compounded pellet contents of 40 g, 190 g and 80 g, respectively. The mold dimension 130 x 130 x 2 mm was finally used to prepare all foam samples. The foam no. 1 and 3-5 (Table 3.9) were performed at 150 °C for 10 min under the pressure of 150 kg/cm². The foam no. 2 and 6-16 were performed at 145 °C under similar compression pressure and time. The foam sample, foam name, the composition of the first extrudates, AZDC and ZnO content (wt%) and AZDC/ZnO weight ratios are listed in Table 3.9. The foam no. 1 and 3-5 were prepared in order to study influence of AZDC/ZnO weight ratios. The foam no. 2 and 6-9 were designed to study influence of RWS particle size and RWS surface treatment on the properties of the foams including pore morphology, mechanical and thermal properties, *in-vitro* degradation and cytotoxicity. The foam no. 10-16 were prepared to study influence of chitosan and/or PEG and treated-RWS on the characteristic of the foams.

Table 3.9 Composition for preparation of PLA compounded foams

No.	Foam sample	Foam name	The PLA compounded pellet content (wt%)				AZDC (wt%)	ZnO (wt%)	AZDC/ZnO ratios (wt/wt)
			PLA	PEG	CH	RWS			
1	PLA0	PLA 3/0.0	100.0	-	-	-	2.00	0.00	3/0.0
2	PLA0.1	PLA 3/0.1	100.0	-	-	-	1.94	0.06	3/0.1
3	PLA0.3	PLA 3/0.3	100.0	-	-	-	1.82	0.18	3/0.3
4	PLA0.5	PLA 3/0.5	100.0	-	-	-	1.71	0.29	3/0.5
5	PLA1.0	PLA 3/1.0	100.0	-	-	-	1.50	0.50	3/1.0
6	T1S	PLA/NaOH 75	95.0	-	-	5.0 ^a	1.94	0.06	3/0.1
7	T2S	PLA/1%GPMS-A 75	95.0	-	-	5.0 ^a	1.94	0.06	3/0.1
8	T0L	PLA/RWS 212-600	95.0	-	-	5.0 ^a	1.94	0.06	3/0.1
9	T2L	PLA/1%GPMS-A 212-600	95.0	-	-	5.0 ^a	1.94	0.06	3/0.1
10	1C0P	PLA-CH1	99.0	-	1.0	-	1.94	0.06	3/0.1
11	3C0P	PLA-CH3	97.0	-	3.0	-	1.94	0.06	3/0.1
12	0C5P	PLA-PEG	95.0	5.0	-	-	1.94	0.06	3/0.1
13	1C5P	PLA-PEG-CH1	94.1	4.9	1.0	-	1.94	0.06	3/0.1
14	3C5P	PLA-PEG-CH3	92.2	4.8	3.0	-	1.94	0.06	3/0.1
15	1C0PR1	PLA-CH1-R1	98.0	-	1.0	1.0 ^b	1.94	0.06	3/0.1
16	1C0PR3	PLA-CH1-R3	96.1	-	0.9	3.0 ^b	1.94	0.06	3/0.1

Footnotes: 1. ^a The RWS type and RWS size were different depending on the foam name.

2. ^b The RWS type was 1%GPMS-A 212-600.

3.3.8 Characterizations

3.3.8.1 Fourier transforms infrared spectroscopy (FTIR)

The chemical structures of treated and untreated RWS were analyzed by using FTIR spectroscopy in attenuated total reflectance (ATR) mode. The RWS was pressed under the pressure of 25 bar to form a disc. The specimens were scanned in the frequency range of 4000 to 400 cm^{-1} with a resolution of 4 cm^{-1} by 132 scan.

3.3.8.2 X-Ray diffraction spectroscopy (XRD)

Crystallinity of treated and untreated RWS was determined using X-ray diffractometer. The specimens were scanned at a speed of 1 sec per step over a 2θ ranging from 3.5 to 63.5°. A generator voltage of 40 kV and a current of 30 mA were applied. The amorphous contribution in the RWS was subtracted from XRD pattern. The crystallinity Index (I_c) was calculated from the equation (1) [2], where $I_{(002)}$ was the peak intensity at 2θ equal to 22.72° and attributed to a specific characteristic of crystalline cellulose and $I_{(am)}$ was the intensity at 2θ equal to 18.01°, which corresponding to the amorphous portion of the cellulose material:

$$I_c = \frac{(I_{(002)} - I_{(am)})}{I_{(002)}} \times 100 \quad (1).$$

3.3.8.3 Surface morphology

The surface morphology of treated and untreated RWS were investigated using SEM at the voltage of 20 kV and magnification of 175X and 1000X. The RWS were mounted on a stub before sputter coating with gold.

3.3.9 Physical and mechanical properties

3.3.9.1 Density and void fraction (VF)

Foam density was measured by the buoyancy method according to ASTM D792. The foamed sheets were cut into square shape with the width and length of 25 mm x 25 mm and specimen thickness was 2.5-3.0 mm depending on the thickness

of the foamed sheet. The specimens were precisely weighed on an analytical balance in air and in n-hexane with density of 0.6954 g/cm³. The densities of five specimens of every sample were measured and the average values calculated from at least 3 specimens were reported. The void fraction (VF) was calculated from the equation (2) [3], where ρ_1 and ρ_2 were density of foamed specimens and unfoamed PLA (1.223 g/cm³), respectively. The density and VF were reported in a unit of g/cm³ and %, respectively:

$$\%VF = 1 - \left(\frac{\rho_1}{\rho_2} \right) \times 100 \quad (2).$$

3.3.9.2 Pore morphology

The pore morphology of the foams were investigated using the scanning electron microscope at the voltage of 20 kV and magnification of 35X. The foamed sheet was cut into 9 zones as shown in Figure 3.1. The specimen from each zone was immersed in liquid nitrogen and then immediately fractured before coating with gold. Base on pore size, approximately 50 to 150, 100 to 200, and 100 to 500 pores were investigated for foam no. 1-5, foam no. 6-9 and foam no. 10-16, respectively. The average pore size in a unit of micron (μm) were calculated and reported.

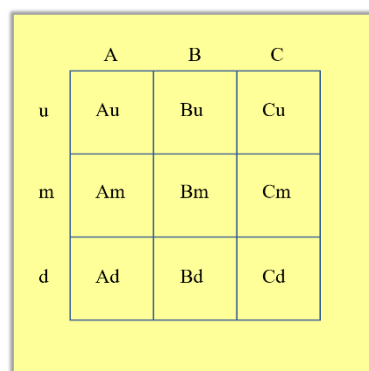


Figure 3.1 The foam sheet showing the specimen zones used to observe pore morphology by using SEM.

3.3.9.3 Impact strength

The Izod and Charpy impact resistance of unfoamed and foamed PLA compounds were determined according to ASTM 256 and ASTM D6110, respectively. The notched and unnotched specimens with rectangular shape were prepared and the specimen dimension was 12.7 x 65.0 mm² with the thickness approximately 2.00 mm. Ten specimens for each sample were tested using a 4 J pendulum. An average value and a standard deviation calculated from at least 6 specimens were reported.

3.3.9.4 Tensile properties

The tensile modulus, tensile strength and elongation at break of unfoamed and foamed PLA compounds were investigated according to ASTM D412 Test C using INSTRON[®] 5569. Twelve specimens for each sample were tested at room temperature. The crosshead speed of 50 mm/min was used for testing the PLA/nontreated RWS samples. The crosshead speed of 5 mm/min was used for testing the unfoamed PLA/treated RWS samples and the PLA compounded foam samples. An average value with standard deviations calculated from at least 6 specimens were reported.

3.3.9.5 Flexural properties

The flexural properties of PLA compounded foams were determined according to ASTM 790 using INSTRON[®] 3365. Ten specimens for each sample with rectangular shape were cut in a width (w) of 12.7 mm and a span length (L) of 50 mm. The testing speed was 1.5 mm/min. An average value with standard deviations calculated from at least 6 specimens were reported [4-5].

3.3.10 Thermal properties

3.3.10.1 Differential scanning calorimeter

The DSC thermograms of PLA compounded pellets and PLA/PEG/CH foams were recorded. The first heating scan was performed from 20°C to 200°C, and then the sample was cooled at the rate of -10°C/min from 200°C to 20°C. The second heating scan was performed from 20°C to 200°C. Both heating scans were performed

at the rate of 10°C/min. The heat of fusion of pure crystalline PLLA (ΔH_{PLA}) was 93 J/g [6]. The degree of crystallinity (X_{c1}) by considering an area under the cold crystallization peak (ΔH_{cc}) and the degree of crystallinity (X_{c2}) by neglecting ΔH_{cc} were calculated from the equation (3) and (4), respectively. The ΔH_m was the heat of fusion of the samples:

$$X_{c1} = \left[\frac{\Delta H_m - \Delta H_{cc}}{\Delta H_{PLA}} \right] \times 100 \quad (3)$$

$$X_{c2} = \frac{\Delta H_m}{\Delta H_{PLA}} \times 100 \quad (4).$$

3.3.10.2 Dynamic mechanical thermal analysis

Dynamic mechanical thermal analysis (DMTA) of the foam specimens was performed in a single cantilever mode. The specimens were trimmed to dimension of 25 mm x 6 mm x 2.5-3.0 mm (length x width x thickness) before testing at a temperature range of 10°C to 140°C with a heating rate of 3°C/min. The frequency was 1 Hz.

3.3.10.3 Thermogravimetric analysis

Thermogravimetric analysis (TGA) of RWS, PLA compounded pellets and PLA compounded foams were carried out at a heating rate of 5°C/min from 30°C to 500°C under nitrogen atmosphere. 7-15 mg of the sample were used.

3.3.11 *In-vitro* degradation testing

The *in-vitro* degradation testing of the foam specimens was performed by 2 methods.

3.3.11.1 *In-vitro* degradation according to Rakmea *et al.* [7]

A phosphated-buffered solution (PBS) at a concentration of 0.1 M and pH 7.4 was in-house prepared by mixing of 0.2 M $\text{Na}_2\text{HPO}_4 \cdot 2\text{H}_2\text{O}$ solution and 0.2 M $\text{NaH}_2\text{PO}_4 \cdot 2\text{H}_2\text{O}$ solution and then adding distilled water to obtain total volume of 200 ml. *In-vitro* degradation was determined by soaking the foam specimens in PBS. Three

specimens with a dimension of 10 mm × 60 mm × 2 mm (width × length × thickness) from each sample with initial weight (W_0) were vertically placed in a test tube filled with 35 ml PBS. The immersed specimens were incubated at 37 °C for 8 weeks. The PBS in all test tubes was weekly replaced by the fresh PBS. At the end of each period, the specimens were removed from PBS, then rinsed by distilled water for 3 times and vacuum dried at a temperature of 65 °C to a constant weight (W_d). The percentage of weight loss of the specimen during immersion in PBS was calculated from the equation (5), where W_0 was an initial weight and W_d was a weight after degradation:

$$\%Weight\ loss = \left[\frac{W_0 - W_d}{W_0} \right] \times 100 \quad (5).$$

3.3.11.2 *In-vitro* degradation according to Zhang and Cui, [8]

Five dry foam specimens (1 × 1 cm) for each sample were added in 500 µl of a lysozyme solution (4 mg of lysozyme in 1 ml of PBS with pH 7.4). The sample was then incubated at 37°C for 8 week. The lysozyme solution was weekly replaced with a fresh solution. At determined time intervals, the specimens were removed from the solution, then washed with distilled water and finally dried in a freeze dryer. The % weight loss was also calculated from the equation (5).

3.3.12 Cell cytotoxicity assay

MG-63 cells were cultured in a 75 ml flask containing alpha-MEM medium with the addition of 1% penicillin-streptomycin, 0.1% fungizone, and 10% fetal bovine serum at 37 °C in an incubator with fully humidified atmosphere at 5% CO₂. MG-63 cells (5×10^4 cells) were seeded onto the surface of foam specimens. The medium was changed every 3 days during the cells culture. An osteogenic medium (OS) was used for osteoblast differentiation of the MG-63 cells [9]. This medium contained 10 mM of β-glycerophosphate, 50 mg/ml of ascorbic acid, and 100 nM of dexamethasone. The MG-63 cells were cultured in a culture plate for 1, 3, 5 and 7 days. The MG-63 cell proliferation was measured by WST-1 assay. The quantification of cell proliferation was measured according to manufacturer's instructions [10]. The absorbance of each specimen was recorded at 420 nm using Multiskan™ GO

Microplate Spectrophotometer. The morphology of cells that adhered on the foam specimen was investigated by scanning electron microscope (FEI® Quanta 400). The seeded foam specimens were washed with PBS and fixed using 10% neutral formalin buffer for 5 h at 4°C. The specimens were dried in a freeze dryer and the specimen surfaces were sputter coated with gold prior to investigation.

3.3.13 Statistical analysis of data

One-way analysis of variance (one-way ANOVA) was performed using SPSS software (version 20.0) at 0.05 significance level ($p < 0.05$). The significance differences among the specimens were analyzed using Tukey's honestly significant difference (HSD) test. Different letters, e.g. A, B, C, D, AB and CD, were used to identify the samples when the average values are significant different at $p < 0.05$.

3.4 References

1. Moigne, N. L., Longerey, M., Taulemesse, J.-M., Bènezet, J.-C. and Bergeret, A. 2014 Study of the interface in natural fibres reinforced poly(lactic acid) biocomposites modified by optimized organosilane treatments. *Industrial Crops and Products*. 52: 481-494.
2. Kamphunthong, W., Hornsby, P. and Sirisinha, K. 2012 Isolation of cellulose nano-fibres from Para rubber wood and their reinforcing effect in Poly(vinyl alcohol) composites. *Journal of Applied Polymer Science*. 125: 1642-1651.
3. Luo, Y., Zhang, J., Qi, R., Lu, J., Hu, X. and Jiang, P. 2013 Polylactide foams prepared by a traditional chemical compression molding method. *Journal of Applied Polymer Science*. 330-337.
4. Zimmermann, M. V. G., Brambilla, V. C., Brandalise, R. N. and Zattera, A. J. 2013 Observations of the effects of different chemical blowing agents on the degradation of poly(lactic acid) foams in simulated soil. *Materials Research*. 16 (6): 1266-1273.
5. Ding, W., Chang, E., Jahani, D., Alemdar, A., Wang, Q., Park, C. B. and Sain, M. 2016 Development of PLA/cellulosic fibre composites foams using injection molding: Foaming and mechanical properties. *SPE ANTEC™ Indianapolis*. 1783-1787.

6. Kawamoto, N., Sakai, A., Horikoshi, T., Urushihara, T. and Tobita, E. 2007 Physical and mechanical properties of poly(L-lactic acid) nucleated by dibenzoylhydrazide compound. *Journal of Applied Polymer Science*. 103: 244-250.
7. Rakmae, S., Ruksakulpiwat, Y., Sutapun, W. and Suppakarn, N. 2012 Effect of silane coupling agent treated bovine bone based carbonated hydroxyapatite on in vitro degradation behavior and bioactivity of PLA composites. *Materials Science and Engineering C*. 32: 1428-1436.
8. Zhang, Z. and Cui, H. 2012 Biodegradability and biocompatibility study of poly (chitosan -g-lactic acid) scaffolds. *Molecules*. 17: 3243-3258.
9. Sangkert, S., Kamonmattayakul, S., Chai, W. L. and Meesane, J. 2016 A bio-functional-modified silk fibroin scaffold with mimic reconstructed extracellular matrix of decellularized pulp/collagen/fibronectin for bone tissue engineering in alveolar bone resorption. *Materials Letter*. 166: 30-34.
10. Hsueh, Y.-S., Savitha, S., Sadhasivam, S., Lin, F.-H. and Shieh, M.-J. 2014 Design and synthesis of elastin-like polypeptides for an ideal nerve conduit in peripheral nerve regeneration. *Materials Science and Engineering C*. 38: 119-126.

CHAPTER 4

RESULTS AND DISCUSSION

4.1 Preparation and properties of unfoamed PLA/RWS compounds

4.1.1 Suitable RWS particle sizes and RWS content

Mechanical properties including impact strength and tensile properties were used to determine the suitable RWS particle sizes for surface treatment and RWS content for preparation of unfoamed PLA/treated-RWS.

4.1.1.1 Impact strength

(i) Particle size of 212-600 μm

Figure 4.1 shows the Charpy impact strength of PLA compounds containing various nontreated-RWS contents. It was found that the Charpy impact strength of the unnotched specimens decreased as increased RWS contents. This trend was also found in the Izod impact strength (Figure 4.2). The addition of 5 wt% and 10 wt% RWS slightly changed the Charpy impact strength of the notched specimens. The PLA/RWS compound containing 15 wt% RWS was very brittle; therefore, the compression molded samples could not be cut as a notched specimen. The Izod impact strength of the notched specimens of PLA and PLA/RWS compound containing 5 wt% and 10 wt% RWS were similar but the addition of 15 wt% of RWS to PLA significantly decreased the Izod impact strength of the notched specimens.

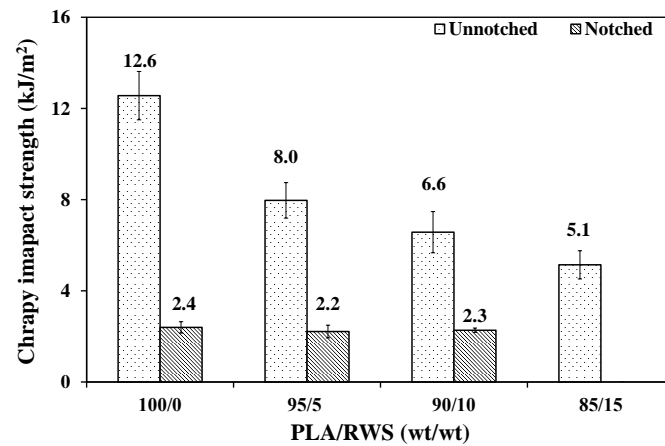


Figure 4.1 Effect of nontreated-RWS contents on Charpy impact strength of PLA (particle size: 212-600 μm).

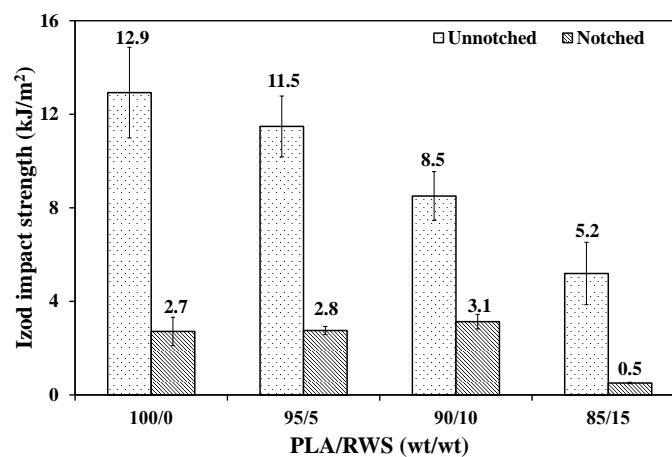


Figure 4.2 Effect of nontreated-RWS contents on Izod impact strength of PLA (particle size: 212-600 μm).

Figure 4.3 and 4.4 display the impact strength obtained from Charpy and Izod testing of unnotched and notched specimens, respectively. It was found that the impact strengths of unnotched and notched specimens tested by Izod method were higher than those of the specimens tested by Charpy method. The difference of the impact strength obtained from Charpy and Izod testing was due to the difference of direction of the specimen placed in the holder and the direction of impact force (pendulum).

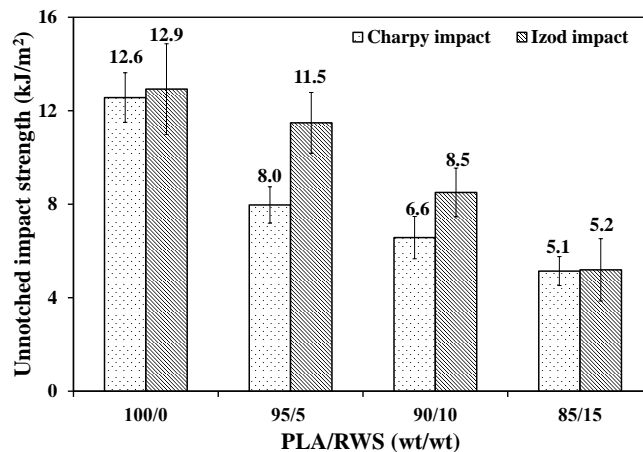


Figure 4.3 Effect of nontreated-RWS contents on unnotched impact strength of PLA (particle size: 212-600 μm).

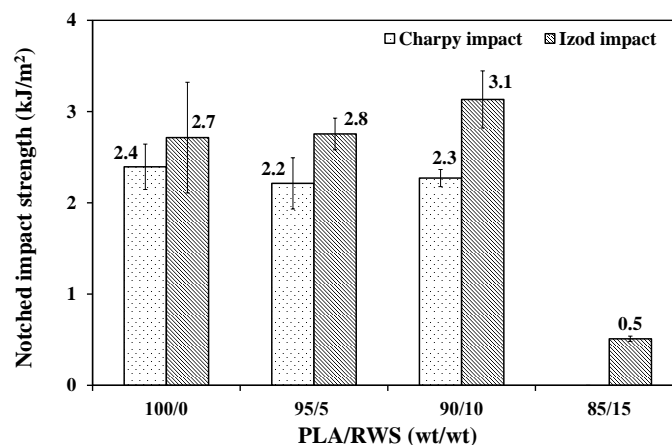


Figure 4.4 Effect of nontreated-RWS contents on notched impact strength of PLA (particle size: 212-600 μm).

(ii) Particle size of $\leq 212 \mu\text{m}$

The addition of RWS decreased the Charpy impact strength of the unnotched specimens of PLA for all PLA/RWS ratios (Figure 4.5). This trend was also found in the Izod impact strength (Figure 4.6). The impact strength slightly changed as increased RWS content from 5 wt% to 10 wt% but it significantly decreased when 15 wt% RWS was used (Figure 4.5 and 4.6). The notch sensitivity of PLA compounds was observed in both Charpy and Izod testing due to significant decreasing of impact strength of notched specimens as compared with the unnotched one.

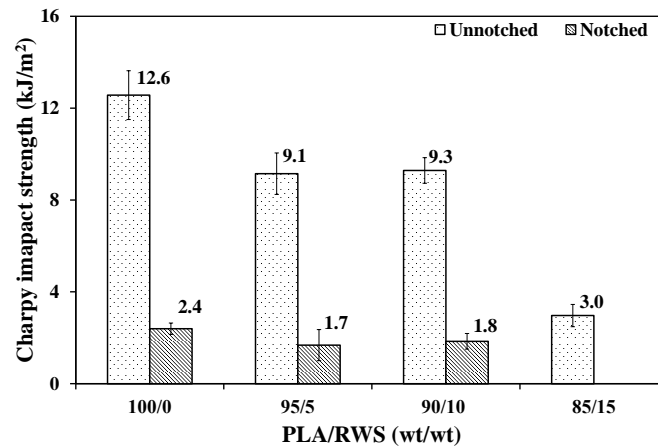


Figure 4.5 Effect of nontreated-RWS contents on Charpy impact strength of PLA (particle size: $\leq 212 \mu\text{m}$).

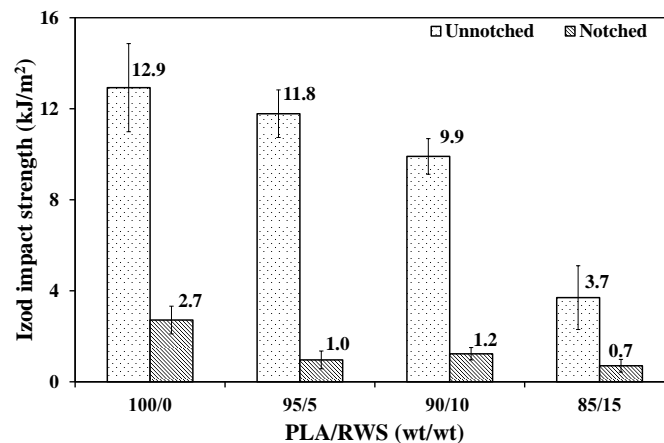


Figure 4.6 Effect of nontreated-RWS contents on Izod impact strength of PLA (particle size: $\leq 212 \mu\text{m}$).

Figure 4.7 shows that the unnotched Izod tested specimens showed higher impact strength than those tested by Charpy method whereas the notched specimens did not show this trend (Figure 4.8). In addition, PLA compounds incorporated with RWS particle size of $212\text{-}600 \mu\text{m}$ and $\leq 212 \mu\text{m}$ exhibited notch sensitivity as shown in Figure 4.1-4.2 and Figure 4.5-4.6, respectively. The impact strength significantly decreased when the specimens were notched. Figure 4.4 and 4.8 demonstrated that PLA compounds incorporated with the larger particle RWS showed lower notch sensitivity than those of the smaller particle size.

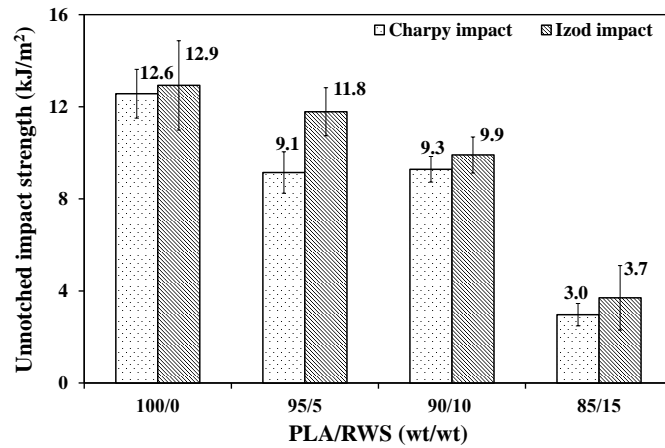


Figure 4.7 Effect of impact testing method on unnotched impact strength of PLA (particle size: $\leq 212 \mu\text{m}$).

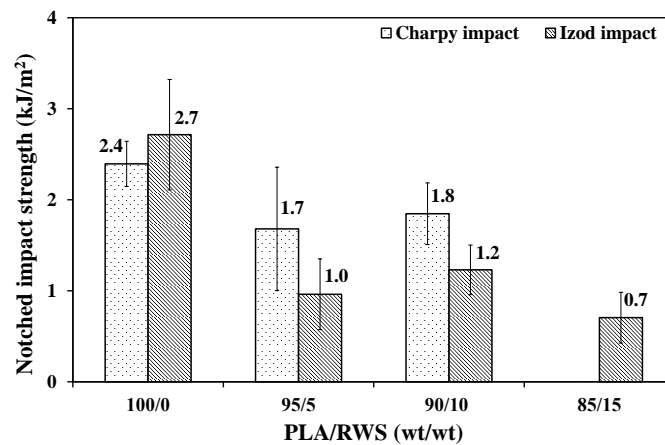


Figure 4.8 Effect of impact testing method on notched impact strength of PLA (particle size: $\leq 212 \mu\text{m}$).

The Charpy and Izod impact testing were applied to the specimens with different direction of specimen located in the holder and the direction of impact force resulting in the difference of impact strength values. In this experiment, the Izod impact strength of the samples was higher than Charpy impact strength, and the Izod testing is commonly used. Thus, only Izod testing method was applied to the specimens in the next experiment. Moreover, the results mentioned above showed that the PLA compounds with the PLA/RWS ratio of 85/15 were very low impact strength. Therefore, this composition was not tested in the next experiment.

(iii) Particle size of 75-150 μm and $\leq 75 \mu\text{m}$

The impact strength of PLA compounds containing the RSW particle sizes of 75-150 μm and $\leq 75 \mu\text{m}$ is shown in Figure 4.9 and 4.10, respectively. The addition of both particle sizes RWS to PLA slightly decreased the impact strength of the unnotched specimens whereas the impact strength of the notched specimens slightly changed, except the addition of 10 wt% of smaller particle RWS ($\leq 75 \mu\text{m}$), it showed very low impact strength.

Figure 4.11 and 4.12 demonstrate effect of RWS on Izod impact strength of PLA containing various particle size RWS at 5 wt% and 10 wt%, respectively. The addition of RWS at 5 wt% and 10 wt% (all particle size) to PLA slightly decreased the impact strength of the unnotched specimens. The impact strength of PLA compounds containing 10 wt% RWS slightly decreased as increased RWS particle size, whereas PLA compounds containing 5 wt% RWS did not show this trend. The addition of RWS at 5 wt% and 10 wt% to PLA slightly changed the impact strength of the notched specimens, except the addition of 5 wt% RWS with particle size of $\leq 212 \mu\text{m}$ (Figure 4.11) and 10 wt% RWS with particle size of $\leq 75 \mu\text{m}$ and $\leq 212 \mu\text{m}$ (Figure 4.12), it decreased the impact strength of PLA.

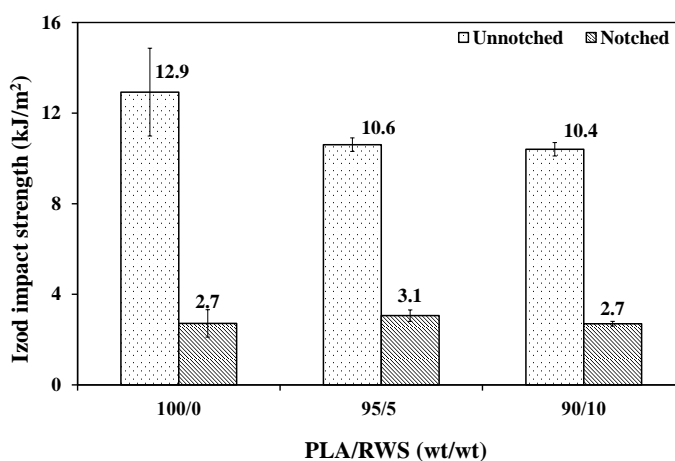


Figure 4.9 Effect of nontreated-RWS contents on Izod impact strength of PLA (particle size: 75-150 μm).

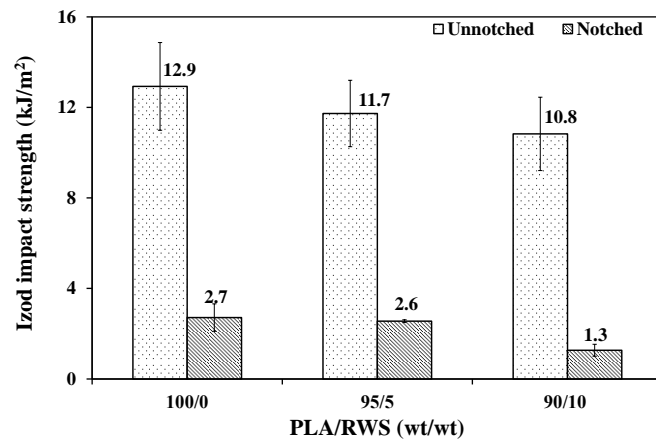


Figure 4.10 Effect of nontreated-RWS contents on Izod impact strength of PLA (particle size: $\leq 75 \mu\text{m}$).

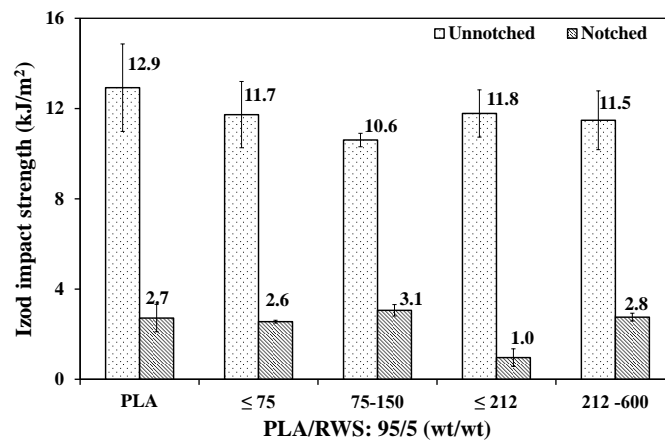


Figure 4.11 Effect of particle size on Izod impact strength of PLA compounds containing 5 wt% of RWS.

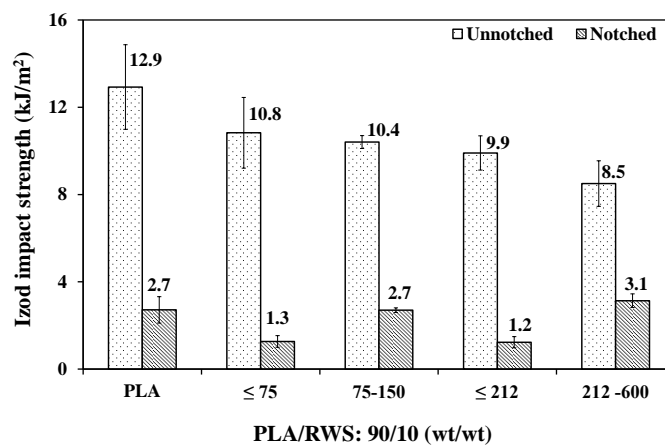
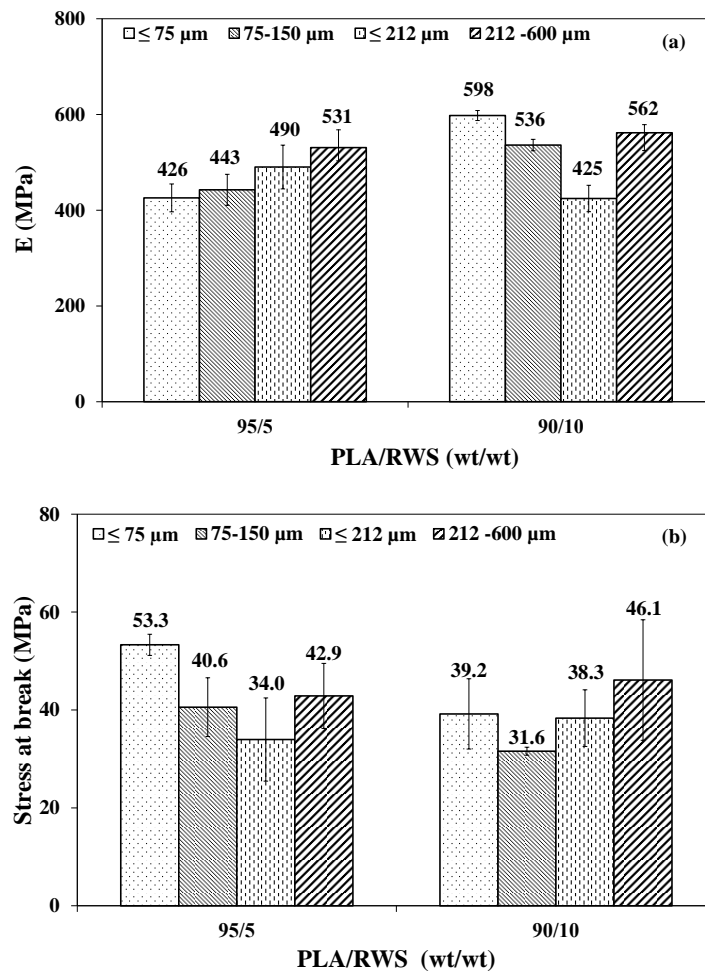


Figure 4.12 Effect of particle size on Izod impact strength of PLA compounds containing 10 wt% of RWS.

4.1.1.2 Tensile properties

Figure 4.13 displays effect of RWS content and particle size on tensile properties of PLA. In the present study, the specimens were tested using crosshead speed of 50 mm/min. All composition of PLA compounds showed brittle fracture without yield point. The result demonstrated that the tensile modulus of PLA compounds containing 5 wt% RWS slightly increased as increased RWS particle size, whereas the compounds containing 10 wt% RWS did not show this trend. The compound containing 5 wt% of the smallest particle ($\leq 75 \mu\text{m}$) showed the highest stress at break and strain at break. The compound containing 10 wt% of the smallest particle ($\leq 75 \mu\text{m}$) showed the highest tensile modulus, and the compound containing 10 wt% the largest particle (212-600 μm) showed the highest stress at break.



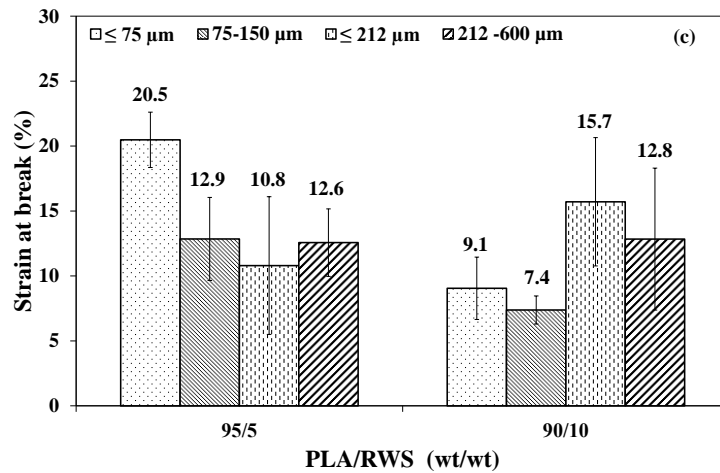


Figure 4.13 Effect of particle size and contents on tensile properties of PLA compounds: (a) modulus, (b) stress at break and (c) strain at break.

The Izod impact strength and tensile properties of PLA compounds containing various sizes of 5 wt% and 10 wt% RWS are listed in Table 4.1. Based on RWS content, the compounds containing 5 wt% RWS showed higher mechanical properties than those of the compounds containing 10 wt% RWS. Based on using 5 wt% RWS obtained by grinding and sieving ($\leq 75 \mu\text{m}$ and $75-150 \mu\text{m}$), the addition of the smaller particle RWS ($\leq 75 \mu\text{m}$) to PLA showed the highest mechanical properties. Based on using 5 wt% RWS obtained by sieving ($\leq 212 \mu\text{m}$ and $212-600 \mu\text{m}$), the compound containing the larger particle ($212-600 \mu\text{m}$) showed the highest notched impact strength and tensile properties. Therefore, the nontreated-RWS with particle size of $\leq 75 \mu\text{m}$ and $212-600 \mu\text{m}$ was selected to prepare treated-RWS using alkaline and/or silane treatment. The PLA/RWS ratio of 95/5 (wt/wt) was used to prepare unfoamed PLA/treated-RWS compounds in the next experiment.

Table 4.1 Mechanical properties of PLA compounds containing 5 wt% and 10 wt% of RWS with various particle size

PLA/RWS ratios	Particle size (μm)	Izod impact strength (kJ/m^2)		Tensile properties		
		Unnotched	Notched	Modulus (MPa)	Stress at break	Strain at break (%)
95/5	≤ 75	11.7 ± 1.5	2.6 ± 0.1	426 ± 29	53.3 ± 2.2	20.5 ± 2.1
	75-150	10.6 ± 0.3	3.1 ± 0.3	443 ± 32	40.6 ± 6.0	12.9 ± 3.2
	≤ 212	11.8 ± 0.9	1.0 ± 0.4	490 ± 46	34.0 ± 8.5	10.8 ± 5.3
	212-600	11.5 ± 1.3	2.8 ± 0.2	531 ± 37	42.9 ± 6.6	12.6 ± 2.6
90/10	≤ 75	10.8 ± 1.6	1.3 ± 0.3	598 ± 10	39.2 ± 7.2	9.1 ± 2.4
	75-150	10.4 ± 0.3	2.7 ± 0.1	536 ± 12	31.6 ± 0.8	7.4 ± 0.58
	≤ 212	9.9 ± 0.8	1.2 ± 0.3	425 ± 26	38.3 ± 5.8	15.7 ± 4.9
	212-600	8.5 ± 1.0	3.1 ± 0.3	562 ± 17	46.1 ± 12.3	12.8 ± 5.5

4.1.2 Characterizations of treated-RWS

4.1.2.1 Chemical structures of RWS

(i) Particle size of 212-600 μm

RWS is a one kind of lignocellulose containing of cellulose, hemicellulose, lignin, pectin and non-essential parts such as waxes, oil and impurities. PLA contains some hydroxyl and carboxylic end groups similarly to RWS; however, its polarity is much lower than that of RWS. This results in low interfacial adhesion between PLA and RWS, causing poor mechanical properties. Therefore, alkaline treatment is required to remove impurities and decrease hydrophilicity of RWS, and silane treatment is required to improve interfacial adhesion between PLA and RWS. Alkaline treatment using NaOH is a typical pathway to eliminate non-essential parts on the surface of cellulosic materials, for example, natural fiber and wood sawdust and reduce hydrophilicity of RWS [1-3]. Silane coupling agents are widely used to improve the interfacial adhesion between polymer and cellulosic materials via the hydrolyzable and organofunctional reactions [2, 4-5]. In the present study, the surface treatment using

GPMS was divided into three methods, method A, B and C. In method A, nontreated-RWS was treated by NaOH followed by GPMS treatment. FTIR technique was utilized to characterize the surface of RWS before and after NaOH and/or silane treatment. Figure 4.14 shows the FTIR spectra of the larger particle RWS (212-600 μm) before and after treatment and the spectra of GPMS and hydrolyzed GPMS. FTIR assignment is listed in Table 4.2. Nontreated-RWS showed strong peaks of OH group at approximately 3000 to 3500 cm^{-1} , C=O of hemicellulose at 1735 cm^{-1} and acetyl group of xylan at 1230 cm^{-1} [6]. After NaOH treatment, the peak at 1735 cm^{-1} was not observed in the spectrum of NaOH-treated RWS and 1%GPMS RWS-A demonstrating disappearance of hemicellulose. The peak in the spectrum of nontreated-RWS at 1230 cm^{-1} became a double peak in the spectrum of NaOH-treated RWS and 1%GPMS RWS-A, at 1227 cm^{-1} and 1267 cm^{-1} . The first and second split peak were assigned to the vibrations of the syringyl structure and guaiacyl structure of lignin, respectively [6]. This result demonstrated that the hemicelluloses and non-essential parts were mostly removed by NaOH treatment. It was in accordance with the previous study [2, 6]

The GPMS treatment, the proposed interaction mechanism of GPMS with RWS and PLA is shown in Figure 4.15 [4]. After hydrolysis, GPMS is transformed to hydrolyzed GPMS or silanols which contain a large number of hydroxyl groups (Figure 4.15(a)). During the hydrolysis process, the Si-O-Si groups can be together formed via self-condensation as shown in Figure 4.15(b). The -Si-O-Si- network structure is formed after the addition of RWS into hydrolyzed GPMS solution obtaining GPMS-treated RWS (Figure 4.15(c)). After melt blending with PLA, GPMS-treated RWS can be grafted with PLA through epoxide ring opening as displayed in Figure 4.15(d). In the present study, after hydrolysis, the peak in the spectrum of GPMS at 1255 cm^{-1} and 909 cm^{-1} assigned to the epoxide ring vibration (Table 4.2) were transformed to 903 cm^{-1} and 844 cm^{-1} , and the peak at 1087 cm^{-1} assigned to Si-O bonds in Si-O-CH₃ of GPMS was transformed to 1102 cm^{-1} assigned to Si-O bonds in Si-O-H (Figure 4.14) which corresponded to the previous study [7]. The spectrum of 1%GPMS-A RWS representing the product of Figure 4.15(c) shows that the presence of hydrolyzed GPMS on the surface of RWS after condensation reaction was not clearly observed. This might be because a very small concentration of GPMS and an overlapped peak. The peaks of hydrolyzed GPMS at 2927 and 2861 cm^{-1} corresponded to C-H

stretching vibration overlapped the broad peak of all RWS samples at 2900 cm^{-1} . Similarly, the epoxide ring peaks in hydrolyzed GPMS overlapped with C-H bending of RWS (Table 4.2) at approximately 900 cm^{-1} and Si-O in the $-\text{Si-O-Si}-$ network structure or Si-O-RWS bond overlapped with C-O stretching of RWS in the wave number range of $1000\text{-}1110\text{ cm}^{-1}$ [8]. Although the GPMS treatment could not be clearly observed, the intensity of the overlapped peaks of C-H stretching vibration at approximately 2971 cm^{-1} and 2901 cm^{-1} increased with increasing GPMS content as shown in Figure 4.16. This indicated relatively good potential of surface treatment by using method A.

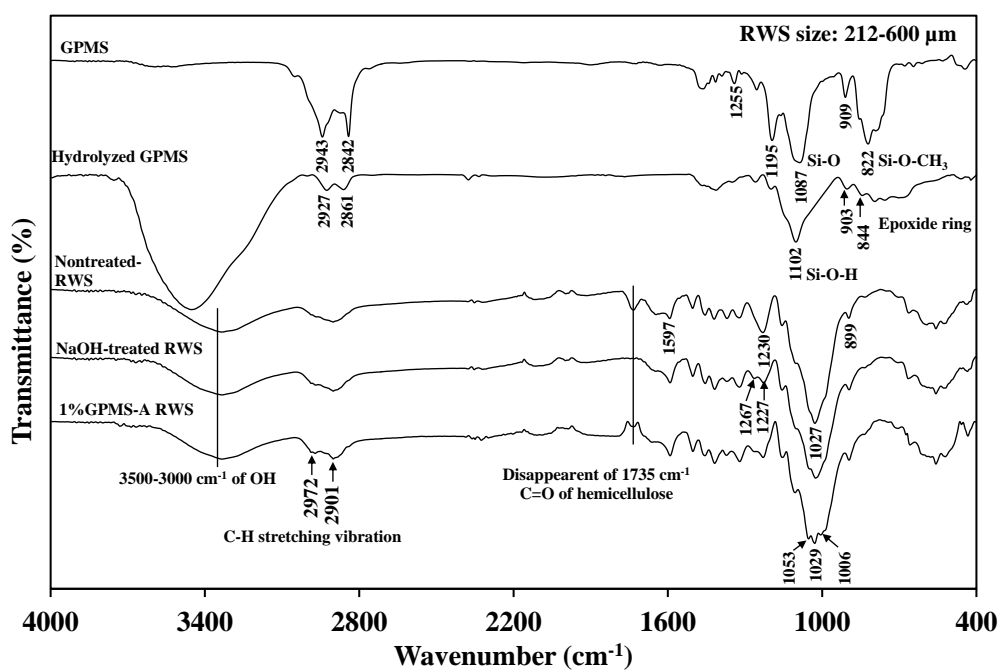


Figure 4.14 FTIR spectra of GPMS and RWS (212-600 μm) before and after surface treatment with NaOH and GPMS using method A.

Table 4.2 FTIR assignment of nontreated RWS and GPMS [2, 6-7, 9].

Peak (cm ⁻¹)	Nontreated-rubber wood sawdust	GPMS
3339	OH stretching vibration	-
2943, 2842	-	C-H stretching vibration
2900	C-H stretching vibration	-
1735	C=O stretching vibration of hemicellulose	-
1643, 1597, 1505	Carboxylic groups	-
1456, 1149	Symmetric bending of CH ₃	-
1370, 1324	C-O stretching vibration of carboxylic group	-
1255, 909	-	Epoxide ring vibration
1230	Acetyl group of xylan	
1195	-	C-O stretching vibration
1087	-	Si-O stretching vibration
1027	C-C-O or C-O-C stretching vibration	-
899	C-H bending of carboxylic	-
822	-	Si-O-CH ₃ deformation

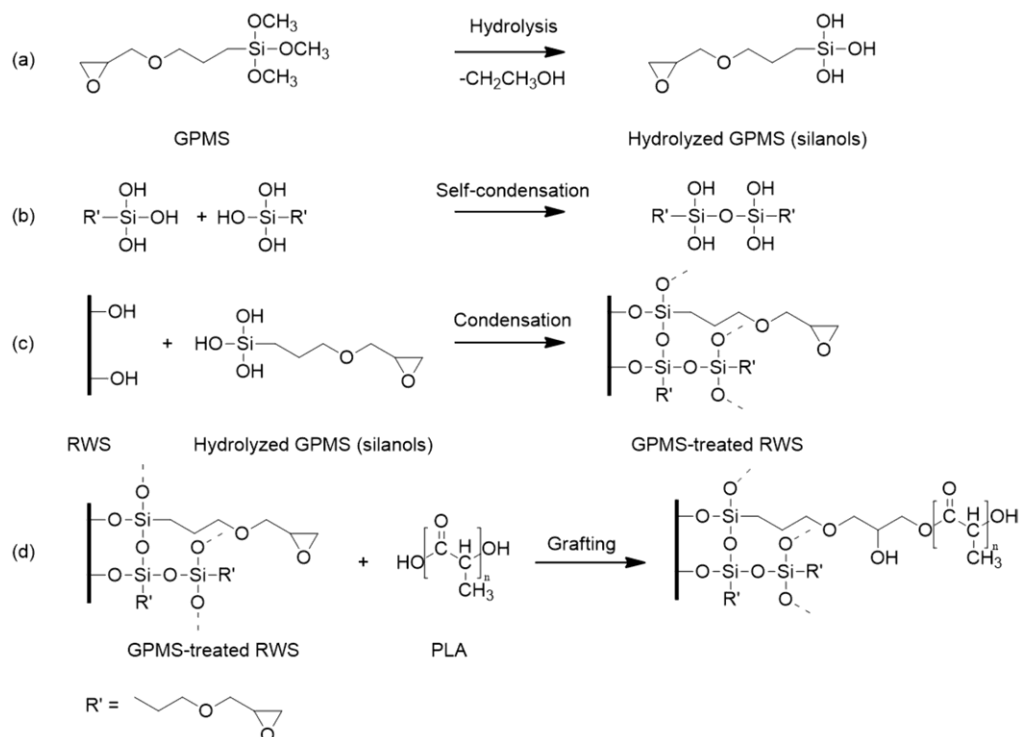


Figure 4.15 Proposed interaction mechanism of GPMS with RWS and PLA [4].

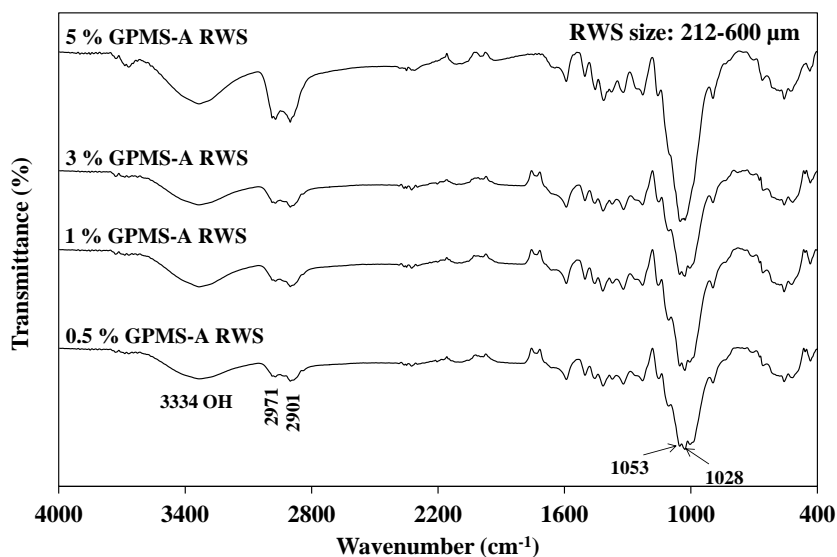


Figure 4.16 FTIR spectra of RWS (212-600 μm) treated with various GPMS content using method A.

APMS silane coupling agent was used for surface treatment of the larger particle RWS (212-600 μm) using method A and method A without pH adjusting to study effects of silane type and pH condition on the surface treatment of RWS. The RWS particle size of 212-600 μm was used because the treatment procedure of this particle size was easier than those of the smaller particle. In addition, Xie *et al.* [5] have been reported that the alkoxy groups of APMS could not be efficiently hydrolyzed in acid condition. Therefore, the method A without pH adjusting to 5 was carried out to study effect of pH condition. FTIR spectra of APMS and treated RWS are shown in Figure 4.17. The characteristic peaks of APMS were the peaks at 2940 cm^{-1} and 2841 cm^{-1} assigned to CH stretching, the peaks at 1596 cm^{-1} and 1463 cm^{-1} assigned to vibration of NH_2 group [3], the peak at 1192 cm^{-1} assigned to C-O stretching, the peak at 1085 cm^{-1} assigned to Si-O stretching, and the peak at 816 cm^{-1} assigned to Si-O- CH_3 deformation [7]. It was found that APMS surface treatment of RWS could not be clearly confirmed by FTIR results. This may be due to the overlapped peaks of APMS and RWS. In addition, no obvious differences were found for APMS treatment between method A and method A without pH adjusting indicating no effect of pH condition on the surface treatment of RWS.

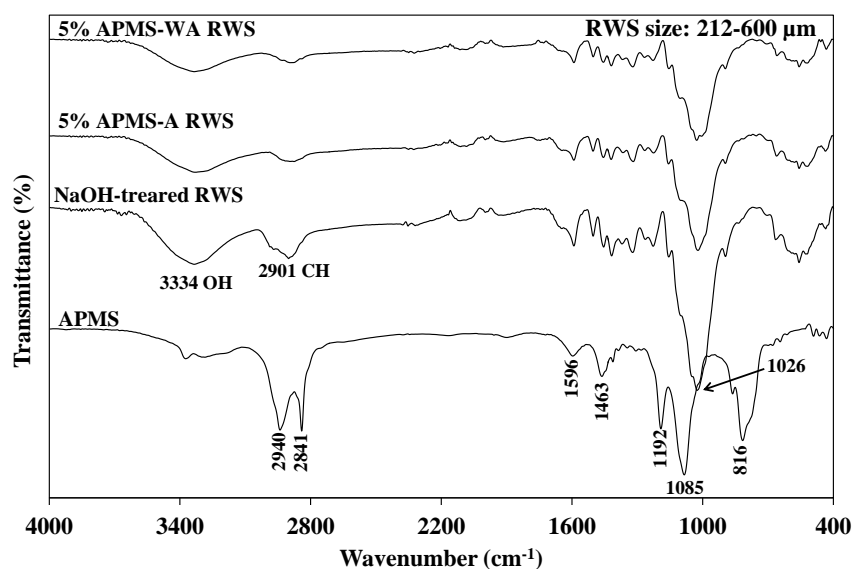


Figure 4.17 FTIR spectra of APMS and treated RWS (212-600 μm) before and after surface treatment with APMS using method A and method A without pH adjusting.

In the GPMS treatment using method B, the nontreated-RWS was not firstly treated by NaOH, and the treatment was carried out without pH adjusting. The spectra of RWS before and after GPMS treatment using method B are shown in Figure 4.18. The presence of the peaks at approximately 1737 cm^{-1} and 1230 cm^{-1} in the FTIR spectrum of 1%, 3% and 5% GPMS RWS-B indicated that the GPMS treatment using method B could not eliminate hemicelluloses and non-essential parts from the surface of nontreated-RWS. In addition, the intensity increment of the overlapped peaks of the C-H stretching vibration as increased GPMS content was not observed in the method B (Figure 4.18). This was because the nontreated-RWS was not firstly treated by NaOH. Therefore, the presence of hemicellulose and non-essential parts on the surface of nontreated-RWS might disrupt the GPMS treatment on the surface of RWS.

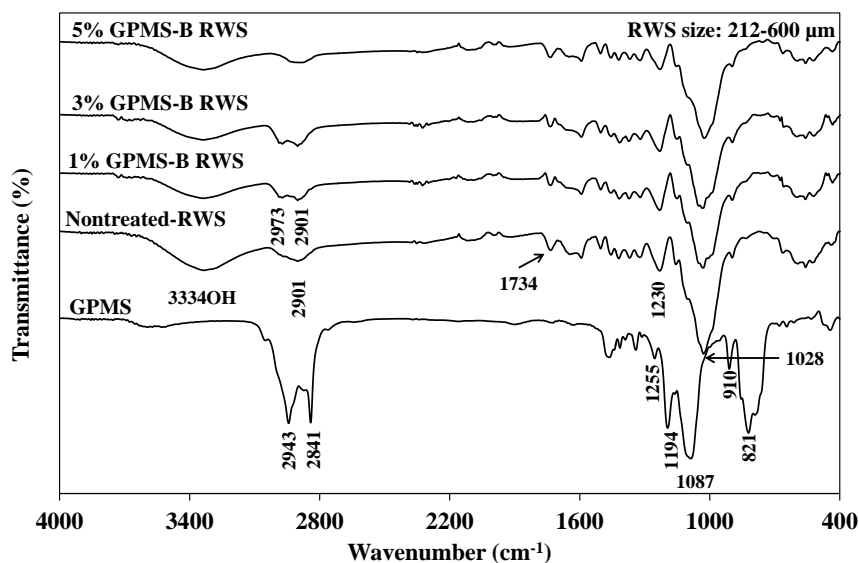


Figure 4.18 FTIR spectra of GPMS and RWS (212-600 μm) before and after surface treatment with various GPMS content using method B.

(ii) Particle size of $\leq 75 \mu\text{m}$

The FTIR spectra of smaller particle RWS ($\leq 75 \mu\text{m}$) before and after surface treatment with GPMS using method A are displayed in Figure 4.19. The chemical structure changes after NaOH treatment and GPMS treatment using method A of the smaller size RWS were found similarly with those of the larger particles. The hemicellulose and non-essential parts were partially removed by NaOH treatment. In addition, GPMS treatment could not clearly observed due to the peak overlapping.

Figure 4.20 displays FTIR spectra of GPMS and the smaller size RWS ($\leq 75 \mu\text{m}$) before and after treatment with GPMS using method B and C. In the treatment using method B, the FTIR spectra showed the similar results to those of the larger particle RWS (Figure 4.18). In the GPMS treatment using method C, the treatment procedure was similar to the method A but nontreated-RWS was not firstly treated by NaOH. The presence of the peaks at about 1735 cm^{-1} and 1230 cm^{-1} in the FTIR spectrum of 5% GPMS RWS-C indicated that GPMS treatment using method C could not eliminate hemicelluloses and lignin and change chemical structure of nontreated-RWS.

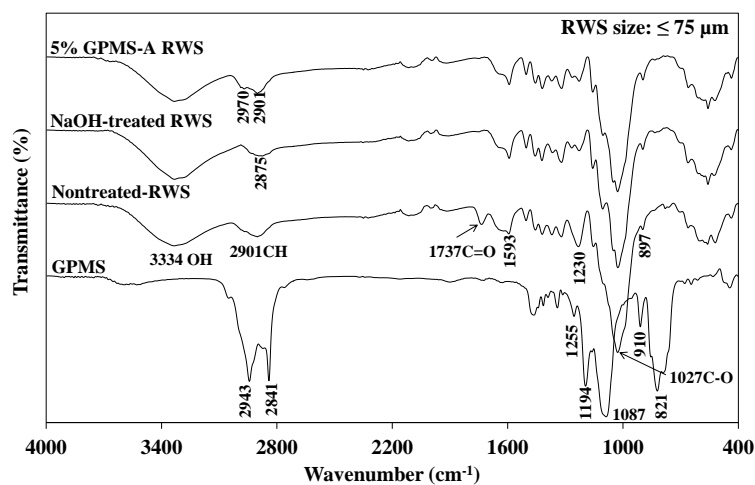


Figure 4.19 FTIR spectra of GPMS and RWS ($\leq 75 \mu\text{m}$) before and after surface treatment with NaOH and GPMS using method A.

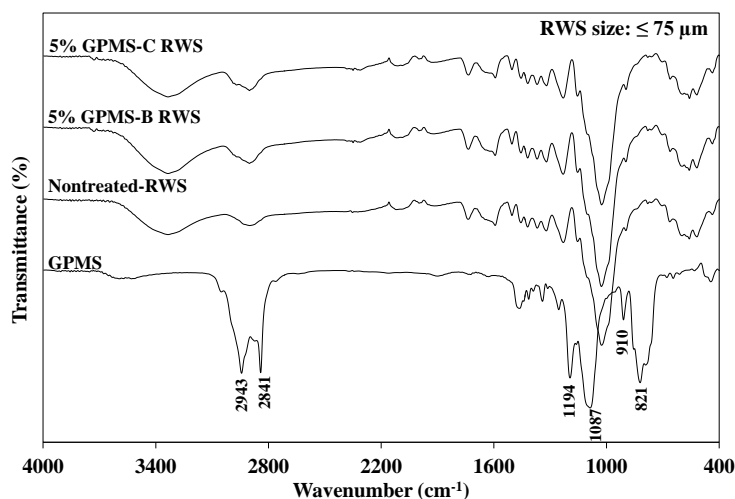


Figure 4.20 FTIR spectra of GPMS and RWS ($\leq 75 \mu\text{m}$) before and after surface treatment with GPMS using method B and C.

All FTIR results showed that NaOH treatment in both particle sizes of RWS could partially eliminate hemicellulose and non-essential parts such as wax and oil from the RWS surfaces. In the GPMS treatment using method A, FTIR results showed the peak overlapping and the increment of the overlapped peak intensity with increasing GPMS content indicated the potentials of this method. The GPMS treatment using method B and C which were applied to nontreated-RWS could not eliminate hemicellulose and non-essential parts. In addition, no difference of FTIR results

between GPMS treatment with and without pH adjusting was found. The surface treatment of RWS with APMS using method A and method A without pH adjusting could not be confirmed by FTIR. The nontreated-RWS, NaOH-treated RWS and GPMS-treated RWS using method A (both particle sizes) were selected to observe crystallinity and thermal degradation properties.

4.1.2.2 Surface morphology of RWS

Effect of surface treatments on the surface of the larger particle RWS (212-600 μm) is shown in Figure 4.21. The SEM images of nontreated-RWS (Figure 4.21(a) and (d)) showed a small particle on the RWS surface. After NaOH treatment (Figure 4.21(b) and (e)) and GPMS treatment (Figure 4.21(c) and (f)), the surface became cleaner and showed a grooved surface due to eliminating of hemicellulose and non-essential parts [2].

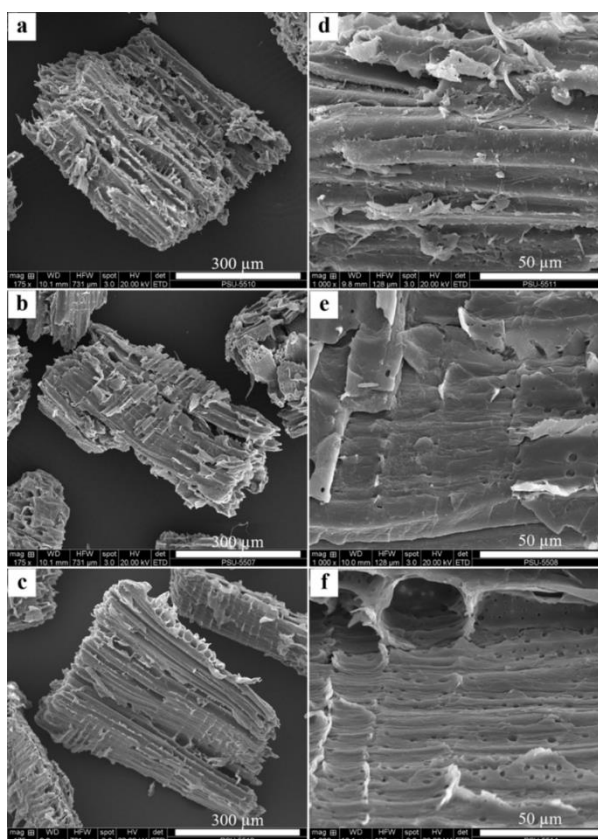


Figure 4.21 SEM images at 175X and 1000X of RWS with particle size of 212-600 μm : (a, d) nontreated-RWS, (b, e) NaOH-treated RWS and (c, f) 1%GPMS-A.

4.1.2.3 Crystallinity Index and thermal degradation of RWS

XRD analysis was used to determine crystallinity of RWS. The XRD pattern of RWS demonstrated the characteristic peaks at $2\theta = 17^\circ$, 22.5° and 35° which corresponded to the crystal plane diffraction peaks of (1 0 1), (0 0 2) and (0 4 0) in cellulose, respectively [10] (Figure 4.22 (a) and (b)). No change in the XRD peak position was found after NaOH treatment and GPMS treatment. It indicated no change in the crystal structure of RWS. This was due to using low concentration of alkaline solution (5% NaOH) which was corresponded to the previous study. Kamphunthong *et al.* [1] found that the crystal structure of rubber wood was not changed until treatment with 17.5% NaOH was applied. The crystallinity index (CI) calculated from the XRD analysis of various types of RWS is listed in Table 4.3. The CI of the smaller particle RWS ($\leq 75 \mu\text{m}$) significantly increased after NaOH treatment and it slightly increased after GPMS treatment. A slightly change in CI of the larger size RWS (212-600 μm) after surface treatment was found (Table 4.3). The CI of the smaller particle (nontreated-RWS 75) was lower than that of the larger particle (nontreated-RWS 212-600) because the smaller particle was prepared from the larger particle by very high speed grinding (25,000 rpm). That might be because the high speed grinding provided very high shear rate which was able to destroy a certain of crystal structure of the larger particle RWS.

Table 4.3 Thermal degradation temperature and crystallinity index of nontreated RWS and RWS treated with NaOH and GPMS using method A

RWS types	$T_{d \text{ onset}} (\text{°C})$	$T_d (\text{°C})$	Crystallinity Index (%)
Nontreated-RWS 75	265	342	61.7
NaOH-treated RWS 75	311	355	87.7
1% GPMS-A 75	319	358	93.1
Nontreated-RWS 212-600	293	332	91.7
NaOH-treated RWS 212-600	291	331	88.6
1% GPMS-A 212-600	311	353	94.4

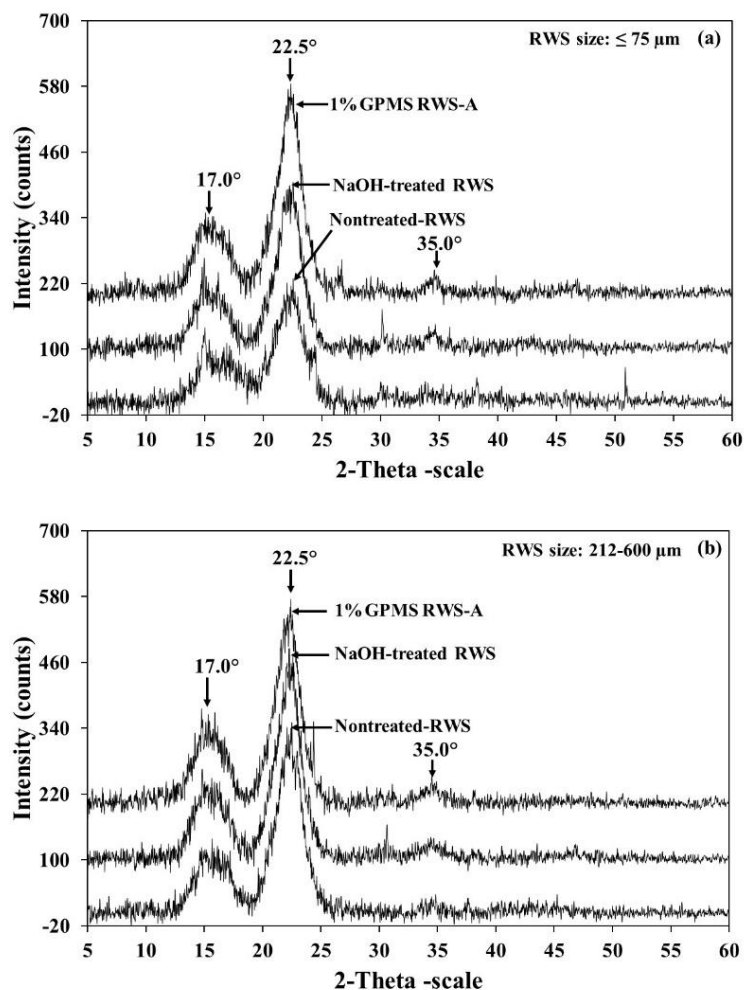


Figure 4.22 XRD patterns of nontreated-RWS, NaOH-treated RWS and 1%GPMS-A with different particle size: (a) $\leq 75 \mu\text{m}$ and (b) 212-600 μm .

TGA and DTG thermograms of the smaller and the larger particle RWS obtained from TGA are displayed in Figure 4.23(a) and (b), respectively. The onset degradation temperature ($T_{d \text{ onset}}$) and the degradation temperature (T_d) of RWS are listed in Table 4.3. $T_{d \text{ onset}}$ was the temperature of degradation at initial weight loss obtained from TGA thermogram, and T_d was the temperature at the peak of DTG thermogram. For the smaller particle RWS ($\leq 75 \mu\text{m}$), it was found that surface treatment increased thermal stability of RWS. NaOH treatment significantly increased the thermal degradation temperatures of RWS which might be because of elimination of some hemicellulose and impurities, and its thermal degradation temperatures slightly

increased after GPMS treatment [1]. For the larger particle RWS (212-600 μm), NaOH treatment did not change thermal stability of RWS, whereas GPMS treatment increased its thermal stability. The higher thermal stability of GPMS treatment might be relevant to the occurrence of Si on the surface of RWS as displayed in Figure 4.15(c).

These results demonstrated that surface treatment by method A could eliminate hemicellulose and non-essential parts which corresponded with FTIR and SEM results. In addition, the eliminating of hemicellulose and non-essential parts which were an amorphous parts increased the crystallinity index (CI) resulting to increase the thermal stability of RWS [1].

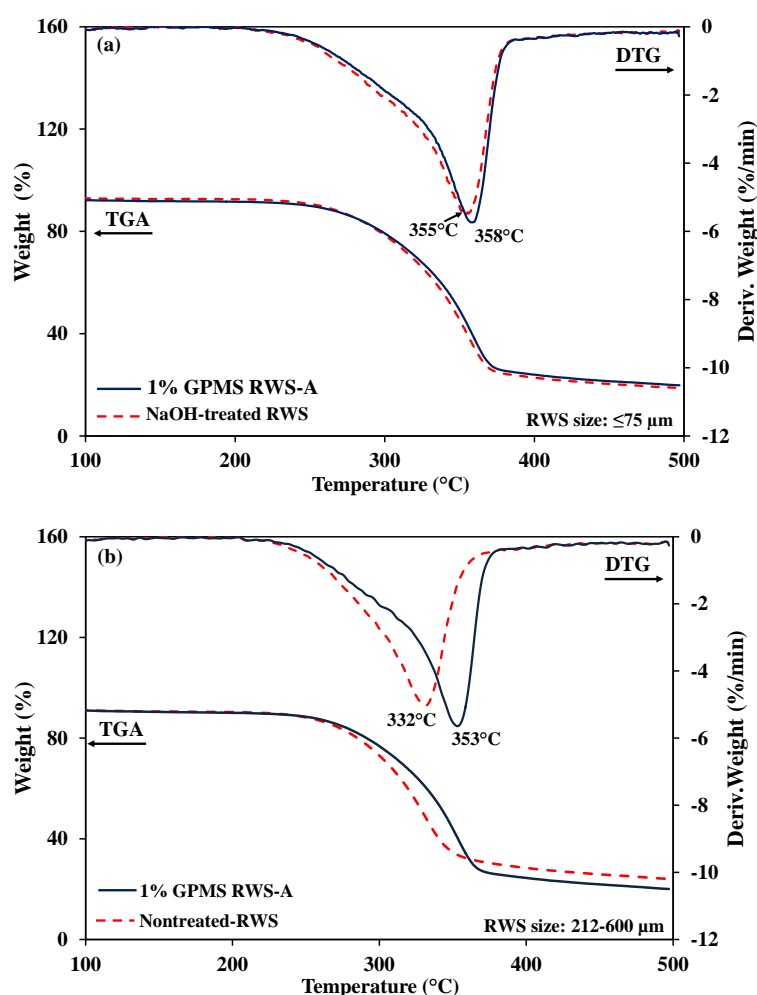


Figure 4.23 TGA and DTG graph of RWS before and after treatment with different particle size: (a) $\leq 75 \mu\text{m}$ and (b) 212-600 μm .

4.1.3 Effect of surface treatment on unfoamed PLA/RWS properties

4.1.3.1 Impact strength

(i) Particle size of $\leq 75 \mu\text{m}$

Figure 4.24 and 4.25 show the impact strength of PLA compounds containing the RWS treated with GPMS using method A and B, respectively. The PLA/RWS sample was the PLA compound containing nontreated-RWS. It was found that NaOH treatment and 1%GPMS-A treatment slightly improved the Izod impact strength of PLA. The addition of 1%GPMS-A 75 to PLA showed the highest impact strength, and the impact strength decreased as increased GPMS-A concentration. It seem that the addition of RWS treated by method A produced the compound showing higher impact strength than that of the addition of RWS treated by method B (Figure 4.26).

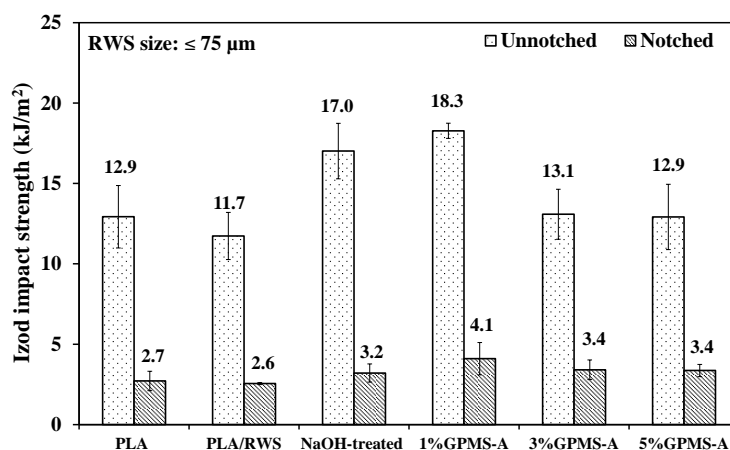


Figure 4.24 Effect of alkaline treatment and GPMS treatment using method A on Izod impact strength of PLA compounds (particle size: $\leq 75 \mu\text{m}$).

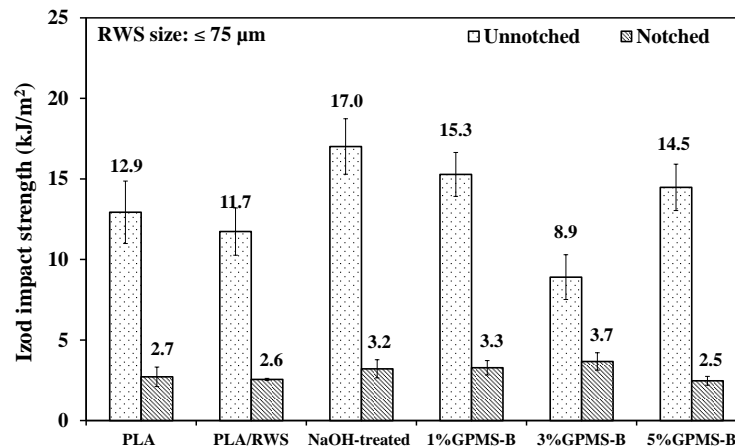


Figure 4.25 Effect of alkaline treatment and GPMS treatment using method B on Izod impact strength of PLA compounds (particle size: $\leq 75 \mu\text{m}$).

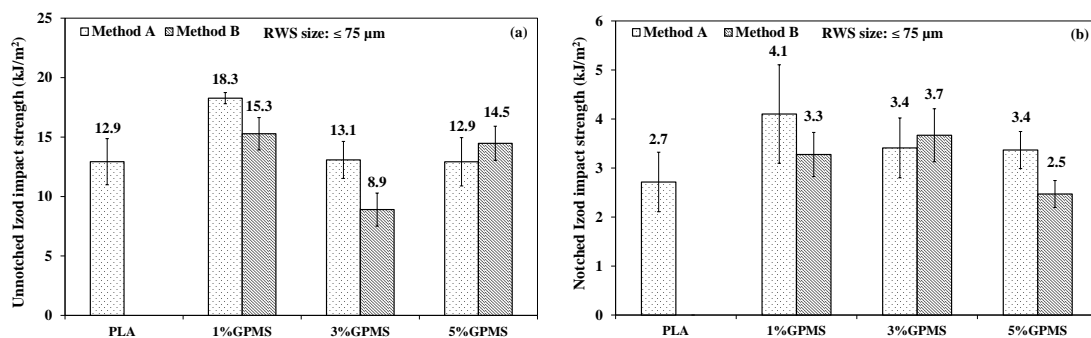


Figure 4.26 Effect of surface treatment method on (a) unnotched Izod impact strength and (b) notched Izod impact strength of PLA compounds (particle size: $\leq 75 \mu\text{m}$).

(ii) Particle size of 212-600 μm

Effect of surface treatment of the larger particle RWS with NaOH and GPMS using method A and B on Izod impact strength are shown in Figure 4.27 - 4.29. It was found that the addition of NaOH-treated RWS to PLA significantly decreased the impact strength (Figure 4.27 and 4.28), and the addition of RWS treated with GPMS by method A produced the compound showing higher impact strength than that of the addition of RWS treated with GPMS by method B, at all GPMS content except at 5 %GPMS (Figure 4.29). GPMS content had effect on the impact strength of PLA compounds depending on the treatment method. For example, the compound of

PLA/5%GPMS-B showed the highest impact strength in the unnotched specimen, and it showed the similar impact strength to PLA and to other PLA/RWS compounds in the notched specimens (Figure 4.28). In addition, PLA/GPMS-A RWS compound using only 1%GPMS showed relatively high impact strength (Figure 4.27), whereas PLA/GPMS-B compound showed high impact strength when the highest GPMS content was used (Figure 4.28). In the GPMS treatment using method A, the RWS was firstly treated by NaOH which could remove hemicellulose and non-essential parts. This resulted to increase surface treatment efficiency, hence, a small amount of GPMS could be used.

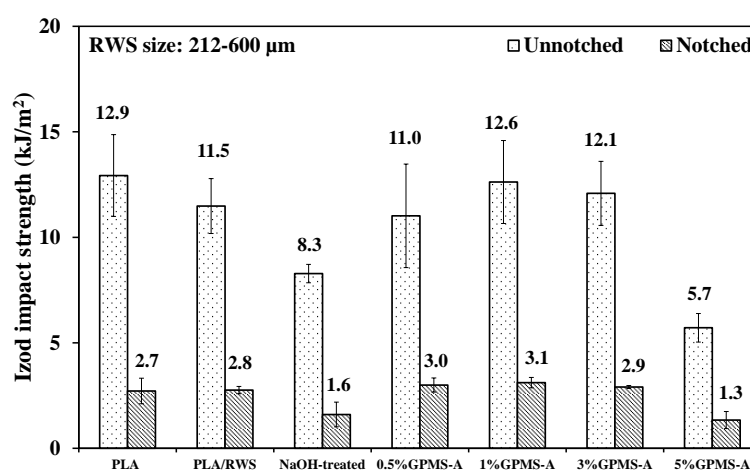


Figure 4.27 Effect of alkaline treatment and GPMS treatment using method A on Izod impact strength of PLA compounds (particle size: 212-600 µm).

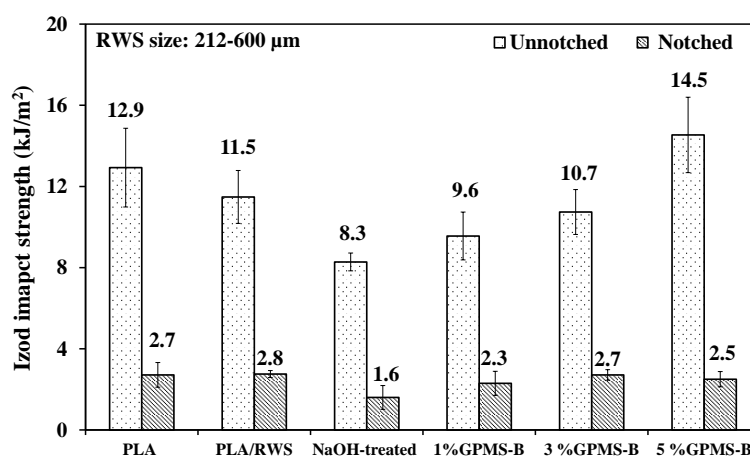


Figure 4.28 Effect of NaOH treatment and GPMS treatment using method B on Izod impact strength of PLA compounds (particle size: 212-600 µm).

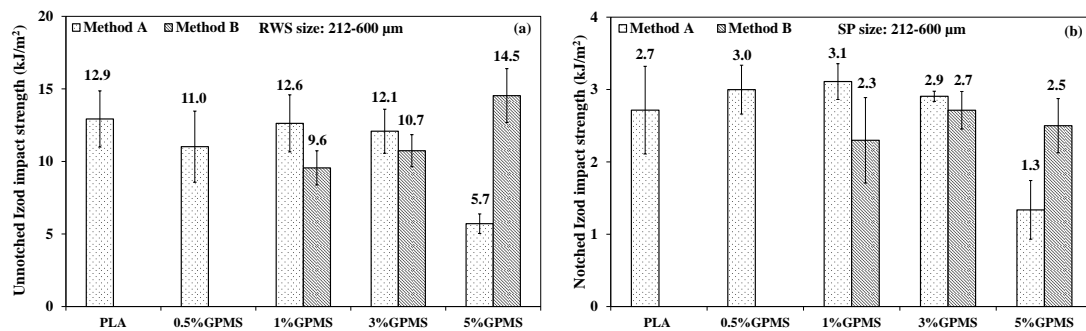


Figure 4.29 Effect of surface treatment method on (a) unnotched Izod impact strength and (b) notched Izod impact strength of PLA compounds (particle size: 212-600 μm).

(iii) Effect of RWS particle size

Effects of RWS particle size and surface treatment method, method A and B, on impact strength of PLA are shown in Figure 4.30 and 4.31. It demonstrated that PLA compounds containing the smaller particle RWS ($\leq 75\mu\text{m}$) showed higher impact strength than that of PLA compounds containing the larger particle RWS.

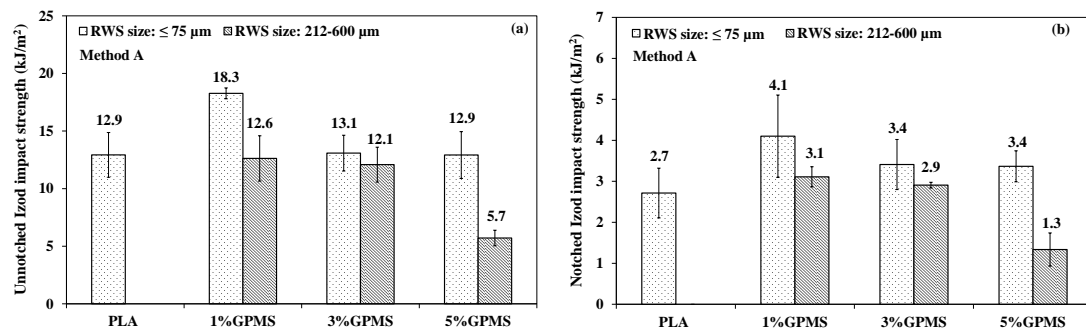


Figure 4.30 Effect of RWS particle size on: (a) unnotched impact strength and (b) notched impact strength of PLA compounds (method A).

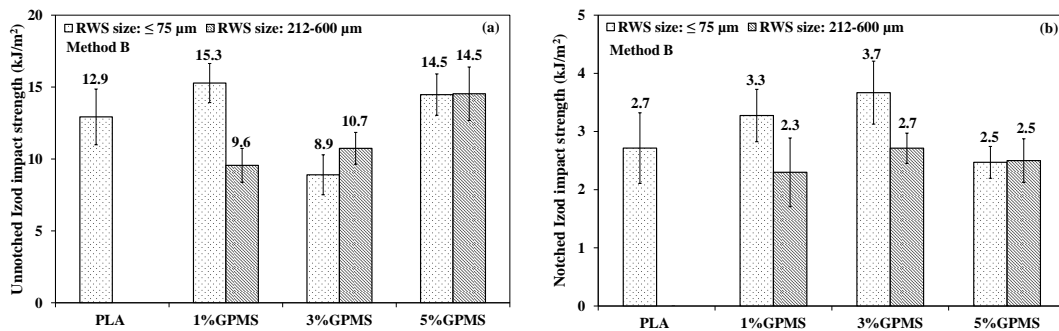
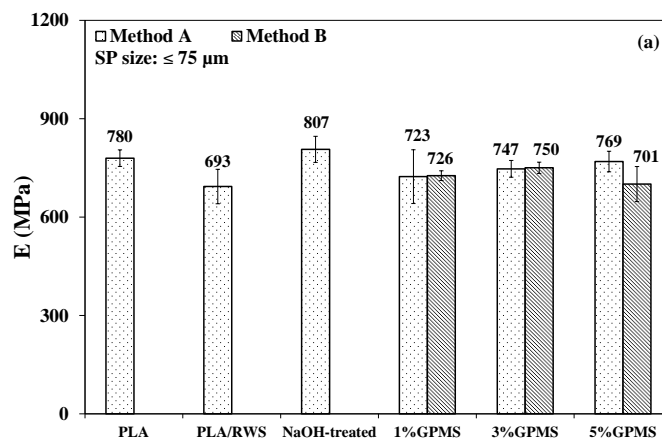


Figure 4.31 Effect of RWS particle size on: (a) unnotched impact strength and (b) notched impact strength of PLA compounds (method B).

4.1.3.2 Tensile properties

Tensile properties of PLA compounds containing the smaller particle RWS ($\leq 75 \mu\text{m}$) are displayed in Figure 4.32(a)-(c). It was found that the addition of nontreated-RWS to PLA decreased tensile properties but the tensile properties increased when the NaOH-treated RWS was used. No significant difference of tensile properties was found when the RWS treated with GPMS by method A and B was used. It seems that the tensile properties of PLA compound containing RWS treated by GPMS using method A was slightly higher than those of the compound containing RWS treated by GPMS using method B.



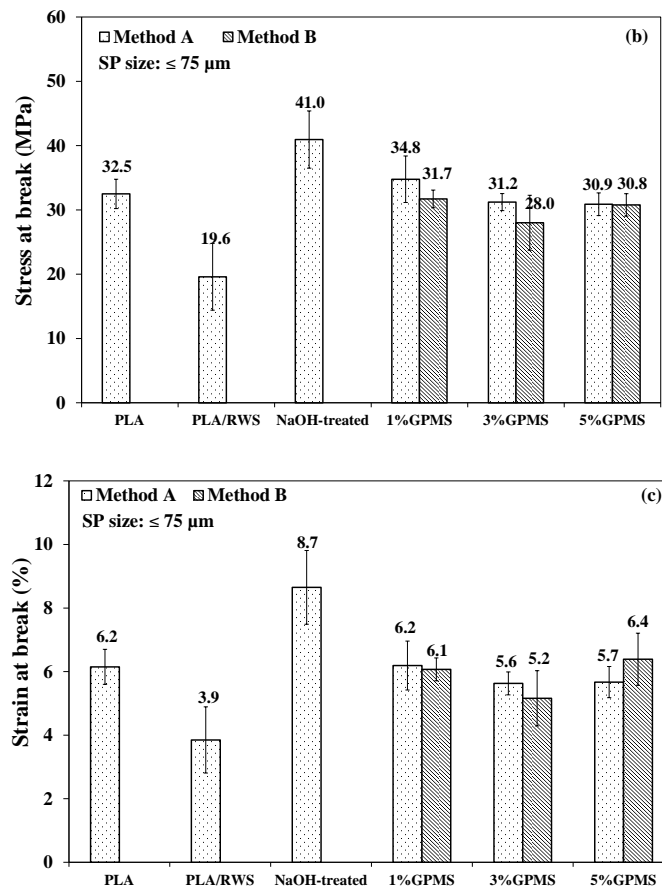


Figure 4.32 Effect of surface treatment method on tensile properties of PLA compounds: (a) modulus, (b) stress at break and (c) strain at break (particle size: $\leq 75 \mu\text{m}$).

Tensile properties of PLA compounds containing the larger particle RWS (212-600 μm) as displayed in Figure 4.33(a)-(c) demonstrated that the addition of nontreated-RWS and NaOH-treated RWS to PLA decreased the tensile properties. The compound incorporated with RWS treated by method A with the suitable GPMS content (1%GPMS-A) showed the highest stress at break and strain at break. The tensile properties of PLA compounds containing GPMS-treated RWS using method A in all GPMS content was slightly higher than those of PLA compounds containing GPMS-treated RWS by method B, except PLA compound containing 5%GPMS-B RWS. The mechanical properties of PLA compounds containing both particle size RWS treated with different surface treatment method at the ratio of 95/5 (PLA/RWS) are listed in Table 4.4.

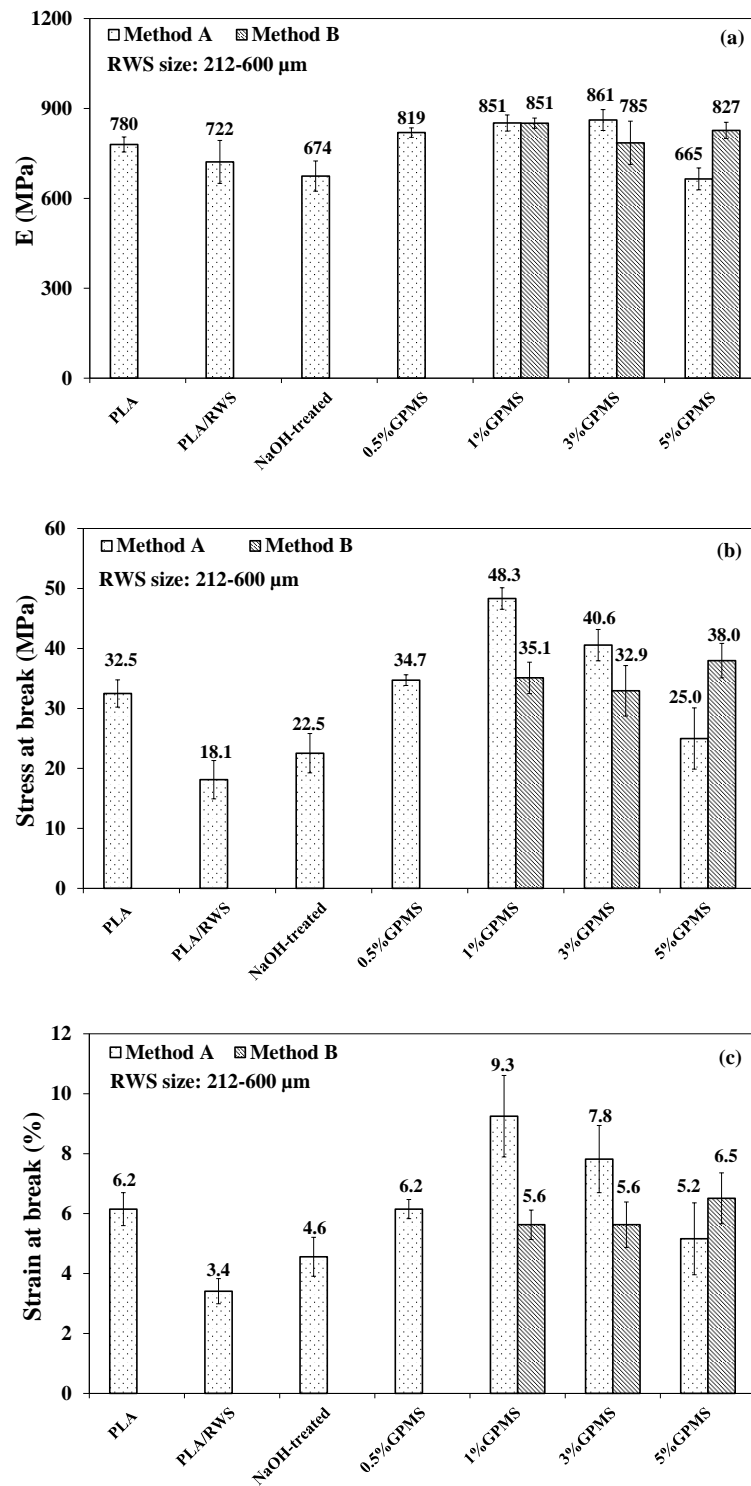


Figure 4.33 Effect of surface treatment method on tensile properties of PLA compounds: (a) modulus, (b) stress at break, and (c) strain at break. (particle size: 212-600 μm).

Table 4.4 Mechanical properties of PLA composites containing 5 wt% of RWS with particle size of $\leq 75 \mu\text{m}$ and 212-600 μm

Composition	Particle size (μm)	Izod impact strength (kJ/m^2)		Tensile properties		
		Unnotched	Notched	Modulus (MPa)	Stress at break (MPa)	Strain at break (%)
PLA	-	12.9 ± 1.9	2.7 ± 0.6	780 ± 25	32.5 ± 2.3	6.2 ± 0.6
PLA/nontreated-RWS	≤ 75	11.7 ± 1.5	2.6 ± 0.1	722 ± 72	18.1 ± 3.2	3.4 ± 0.4
PLA/NaOH-RWS		17.0 ± 1.7	3.2 ± 0.6	806 ± 40	41.0 ± 4.4	8.7 ± 1.2
PLA/1%GPMS-A		18.3 ± 0.5	4.1 ± 1.0	723 ± 82	34.8 ± 3.6	6.2 ± 0.8
PLA/3%GPMS-A		13.1 ± 1.6	3.4 ± 0.6	747 ± 26	31.2 ± 1.3	5.6 ± 0.4
PLA/5%GPMS-A		12.9 ± 2.0	3.4 ± 0.6	769 ± 31	30.9 ± 1.8	5.7 ± 0.5
PLA/1%GPMS-B		15.3 ± 1.4	3.3 ± 0.4	726 ± 15	31.7 ± 1.4	6.1 ± 0.4
PLA/3%GPMS-B		8.9 ± 1.4	3.7 ± 0.5	750 ± 17	28.0 ± 4.3	5.2 ± 0.9
PLA/5%GPMS-B		14.5 ± 1.4	2.5 ± 0.3	701 ± 53	30.8 ± 1.8	6.4 ± 0.8
PLA/nontreated-RWS		212-600	11.5 ± 1.3	2.8 ± 0.2	758 ± 53	19.6 ± 5.2
PLA/NaOH-RWS	8.3 ± 0.4		1.6 ± 0.6	674 ± 50	22.5 ± 3.3	4.6 ± 0.7
PLA/0.5%GPMS-A	11.0 ± 2.5		3.0 ± 0.3	819 ± 16	34.7 ± 0.9	6.2 ± 0.3
PLA/1%GPMS-A	12.6 ± 2.0		3.1 ± 0.3	851 ± 27	48.3 ± 1.8	9.3 ± 1.4
PLA/3%GPMS-A	12.1 ± 1.5		2.9 ± 0.1	861 ± 35	40.6 ± 2.6	7.8 ± 1.1
PLA/5%GPMS-A	5.7 ± 0.7		1.3 ± 0.4	665 ± 37	25.0 ± 5.1	5.2 ± 1.2
PLA/1%GPMS-B	9.6 ± 1.2		2.3 ± 0.6	851 ± 17	35.1 ± 2.6	5.6 ± 0.5
PLA/3%GPMS-B	10.7 ± 1.1		2.7 ± 0.3	785 ± 72	32.9 ± 4.2	5.6 ± 0.8
PLA/5%GPMS-B	14.5 ± 1.9		2.5 ± 0.4	827 ± 27	38.0 ± 2.9	6.5 ± 0.9

4.1.4 Effect of silane type on unfoamed PLA/RWS properties

Based on mechanical properties in Table 4.4, the PLA/RWS compounds exhibiting relatively high mechanical were selected to compare with PLA compounds containing RWS treated with 3-aminopropyl trimethoxysilane (APMS). The compositions were shown in Table 4.5 and effect of silane type on mechanical and thermal properties of PLA compounds were observed as following.

Table 4.5 Composition of unfoamed PLA/treated-RWS compounds to observe effect of silane type on mechanical properties of PLA compounds

Compounds	Particle size (μm)	PLA/treated-RWS ratios
2 nd ext PLA	-	100/0
PLA/NaOH 75	$\leq 75\mu\text{m}$	95/5
PLA/1% GPMS-A 75	$\leq 75\mu\text{m}$	95/5
PLA/1% APMS-A 75	$\leq 75\mu\text{m}$	95/5
PLA/1% GPMS-A 212-600	212–600 μm	95/5
PLA/1% APMS-A 212-600	212–600 μm	95/5

4.1.4.1 Impact strength

Effect of silane type on Izod impact strength is shown in Figure 4.34. It was found that the PLA compounds containing 1%GPMS-A (both particle sizes) showed higher impact strength than that of PLA compounds containing 1%APMS-A. In addition, the compounds of PLA/NaOH-treated 75 and PLA/1%GPMS-A 75 showed the higher impact strength than that of the neat PLA, and the compound of PLA/1%GPMS-A 75 showed the highest impact strength.

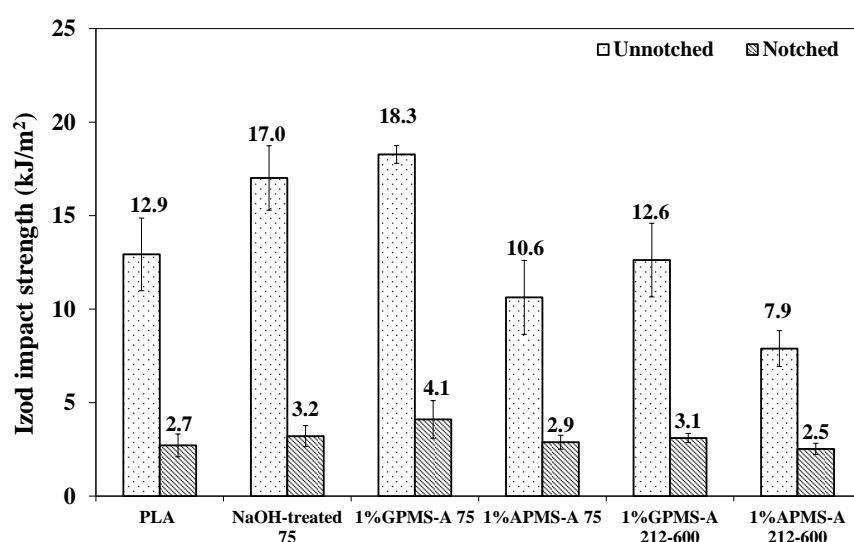
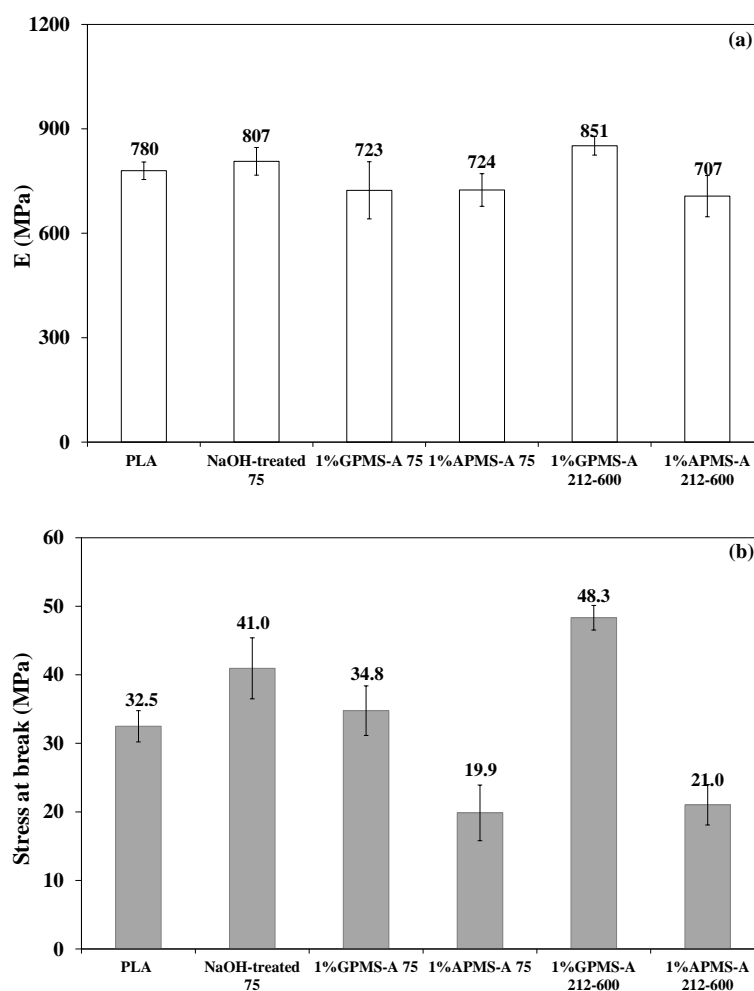


Figure 4.34 Effect of silane type on Izod impact strength of PLA compounds.

4.1.4.2 Tensile properties

Effect of silane type on tensile properties of the PLA compounds are displayed in Figure 4.35(a)-(c). The tensile stress and strain at break of PLA blended with 1%GPMS-A RWS (both particle sizes) were higher than those of PLA blended with 1%APMS-A RWS (Figure 4.35 (b) and (c)). The compound of PLA/1%GPMS 212-600 showed the highest tensile properties. The mechanical properties of PLA compounds indicated that the PLA compounds containing RWS treated with NaOH or GPMS by method A showed the higher mechanical properties than those of PLA compounds containing with RWS treated with APMS.



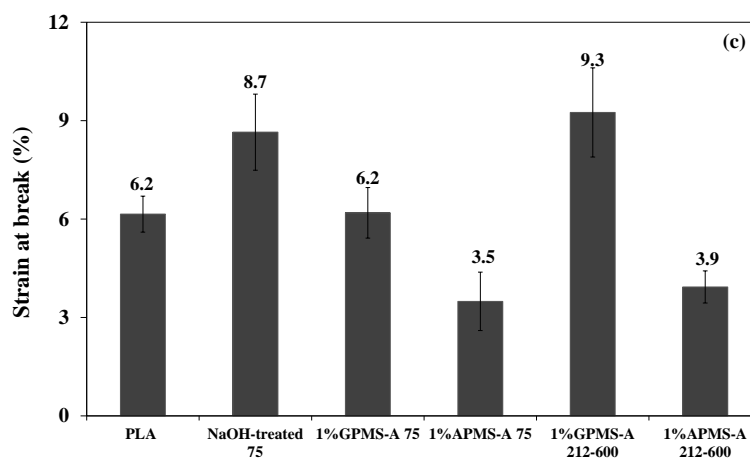


Figure 4.35 Effect of silane coupling agent type on tensile properties of PLA compounds: (a) modulus, (b) stress at break and (c) strain at break.

4.1.4.3 Thermal properties

Thermal properties of PLA and PLA compounded pellets containing 1 wt% RWS were characterized by DSC. Figure 4.36 and 4.37 display DSC thermograms PLA and PLA blended with the smaller particle RWS ($\leq 75\mu\text{m}$) and the larger particle RWS (212-600 μm), respectively. The thermal transition temperature determined from the first and second heating scan DSC thermograms are listed in Table 4.6 and 4.7, respectively. In the first heating scan DSC thermograms (Figure 4.36(a) and 4.37(a)), the cold crystallization peak was not found in the PLA curve but it was observed in PLA 2nd ext (the PLA pellet obtained from twice time extrusion) and all PLA compounds. It indicated that recrystallization of the polymer occurred during heating caused by a small molecule occurred during twice time extrusion. The cold crystallization had not effect on mechanical properties of the PLA 2nd ext and PLA compounds but it had effect on their melting transition. Two endothermic melting with border peaks were found in all PLA compounds, except the compound of PLA/RWS. The endothermic peaks were at around 152 °C and 158 °C corresponding to melting temperatures of α' crystalline form occurred during recrystallization and ordered α crystalline form of PLA, respectively [11]. The PLA/RWS compound showed only one endothermic melting peak but the peak was wider and border than that of PLA. In addition, all samples showed the glass transition peaks due to residual stress caused by

quickly cooling after melt blending in extruder which normally found in polyester such as PLA. It could be seen that the glass transition peaks disappeared after second heating by DSC (Figure 4.36(c) and 4.37(c)).

The second heating scan DSC thermograms were used to observed thermal properties of PLA and PLA compounds because the different thermal history of all samples were completely deleted. T_g and T_m of PLA were 56.8°C and 155°C, respectively. After twice time extrusion, the T_g and T_m of PLA 2nd ext were slightly increased to 61.6°C and 158°C, respectively. The cold crystallization peaks and two melting peaks were clearly observed in PLA 2nd ext and all PLA compounded samples. No significant changes of thermal temperature were found in all PLA compounds. The T_g and T_m of PLA blended with smaller particle RWS ($\leq 75 \mu\text{m}$) were ranging from 56.0 to 60.6°C and 155 to 158°C, respectively. The T_g and T_m of PLA blended with larger size RWS (212-600 μm) were ranging from 53.2 to 55.9°C and 154 to 156°C, respectively (Table 4.7).

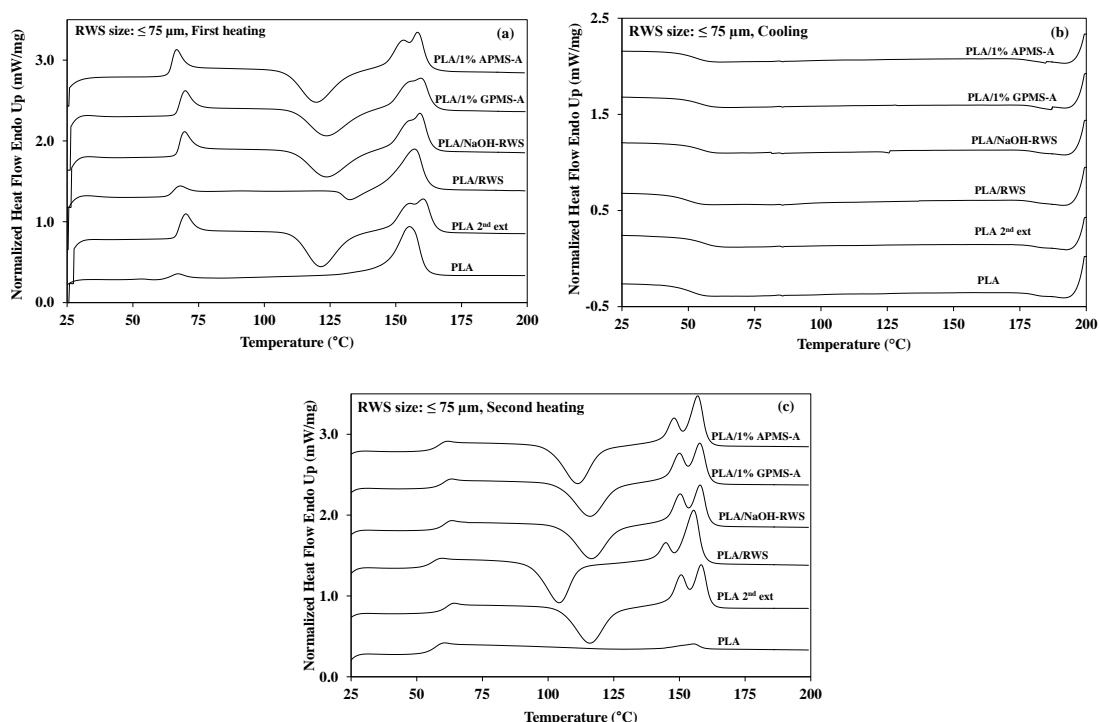


Figure 4.36 DSC thermograms of PLA and PLA compound pellets containing 1 wt% RWS (particle size: $\leq 75 \mu\text{m}$).

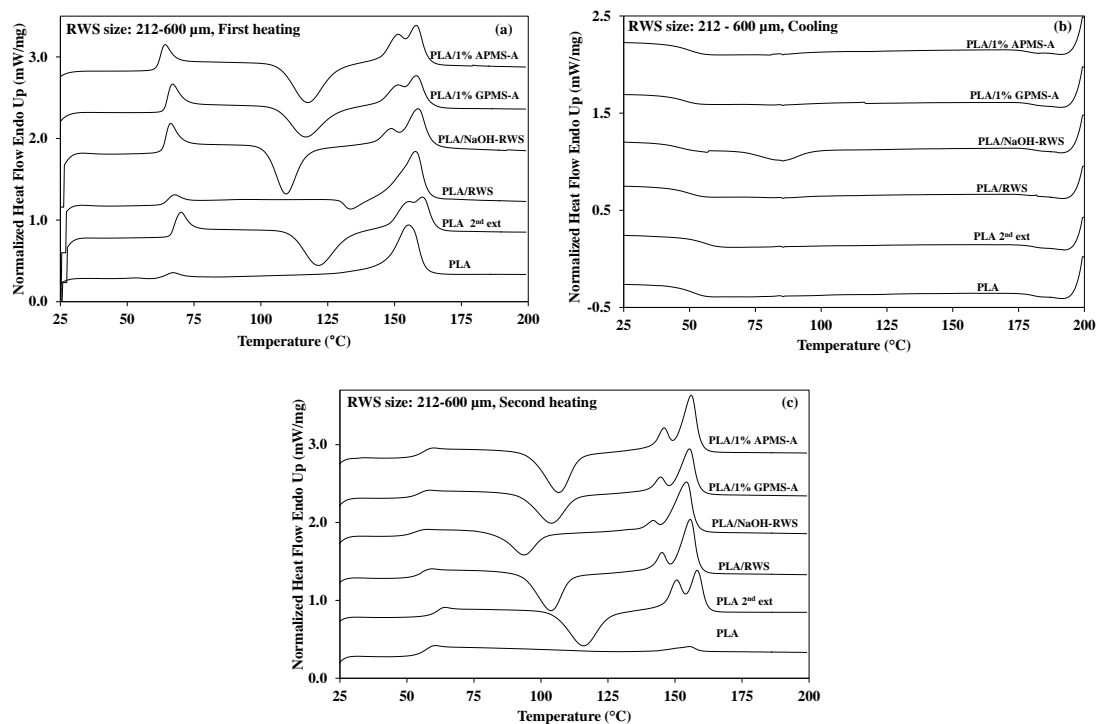


Figure 4.37 DSC thermograms of PLA and unfoamed PLA composite with 1 wt% of RWS (particle size: 212-600 μm).

Table 4.6 Thermal properties determined from the first heating and cooling scan of DSC thermograms

Sample	First heating			Cooling	
	T_g ($^{\circ}\text{C}$)	T_m ($^{\circ}\text{C}$)		T_g ($^{\circ}\text{C}$)	
PLA	64.8	-	155	-	51.0
PLA 2 nd ext	68.3	155	160	122	55.1
PLA/RWS 75	65.8	-	157	133	50.1
PLA/NaOH-RWS 75	68.0	-	159	124	54.9
PLA/1%GPMS-A 75	68.2	154	159	124	53.6
PLA/1%APMS-A 75	65.2	153	158	120	52.6
PLA/RWS 212-600	65.8	-	158	134	50.3
PLA/NaOH-RWS 212-600	64.7	149	159	109	46.1
PLA/1%GPMS-A 212-600	65.4	151	158	117	48.2
PLA/1%APMS-A 212-600	62.7	151	158	118	49.7

Footnote: (PLA/RWS = 95/5, wt/wt)

Table 4.7 Thermal properties determined from the second heating scan of DSC thermograms

Sample	T _g (°C)	T _m (°C)		T _{cc} (°C)	ΔH _m (J/g)	ΔH _{cc} (J/g)	X _{c1} (%)	X _{c2} (%)
PLA	56.8	-	155	-	4.1	-	4.4	4.4
PLA 2 nd ext	61.6	151	158	116	36.1	-33.2	3.1	38.8
PLA/RWS 75	56.0	145	155	104	40.6	-32.8	8.4	43.7
PLA/NaOH-RWS 75	60.6	150	158	116	34.5	-33.8	0.8	37.1
PLA/1%GPMS-A 75	60.3	150	158	116	34.7	-32.9	1.9	37.4
PLA/1%APMS-A 75	58.3	148	157	111	38.7	-35.0	4.0	41.7
PLA/RWS 212-600	55.6	145	156	104	39.7	-31.9	8.5	42.7
PLA/NaOH-RWS 212-600	53.2	142	154	93.8	39.8	-20.8	20.5	42.9
PLA/1%GPMS-A 212-600	54.6	145	155	104	34.1	-29.6	4.8	36.7
PLA/1%APMS-A 212-600	55.9	146	156	107	42.3	-37.2	5.5	45.5

Footnote: (PLA/RWS = 95/5, wt/wt)

The degree of crystallinity by excluding ΔH_{cc} (X_{c1}) and the total degree of crystallinity (X_{c2}) were determined from the second heating scan DSC curves as listed in Table 4.7. By excluding ΔH_{cc} , the addition of the larger particle RWS (212-600 μm) to PLA increased X_{c1} . It was clearly showed in the compound of PLA/NaOH-RWS 212-600. The addition of NaOH-RWS 212-600 to PLA increased X_{c1} from 4% (PLA) to 21%. The addition of the smaller particle RWS ($\leq 75\mu\text{m}$) to PLA decrease X_{c1} of PLA, except the addition of nontreated-RWS (RWS75), it increased X_{c1} of PLA from 4% to 9%. The addition of RWS (both particle sizes) to PLA increased the total degree of crystallinity (X_{c2}).

4.2 Properties and characterization of PLA foams

The suitable average pore size is required for using as scaffold in tissue engineering. Thus, amount of blowing agent and accelerator in PLA foam preparation is important. In the present study, AZDC and ZnO were used as chemical blowing agent and accelerator, respectively. The effect of ZnO content on cellular structure and average pore size was observed to determine a suitable AZDC/ZnO ratio for preparation

PLA/RWS, PLA/PEG/CH and PLA/CH/RWS foams. The AZDC/ZnO ratio was varied to 3/0, 3/0.3, 3/0.5 and 3/1.0 as shown in Table 3.9. The PLA foam prepared by using AZDC/ZnO ratio of 3/0.1 was not used in this experiment because it was prepared with different instrument condition. This foam was discussed in the topic 4.3 and 4.4. Three mold dimension were used to prepare PLA foam (Topic 3.3.7.2). It was found that the PLA foams were successfully prepared by using the mold dimension of 13 cm x 13 cm x 2 mm at 150°C for 10 min at the pressure of 150 kg/cm². The PLA foam properties including pore structure, average pore size, foam density, void fraction, mechanical and thermal properties and *in-vitro* degradation were observed.

4.2.1 Morphology and physical properties

The SEM images demonstrating nine zones of pore morphology of foam specimens in the present study are displayed in appendix A (Figure A2 to A4). The SEM images of PLA foams containing different AZDC/ZnO ratio, 3/0.3, 3/0.5 and 3/1.0, are shown in Figure 4.38. The pore morphology of PLA foam containing 3/0 AZDC/ZnO ratio was not examined because the foam sample was very dense. The closed cell morphology with irregular direction was observed in all PLA foam samples.

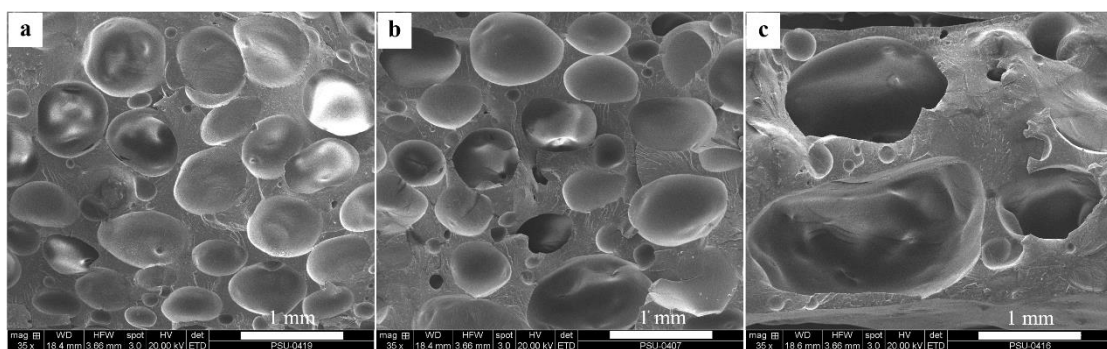


Figure 4.38 SEM image of PLA foams with different AZDC/ZnO ratios: (a) 3/0.3, (b) 3/0.5 and (c) 3/1.0.

The average pore size for each zone (Zone A, B and C), the average pore size of 3 zones, density and void fraction (% VF) of PLA foam were determined as listed in Table 4.8. Average pore sizes of zone A and B of PLA foam increased as increased

ZnO content whereas average pore size of zone C did not show this trend (Figure 4.39). The PLA foam without ZnO (PLA0) exhibited the highest density and the lowest %VF (Table 4.8). As increased ZnO content, the average pore size and %VF of PLA foam increased, whereas its density decreased (Figure 4.40). It was due to increasing the efficiency of AZDC decomposition by increasing of ZnO content [12].

Table 4.8 Average pore size and physical properties of PLA foams with different ZnO contents

Foam sample	Average pore size for each zone (μm)			Average pore size of 3 zones	Density (g/cm^3)	%VF
	Zone A	Zone B	Zone C			
PLA0	N/A	N/A	N/A	N/A	0.815	33.4
PLA0.3	684 ± 106	890 ± 77	808 ± 110	794 ± 104	0.695	43.1
PLA0.5	904 ± 165	1131 ± 59	746 ± 33	927 ± 193	0.652	46.7
PLA1.0	1238 ± 298	1156 ± 191	1280 ± 132	1224 ± 63	0.628	48.7

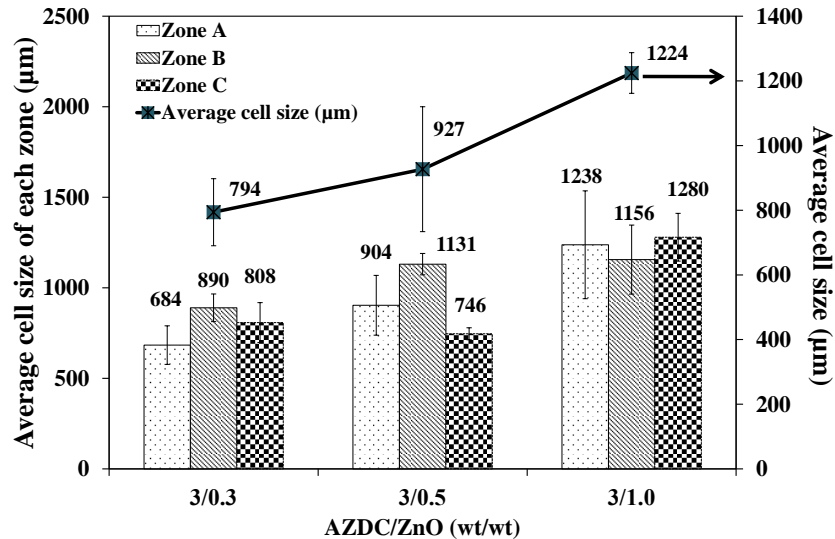


Figure 4.39 Effect of ZnO content on average pore size of PLA foams.

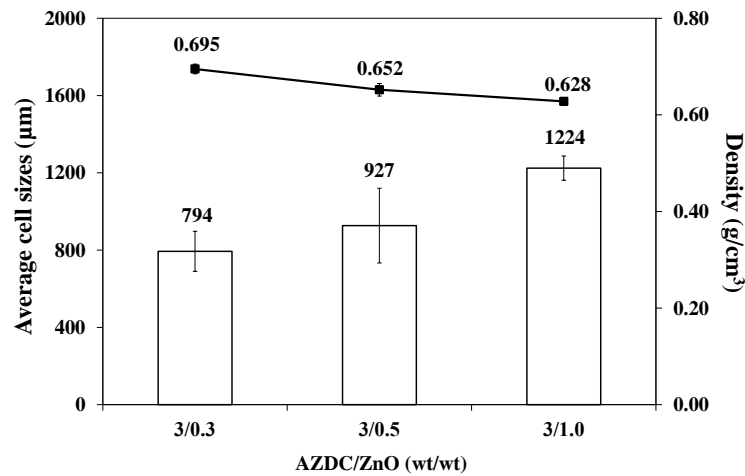


Figure 4.40 Effect of ZnO content on the relation of average pore size and density of PLA foams.

4.2.2 Mechanical properties

The notched Izod impact strength of PLA foam significantly decreased with the incorporation of ZnO and it slightly decreased as increased ZnO content (Figure 4.41). The effect of ZnO content on tensile and flexural properties was found similarly to the impact strength as shown in Figure 4.42 and 4.43, respectively. As mentioned above, ZnO acted as the accelerator to increase AZDC decomposition efficiency resulting to decrease density and increase average pore size of PLA foams. The larger average pore size caused the lower mechanical properties of PLA foams.

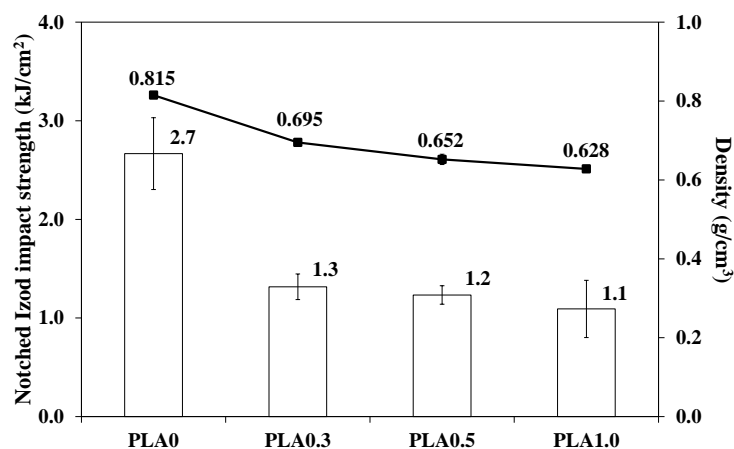


Figure 4.41 Effect of ZnO contents on notched Izod impact strength and density of PLA foams.

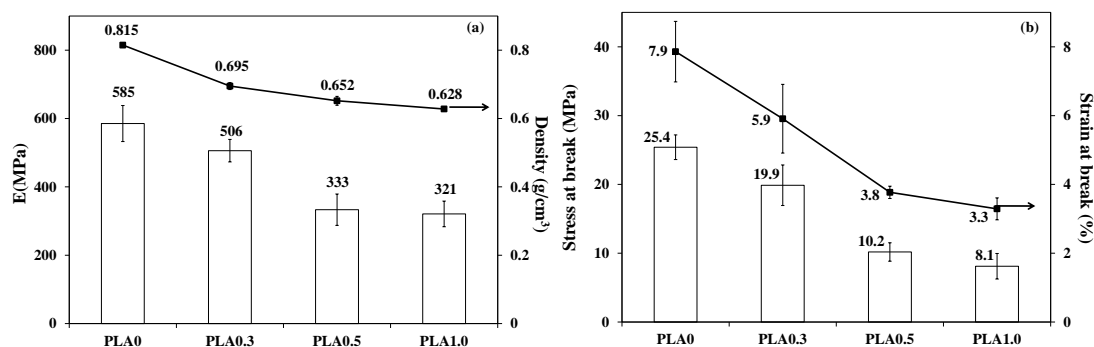


Figure 4.42 Effect of ZnO contents on tensile properties of PLA foams: (a) modulus and (b) stress at break and strain at break.

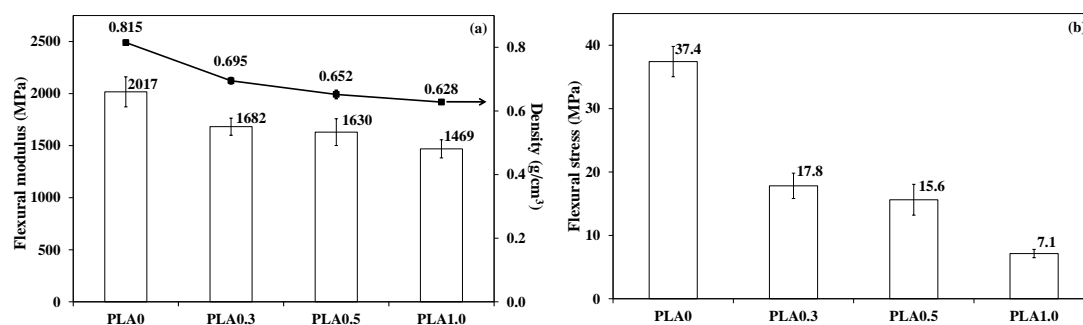


Figure 4.43 Effect of ZnO contents on flexural properties of PLA foams: (a) flexural modulus and density and (b) flexural stress.

4.2.3. Thermal degradation properties

The thermal decomposition of AZDC was determined using TGA technique. The TGA and DTG thermograms are displayed in Figure 4.44. Reyes *et al.* [13] reported that the decomposition of AZDC generated from the competition of at least 3 exothermic reactions. The decomposition of AZDC produces solids and gaseous mixtures of nitrogen, carbon monoxide, ammonia and cyanic acid. The present study found that AZDC demonstrated three decomposition temperatures (T_d) containing 218°C, 242°C and 316°C corresponded to 3 different exothermic reactions [13].

Figure 4.45 shows TGA and DTG thermograms of PLA pellets and PLA foams with different ZnO content and the thermal degradation temperature are listed in Table 4.9. The thermal stability of PLA foam decreased as increased ZnO content. PLA pellet showed only one thermal degradation temperature (T_{d2}) at 359°C but PLA foams

showed 2 thermal degradation temperature: the very small peak (T_{d1}) and the sharp peak (T_{d2}). The T_{d1} was expected to be a decomposition of remaining AZDC and T_{d2} corresponded to thermal degradation temperature of PLA. In addition, it could be seen that the $T_{d\text{ onset1}}$ and T_{d1} of PLA foam decreased with increasing ZnO content. This demonstrated that ZnO activated decomposition rate and decreased decomposition temperature of AZDC (Table 4.9). It was in accordance with the previous study [12].

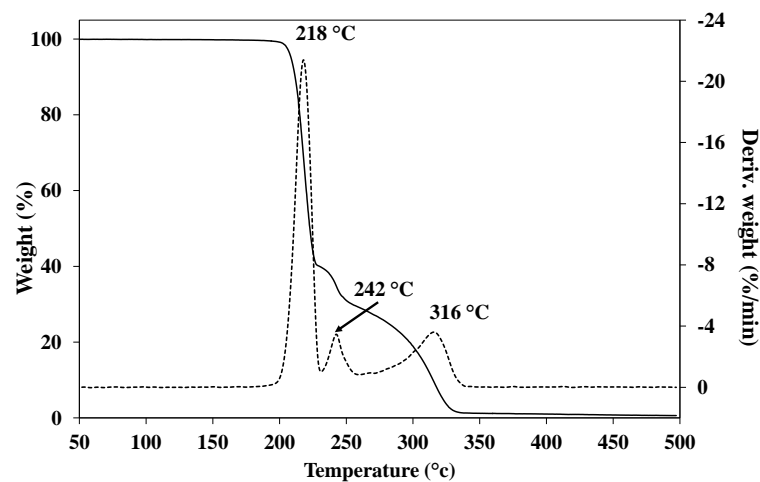


Figure 4.44 TGA and DTG curves of AZDC.

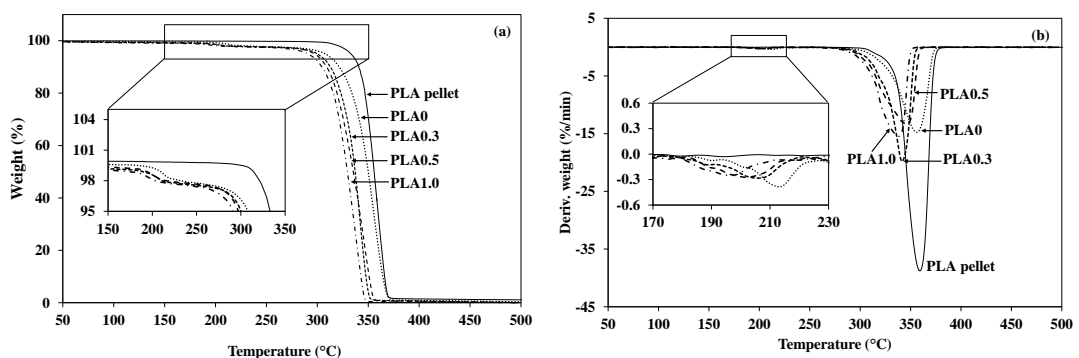


Figure 4.45 (a) TGA and (b) DTG curves of PLA and PLA foams with different AZDC/ZnO ratios

Table 4.9 Thermal degradation temperatures of PLA and foamed PLA with different ZnO contents

Sample	T _{d onset1} (°C)	T _{d onset2} (°C)	T _{d1} (°C)	T _{d2} (°C)	T _{d end} (°C)
PLA (pellet)	-	344	-	359	368
PLA0	201	334	213	356	367
PLA0.3	196	329	206	342	348
PLA0.5	188	317	201	346	346
PLA1.0	182	314	197	338	338

4.2.4. FTIR analysis

FTIR technique was utilized to confirm the remaining AZDC in the PLA foams as shown in Figure 4.46. The shifted characteristic peaks of AZDC/ZnO (3/1) was observed in the FTIR spectrum of PLA1.0 foam. The characteristic peak at 1115 cm⁻¹ corresponded to the stretching vibration of C=O and N-C of AZDC shifted to 1127 cm⁻¹, and the peak at 1364 cm⁻¹ corresponded to the bending vibration of N-C=O of AZDC shifted to 1361 cm⁻¹ [14]. The thermal degradation and FTIR results indicated the remaining of AZDC in the PLA foams.

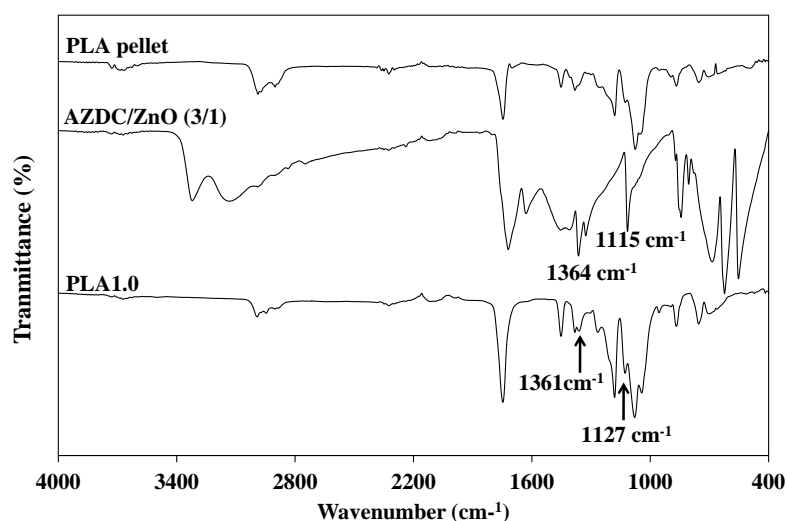


Figure 4.46 FTIR spectra of PLA pellet, AZDC/ZnO (3/0.1 wt/wt) and PLA1.0 foam.

4.2.5 *In-vitro* degradation properties

Scaffold requires a suitable time in degradation and resorption until the tissue engineering transplant process is successfully remodeled by the host tissue [15]. Thus, *in-vitro* degradation testing in term of weight loss percentage (% weight loss) was used in this research to preliminary evaluate the suitability of the PLA foams for bone scaffold application. The % weight loss after immersion in PBS for 8 weeks of PLA foam specimen is displayed in Figure 4.47. It was found that ZnO content influentially affected foam degradation behavior. The degradation rate of all foam specimens was similar in the first week. Since the second week, the % weight loss and *in-vitro* degradation rate increased with increasing ZnO content. The rate of degradation decreased after 4 weeks, and the % weight loss and degradation rate still increased with increasing ZnO content. It was because the higher ZnO content provided the lager average pore size which enhanced the PBS penetration to degrade the foam specimens [16]. After the end of testing, the % weight loss of PLA foams ranked from 0.66 to 1.73%. It was lower than those of PLA scaffold fabricated by solvent casting followed by porogen leaching method [17]. This indicated that PLA foams showed relatively low *in-vitro* degradation.

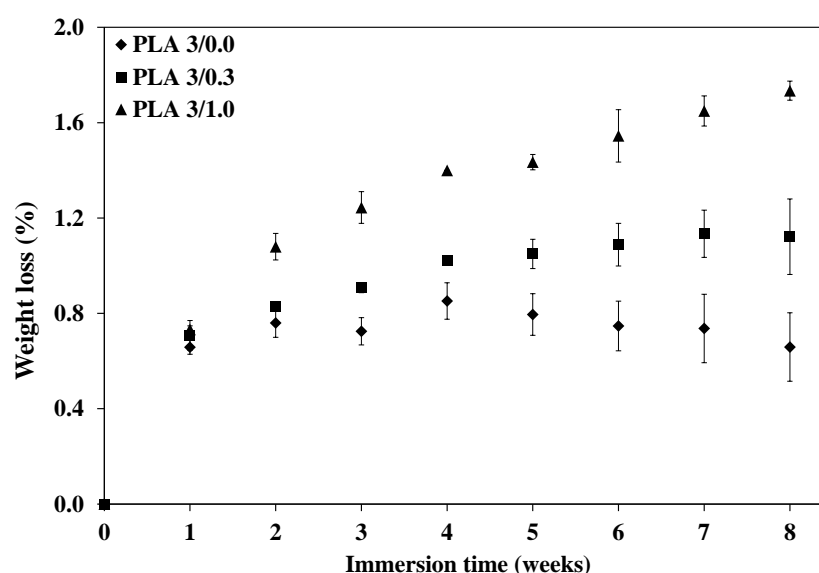


Figure 4.47 Effect of ZnO contents on *in-vitro* degradation of PLA foams.

4.3 Properties and characterization of PLA/RWS compounded foams

Based on mechanical properties of unfoamed PLA blended with various nontreated-RWS particles sizes and contents (Table 4.1), we concluded that the 5 wt% RWS with particle sizes of $\leq 75 \mu\text{m}$ and 212-600 μm were the optimal condition in this topic. The mechanical properties of unfoamed PLA blended with nontreated- and treated-RWS as shown in Table 4.4 demonstrated that PLA blended with the larger particles of nontreated RWS (212-600 μm) showed slightly higher mechanical properties than those of PLA blended with the smaller particles of nontreated RWS ($\leq 75 \mu\text{m}$). In addition, PLA blended with the smaller particles of NaOH-treated RWS ($\leq 75 \mu\text{m}$) showed higher mechanical properties than those of PLA blended with the larger particles of NaOH-treated RWS (212-600 μm). It was found that GPMS treatment by method A had better treatment efficiency than other methods. After silane treatment by method A, the mechanical properties of PLA blended with the smaller and the larger particles RWS were similar and 1wt% GPMS was the optimal concentration. Therefore, the compositions for foam preparation in this topic were PLA/NaOH-RWS 75, PLA/1%GPMS-A 75, PLA/nontreated RWS 212-600 and PLA/1%GPMS-A 212-600. The nomenclature of the foams prepared in this topic are listed in Table 3.9 (foam no. 2 and foam no. 6 to 9). In addition, based on the topic 4.2, the PLA foam containing 3/0.3 AZDC/ZnO ratio showed the least average pore size, $794 \pm 104 \mu\text{m}$, but the pore size suggested for bone regeneration is in the range of 50-710 μm [18]. Therefore, The AZDC/ZnO ratio of 3/0.1 was used to prepare PLA/RWS compounded foams in this topic for lowering foam average pore size. All of PLA/RWS compounded foams were successfully prepared by compression molding at 145°C with the pressure of 150 kg/cm^2 for 10 min. The physical, thermal, mechanical properties, *in-vitro* degradation and cytotoxicity of the foams were observed as following.

4.3.1 Morphology and physical properties

The SEM images demonstrating nine zones of PLA0.1 foam and PLA/RWS compounded foam specimens are displayed in appendix A, Figure A1 and Figure A5 to A8, respectively. The effect of surface treatment and particle size of RWS on pore morphology of the foams is shown in Figure 4.48. All foam samples showed the oval-shaped and closed-cell morphology. Figure 4.48(a) displays pore structure of

PLA0.1 foam without RWS. The pore morphology of All PLA compounded foams, except T0L foam, looked similar to that of the PLA0.1 foam. The very large and very small pore size were found in T0L foam (Figure 4.48(d)), resulting in the largest average pore size and the highest standard deviation. Surface treatment of RWS significantly changed cellular structure which was visible in the T2L foam (Figure 4.48(e)). This foam showed smaller average pore size, lower pore size distribution and better pore uniformity. The surface treatment improved interfacial adhesion between PLA and treated RWS providing a finer pore structure of the foams. This was in accordance with the previous study reported by Mihai *et al.* [19]. They found that the interfacial modification using maleated-PLA as a coupling agent was necessary to obtain fine pore structure in thermoplastic starch (TPS)/PLA blended foam. This phenomena also has been found in wood fiber/HDPE composite foam prepared by extrusion foaming using maleic anhydride grafted HDPE as a coupling agent reported by Guo *et al.* [20].

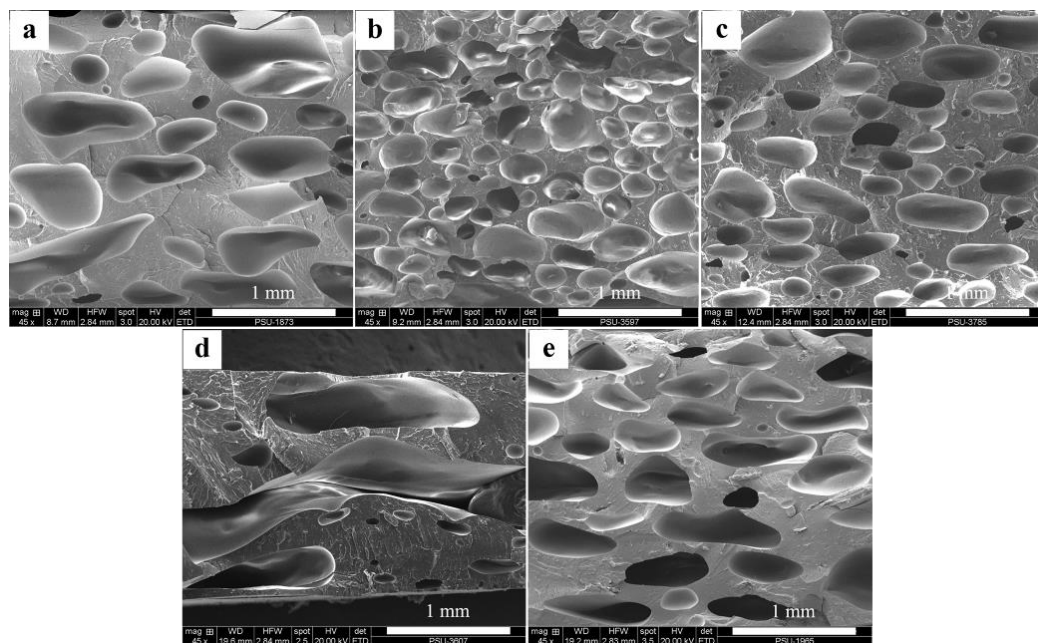


Figure 4.48 Effect of particle size and surface treatment of RWS on pore morphology of the foams: (a) PLA0.1, (b) T1S, (c) T2S, (d) T0L and (e) T2L.

The effect of RWS particle size on pore size was clearly observed. The PLA compounded foams containing the smaller particle RWS (T1S and T2S foams) exhibited smaller average pore size than that of the foams containing the larger particle RWS (T0L and T2L) (Table 4.10). This was because RWS acted as a nucleating agent for heterogeneous foam nucleation, and the smaller particle RWS with higher nucleation sites than those of the larger particle RWS affected to enhance foam nucleating. It was in accordance with the previous work reported by Guo *et al.* [20]. They found that the addition of the smaller wood fiber size provided the foam with smaller pore size and lower foam density. The foam density importantly depended on its void fraction. The foam exhibiting higher void fraction also showed lower density. The lowest density and the highest void fraction were found in T1S foam, whereas the highest density and the lowest void fraction were found in T0L foam. This was because the foam density and void fraction are related to each other. High void fraction means high amount of void in the foam samples resulting in low density. In addition, the average pore size of the foams did not depend on void fraction. However, T1S foam showed the smallest pore size, and T0L showed the highest pore size. This might due to the effect of surface treatment of RWS and RWS particle size.

Table 4.10 Average pore size and physical properties of PLA/RWS compounded foams

Foam sample	Average pore size for each zone (μm)			Average pore size of 3 zones (μm)	Density (g/cm^3)	%VF
	Zone A	Zone B	Zone C			
PLA0.1	611 ± 17	579 ± 31	396 ± 47	495 ± 200	0.746	39.0
T1S	328 ± 38	367 ± 34	328 ± 15	336 ± 111	0.593	51.9
T2S	436 ± 86	509 ± 178	566 ± 58	466 ± 196	0.932	24.4
T0L	1144 ± 306	755 ± 376	1418 ± 508	1022 ± 651	1.018	17.2
T2L	648 ± 235	609 ± 25	637 ± 43	608 ± 235	0.790	36.0

4.3.2 Mechanical properties

The mechanical properties including Izod impact strength, tensile properties and flexural properties of PLA/RWS compounded foams were determined. The data were statistically analyzed, and the various letters were utilized to identify the foam sample when the average value were significant different at $p < 0.5$. The mechanical properties data are listed in Table 4.11. The relation between density and Izod impact strength, tensile properties and flexural properties of the foam samples display in Figure 4.49, 4.50 and 4.51, respectively. It was found that the tendency of the impact strength and the tensile properties were relatively similar whereas these properties were slightly different to the flexural properties. The addition of the smaller particle RWS ($\leq 75 \mu\text{m}$) to PLA decreased the Izod impact strength and the tensile properties of the foams (T1S and T2S foams), and the mechanical properties of the PLA foam slightly changed when the larger particle RWS (212-600 μm) was added. The surface treatments were proved to be necessary. The unnotched impact strength, tensile properties and flexural strength of T2L foam were better than those of T0L foam. The necessary of GPMS treatment using method A was clearly observed when the mechanical properties between T1S and T2S foam were compared. The unnotched impact strength, tensile and flexural properties of T2S foam which was the foam containing 1%GPMS-A 75 RWS were significantly higher than those of T1S foam which was the foam containing RWS without GPMS treatment. In addition, T1S foam exhibited the smallest pore size but showed the worst mechanical properties, and T1S foam showed the lowest density and the highest void fraction (Table 4.10). It should be note that some of mechanical properties (notched impact strength and flexural modulus) of T0L foam was relatively higher than those of T2L foam because T0L foam showed higher density and lower void fraction, and the effect of GPMS treatment provided T2L foam with higher some of mechanical properties than T0L foam. The results demonstrated that the mechanical properties of PLA/RWS foams were controlled by many factors and any specific factor may not play an important role in all of foam samples.

Table 4.11 Izod impact strength, tensile properties and flexural properties of PLA/RWS foams

Foam sample	Izod impact strength		Tensile properties			Flexural properties	
	Unnotched (kJ/cm ²)	Notched (kJ/cm ²)	Modulus (MPa)	Stress at break (MPa)	Strian at break (%)	Modulus (MPa)	Strength (MPa)
PLA0.1	4.9 ± 1.0 ^A	1.6 ± 0.2 ^{AB}	366 ± 20 ^A	18.4 ± 2.1 ^A	8.3 ± 1.3 ^B	1923 ± 61 ^{BC}	29.5 ± 3.3 ^B
T1S	1.3 ± 1.0 ^C	1.1 ± 1.0 ^C	206 ± 20 ^B	5.4 ± 1.1 ^C	3.9 ± 0.7 ^C	1189 ± 129 ^D	6.9 ± 0.5 ^D
T2S	3.1 ± 0.5 ^B	1.4 ± 1.0 ^{BC}	341 ± 30 ^A	17.1 ± 0.2 ^A	7.5 ± 0.5 ^B	2187 ± 169 ^A	36.5 ± 3.6 ^A
T0L	4.5 ± 1.0 ^A	2.0 ± 0.4 ^A	349 ± 73 ^A	11.1 ± 2.7 ^B	4.3 ± 1.2 ^C	2123 ± 180 ^{AB}	23.7 ± 2.8 ^C
T2L	5.2 ± 0.5 ^A	1.8 ± 1.0 ^{AB}	350 ± 28 ^A	20.1 ± 1.6 ^A	10.4 ± 1.6 ^A	1835 ± 149 ^C	24.8 ± 3.4 ^{BC}

Footnotes: Average values with different letters in the same column are significantly different at $p < 0.05$.

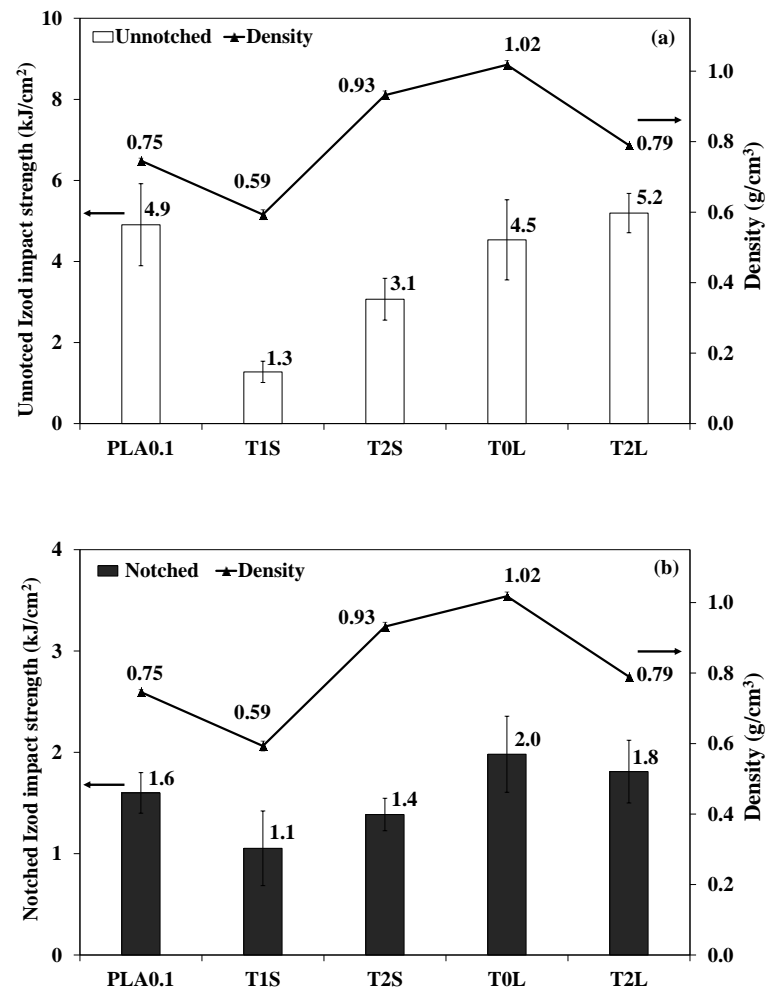


Figure 4.49 Effect of particle size and surface treatment of RWS on Izod impact strength of the foams: (a) unnotched specimens and (b) notched specimens.

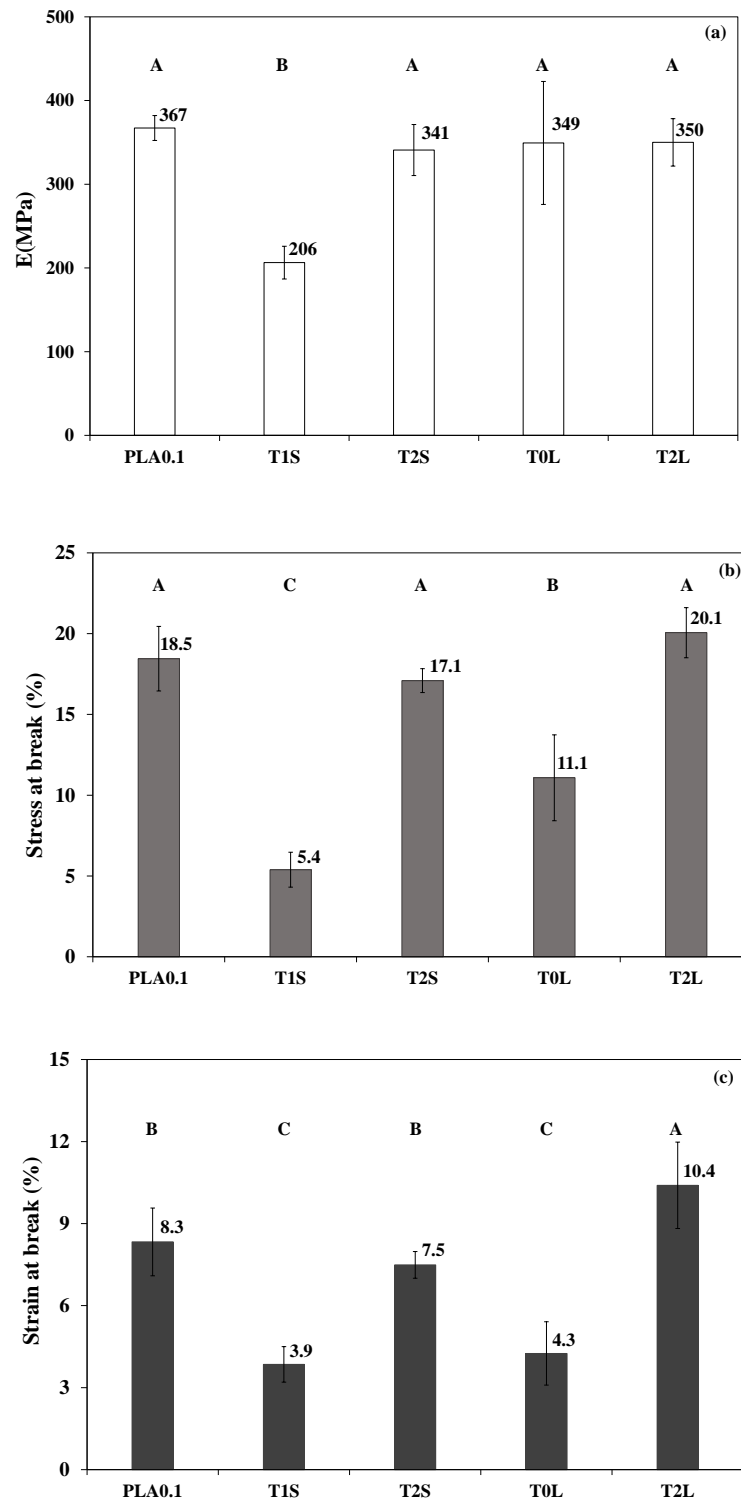


Figure 4.50 Effect of particle size and surface treatment of RWS on tensile properties of the foams: (a) modulus, (b) stress at break and (c) strain at break, average values with different letters are significantly different at $p < 0.05$).

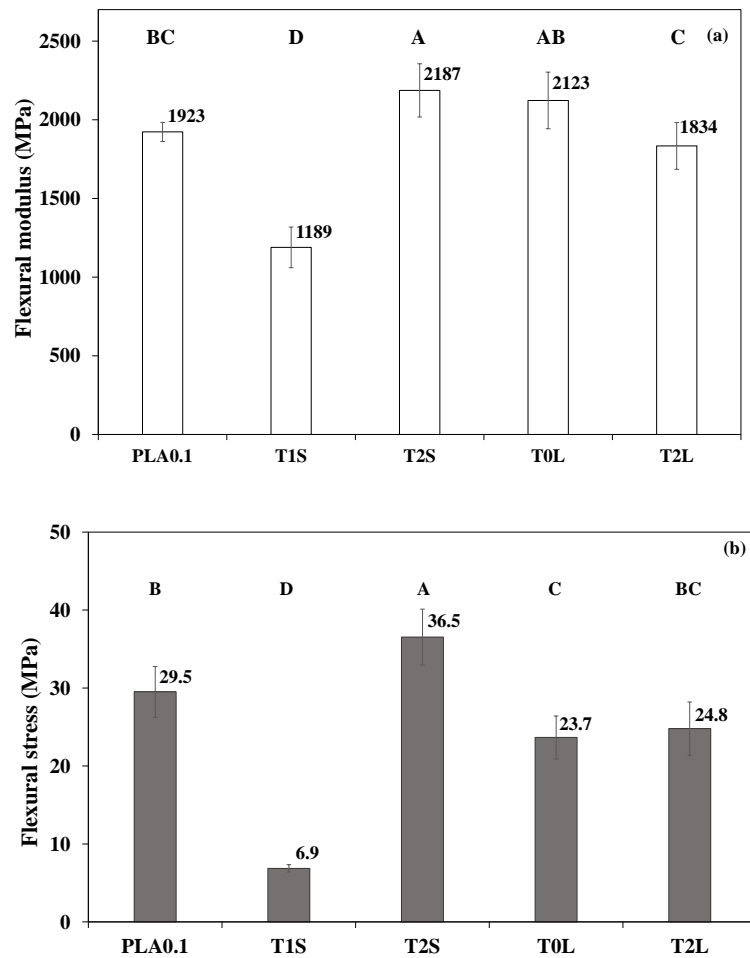


Figure 4.51 Effect of particle size and surface treatment of RWS on flexural properties of the foams: (a) flexural modulus and (b) flexural stress, average values with different letters are significantly different at $p < 0.05$.

4.3.3 Characterizations of PLA compounded foams

4.3.3.1 DMTA analysis

The influence of particle size and surface treatment of RWS on storage modulus (E') and damping factor ($\tan \delta$) are displayed in Figure 4.52(a) and (b), respectively. Similarly to mechanical properties, T1S foam exhibited the lowest storage modulus (E'), and T2L foam exhibited the highest storage modulus (Figure 4.52(a)). At below glass transition temperature, storage modulus of T0L and T2L foams was higher than PLA foam, T1S and T2S foams. At the temperature range of 50°C to 60°C,

the storage modulus of the foams was sharply decreased which correspond to the α -relaxation of amorphous region of PLA [21]. No significant different of storage modulus was found in this temperature range.

Figure 4.52(b) displayed $\tan \delta$ peak as a function of temperature. An increase of area under the α -relaxation in $\tan \delta$ peak of a polymer indicates increasing degree of molecular chains mobility affecting to increase damping properties of material [21]. The maximum $\tan \delta$ peak corresponding to the α -relaxation temperature of PLA foam and PLA compounded foams ranked from 61.4 to 63.6 °C. The higher relaxation temperature ranging from 85 to 105 °C was due to cold crystallization of PLA. It was found that both relaxation temperatures of PLA foam were insignificantly changed by the addition of RWS.

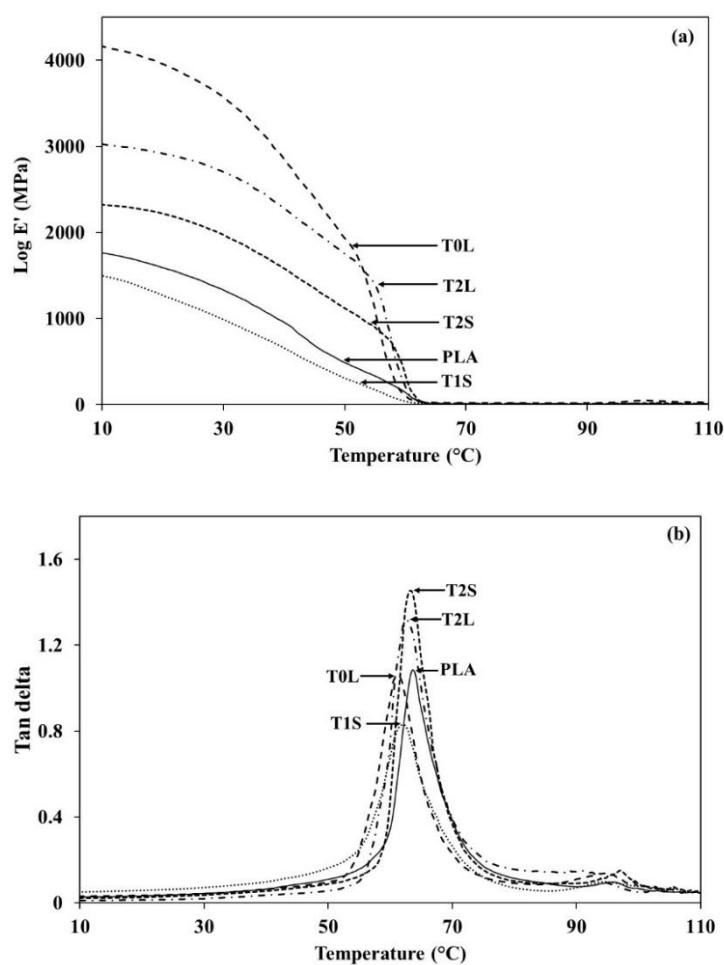


Figure 4.52 (a) Storage modulus and (b) $\tan \delta$ as a function of temperature of PLA foam and PLA/RWS foams.

4.3.3.2 TGA analysis

The thermal stability of PLA and PLA compounded foams was characterized by TGA as shown in Figure 4.53(a) and (b). The very small peak of transition temperature at around 200 °C corresponding to decomposition of AZDC was also observed (Figure 4.53(a)), as mentioned in the topic of 4.2.3. The $T_{d\ onset}$ and T_d of the foams are listed in Table 4.12. It showed that the presence of RWS decreased thermal stability of PLA foam, and the thermal stability of the foams containing the smaller particle RWS ($\leq 75\ \mu\text{m}$) and the foams containing the larger particle RWS (212-600 μm) were similar.

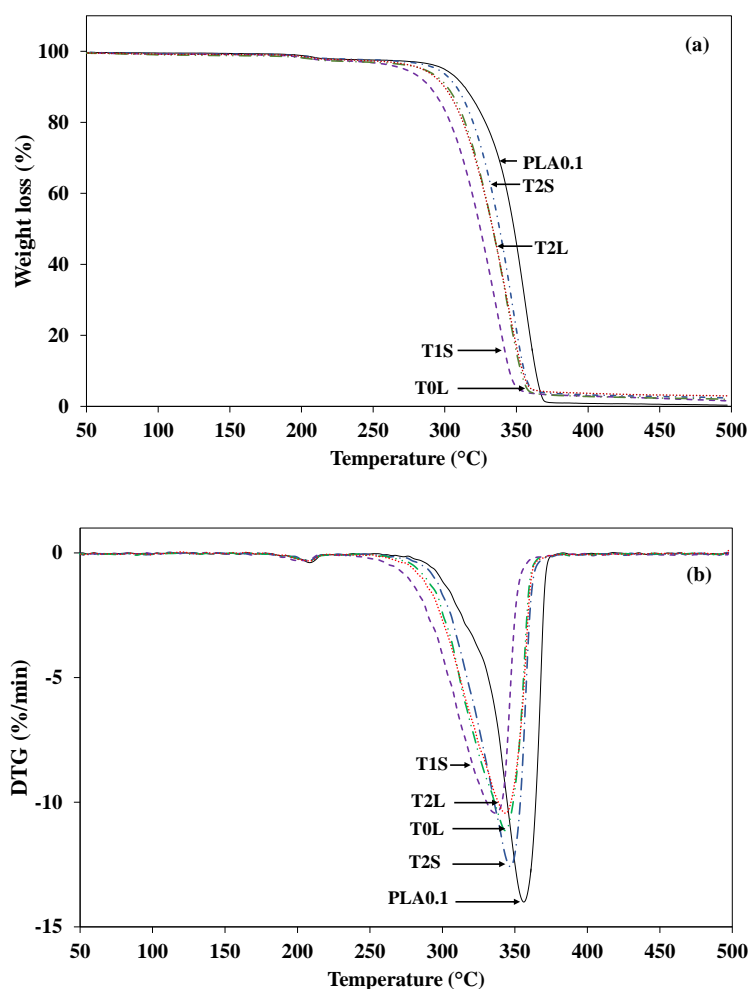


Figure 4.53 (a) TGA and (b) DTG curves of PLA foam and PLA/RWS foams.

Table 4.12 Thermal degradation temperatures of PLA foam and PLA/RWS foams

Foam sample	T _{d onset} (°C)	T _d (°C)
PLA0.1	332	356
T1S	302	337
T2S	312	343
T0L	319	347
T2L	310	344

4.3.4 *In-vitro* degradation properties

The % weight loss of PLA and PLA/RWS compounded foams after incubation in PBS in the presence of lysozyme for 8 weeks is displayed in Figure 4.54. The data were statistically analyzed. Different letters were utilized to identify the foam samples when the average % weight loss were significantly different at $p < 0.05$. The weight loss of all samples increased as increased incubation time. The PLA0.1 foam showed a rapid weight loss at first 2 weeks and then the % weight loss remained constant at 5% until the end of experiment. All of PLA compounded foams, except T0L foam, exhibited a similar change of weight loss. A quick change of weight loss occurred in the first week and, then, the rate of weight loss decreased and became constant after 2 weeks of incubation. The T0L foam showed very slow rate of weight loss and remained constant at approximately 2% after incubation for 6 weeks. After 3 weeks of incubation, the rates of weight loss of T1S and T2S foam were similar and higher than that of T2L foam. At the end of the experiment, the weight loss of the foam samples could be ranked in the following order: T0L < T2L < PLA0.1 < T2S < T1S. A higher weight loss demonstrates more degradation. Although the larger particle RWS (212-600 μm) reduced the weight loss of PLA0.1 foam and the smaller particle RWS ($\leq 75 \mu\text{m}$) increased the weight loss, it should be remembered that surface treatment, pore morphology, density and void fraction have to be considered as well. The very low weight loss of T0L foam came from the relatively high density and low void fraction. The degradation resistance of T2L foam was higher than that of PLA0.1 foam, implying a high interfacial adhesion between PLA and RWS that could correspond to the good mechanical properties of this sample. Two factors were presumed to be involved in the

low degradation resistance of T1S foam including the high void fraction and low interfacial adhesion. Both factors also affected the mechanical properties of T1S foam.

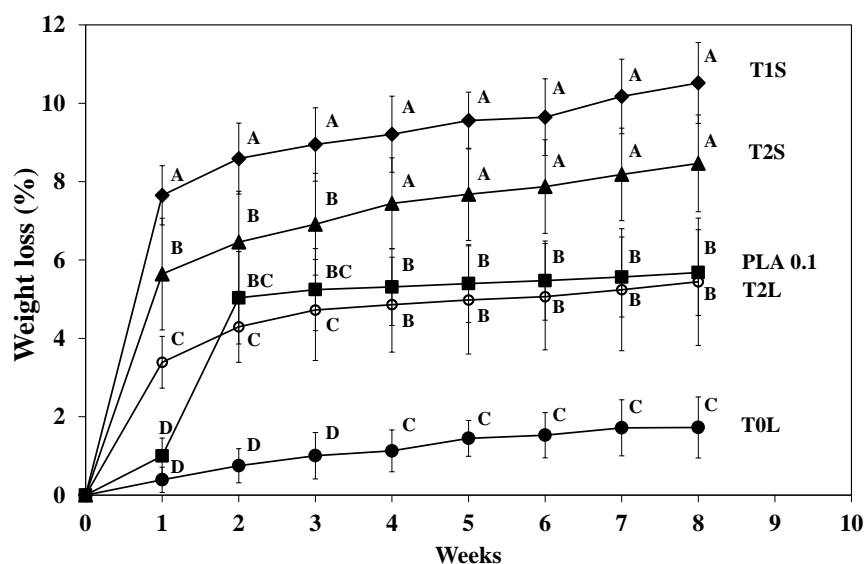


Figure 4.54 Weight loss (%) as a function of incubation time of foam specimens, average values with different letters in the same week are significantly different at $p < 0.05$.

4.3.5 Cytotoxicity properties

The cytotoxicity were determined to preliminary investigate the suitability of obtained foams for bone scaffold applications. The culturing of MG-63 cell, osteoblast-liked cell, and cell proliferation testing by using WST-1 assay were utilized to evaluate cytotoxicity of the foam samples. The WST-1 assay is colorimetric method to measure viable cells in cell culture [22]. When added to the sample, WST-1 is reduced by living cells to water soluble formazan through cellular dehydrogenase. The dark yellow water soluble formazan can be measured from absorbance at 420 nm. The degree of conversion, indicated by the intensity of color, is directly correlated with the amount of metabolic activity in viable cells. An increase of viable cells with increasing culture time indicates increased cell proliferation [23]. MG63 cell proliferation is shown in Figure 4.55. The data were also statistically analyzed as described in the topic 4.3.4. The PLA0.1 foam sample was used as a control sample.

Cell proliferation increased with cell culture time, demonstrating the non-cytotoxicity of the foam samples. MG63 cell proliferation on the surface of the foam samples could be ranked as following order: PLA0.1 > T0L > T2S > T2L > T1S. The trend of cell proliferation of T0L foam was unpredictable. The relatively large pore sizes of T0L foam might have contributed to this result. In contrast, T1S foam which had the highest void fraction, did not promote the cell proliferation so much, it might be due to its small pore size. PLA is a polymer with low hydrophilicity, thus, large pores may be helpful for cell proliferation.

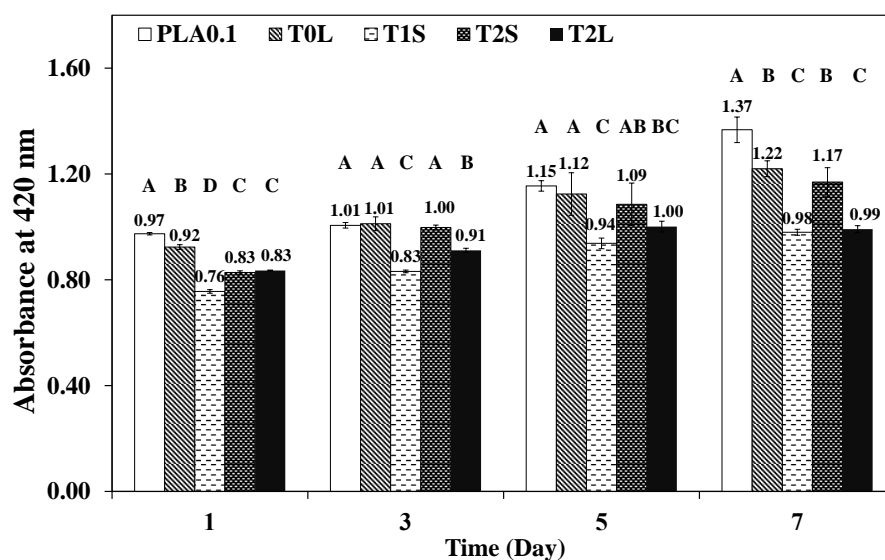


Figure 4.55 Cell proliferation on the polished surface of foam specimens at 1, 3, 5 and 7 days, average values with different letters in the same day are significantly different at $p < 0.05$.

Cell adhesion on the surface of foam samples was observed by SEM. Figure 4.56(a) displays the surface of PLA0.1 foam without cell culture, it was referred to as a blank. Figure 4.56(b)-(f) show the surface of the foam samples after cell culture for 7 days. MG-63 cells of various shape were observed and are indicated by white arrows in the figures. The spindle-shaped cells were present on the surface of the PLA0.1 foam (Figure 4.56(b)). The appearance of cell adhesion on the surfaces of the foam samples also demonstrated non-cytotoxic reactivity.

In the present study, the %VF and average pore size of the obtained foams were in the range of 17.2 to 51.9% and 336 to 1022 μm , respectively (Table 4.10). The porosity of cancellous bone is in the range of 30 to 90%. [24] The optimum pore sizes for bone regeneration and collateral bone ingrowth were in the range of 50-710 μm and 100-1000 μm , respectively [25-26]. In addition, bone fixations must have a slow rate of degradation [17], and both PLA foam and PLA/RWS foams showed slow rates of degradation (< 6% after 8 weeks in T2L foam). All experimental results in this topic including average pore size, void fraction, mechanical properties, cytotoxicity and *in-vitro* degradation indicated the suitability of PLA0.1, T2S and T2L foams for bone applications.

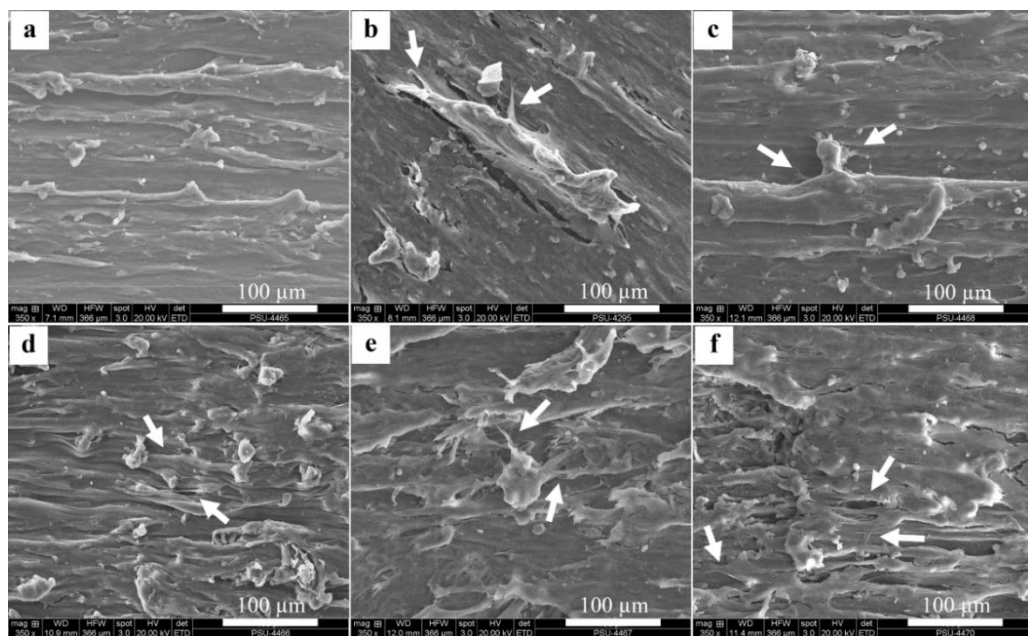


Figure 4.56 SEM images of freeze-fractured surfaces of foam specimens demonstrating cell adhesion after 7 days: (a) blank, (b) PLA0.1, (c) T0L, (d) T1S, (e) T2S and (f) T2L.

4.4 Properties and characterization of unfoamed and foamed PLA compounds

4.4.1 Properties of unfoamed PLA/PEG/chitosan

The effect of chitosan (CH) and PEG on mechanical of unfoamed PLA compounds was observed by impact and tensile testing in order to obtain appropriate compositions to prepare PLA compound foams.

4.4.1.1 Mechanical properties

The Izod impact strength and tensile properties were used to study the mechanical properties of PLA/PEG/CH compounds. Figure 4.57(a) and (b) show the Izod impact strength of the unnotched and notched specimens, respectively, and Figure 4.58(a)-(c) display the tensile properties of the unfoamed PLA compounds. The compound of PLA-PEG-CH5 was very brittle so that the compression molded sample could not cut as a tensile specimen for testing. It was found that the addition of chitosan and increasing of chitosan content decreased the impact strength of PLA and plasticized PLA. This trend was also found in the tensile properties (Figure 4.58(a)-(c)). The addition of PEG significantly increased the impact strength of the unnotched specimens of PLA and slightly increased the impact strength of PLA-CH1 blends, whereas the addition of PEG to PLA and PLA/chitosan blends decreased the tensile properties.

The mechanical properties of the PLA compounds demonstrated that a small content of chitosan acted as a microdomain in the continuous phase of PLA and inherent incompatibility between PLA and chitosan resulted in a decrease of the impact strength and the tensile properties of PLA and PLA blends. It was in accordance with the previous study reported by Rápá *et al.* [27]. Tributyl o-acetyl citrate (ATBC) was used as a plasticizer, and they found that the addition of chitosan and increasing chitosan content (1, 3, 5 wt%) decreased the tensile strength and the strain at break of plasticized PLA. In the present study, the addition of PEG to PLA could increase the impact strength, whereas the addition of PEG could not improve the tensile properties of PLA. Although the addition of chitosan and/or PEG to PLA could not improve the mechanical properties, good biocompatible and non-toxicity of chitosan remain

interesting. Thermal properties characterized by DSC of the compounds of PLA, chitosan, and PEG were tested, and PLA/PEG/CH foam samples were prepared in the next experimental.

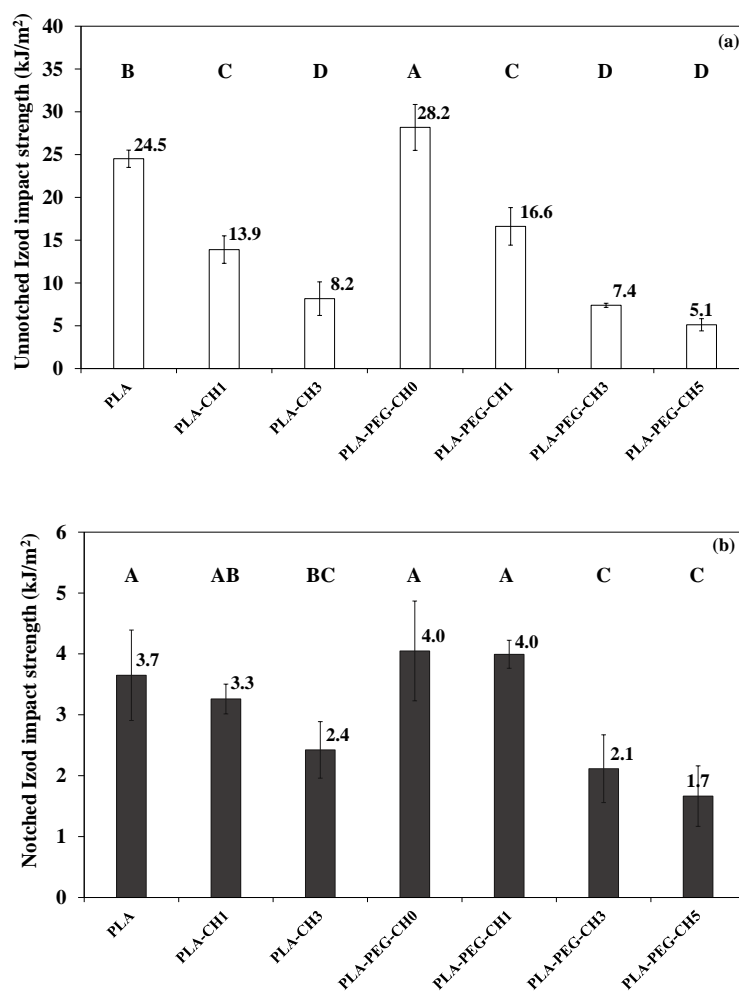


Figure 4.57 Effect of chitosan and PEG on Izod impact strength of unfoamed PLA (a) unnotched specimens and (b) notched specimens, average values with different letters are significantly different at $p < 0.05$.

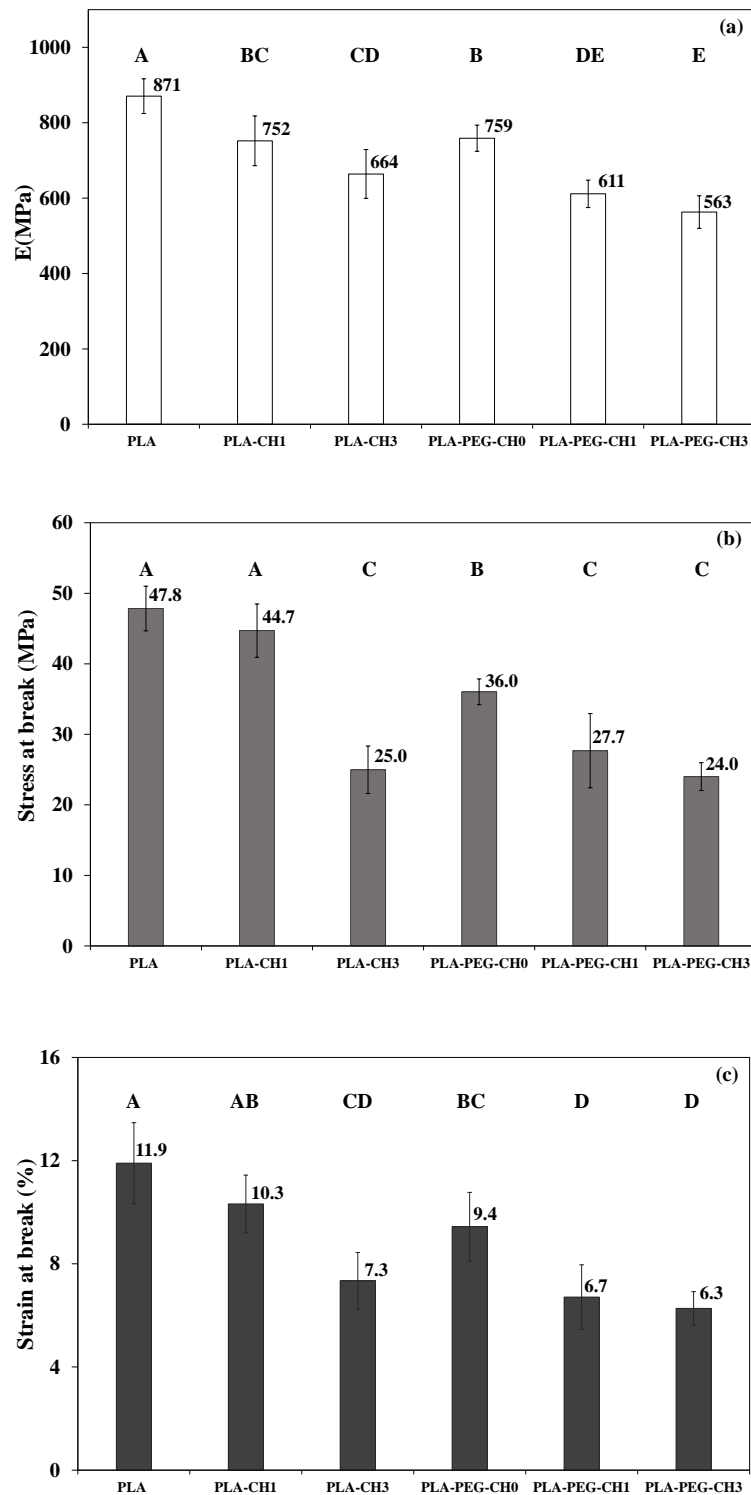


Figure 4.58 Effect of chitosan and PEG on Izod impact strength of unfoamed PLA: (a) modulus, (b) stress at break and (c) strain at break, average values with different letters are significantly different at $p < 0.05$.

4.4.1.2 Thermal properties

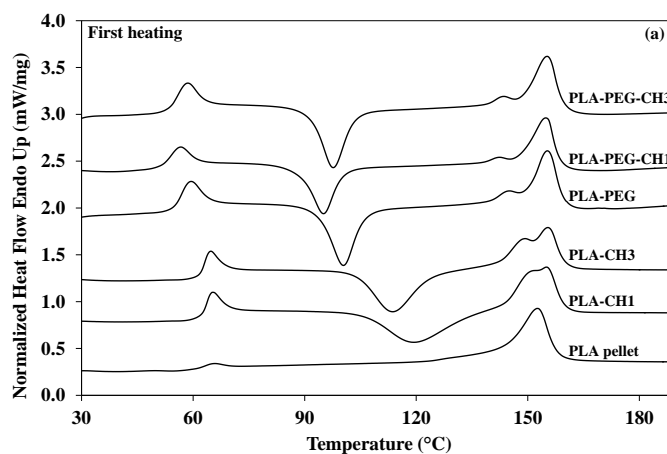
Figure 4.59 shows DSC thermograms of PLA and PLA compounded pellets. The thermal transition temperature evaluated from the first and the second heating scan DSC thermograms are listed in Table 4.13 and 4.14, respectively. The first heating scan DSC thermograms (Figure 4.59(a)), all samples exhibited the glass transition peaks, and it disappeared after the second heating (Figure 4.59(c)). In addition, the glass transition temperatures evaluated from the first heating scan DSC thermograms of PLA and PLA compounded pellets were decreased as compared with those evaluated from the second heating scan of DSC thermograms. This was due to the second heating scan deleted its thermal history. In the second heating scan DSC thermograms (Figure 4.59(c)), the plasticization effect of PEG in PLA was clearly observed by the reduction of T_g from 56.2°C to 48.1°C. It seem that chitosan also acted as a plasticizer of PLA and promoted plasticization effect of PEG, it was observed by a slightly decreased T_g of plasticized PLA after the addition of chitosan. The cold crystallization temperature (T_{cc}) corresponding to recrystallization during heating was found in all samples, except PLA pellets. The addition of chitosan generated cold crystallization peak (PLA-CH1 and PLA-CH3), and it slightly decreased T_{cc} of plasticized PLA (PLA-PEG-CH1 and PLA-PEG-CH3). In addition, the degree of crystallinity (X_{c1}) and the degree of crystallinity by excluding ΔH_{cc} (X_{c2}) of PLA increased with the addition of PEG and/or chitosan (Table 4.14). This results indicated that chitosan and PEG acted as nucleating agent of PLA which was in accordance with the previous study [28-29]. Two melting peaks were found after the addition of chitosan and/or PEG at approximately 142°C and 154°C. The smaller melting peak at lower temperature corresponded to melting of disordered α' crystals of PLA formed during cold crystallization, and the melting peak at higher temperature corresponded to melting of ordered α crystals of PLA as explained in the topic 4.1.4.3 [11].

Table 4.13 Thermal properties determined from the first heating and cooling scan of DSC thermograms

Sample	First heating				Cooling
	T_g (°C)	T_{cc} (°C)	T_m (°C)		T_g (°C)
PLA pellet	63.6	-	-	152	49.4
PLA-CH1	63.8	119	152	155	51.0
PLA-CH3	63.3	104	149	155	48.1
PLA-PEG	57.4	101	150	155	40.9
PLA-PEG-CH1	54.7	95.1	143	154	36.9
PLA-PEG-CH3	56.5	97.7	144	155	38.4

Table 4.14 Thermal and crystallinity properties determined from the second heating scan of DSC thermograms

Sample	T_g (°C)	T_{cc} (°C)	T_m (°C)		ΔH_m (J/g)	ΔH_{cc} (J/g)	X_{c1} (%)	X_{c2} (%)
PLA pellet	56.2	-	-	153	0.78	-	0.8	0.8
PLA-CH1	56.7	116	148	155	38.6	-34.9	4.0	41.6
PLA-CH3	55.2	107	145	154	36.6	-33.4	3.4	39.3
PLA-PEG	48.1	93.6	141	154	39.2	-30.2	9.6	42.1
PLA-PEG-CH1	43.8	86.7	139	153	31.8	-19.5	13.2	34.2
PLA-PEG-CH3	45.9	87.2	140	154	37.0	-21.1	17.1	39.7



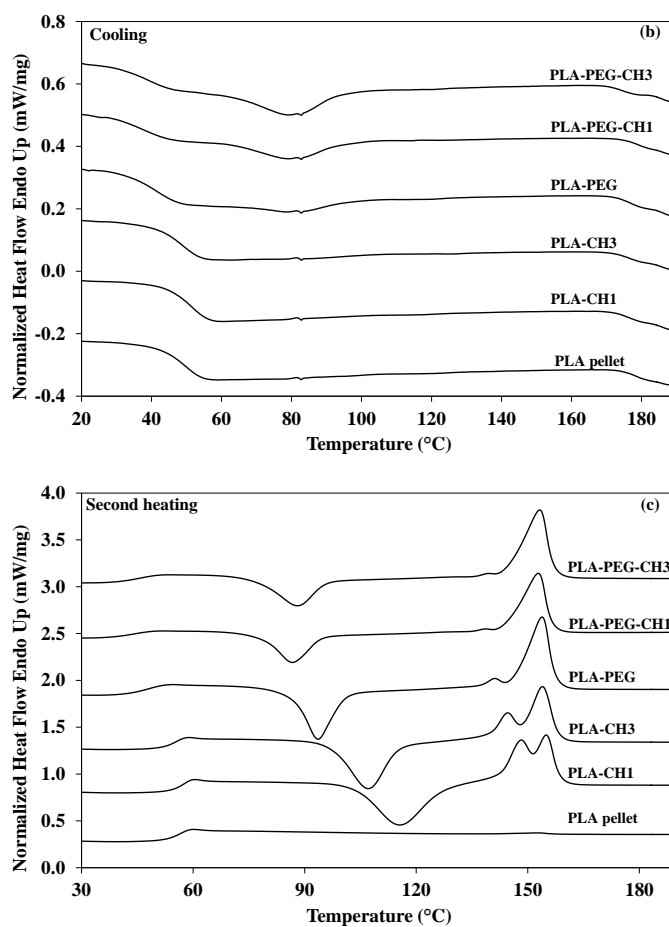


Figure 4.59 DSC thermograms of unfoamed PLA compounds.

4.4.2 Properties of PLA/PEG/chitosan foams

4.4.2.1 Morphology and physical properties

SEM images demonstrating 9 zones of PLA0.1 foam and PLA compounded foam samples are shown in appendix A, Figure A1 and A9 to A13, respectively. SEM images compared between PLA0.1 foam and PLA compounded foams containing PEG and/or chitosan display in Figure 4.60. A closed-cell morphology with oval shape was visible in all foam samples. These have been found in polyethylene foam [29] and PLA foam [30] prepared by compression molding using AZDC. Figure 4.60(a) shows the cell morphology of the neat PLA foam. The addition of chitosan and PEG decreased the average pore size and pore size distribution of the foams (Table 4.15). It seems that chitosan and PEG acted as nucleating agent for

heterogeneous foam nucleation which was in accordance with the previous study by Vázquez *et al.* [31]. They found that chitosan acted as nucleating agent for heterogeneous foam nucleation and decreased pore size of polystyrene (PS) and polypropylene (PP) foam processed by extrusion foaming using AZDC as a blowing agent [31]. In addition, it also has been found that the addition of 10 wt% of PEG decreased pore size of PLA porous scaffold produced by supercritical CO₂ foaming with particle leaching [32]. The similar characteristics of nucleating agents used in thermoplastic foaming have been reported in previous study by Abbasi *et al.* [33] and Zhai *et al.* [34]. Nucleating agents used in thermoplastic foaming were nano-calcium carbonate in LDPE foams [33] and nano-silica in polycarbonate foams [34]. Density and void fraction (%VF) of foam samples are listed in Table 4.15. The foam density was intently effected by void fraction. The foam with higher void fraction demonstrated the lower density. These values were ranking in the same order. The average pore size could not be ranked in the same order with the void fraction or the density.

Table 4.15 Physical properties and average pore diameters of PLA foam samples

Foam sample	Average pore size (μm)	Density (g/cm^3)	VF (%)
PLA0.1	495 ± 200	0.746 ± 0.007	39.0 ± 0.5
1C0P	450 ± 175	0.723 ± 0.002	40.9 ± 0.2
3C0P	316 ± 60	0.819 ± 0.009	33.0 ± 0.7
0C5P	355 ± 157	0.760 ± 0.003	37.8 ± 0.2
1C5P	282 ± 107	0.816 ± 0.004	33.3 ± 0.3
3C5P	300 ± 77	0.759 ± 0.014	37.9 ± 1.1

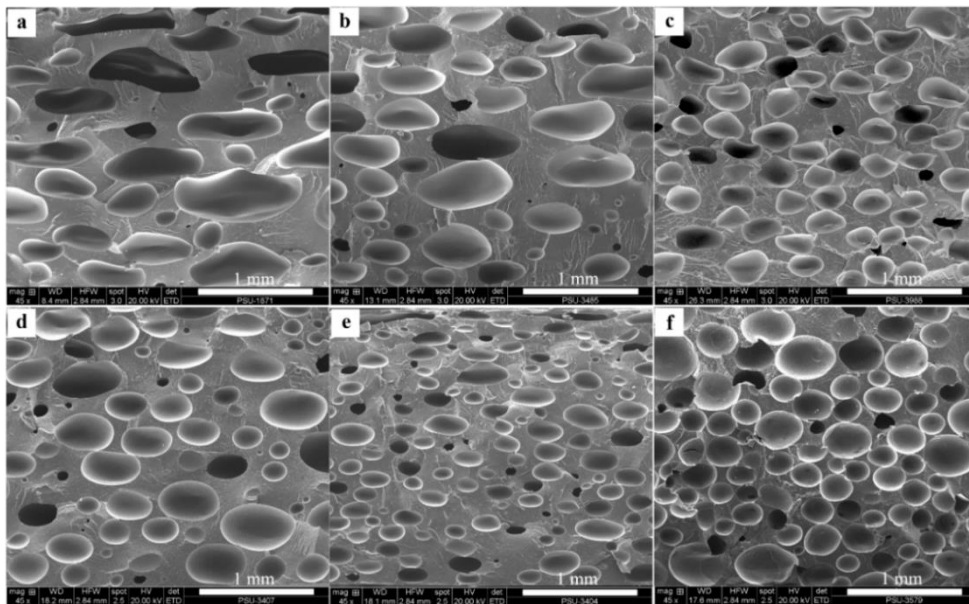


Figure 4.60 SEM images of foam samples: (a) PLA0.1, (b) 1C0P, (c) 3C0P, (d) 0C5P, (e) 1C5P and (f) 3C5P.

4.4.2.2 Thermal properties

(i) DSC analysis

Figure 4.61 displays DSC thermograms of the PLA and PLA compounded foams. The thermal transition temperatures evaluated from the first and the second heating scan of DSC thermograms are listed in Table 4.16 and 4.17, respectively. The first heating scan DSC thermograms of all foam samples (Figure 4.61(a)) showed the glass transition peaks, and the glass transition temperatures evaluated from the first and the second heating scan DCS thermograms were significant different which were similar to those of PLA compounded pellets (Topic 4.4.1.2). The glass transition temperatures in the cooling and the second heating scan of the foams containing PEG (0C5P, 1C5P and 3C5P foams) could not clearly observed in the temperature range of the testing (Figure 4.61(b) and (c)). In addition, the thermal characteristics of polymeric foams have been studied from the first heating scan DSC thermograms in the previous works by Zimmermann *et al.* [30], Litauszki and Kmetty [35] and Sun *et al.* [36]. Therefore, the thermal characteristic of PLA compounded foams in the present study was examined from the first heating scan DSC thermograms

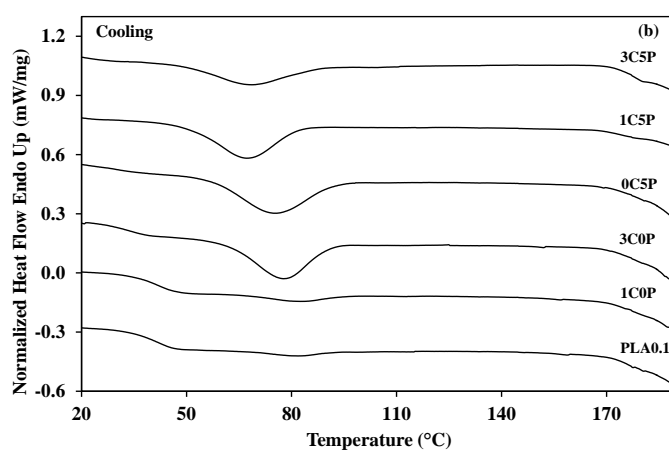
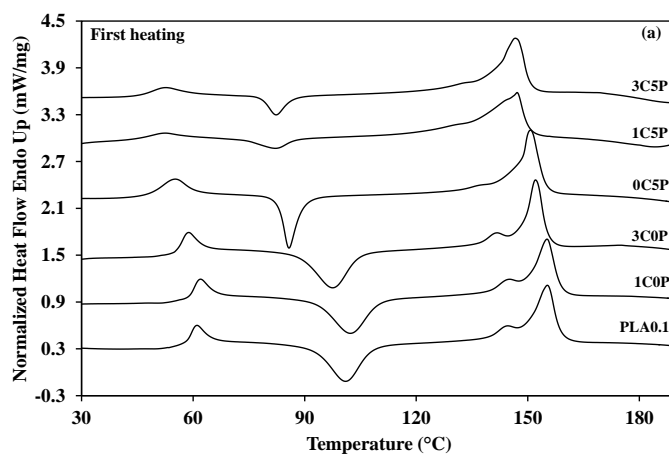
(Figure 4.61(a)). All foam samples showed cold crystallization temperature (T_{cc}) resulting to a double endothermic peaks, and the glass transition peaks were found. The thermal transition temperature (T_g , T_{cc} , T_{m1} and T_{m2}) and degrees of crystallinity (X_{c1} and X_{c2}) are listed in Table 4.16. The addition of PEG showed effective plasticization on PLA foam by significant decreasing T_g of PLA when approximately 5 wt% was added to the blend. Chitosan also acted as a plasticizer and enhanced plasticization effect of PEG. It could be observed in the 3C5P foam demonstrating the lowest T_g . Both PEG and chitosan were acted as nucleating agent indicated by decreasing T_{cc} of PLA, and the lowest T_{cc} was found in 3C5P sample containing a mixture of PEG and chitosan. Chitosan had no effect on the degree of crystallization by excluding ΔH_{cc} (X_{c1}) of PLA in the foam without PEG, whereas the addition of PEG and a mixture of PEG and chitosan significantly increased X_{c1} of PLA. Nevertheless, the total degree of crystallinity (X_{c2}) of the samples insignificantly changed by the addition of PEG and chitosan.

Table 4.16 Thermal and crystallinity properties determined from the first heating and cooling scan of DSC thermograms of PLA compounded foams

Foam sample	First heating						Cooling	
	T_g (°C)	T_{cc} (°C)	T_{m1} (°C)	T_{m2} (°C)	X_{c1} (%)	X_{c2} (%)	T_g (°C)	T_{cc} (°C)
PLA	59.6	101	145	155	9.0	43.4	41.2	-
1C0P	60.5	102	145	155	7.8	41.6	41.2	-
3C0P	57.4	97.6	142	152	7.4	39.8	33.6	77.7
0C5P	51.8	85.8	139	151	24.1	44.4	-	77.8
1C5P	50.3	82.4	132	147	43.7	49.7	-	67.1
3C5P	49.7	82.0	134	147	36.3	44.1	-	68.7

Table 4.17 Thermal and crystallinity properties determined from the second heating scan of DSC thermograms of PLA compounded foams

Foam sample	T_g (°C)	T_{cc} (°C)	T_{m1} (°C)	T_{m2} (°C)	X_{c1} (%)	X_{c2} (%)
PLA	47.2	96.1	139	151	11.4	47.4
1C0P	46.8	95.2	139	151	9.0	45.6
3C0P	39.2	80.9	132	146	34.5	48.0
0C5P	-	76.9	-	145	34.5	46.7
1C5P	-	70.7	-	133	28.0	41.6
3C5P	-	74.6	-	136	24.2	43.2



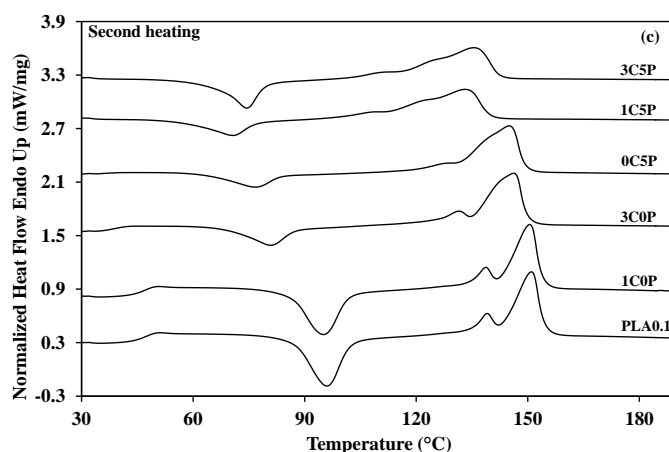
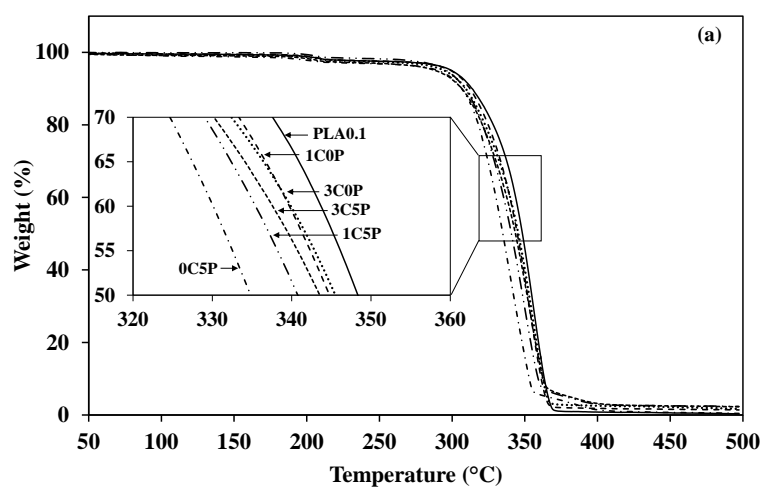


Figure 4.61 DSC thermograms of PLA compounded foams.

(ii) TGA analysis

Thermal stability of PLA compounded foams was determined by thermogravimetric analysis. TGA and DTG curves are shown in Figure 4.62(a) and (b), respectively. $T_{d\text{ onset}}$ and $T_{d\text{ endset}}$ evaluate T_d from TGA curve and T_d evaluated from DTG curve are listed in Table 4.18. The addition of chitosan to PLA slightly changed thermal degradation temperature of the foams without PEG. The addition of PEG in to PLA decreased thermal stability of the foam (0C5P foam) but the addition of chitosan slightly increased thermal stability of the foams containing PEG, (1C5P and 3C5P foam).



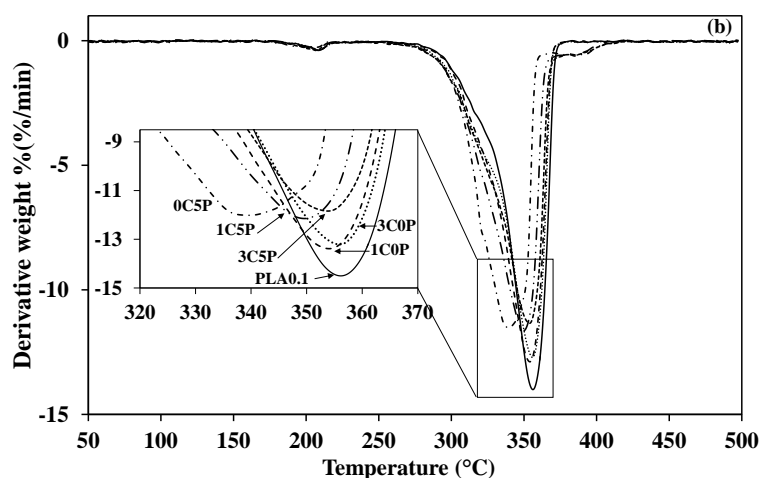


Figure 4.62 (a) TGA and (b) DTG curves of PLA foam and PLA compounded foams.

Table 4.18 Thermal degradation properties of the foams

Foam sample	$T_{d\ onset}$ (°C)	T_d (°C)	$T_{d\ endset}$ (°C)
PLA0.1	332	356	366
1C0P	326	354	364
3C0P	327	356	365
0C5P	314	340	357
1C5P	326	354	365
3C5P	323	354	365

4.4.2.3 Mechanical properties

The Izod impact strength, tensile and flexural properties were utilized to observe mechanical properties of the foam samples as listed in Table 4.19 and Figure 4.63-4.64. The data were statistically analyzed. In the present study, chitosan was not expected to improve mechanical properties of PLA. The addition of chitosan reduced the Izod impact strength and tensile properties of PLA (Table 4.19). The incompatibility between PLA and chitosan might have been due to the relatively large particle size of the chitosan ($\sim 149\ \mu\text{m}$). Reduced tensile properties were previously reported for PLA/chitosan blend [27]. Likewise, chitosan decreased the tensile strength of LLDPE

[37]. The plasticized PLA without chitosan (0C5P) showed increased the Izod impact strength and the highest toughness of all the samples tested. The impact strength of the plasticized PLA foams decreased with increasing chitosan content ($3C5P < 1C5P < 0C5P$). All the plasticized PLA foams, with and without chitosan, showed poorer tensile properties than those of PLA foam. The impact strength might be more affected by chitosan than by the degree of crystallinity, foam density and pore size. Notably, 1C5P, having higher density, the highest degree of crystallinity and the lowest average pore size, showed lower impact strength, modulus and tensile strength than 0C5P. The data presented in Figure 4.63-4.64 confirmed that, as with impact strength, density did not have a significant effect on the modulus and tensile strength

Table 4.19 Impact strength and tensile properties of foam samples

Foam sample	Izod impact strength (kJ/m ²)		Tensile properties		
	Unnotched	Notched	E (MPa)	σ_b (MPa)	ϵ_b (%)
PLA0.1	4.9 ± 1.0^B	1.6 ± 0.2^{AB}	366 ± 20^A	18.4 ± 2.1^A	8.3 ± 1.3^B
1C0P	3.4 ± 0.4^C	1.3 ± 0.3^B	216 ± 12^{DE}	7.5 ± 1.4^C	5.6 ± 1.2^{CD}
3C0P	4.8 ± 0.5^B	1.5 ± 0.1^{AB}	275 ± 40^{BC}	10.8 ± 1.8^B	6.6 ± 1.6^{BC}
0C5P	7.3 ± 0.8^A	2.0 ± 0.3^A	319 ± 30^B	16.6 ± 0.6^A	7.8 ± 0.5^{BC}
1C5P	5.0 ± 1.0^B	1.7 ± 0.4^{AB}	258 ± 27^{CD}	10.6 ± 0.5^B	10.7 ± 2.1^A
3C5P	3.7 ± 0.8^{BC}	1.5 ± 0.3^{AB}	194 ± 24^E	5.0 ± 0.8^D	3.7 ± 0.5^D

Footnotes: Average values with different letters in the same column are significantly different at $p < 0.05$.

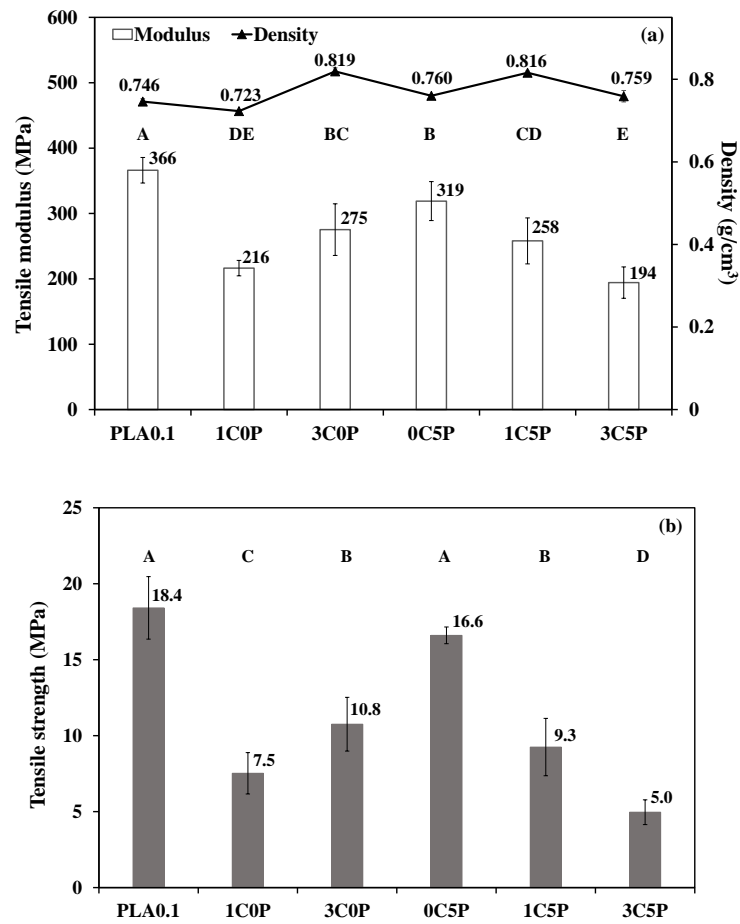
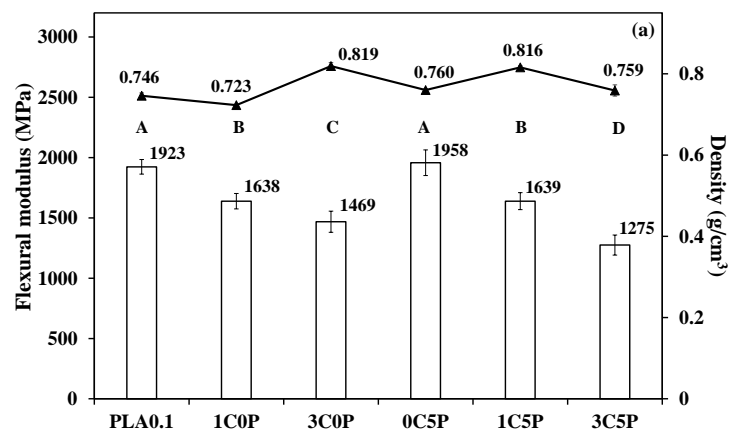


Figure 4.63 Tensile properties of foam samples: (a) tensile modulus and (b) tensile strength, average values with different letters are significantly different at $p < 0.05$.



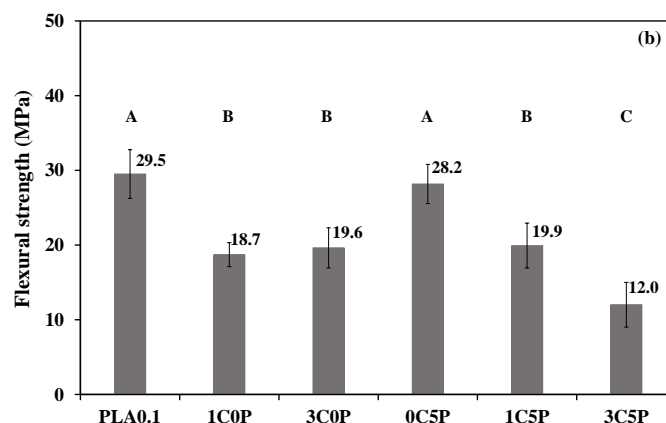


Figure 4.64 Flexural properties of foam samples: (a) flexural modulus and (b) flexural strength, average values with different letters are significantly different at $p < 0.05$.

4.4.2.4 *In-vitro* degradation properties

The % weight loss of PLA compounded foams were weekly determined after incubation is shown in Figure 4.65. The data were statistically analyzed and the average values were significantly different at $p < 0.05$. The weight loss of all samples increased with increasing incubation time, and PLA showed the highest weight loss (Figure 4.65). At the end of the second week, PLA showed a 5% weight loss while the weight loss of the other samples ranged from 0.5% to 1.3%. After 2 weeks, the weight loss of PLA was almost constant, whereas the other samples showed a constant weight loss from the 6th week. At the end of the experiment, the samples could be ranked by weight loss in the following order: 3C0P < 0C5P < 1C0P < 3C5P < 1C5P < PLA. PLA showed a 5.7% weight loss while the weight lost by of the other samples ranged from 1.4% to 3.0%. The addition of chitosan to PLA significantly reduced weight loss. Chitosan reduced %weight loss by neutralizing the acid product of the degradation of PLA and restraining self-catalysis in the PLA degradation process [38]. Paradoxically, 0C5P showed relatively little weight loss. This sample will be investigated more deeply in future study.

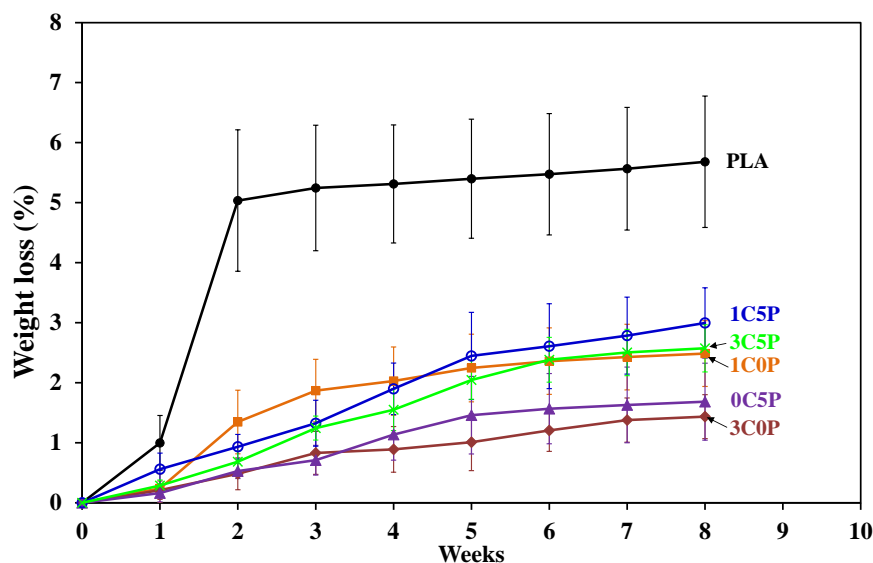


Figure 4.65 Weight loss as a function of incubation time of PLA compounded foams.

4.4.2.5 Cytotoxicity properties

The WST-1 assay used in the cytotoxicity evaluation is a colorimetric assay using tetrazolium salt (WST-1) for the quantitation of viable cells as described in the topic 4.3.5. The data were statistically. The proliferation of MG-63 cells increased with cell culture time (Figure 4.66). This result demonstrated the non-cytotoxicity of all the foam samples. The addition of 1 wt% chitosan (1C0P) slightly changed cell proliferation on PLA whereas 3 wt% chitosan (3C0P) reduced proliferation more significantly. The addition of PEG (0C5P) did not inhibit cell proliferation on PLA. The addition of chitosan in conjunction with PEG inhibited cell proliferation on PLA. This result was similar to the result from the *in-vitro* degradation test.

MG-63 cells on the surface of samples after 7 days of cell culture are shown in SEM micrographs (Figure 4.67). The white arrows indicate areas covered by spreading cells [39]. Cell adhesion is visible in the white circles. The appearance of cells on the surfaces of all samples verified the non-cytotoxic reactivity of the samples. Scaffold for bone tissue engineering requires relatively low weight loss and high cell proliferation. In the present study, 1C0P and 0C5P were better in regard to these properties than PLA.

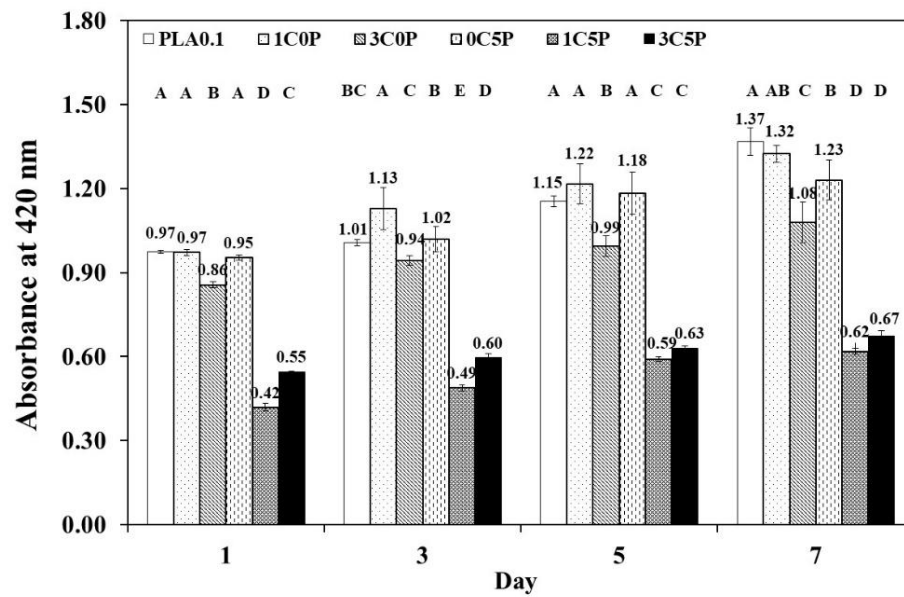


Figure 4.66 MG-63 cell proliferation on the polished surface of samples at 1, 3, 5 and 7 days, average values with different letters in the same day are significantly different at $p < 0.05$.

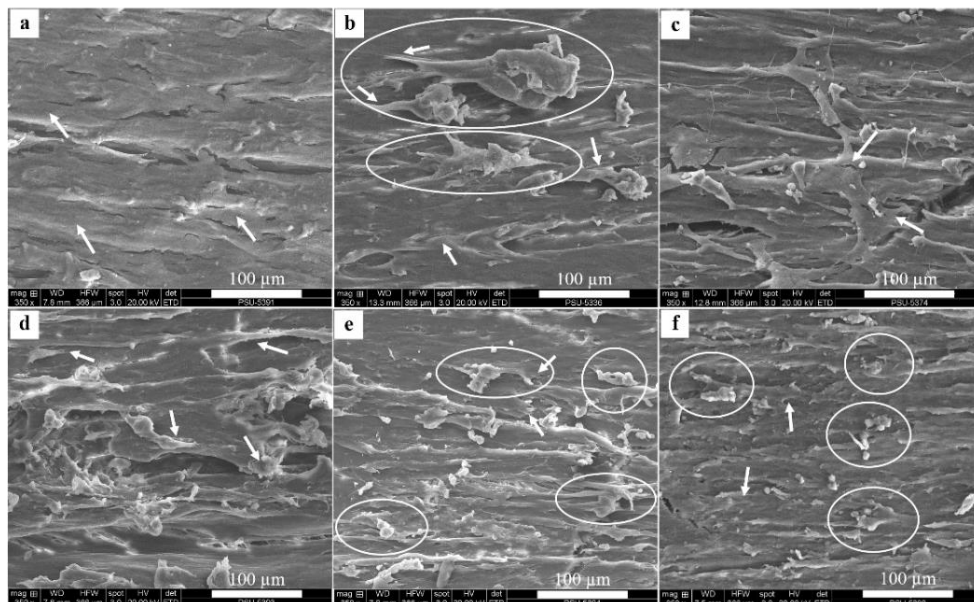


Figure 4.67 SEM images of cell adhesion on the polished surface of foam samples after 7 days of cell culture: (a) PLA, (b) 1C0P, (c) 3C0P, (d) 0C5P, (e) 1C5P and (f) 3C5P.

4.5 Properties and characterization of PLA/chitosan/RWS foams

4.5.1 Morphology and physical properties

Based on properties of the foam samples prepared in the topic 4.4, the 1COP foams exhibited relatively low *in-vitro* degradation and high cell proliferation but its mechanical properties was relatively low. In addition, the PLA/RWS foams prepared in the topic 4.3 showed that the addition of treated RWS (1%GPMS-A 212-600) obtained T2L foam showed relatively high impact strength, tensile strength and tensile strain. Therefore, in the present study the 1COP foam was incorporated with 1%GPMS-A 212-600 RWS with the content of 1wt% and 3 wt% to obtain 1COPR1 and 1COPR3 foams, respectively, to study effect of the treated RWS (1%GPMS-A 212-600) on the 1COP foam. The pore morphology showing nine zones of 1COPR1 and 1COPR3 foam samples are shown in appendix A (Figure A14 and A15). Influence of treated RWS on pore morphology of the foams is shown in Figure 4.68. All foam samples showed closed cell with oval shape. Density, void fraction (%VF) and average pore size of the foam samples are listed in Table 4.20. The addition 1 wt% of 1%GPMS-A 212-600 RWS (1COPR1) increased foam density whereas it lowered void fraction, average pore size and pore size distribution as compared with PLA0.1 and 1COP foams. As increasing of 1%GPMS-A 212-600 RWS content to 3 wt%, the foam density and void fraction slightly changed, whereas average pore size increased. It was found that foam density was effected by void fraction, similarly to the foams in the topic 4.4. The average pore size could not be ranked in the same order with the void fraction or the density.

Table 4.20 Physical properties of foam samples

Foam sample	Average pore size (μm)	Density (g/cm^3)	VF (%)
PLA0.1	495 ± 200	0.746 ± 0.007	39.0 ± 0.5
1COP	450 ± 175	0.723 ± 0.002	40.9 ± 0.2
1COPR1	371 ± 104	0.828 ± 0.005	32.3 ± 0.4
1COPR3	439 ± 130	0.826 ± 0.004	37.8 ± 03

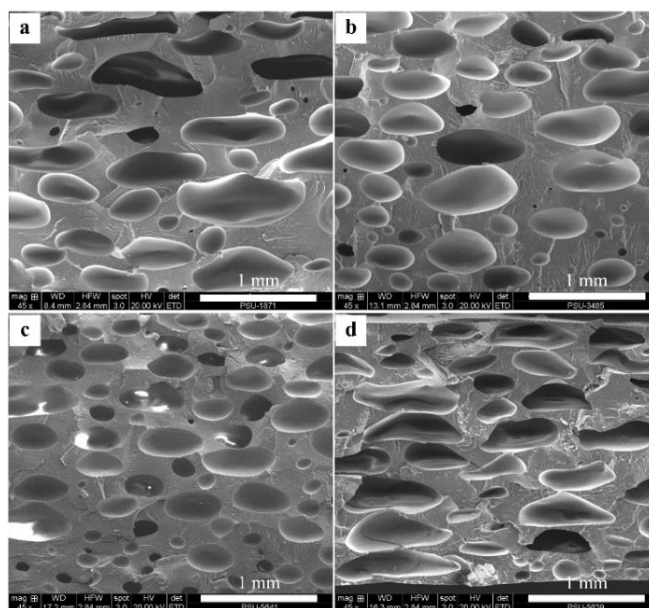


Figure 4.68 Cell morphology of PLA compounded foams: (a) PLA0.1, (b) 1C0P, (c) 1C0PR1 and 1C0PR3 foam.

4.5.2 Mechanical properties

The effects of 1% GPMS-A 212-600 RWS on the Izod impact strength, tensile properties and flexural properties of the foams are displayed in Figure 4.69, 4.70 and 4.71, respectively. The data were statistically analyzed, and these are listed in Table 4.21. All of mechanical properties exhibited the similar trend, except strain at break. The addition of 1% GPMS-A 212-600 RWS increased the mechanical properties as compared with PLA0.1 and 1C0P foams. However, the mechanical properties decreased with increasing treated-RWS content from 1 to 3 wt%. It seems that mechanical properties of the foams were influenced by foam density and void fraction. The 1C0PR1 foam exhibiting the highest density and the lowest void fraction showed the highest mechanical properties, whereas the 1C0P exhibiting the lowest density and the highest void fraction showed the lowest mechanical properties.

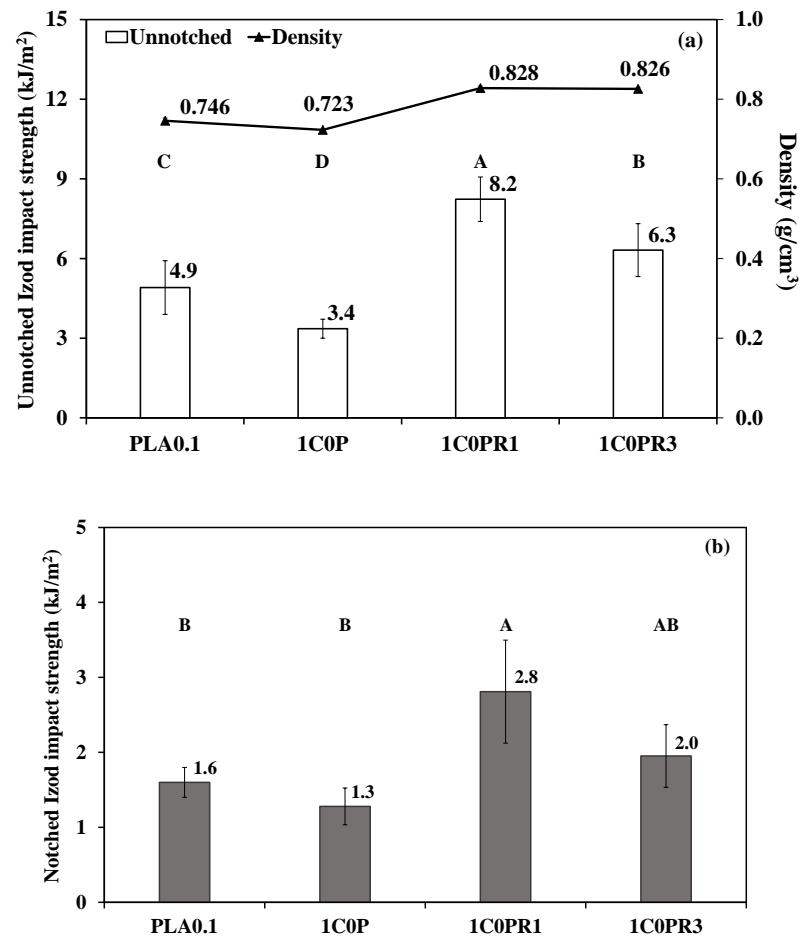
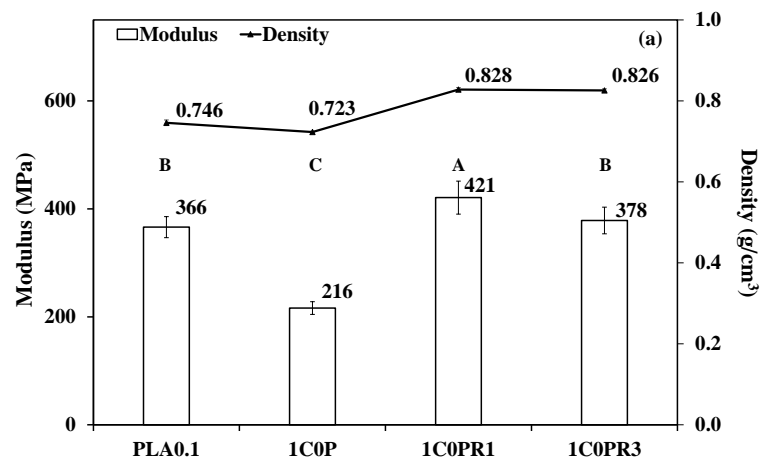


Figure 4.69 Izod impact strength of foam samples: (a) unnotched and (b) notched specimens, average values with different letters are significantly different at $p < 0.05$.



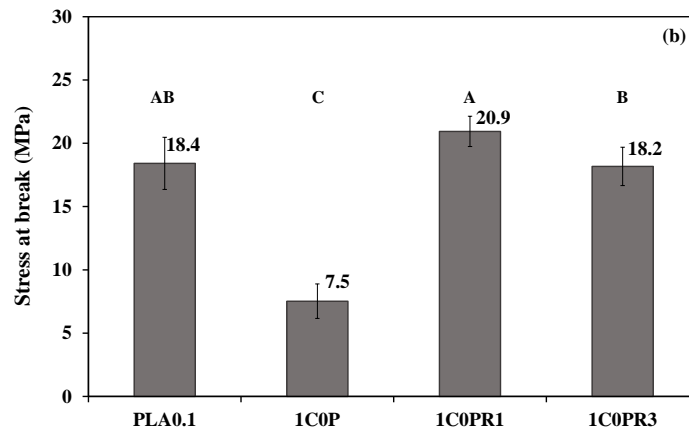


Figure 4.70 Tensile properties of foam samples: (a) tensile modulus and (b) stress at break, average values with different letters are significantly different at $p < 0.05$.

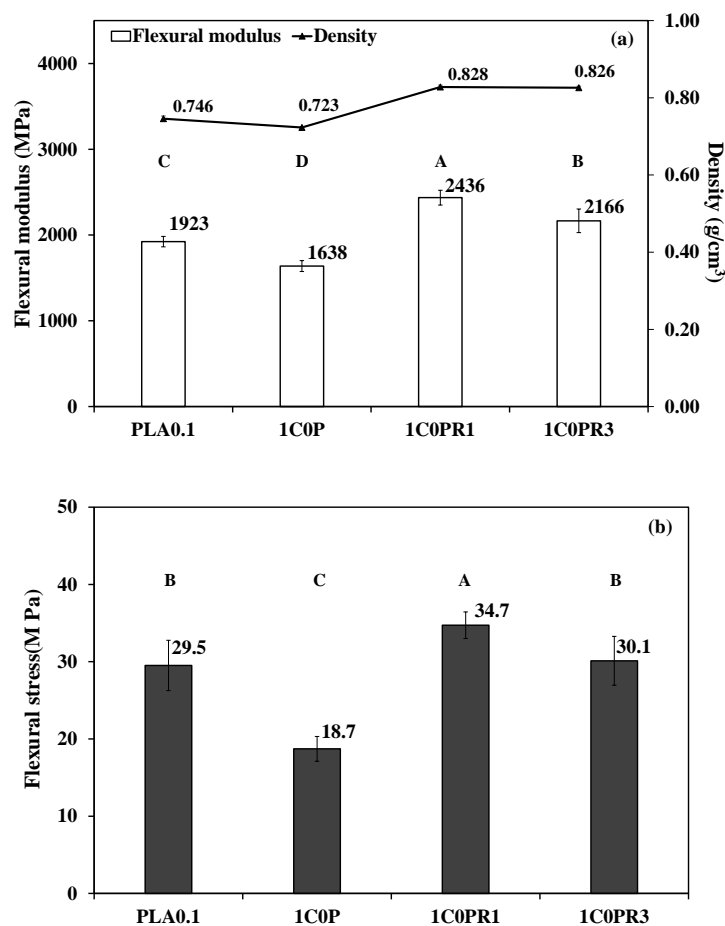


Figure 4.71 Flexural properties of foam samples: (a) flexural modulus and (b) flexural stress, average values with different letters are significantly different at $p < 0.05$.

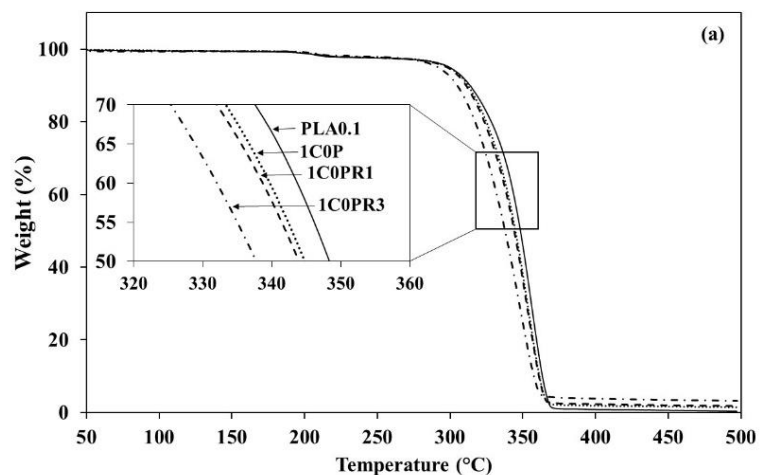
Table 4.21 Mechanical and thermal degradation properties of foam samples

Foam samples	PLA0.1	1C0P	1C0PR1	1C0PR3
Unnotched impact strength (kJ/m ²)	4.9 ± 1.0 ^C	3.4 ± 0.4 ^D	8.2 ± 0.8 ^A	6.3 ± 1.0 ^B
Notched impact strength (kJ/m ²)	1.6 ± 0.2 ^B	1.3 ± 0.3 ^B	2.7 ± 0.7 ^A	2.0 ± 0.4 ^{AB}
Tensile modulus (MPa)	366 ± 20 ^B	216 ± 12 ^C	421 ± 31 ^A	378 ± 25 ^B
Tensile strength (MPa)	18.4 ± 2.1 ^{AB}	7.5 ± 1.4 ^C	20.9 ± 1.1 ^A	18.2 ± 1.5 ^B
Strain at break (%)	8.3 ± 1.3 ^A	5.6 ± 1.2 ^B	7.7 ± 1.5 ^A	8.2 ± 0.7 ^A
Flexural modulus (MPa)	1923 ± 61 ^B	1638 ± 64 ^C	2436 ± 87 ^A	2166 ± 137 ^B
Flexural strength (MPa)	29.5 ± 3.3 ^{AB}	18.7 ± 1.6 ^C	34.7 ± 1.7 ^A	30.0 ± 3.2 ^B
T _{d onset} (°C)	332	326	325	315
T _d (°C)	356	354	353	347

Footnotes: Average values of mechanical properties with different letters in the same column are significantly different at $p < 0.05$.

4.5.3 Thermal degradation properties

Figure 4.72(a) and (b) displayed TGA and DTG thermograms of the foams, respectively. T_{d onset} evaluated from TGA thermogram and T_d at the peak of DTG thermogram are listed in Table 4.20. It was found that the addition of chitosan (1C0P) and mixture of chitosan and 1%GPMS-A 212-600 RWS (1C0PR1 and 1C0PR3) slightly decreased thermal stability of the foams.



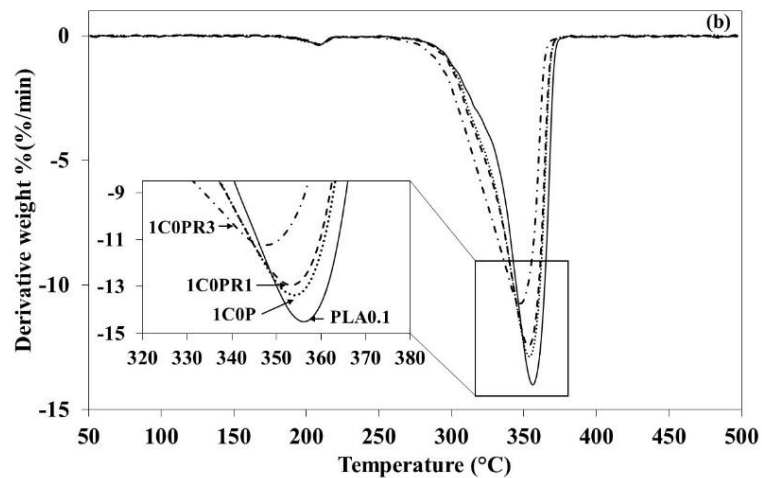


Figure 4.72 (a) TGA and (b) DTG curves of PLA foam and PLA/CH/RWS foams.

4.6 References

1. Kamphunthong, W., Hornsby, P. and Sirisinha, K. 2012 Isolation of cellulose nanofibers from Para rubber wood and their reinforcing effect in poly(vinyl alcohol) composites. *Journal of Applied Polymer Science*. 125: 1642–1651.
2. Moigne, N. L., Longerey, M., Taulemesse, J.-M., Bènèzet, J.-C. and Bergeret, A. 2014 Study of the interface in natural fibres reinforced poly(lactic acid) biocomposites modified by optimized organosilane treatments. *Industrial Crops and Products*. 52: 481-494.
3. Zhou, F., Cheng, G. and Jiang, W. 2014 Effect of silane treatment on micro structure of sisal fibers. *Applied Surface Science*. 292: 806-812.
4. Lv, S., Tan, H., Gu, J. and Zhang, Y. 2015 Silane modified wood flour blended with poly(lactic acid) and its effects on composite performance. *Bio Resources*. 10 (3): 5426-5439.
5. Xie, Y., Hill, C. A. S., Xiao, Z., Militz, H. and Mai, C. 2010 Silane coupling agents used for natural fiber/polymer composites: A review. *Composites Part A*. 41: 806-819.
6. Jaya, H., Omar, M. F., Akil, H. M., Ahamd, Z. A., Zulkepli, N. N., Abdullah, M. M. a. B., Sandu, I. G. and Vizureanu, P. 2016 Effect of surface modification on sawdust reinforced high density polyethylene composites under a wide range of strain rates. *Materials Plastic*. 53 (1): 85-90.

7. Shukla, D. K., Kasisomayajula, S. V. Parameswaran, V. 2008 Epoxy composites using functionalized alumina platelets as reinforcements. *Composites Science and Technology*. 68: 3055-3063.
8. Tee, Y. B., Talib, R. A., Abdan, K., Chin, N. L., Basha, R. K. and Yunus, K. F. M. 2013 Thermally grafting aminosilane onto kenaf-derived cellulose and its influence on the thermal properties of poly(lactic acid) composites. *Bio Resources*. 8 (3): 4468-4483.
9. Wahab, M. A., Jellali, S. and Jedidi, N. 2010 Ammonium biosorption onto sawdust: FTIR analysis, kinetics and adsorption isotherms modeling. *Bioresource Technology*. 101: 5070-5075.
10. Liu, R., Luo, S., Cao, J. and Peng, Y. 2013 Characterization of organo-montmorillonite (OMMT) modified wood flour and properties of its composites with poly(lactic acid). *Composites Part A*. 51: 33-42.
11. Tábi, T., Sajó, I. E., Szabó, F., Luyt, A. S. and Kovács, J. G. 2010 Crystalline structure of annealed polylactic acid and its relation to processing. *eXPRESS Polymer Letters*. 4 (10): 659-668.
12. Luo, Y., Zhang, J., Qi, R., Lu, J., Hu, X. and Jiang, P. 2013 Polylactide foams prepared by a traditional chemical compression molding method. *Journal of Applied Polymer Science*. 330-337.
13. Reyes-Labrata, J. A. and Marcilla, A. 2008 Kinetic study of the decomposition involved in the thermal degradation of commercial azodicarbonamide. *Journal of Applied Polymer Science*. 107: 339-346.
14. Xie, Y., Li, P., Wang, H., Qian, H. and Yao, W. 2013. Comparative studies by IR, Raman, and surface-enhanced Raman spectroscopy of azodicarbonamide, biurea and semicarbazide hydrochloride. *Spectrochimica Acta Part A: Molecular and Biomolecular Spectroscopy Engineering*. 144: 80-84.
15. Hutmacher, D. W. 2000 Scaffolds in tissue engineering bone and cartilage. *Bio materials*. 21: 2529-2543.
16. Rakmae, S., Ruksakulpiwat, Y., Sutapun, W. and Suppakarn, N. 2012 Effect of silane coupling agent treated bovine bone based carbonated hydroxyapatite on *in-vitro* degradation behavior and bioactivity of PLA composites. *Materials Science and Engineering C*. 32: 1428-1436.

17. Revati, R., Abdul Majid, M. S., Ridzuan, M. J. M., Basaruddin, K. S., M. N. Rahman Y., Cheng, E. M. and Gibson, A. G. 2017 *In-vitro* degradation of a 3D porous Pennisetum purpureum/PLA biocomposite scaffold. *Journal of the Mechanical Behavior of Biomedical Materials*. 74: 383-391.
18. Kramschuster, A., and Turng, L.-S. 2013. Fabrication of tissue engineering scaffolds. *Handbook of Biopolymers and Biodegradable Plastics*. <http://dx.doi.org/10.1016/B978-1-4557-2834-3.00017-3>. (accessed 10/8/2018).
19. Mihai, M., Huneault, M. A., Favis, B. D. and Li, H. 2007 Extrusion foaming of semi-crystalline PLA and PLA/thermoplastic starch blends. *Macromolecules Bioscience*. 7: 907-920.
20. Guo, G., Lee, Y. H., Rizvi, G. M. and Park, C. B. 2008 Influence of wood fiber size on extrusion foaming of wood fiber/HDPE composites. *Journal of Applied Polymer Science*. 107: 3505-3511.
21. Mofokeng, J. P., Luyt, A. S., Tábi, T. and Kovács, J. 2011 Comparison of injection moulded, natural fibre-reinforced composites with PP and PLA as matrices. *Journal of Thermoplastic Composite Materials*. 25 (8): 927–948.
22. Hsueh, Y.-S., Savitha, S., Sadhasivam, S., Lin, F.-H. and Shieh, M.-J. 2014 Design and synthesis of elastin-like polypeptides for an ideal nerve conduit in peripheral nerve regeneration. *Materials Science and Engineering C*. 38: 119-126.
23. Wood, K., Szewczuk, M. R., Rousseau, D. and Neufeld, R. J. 2018 Oseltamivir phosphate released from injectable Pickering emulsions over an extended term disables human pancreatic cancer cell survival. *Oncotarget*. 9 (16): 12754-12768.
24. Zhou, H., Lawrence, J. G. and Bhaduri, S. B. 2012 Fabrication aspects of PLA-CaP/PLGA-CaP composites for orthopedic application: A review. *Acta Biomaterialia*. 8: 1999-2016.
25. Bose, S., Roy, M. and Bandyopadhyay, A. 2012 Recent advances in bone tissue engineering scaffolds. *Trends Biotechnol*. 30 (10): 546-554.
26. Dutta, R. C., Dey, M., Dutta, A. K. and Basu, B. 2017 Competent processing techniques for scaffolds in tissue engineering. *Biotechnology Advances*. 35: 240-250.

27. Râpă, M., Mitelut, A. C., Tanase, E. K., Grosu, E., Popescu, P., Popa, M. E., Resnes, J. T., Sivertsvik, M., Darie-Nită, R. N. and Vasile, C. 2016 Influence of chitosan on mechanical, thermal, barrier and antimicrobial properties of PLA-biocomposites for food packaging. *Composites Part C*. 102: 112-121.
28. Zhang, W., Chen, B., Zhao, H., Yu, P., Fu, D., Wen, J. and Peng, X. 2013 Processing and characterization of supercritical CO₂ batch foamed poly(lactic acid)/poly(ethylene glycol) scaffold for tissue engineering application. *Journal of Applied Polymer Science*. 3066-3073.
29. Almeida, M. G., Demori, R., Zattera, A. J. and Zeni, M. 2007 Morphological analysis of polyethylene foams with post-use material incorporated. *Polymer Bulletin*. 59: 83-90.
30. Zimmermann, M. V. G., Brambilla, V. C., Brandalise, R. N. and Zattera, A. J. 2013 Observations of the effects of different chemical blowing agents on the degradation of poly(lactic acid) foams in simulated soil. *Materials Research*. 16 (6): 1266-1273.
31. Vázquez, M. O., Ramírez-Arreola, D. E., Bernache, J., Gómez, C., Robledo-Ortiz, J. R., Rodrigue, D. and González-Núñez, R. 2009 Using chitosan as a nucleation agent in thermoplastic foams for heavy metal adsorption. *Mecromolecular Symposia*. 283-284: 152-158.
32. Chen, B.-Y., Jing, X., Mi, H.-Y., Zhao, H., Zhang, W.-H., Peng, X.-F. and Turng, L.-S. 2015 Fabrication of polylactic acid/polyethylene glycol (PLA/PEG) porous scaffold by supercritical CO₂ foaming and particle leaching. *Polymer Engineering and Science*. 1339-1348.
33. Abbasi, M., Khorasani, S. N., Bagheri, R. and Esfahani, J. M. 2011 Microcellular foaming of low-density polyethylene using Nano-CaCO₃ as a nucleating agent. *Polymer Composites*. 1718-1725.
34. Zhai, W., Yu, J., Wu, L., Ma, W. and He, J. 2006 Heterogeneous nucleation uniformizing cell size distribution in microcellular nanocomposites foams. *Polymers*. 47: 7580-7589.
35. Litauszki, K. and Qi Kmetty, A. 2018 Development and characterization of innovative biopolymer foams. *Materials Science and Engineering*. 426: 1-9.

36. Sun, P., Qian, T. Y., Ji, X. Y., Wu, C., Yan, Y. S. and Qi, R. R. 2018 HDPE/UHMWPE composite foams prepared by compression molding with optimized foaming capacity and mechanical properties. *Journal of Applied Polymer Science*. 46768: 1-12.
37. Isa, S. A. B. M. and Mohammed, R. 2015 Physical and mechanical properties of chitosan and polyethylene blend for food packaging film. *International Journal of Mechanical and Production Engineering*. 3 (10): 51-55.
38. Li, L., Ding, S. and Zhou, C. 2004 Preparation and degradation of PLA/chitosan composite materials. *Journal of Applied Polymer Science*. 91: 274-277.
39. Balu, R., Sampath Kumar, T. S., Ramalingam, M. and Ramakrishna, S. 2011 Electrospun polycaprolactone/poly(1,4-butylene adipate-co-polycaprolactone) blends: potential biodegradable scaffold for bone tissue regeneration. *Journal of Biomaterials and Tissue Engineering*. 1: 30-39.

CHAPTER 5

CONCLUSIONS

5.1 Preparation and characterization of PLA/RWS compounds

The unfoamed sheets of PLA compounded with nontreated-RWS with four particle size ranges were prepared by melt blending in twin screw extruder followed by compression molding, and the mechanical properties were tested. Based on the mechanical properties, the RWS content of 5 wt% and RWS particle size of ≤ 75 μm and 212-600 μm were used to prepare unfoamed PLA/treated RWS, and these two particle size ranges were treated with NaOH and/or silane (GPMS or APMS) using method A, B and C. The RWS surface modification was characterized by FTIR, TGA, SEM and XRD analysis. It was found that the surface treatment using NaOH followed by GPMS (method A) partially eliminated hemicellulose and non-essential parts from RWS surface confirmed by FTIR. The SEM images showed that the surface of RWS became cleaner and showed a grooved surface after surface treatment. The surface modification did not change the crystal structure of RWS, whereas the thermal stability of RWS increased after surface treatment. In addition, the crystallinity index (CI) of the smaller particle RWS (≤ 75 μm) increased, whereas the CI of the larger particle RWS (212-600 μm) slightly changed after GPMS treatment using method A. Thermal properties of PLA/treated-RWS compounds were characterized by DSC analysis. It was found that the addition of the larger particle RWS (212-600 μm) to PLA increased degree of crystallinity (X_{c1}), whereas the X_{c1} decreased when the smaller particle RWS (≤ 75 μm) was added, except the addition of nontreated-RWS 75. The addition of both particle RWS increased degree of crystallinity by excluding ΔH_{cc} (X_{c2}) of PLA. The mechanical properties including impact strength and tensile properties showed that the compounds of PLA/NaOH-treated 75, PLA/1%GPMS-A 75 and PLA/1%GPMS-A 212-600 exhibited relatively high mechanical properties. These compounds were used to prepare PLA/RWS foams.

5.2 Preparation and characterization of PLA foams and PLA/RWS foams

PLA foams were successfully prepared by compression molding using AZDC as a chemical blowing agent and ZnO as an accelerator. The ZnO content was varied. The foams showed closed-cell morphology. The void fraction (%VF) and average pore sizes of PLA foam increased as increased ZnO content. As ZnO content increased, the thermal degradation of PLA foam decreased. The remaining AZDC was found in the PLA foams confirmed by TGA and FTIR analysis. Furthermore, increasing ZnO content decreased foam density, mechanical properties and *in-vitro* degradation of the foam because of increasing its average pore size. The PLA/RWS foams were also successfully prepared using the similar method to the PLA foams. The PLA/RWS foams also showed closed-cell morphology. The foam exhibiting higher density showed the lower %VF. The density of the foam samples ranked in the following order: T1S < PLA0.1 < T2L < T2S < T0L, and the %VF of the foam showed the vice versa ranking. Average pore size of the foam ranked from 336 to 608 μm , except T0L foam, it showed very large average pore size (1022 μm) and pore size distribution. RWS particle sizes, surface treatment, foam density and %VF were factors controlling the mechanical properties of the foams. The addition of RWS increased or decreased the mechanical properties depending on the mentioned factors. The T2L foam showed the highest mechanical properties, whereas T1S foam showed the lowest mechanical properties. The preliminary investigation of cytotoxicity and *in-vitro* degradation could confirm that these foams were suitable for bone scaffold application. All foams samples showed non-toxicity proved by increasing cell proliferation throughout the cell culture time, and the *in-vitro* degradation testing showed that T2L and T2S foams demonstrated a slow biodegradation. The results including average pore size, void fraction, *in-vitro* degradation and cytotoxicity indicated the suitability of PLA0.1, T2S and T2L foams for bone scaffold applications.

5.3 Preparation and characterization of PLA/PEG/CH compounds, PLA/PEG/CH foams and PLA/CH/RWS foams

The unfoamed PLA/PEG/CH compounded sheets were prepared by melt blending in twin screw extruder followed by compression molding, and the mechanical and thermal properties were tested. It was found that the addition of chitosan and increasing chitosan content decreased the Izod impact strength and tensile properties of PLA and plasticized PLA. The addition of PEG to PLA or PLA/CH blend decreased the tensile properties. However, the Izod impact strength of PLA and PLA/chitosan blend were enhanced by the addition of PEG. The thermal properties characterized by DSC demonstrated that PEG and chitosan acted as nucleating agent of PLA. The PLA foam with and without PEG and/or chitosan was successfully prepared by the similar procedure to PLA foams and PLA/RWS foams. Chitosan was used as a bioactive compound, and PEG was used as a plasticizer. The thermal properties characterized by DSC of the foams also showed that PEG and chitosan acted as nucleating agent of PLA. The PLA foam containing the mixing of PEG and chitosan (3C5P) showed the lowest T_g , T_{cc} and T_m . The compounded foams showed closed-cell morphology and the addition of chitosan and/or PEG decreased average pore size and pore size distribution of the foams. The Izod impact strength of 0C5P and 1C5P foam samples were higher than that of PLA foam, whereas the other foam samples showed lower impact strength. The addition of PEG and/or chitosan degraded the tensile properties of the foams. The cytotoxicity test evaluated from the cell proliferation obtained from cell culturing of MG63 (osteoblast-liked cell) on the foam specimens of 1C0P and 0C5P showed slightly lower than that of PLA foam which demonstrated the suitability of these foam for bone scaffold application. The addition of RWS (1% GPMS-A 212-600) to 1C0P foam increased the density and decreased void fraction, average pore size and pore size distribution of the foam, thereby increasing the mechanical properties of the foam.

5.4 Perspectives

In the present study, PLA foams, PLA/RWS foams, PLA/PEG/CH foams and PLA/CH/RWS foams were successfully prepared, and the physical and mechanical properties of these foams were investigated. It was found that average pore size, void fraction and *in-vitro* degradation of the PLA compounded foams (PLA0.1, T1S, T2S, T2L, 0C5P, 1C0P foams) were suitable for bone scaffold application. Furthermore, all foams showed non-cytotoxicity. However, the obtained foams showed closed-cell morphology, whereas bone scaffold requires opened-cell morphology. Therefore, an idea for further research is development closed-cell morphology of the PLA compounded foams mentioned above to be the foams with opened-cell morphology by following methods:

- 1) Adding of additives to improved melt-viscosity and elasticity of PLA compounded foam.
- 2) Adjusting of processing condition. The mold-opening temperature should be varied in the further research to design pore morphology of the foams
- 3) Changing of foaming method. 3D printing is an interesting method which can design to obtain the foam with opened-cell morphology. Therefore, preparation of PLA foams with the formulae mentioned above by using 3D printing method is an interesting for the further research.

APPENDICES

APPENDIX A

SEM images demonstrating pore morphology of nine zones of the foam specimens

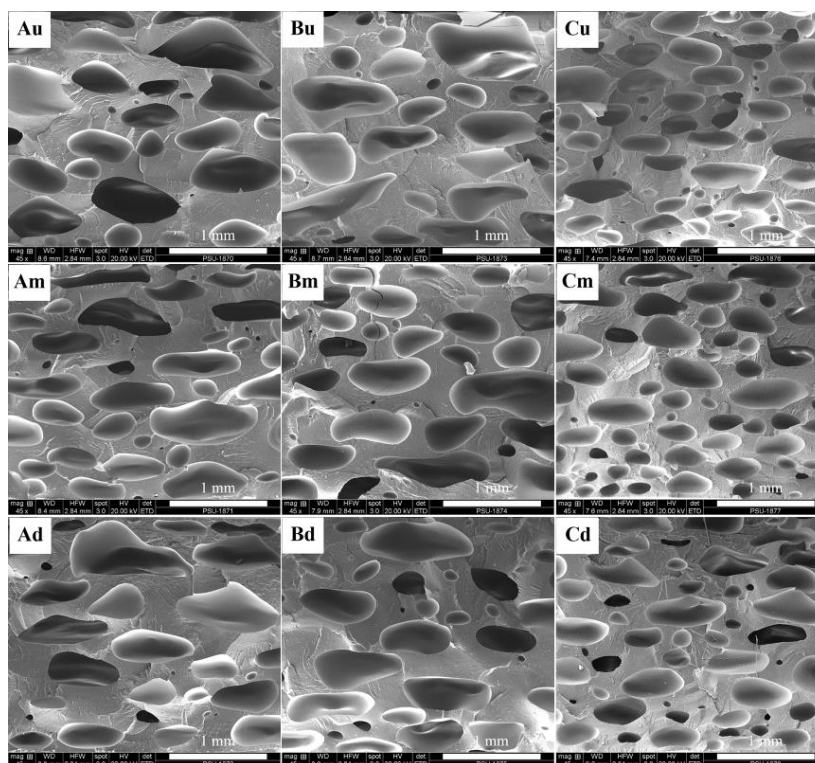


Figure A1 Pore morphology of PLA0.1 foam.

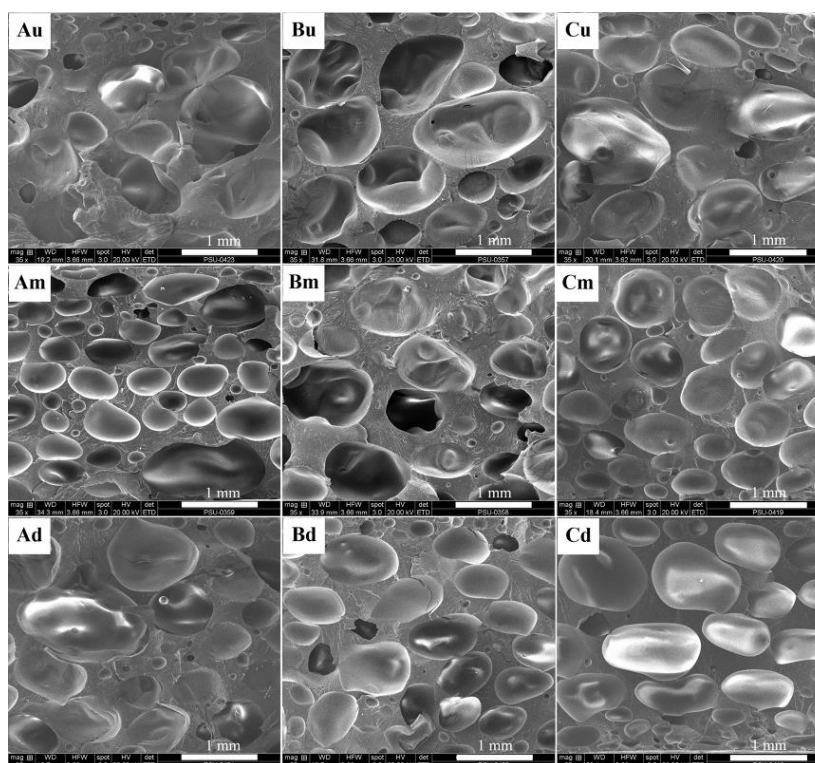


Figure A2 Pore morphology of PLA0.3 foam.

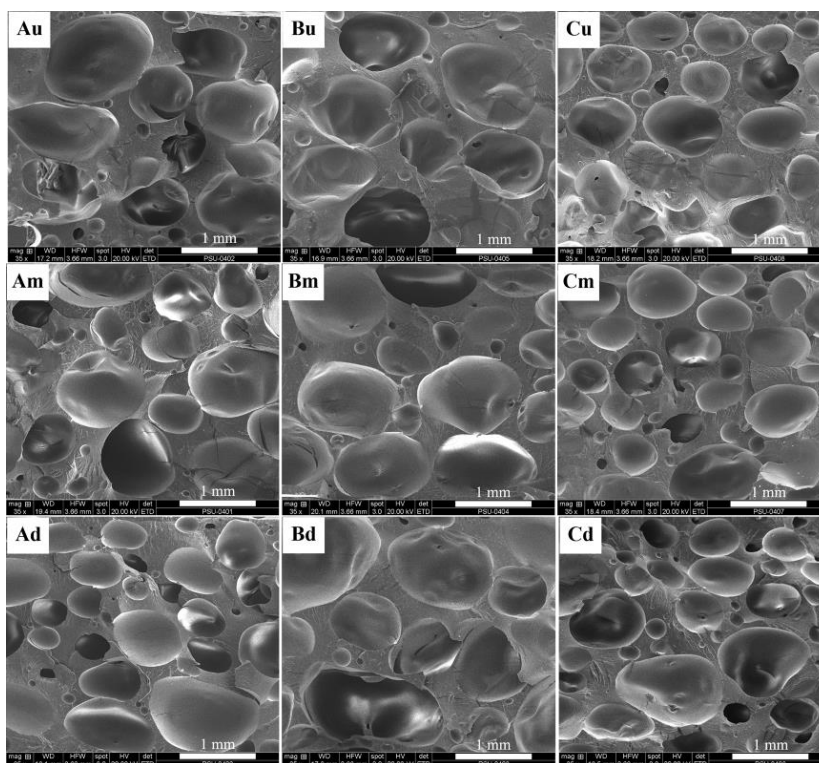


Figure A3 Pore morphology of PLA0.5 foam.

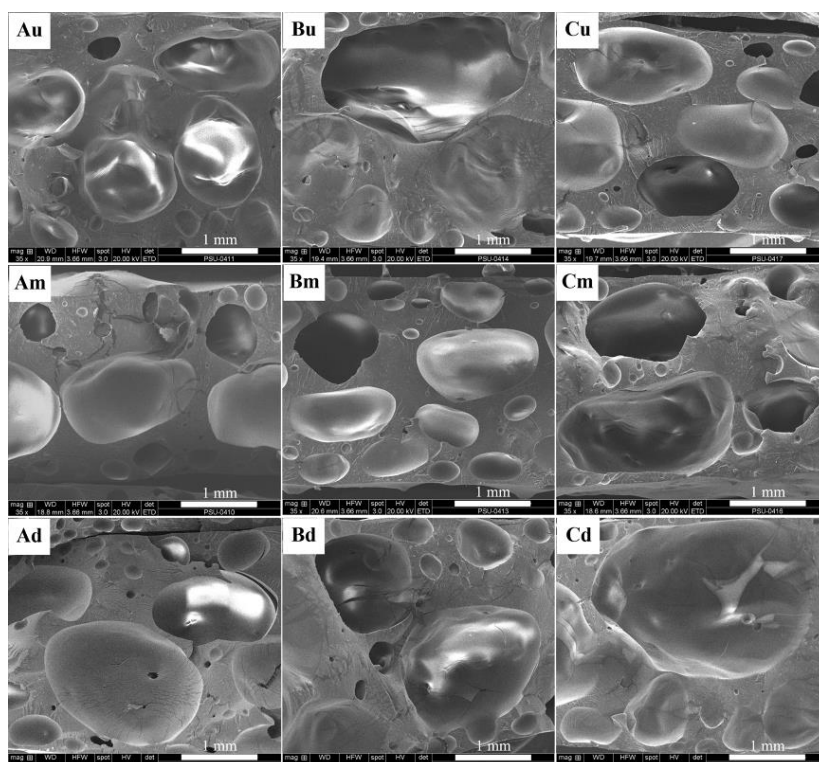


Figure A4 Pore morphology of PLA1.0 foam.

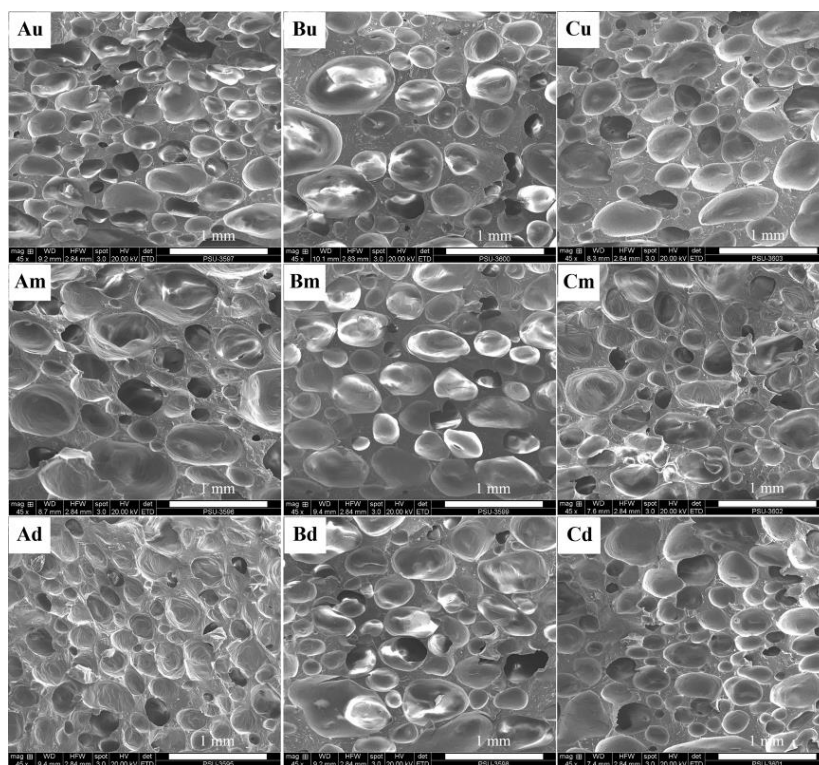


Figure A5 Pore morphology of T1S foam.

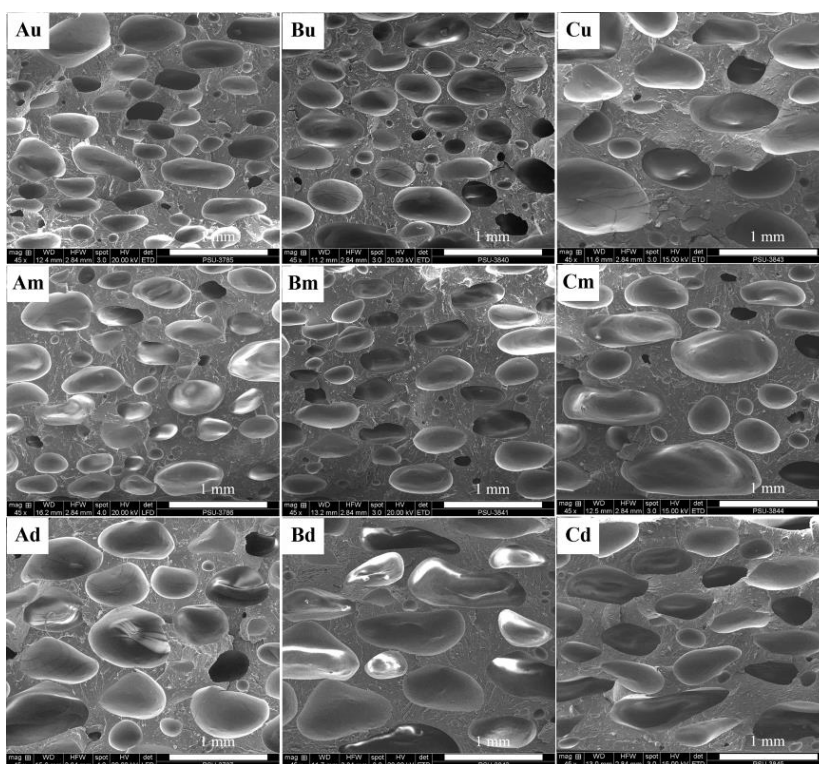


Figure A6 Pore morphology of T2S foam.

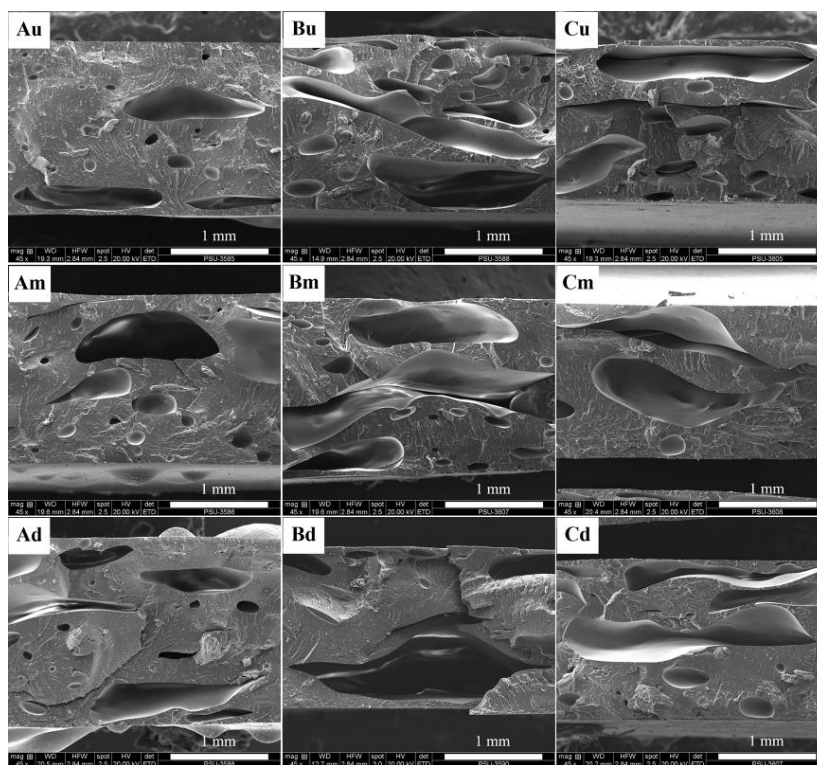


Figure A7 Pore morphology of T0L foam.

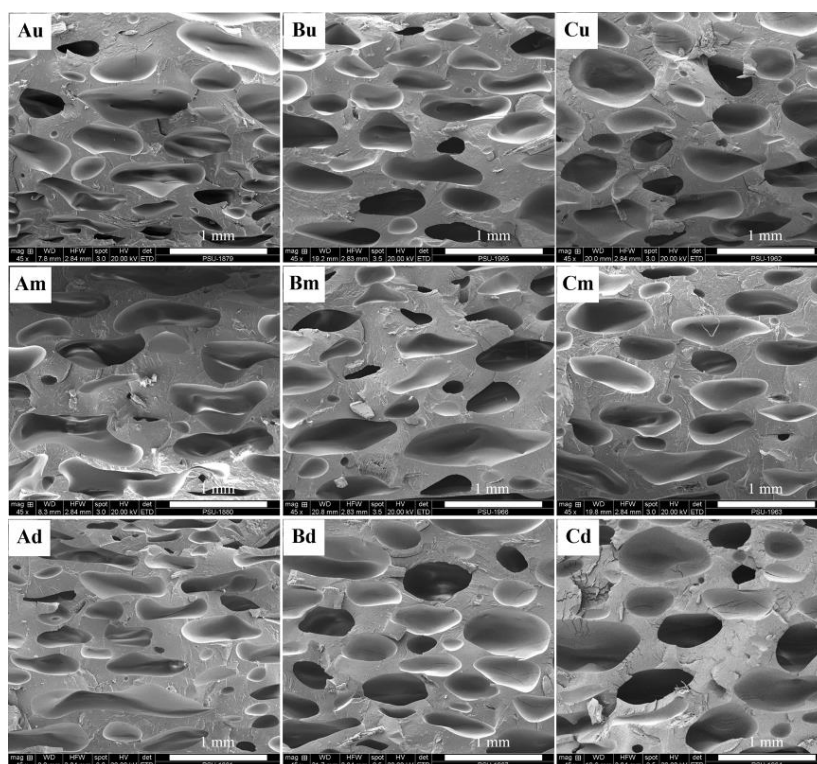


Figure A8 Pore morphology of T2L foam.

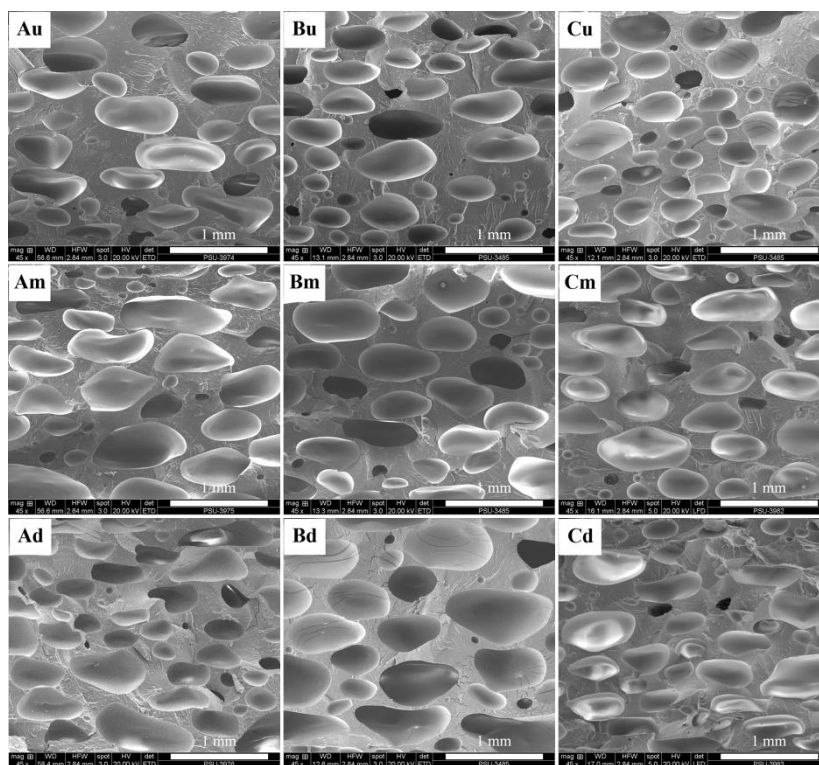


Figure A9 Pore morphology of 1COP foam.

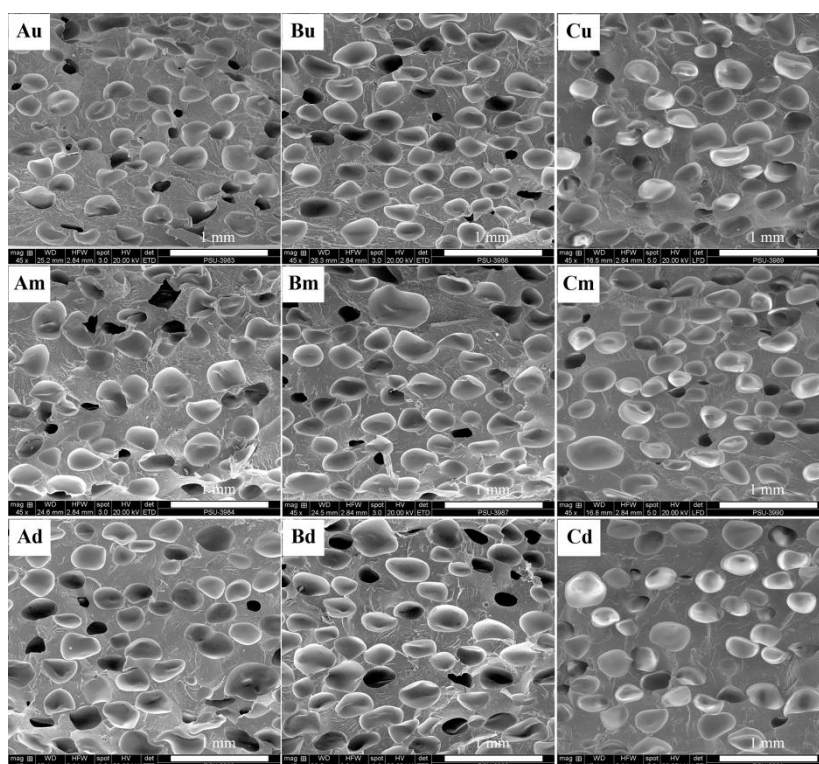


Figure A10 Pore morphology of 3COP foam.

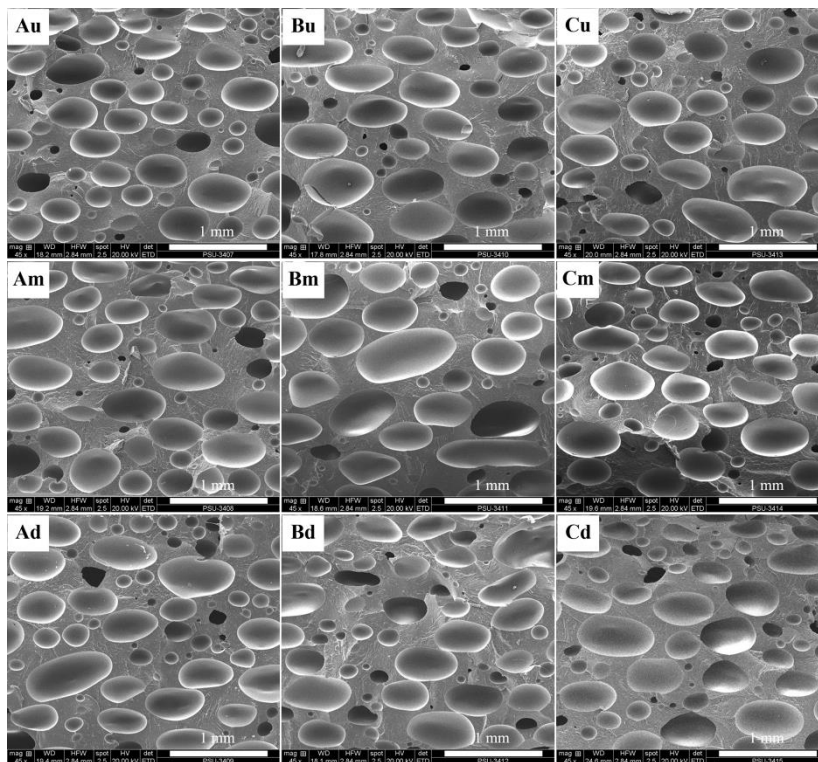


Figure A11 Pore morphology of 0C5P foam.

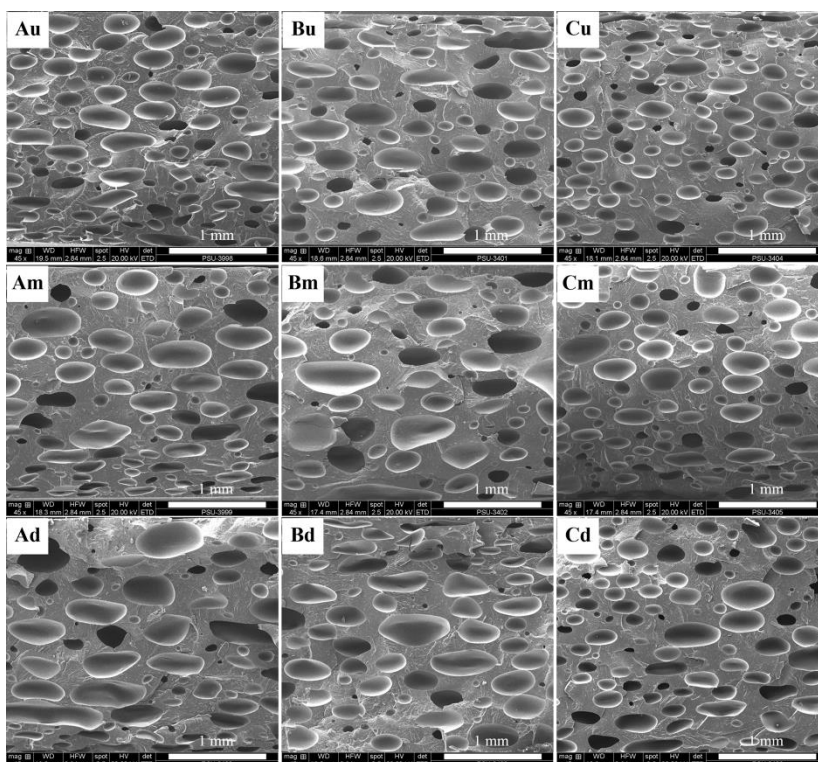


Figure A12 Pore morphology of 1C5P foam.

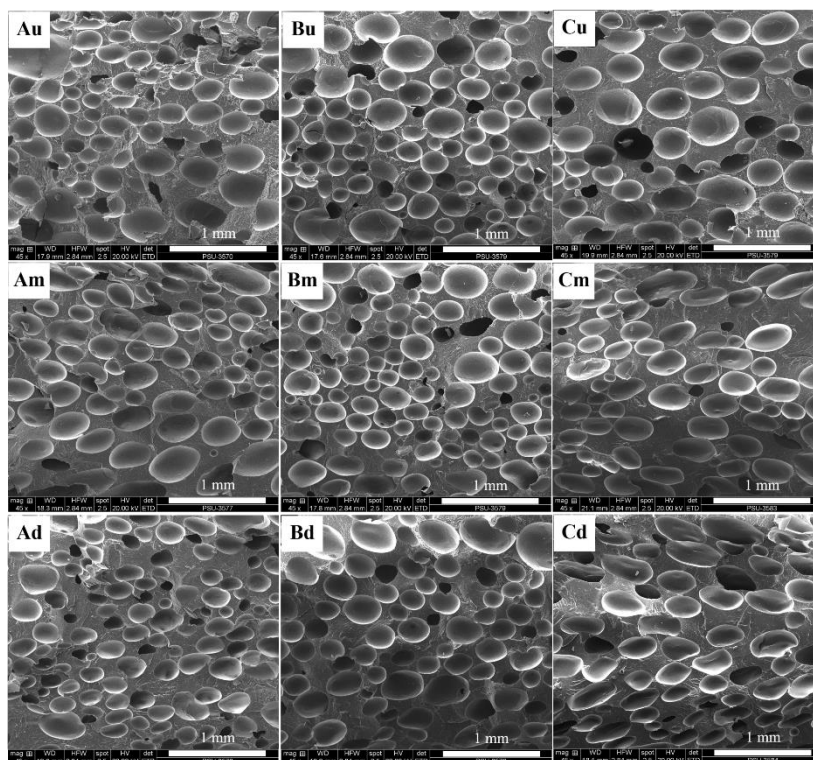


Figure A13 Pore morphology of 3C5P foam.

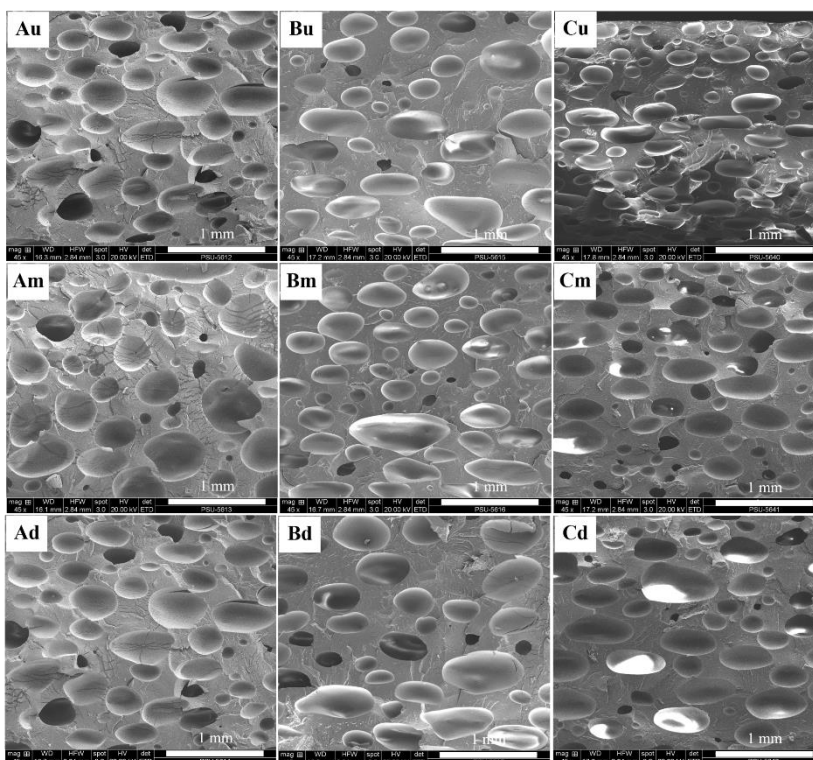


Figure A14 Pore morphology of 1C0PR1 foam.

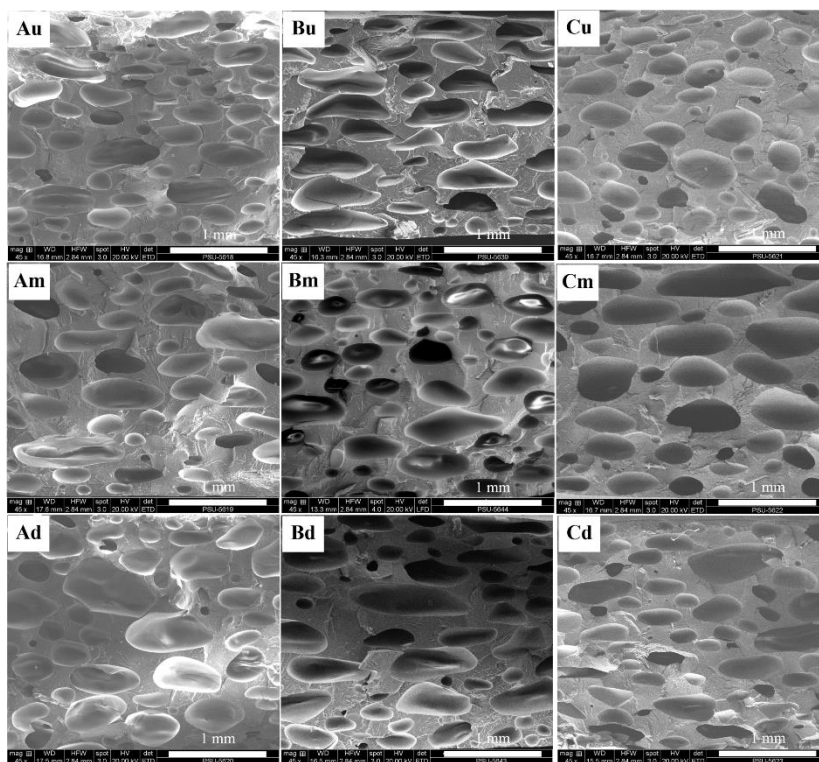


Figure A15 Pore morphology of 1C0PR3 foam.

APPENDIX B

(Abstract)

Topic: Effect of zinc oxide content on morphology and tensile properties of PLA foam prepared by compression molding

Conference name: The 11th SPSJ International Polymer Conference (IPC 2016)

Organization name: The Society of Polymer Science Japan

Date/Place: December 13-16, 2016, Fukuoka International Congress Center, Fukuoka, Japan

14P-S7-050b

Effect of Zinc Oxide Content on Morphology and Tensile Properties of PLA Foam

Prepared by Compression Molding

P. Sungsee and V. Tanrattanakul

Department of Materials Science and Technology, Faculty of Science,

Prince of Songkla University, Hatyai, Songkhla, 90110, Thailand

Phone: +66-74-288-362; Fax: +66-74-446-925; Email: varaporn.t@psu.ac.th

Introduction

Scaffold is an artificial structure which is able to support three-dimensional tissue formation. Scaffold can be cultured with many types of cells in order to induce tissues formation in vitro and in vivo. Poly (lactic acid) (PLA) is a biocompatible polymer widely used in the scaffold application. PLA scaffold is normally fabricated by many methods such as solvent casting and particulate leaching, supercritical gas foaming, electrospinning and melt processing etc. In this research, PLA foams were processed by compression molding using azodicarbonamide (AZDC) as a chemical blowing agent and zinc oxide (ZnO) as an accelerator.

This paper reported morphology of PLA foam and effects of ZnO contents on PLA foam cell sizes and tensile properties of PLA foam were examined.

Results and Discussion

PLA foams were prepared by 2 steps. The first step was a preparation of PLA compound. PLA, AZDC and ZnO were blended in a twin screw extruder. The second step was a foaming process. A sheet of PLA foam was fabricated by compression molding at 150 °C with the pressure of 150 kg/cm² for 10 min. The foam sheet was divided into 3 zones (A, B, and C) to observe cellular structure by SEM. The closed cell morphology was found and the cell size of each zone is shown in Figure 1a. The average cell size of PLA foam increased with increasing ZnO. Figure 1b represents the stress-strain curves of PLA foams. In general, larger cell size of foam causes the lower mechanical properties. Thus, an increase in ZnO content decreased the tensile properties of PLA foams.

References

- 1) Reyes-L., J. A. and Marcilla, A. *J. APPL POLYM. SCI.* **2007** (Published online in Wiley Inter Sci.)
- 2) Zhou, J. et al. *J. APPL POLYM. SCI.* **2014**, 131, 40473.

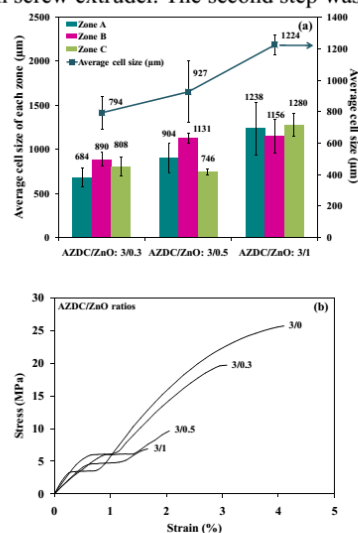


Figure 1. Effect of ZnO content: (a) average cell sizes and (b) stress-strain curves of PLA foams.

APPENDIX C

(Full Proceeding)

Topic: PLA foams for scaffold application

Conference name: Pure and Applied Chemistry International Conference 2018
(PACON2018)

Organization name: The Chemical Society of Thailand and in association with
Faculty of Science, Prince of Songkla University, Thailand

Date/Place: February 7-9, 2018, The 60th Anniversary of His Majesty the King's
Accession to the Throne International Convention Center, Hat Yai,
Songkhla, Thailand



PLA foams for scaffold application

Pasuta Sungsee, Varaporn Tanrattanakul*

Department of Materials Science and Technology, Faculty of Science,
Prince of Songkla University, Hat Yai, Songkhla 90110, Thailand

*E-mail: varaporn.t@psu.ac.th

Abstract:

Poly(lactic acid), PLA, is a biodegradable biomaterial used as a scaffold in tissue engineering application. PLA scaffold can be normally processed by many methods such as electrospinning, 3D printing, polymer phase separation, melt processing etc. Cellular structure or foam is a required structure of materials for the scaffold application. The present work is a preliminary study that focuses on a typical foam formation by using azodicarbonamide (AZDC) and zinc oxide (ZnO) as a chemical blowing agent and accelerator, respectively. PLA foam was prepared by compression molding. The objective of the present study is to evaluate the influence of ZnO content on properties of PLA foam including mechanical, thermal degradation, and in-vitro degradation properties. This is because ZnO content is one of important factors controlling the cellular structure of PLA foam. It was found that PLA foam presented closed cell morphology. The mechanical properties including notched Izod impact strength, tensile and flexural properties decreased as ZnO content increased. The in-vitro degradation study of PLA foam was determined in term of %weight loss in 2 months and demonstrated that an increment in ZnO content increased the %weight loss of PLA foam due to an increase of its average cell size.

1. Introduction

Scaffold is artificial structure with cellular form which is suitably cultured with many types of cells in order to induce cell proliferation, differentiation and tissue formation in vitro and in vivo.¹ Biomaterials mainly used to fabricate scaffold is divided into 3 types which are ceramic, natural polymer and synthetic polymer. Poly(lactic acid) (PLA) is a hydrophobic aliphatic polyester and is widely used in biomedical applications. It is easy to process which allows PLA to use in medical application in various shapes including sutures, nanoparticles, micelles rods films and scaffold.² PLA scaffold has been prepared by various techniques such as solvent casting/porogen leaching, thermal phase separation (TIPS), electrospinning, 3D printing, and melting process. PLA foam prepared by melting process using physical blowing agent have been reported.³⁻⁵ PLA foam prepared by physical foaming method (supercritical CO₂) contains the microcellular structure but it is required expensive special equipment.

Preparation of PLA foam by melting process and chemical blowing agent are an alternative choice because of easy operation, low cost and simple equipment. Chemical blowing agents (CBA) are divided into endothermic and exothermic blowing agents. Azodicarbonamide (AZDC) is a common chemical blowing agent and has been used in PLA foam preparation.^{6,7} Normally, zinc oxide (ZnO) is used as an accelerator of AZDC to decrease foaming temperature. Lou *et al.*⁸ found that AZDC/ZnO contents and mold opening temperature affected the average cell sizes, void fraction (%VF), mechanical properties and degradability of PLA foam prepared by melt blending in an internal mixer followed by compression molding. However, the effect of ZnO contents on PLA foam prepared by compression molding and opportunity to utilize the obtained foam as a scaffold in tissue engineering application have not been reported. The objective of the present study was to determine the effect of ZnO content in PLA foam in terms of cell

morphology, thermal degradation, *in-vitro* degradation and mechanical properties.

2. Materials and Methods

2.1 Materials

PLA 4042D was produced by Nature Works LLC (USA). Azodicarbonamide (AZDC) was purchased from Greatchem and Supply Pty., Ltd. (Thailand) and Zinc Oxide (ZnO) was purchased from Kit Phaibun Chemistry Ltd., Part (Thailand).

2.2 PLA foam preparation

PLA, AZDC, and ZnO were mixed together and then melt blending was carried out in a twin screw extruder at 150 °C with a screw speed of 150 rpm. It was necessary to avoid AZDC decomposition during extrusion. The compounded PLA was finally pressed in a closed mold (130 x 130 x 2 mm³) with a temperature of 150 °C under a pressure of 150 kg/cm² for 10 min to obtain the foam samples. The AZDC/ZnO weight ratio were varied into 3/0, 3/0.1, 3/0.5, and 3/1 wt/wt and total content of AZDC/ZnO was 2wt%. The obtained PLA foams were named PLA0, PLA0.3, PLA0.5, and PLA1.0, respectively.

2.3 PLA foam characterizations

The density of PLA foam (ρ_f) was measured by buoyancy method (ASTM D792). Three specimens were weighted in air and in n-hexane on analytical balance. The average densities were calculated. The void fraction (VF) was calculated according to equation (1)

$$\%VF = [1 - (\rho_f/\rho_s)] \times 100 \quad (1)$$

where ρ_s is a density of unfoamed PLA (1.223 g/cm³) and ρ_f is a density of foamed PLA.⁸ The morphology of PLA foam was investigated by using SEM-FEI® Quanta 400. All specimens were immersed in liquid nitrogen and then immediately fractured before coating with gold. The longest diameter of each pore was measured from SEM micrographs and average cell sizes were calculated. Thermogravimetric analysis (TGA) was carried out using STA449F3 Jupiter® (NETZSCH) with a heating rate of

5 °C/min from 30 °C to 500 °C under nitrogen atmosphere. Fourier Transform Infrared (FTIR) analysis was carried out using a Bruker® TENSOR 27 spectrometer in ATR mode. FT-IR spectra of the samples were recorded in the range 4000–400 cm⁻¹ with resolution of 4 cm⁻¹ and 132 scans.

2.4 Mechanical properties testing

The notched Izod impact strength and tensile properties were determined according to ASTM 256 and ASTM D412 die C, respectively. The crosshead speed was a 5 mm/min for tensile testing. Six specimens were used for every sample. An average value with standard deviations was reported.

2.5 *In-vitro* degradation testing

A phosphated-buffered solution (PBS) at a concentration of 0.1 M and pH 7.4 was in-house prepared according to Rakmae *et al.*⁹ *In-vitro* hydrolytic degradation of PLA foam was determined by soaking a specimen in PBS. Three specimens (2 x 10 x 60 mm³) from each sample were firstly weight to obtain an initial weight (W_o) and were then vertically placed in a 100 mL test tube filled with 35 mL PBS solution. The immersed specimens were incubated at 37 °C for 8 weeks. The PBS in all test tubes was weekly replaced by the fresh one. At the end of each period, the specimens were removed from PBS and wiped with a filter paper to remove surface water. After that, these specimens were rinsed by distilled water for 3 times and vacuum dried at a temperature of 65 °C to a constant weight (W_d). The percentage of weight loss of the specimen during immersion in PBS solution was calculated by equation (2).⁹

$$\%Weight\ loss = \left[\frac{W_o - W_d}{W_o} \right] \times 100 \quad (2)$$

3. Results and Discussion

3.1 PLA foam characterizations

PLA foam was successfully prepared by chemical compression molding method. The closed cell morphology observed by

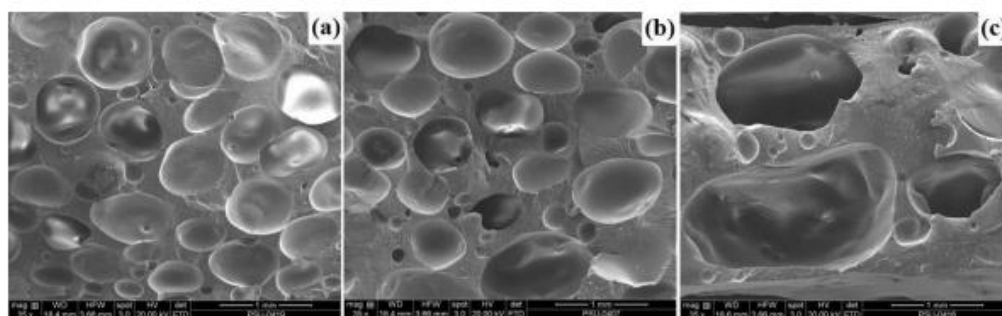


Figure 1. SEM micrograph of PLA foams with different AZDC/ZnO ratios: (a) 3/0.3, (b) 3/0.5, and (c) 3/1.0

SEM was found for all foam samples (Figure 1). The foam properties including in Table 1. It was found that PLA foam without ZnO (PLA0) showed the highest density. As ZnO content increased, the average cell size and %VF increased whereas the densities decreased. This was because an increase in ZnO content increased an efficiency of AZDC decomposition.⁸

Table 1. Properties of PLA foams

Sample	Density (g/cm ³)	%VF	Average cell size (μm)
PLA0	0.815	33.4	N/A
PLA0.3	0.695	43.1	794 ± 104
PLA0.5	0.652	46.7	914 ± 195
PLA1.0	0.628	48.7	1224 ± 63

Thermal stability of AZDC and PLA foams with different ZnO content was determined from TGA results. The TGA and DTG thermograms of AZDC are displayed in Figure 2. The decomposition of AZDC occurs through the competition of at least 3 exothermic reactions producing solids and gaseous mixtures of nitrogen, carbon monoxide, cyanic acid and ammonia.¹⁰ In the present study, AZDC displayed three decomposition temperature (T_d): 217.9 °C, 242.4 °C, and 315.7 °C; corresponding to three different reactions of AZDC decomposition.¹⁰

Figure 3 displayed TGA and DTG thermograms of PLA pellet and PLA foams.

The thermal degradation temperatures are listed in Table 2. The thermal stability of PLA foams decreased as ZnO content increased. The PLA pellet exhibited only one transition temperature (T_{d2}) at 359 °C whereas PLA foams exhibited 2 transition temperatures. The very small peak (T_{d1}) expected to be a decomposition of remaining AZDC and the sharp peak (T_{d2}) corresponded to decomposition of PLA foams.

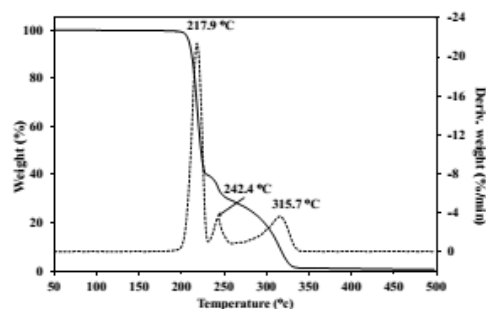


Figure 2. TGA and DTG thermograms of AZDC

Table 2. Thermal degradation temperature of PLA foams

Foam name	$T_{d\text{ onset}1}$ (°C)	$T_{d\text{ onset}2}$ (°C)	T_{d1} (°C)	T_{d2} (°C)
PLA pellet	-	344	-	359
PLA0	201	334	213	356
PLA0.3	196	329	206	342
PLA0.5	188	317	201	346
PLA1.0	182	314	197	338

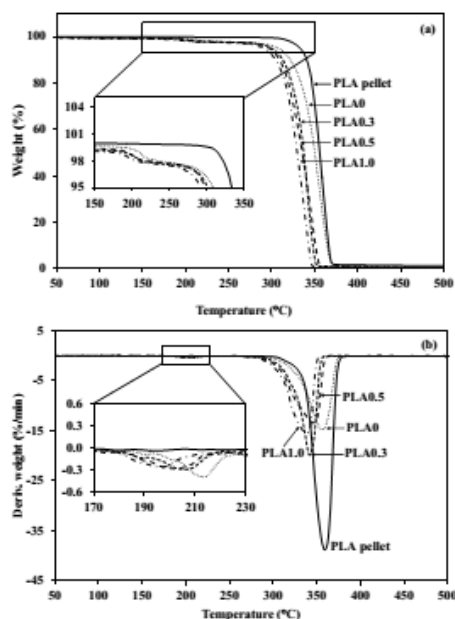


Figure 3. (a) TGA and (b) DTG thermograms of PLA pellet and PLA foams

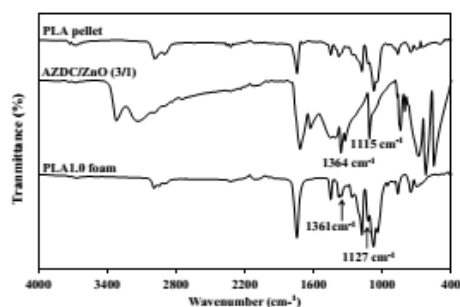


Figure 4. FTIR spectra of PLA pellet, AZDC/ZnO (3/1 wt/wt) and PLA1.0 foam

The remaining AZDC could be confirmed by FTIR results. The shifted characteristic peaks of AZDC/ZnO (3/1) were observed in the spectra of PLA1.0 foam as showed in Figure 4. The shifted characteristic peak from 1115 to 1127 cm⁻¹ assigned to the stretching vibration of C=O and N-C of AZDC. The shifted characteristic peak from 1364 to 1361 cm⁻¹ assigned to the bending vibration of N-C=O of AZDC.¹¹ Furthermore, it was found that $T_{d\ onset}$ and T_{d1} of PLA foam decreased as ZnO content increased (Table 2). This indicated that ZnO decreased the decomposition temperature and activated

decomposition rate of AZDC which was consistent with the previous work.⁸

3.2 Mechanical properties

The notched Izod impact strength of PLA significantly decreased with the addition of ZnO, and ZnO content showed slightly effect on the impact strength (Figure 5). The impact strength related to the density. The lower density showed the lower impact strength. ZnO content also affected the tensile and flexural properties as shown in Figures 6 and 7, respectively.

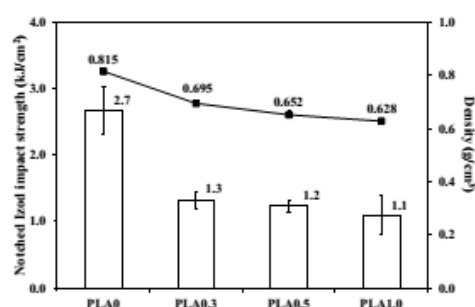


Figure 5. Effect of ZnO content on density and notched Izod impact strength of PLA foams

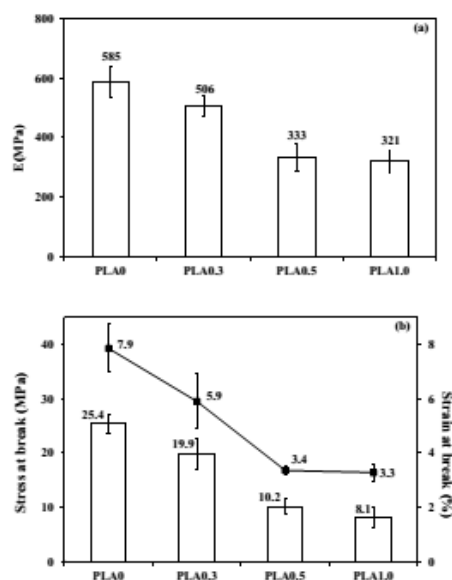


Figure 6. Effect of ZnO content on tensile properties of PLA foams: (a) Young's modulus and (b) stress at break and strain at break

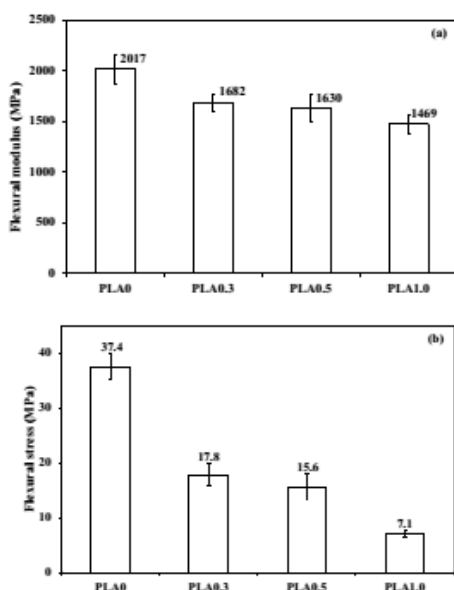


Figure 7. Effect of ZnO content on flexural properties of PLA foams: (a) flexural modulus and (b) flexural stress

As mentioned above, increasing of ZnO content increased the efficiency of the decomposition of AZDC attributing to an increase in the average cell size and a decrease in the density of PLA foam. In general, the larger cell size of foams causes the lower mechanical properties. Therefore, the increase in ZnO content decreased over all mechanical properties of PLA foams. Furthermore, %VF and the cell morphology of foam affected the mechanical properties. The %VF of the PLA foams was in the range of 33.4–48.7% corresponding to those of human cancellous bone (30–90%).¹² The tensile modulus and stress at break of the PLA foams were in the range of 321–585 MPa and 8.1–25.4 MPa, respectively, which were also close to those of human cancellous bone. The tensile strength and modulus of cancellous bone are 400 MPa and 7–20 MPa, respectively.¹³ However, the PLA foams in the present study exhibited closed cell morphology whereas scaffold for bone tissues engineering requires the inter-connected cell morphology.

3.3 *In-vitro* degradation

In-vitro degradation testing in term of %weight loss was used to initially determine the opportunity to utilize obtained PLA foam as a scaffold in tissue engineering. Because the scaffold needs appropriate time for degradation and resorption until the tissue engineered transplant is completely remodeled by the host tissue. Thus, *in-vitro* degradation testing is important.¹⁴ Figure 8 displays the variations of %weight loss of PLA foam specimens after immersion in PBS for 8 weeks. ZnO content strongly affected the degradation behavior. In the first week, rate of degradation of all samples was similar. Since the second week, the higher ZnO content provided the higher %weight loss and degradation rate. Degradation rate of all samples decreased after 4 weeks and higher ZnO content still provided the higher %weight loss and degradation rate. This was because the higher ZnO content yielded the

larger cell size in foams that enhanced PBS penetration.⁹ The %weight loss of the foam samples after the end of the experiment was in the range of 0.66–1.73% which were lower than that of PLA scaffold prepared by the solvent casting and particular leaching method.¹⁵

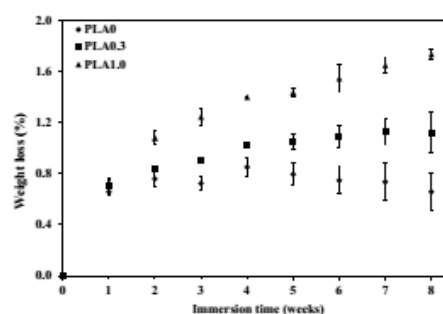


Figure 8. Effect of ZnO content on %weight loss of PLA foams

4. Conclusion

This study showed the success in preparation of PLA foams through compression molding using AZDC and ZnO as blowing agent and accelerator, respectively. The obtained foams exhibited

closed cell morphology. The thermal stability of PLA foam decreased as ZnO content increased. The remaining AZDC was found in PLA foams confirmed by TGA and FTIR results. In addition, an increase of ZnO content decreased the density, the mechanical properties and the *in-vitro* degradation of PLA foam owing to increase of its average cell size.

Acknowledgements

This work was financial supported by Prince of Songkla University, the grant number SCI5901465.

References

- Chen, B-Y.; Jing, X.; Mi, H-Y.; Zhao, H.; Zhang, W-H.; Peng, X-F.; Turng, L-S. *Polym. Eng. Sci.* **2015**, 1339-1348: DOI 10.1002/pen.24073.
- Tyler, B.; Gullotti, D.; Mangraviti, A.; Utsuki, T.; Brem, H. *Adv. Drug. Deli. Rev.* **2016**, 107, 163–175.
- Ameli, A.; Jahani, D.; Nofar, M.; Jung, P. U.; Park, C. B. *Compos. Sci. Technol.* **2014**, 90, 88–95.
- Pilla, S.; Kim, S. G.; Auer, G. K.; Gong, S.; Park, C. B. *J. Meter. Sci. Eng. C.* **2010**, 30, 255–262.
- Wang, J.; Zhu, W.; Zhang, H.; Park, C. B. *Chem. Eng. Sci.* **2012**, 75, 390–399.
- Zimmermann, M. V. G.; Brambilla, V. C.; Bradalise, R. N.; Zattera, A. J. *J. Mater. Res.* **2013**, 16 (6), 1266–1273.
- Najafi, N.; Heuzey, M-C.; Carreau, P. J.; Therriault, D.; Park, C. B. *J. Euro. Polym. J.* **2015**, 73, 455–465.
- Luo, Y.; Zhang, J.; Qi, R.; Lu, J.; Jiang, P. *J. Appl. Polym. Sci.* **2013**, 330–337.
- Rakmea, S.; Ruksakulpiwat, Y.; Sutapan, W.; Suoakarn, N. *Meter. Sci. Eng. C.* **2012**, 32, 1428–1436.
- Reyes-L., J. A.; Marcilla, A. *J. Appl. Polym. Sci.* **2007**, DOI 10.1002/app.26922
- Xie, Y.; Li, P.; Zhang, J.; Wang, H.; Yao, W. *Mol. Biomol. Spectro.* **2013**, 114, 80–84.
- Zhou, H.; Lawrence, J. G.; Bhaduri, S. B. *Acta. Biometer.* **2012**, 8, 1999-2016.
- Harper, L. T.; Ahmed, I.; Felfel, R. M.; Qian, C. *J. Mecha. Behav. Biomed. Mater.* **2012**, 15, 13–23.
- Hetmacher, D. W. *Biomater.* **2000**, 21, 2529–2543.
- Revati, R.; Abdul Majid, M. S.; Ridzuan, M. J. M.; Basaruddin, K. S.; Rahman Y., M. N.; Cheng, E. M.; Gibson, A. G. *J. Mecha. Behav. Biomed. Mater.* **2017**, 74, 383–391.

APPENDIX D

(Abstract)

Topic: Effects of Chitosan and Poly(ethylene glycol) on Mechanical and Thermal Properties of Poly(lactic acid)

Conference name: The 47th World Polymer Congress (MACRO 2018)

Organization name: International Union of Pure and Applied Chemistry (IUPAC),
Royal Australian Chemical Institute and Queensland government

Date/Place: July 1-5, 2018, Cairns Convention Center, Queensland, Australia

Effects of Chitosan and Poly(ethylene glycol) on Mechanical and Thermal Properties of Poly(lactic acid)

P. Sungsee¹ and V. Tanwatanakul¹

¹Department of Materials Science and Technology, Faculty of Science, Prince of Songkla University, Hatyai, Songkhla, 90110, Thailand

Poly(lactic acid) (PLA) is a well-known biodegradable polymer widely used in bone tissue engineering application with the advantages of easy to process and easy to control decomposition rate. However, its drawbacks are brittleness and rather low bioactivity. Chitosan is a polysaccharide and a good bioactive compound containing good antimicrobial activity and non-toxicity, and it is known quite well to use in orthopedic tissue engineering.^{1,2} It is found that the addition of chitosan increases bioactivity of PLA. Poly(ethylene glycol), PEG, is a water-soluble polymer used in medical filed because of its nontoxic and biocompatibility. PEG has been used as a plasticizer of PLA to increase PLA chain mobility.³ The purpose of this work is to evaluate the effect of chitosan and PEG on the mechanical and thermal properties of PLA. Polymer blend was prepared by melt blending in a twin screw extruder. 1 and 3 wt% of chitosan was added and PEG content was 5 wt%. The tensile properties and Izod impact strength of the blends were investigated. The thermal properties was determined by DSC. The addition of chitosan decreased the Izod impact strength of PLA and the addition of PEG increased the Izod impact strength of PLA and PLA/chitosan blends (Figure 1a). Deplasticization was observed in the plasticized blend containing 3 wt% chitosan (PLA-PEG-CH3) due to a decrease in the impact strength. The addition of PEG decreased the tensile properties of PLA and PLA/chitosan blends, and depasticization was also observed in the tensile properties. Chitosan and PEG acted as a nucleating agent of PLA. They decreased the cold crystallization temperature (T_{cc}) of PLA (Figure 1b). The plasticization effect of PEG in PLA was clearly shown in the reduction of the glass transition temperature (T_g) from 56.2°C to 48.1°C. T_g of PLA-PEG-CH3 was higher than that of PLA-PEG-CH1. This might relate to the depasticization effect.

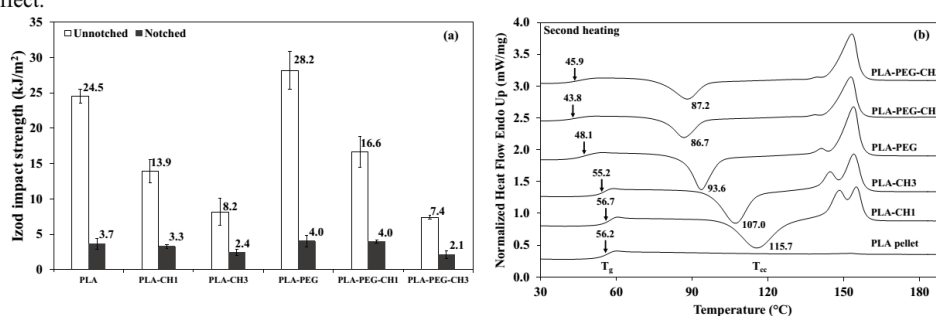


Figure 1. (a) Izod impact strength and (b) DSC thermogram (second heating) of PLA/chitosan and plasticized PLA/chitosan biopolymer.

¹C. E. Tanase, I. Spiridon, *Meter. Sci. Eng. C.* **2014**, *40*, 242–247

²A. D. Martino, M. Sittinger, M. V. Risbud. *Biometer.* **2005**, *26*, 5983-5990

³B-Y. Chen, X. Jing, H-Y. Mi, H. Zhao, W-H. Zhang, X-F. Peng, L-S. Turng, *Polym. Eng. Sci.* **2015**, 1339-134

Pasuta Sungsee

Title: PhD Student

Affiliation, Country: Department of Materials Science and Technology, Faculty of Science, Prince of Songkla University, Hatyai, Songkhla, 90110, Thailand

Phone: +6699-685-9563 Fax: +66-74-446-925 E-mail: nuruk@hotmail.com

Alternate Co-author E-mail: varaporn.t@psu.ac.th

Personal History:

2009-2010 Production planning supervisor at DMS Tech Co., Ltd., Thailand

2010-2014 Lecturer at Nakhon Si Thammarat Rajabhat University, Thailand

Since 2014 Phd student at Prince of Songkla University, Thailand

Research interests: Biodegradable polymer, Bioplastic, Poly(lactic acid)



APPENDIX E

(Research Article)

Topic: Biocomposite foams from poly(lactic acid) and rubber wood sawdust:
Mechanical, properties, cytotoxicity and in vitro degradation

Journal: Journal of Applied Polymer Science

Journal of Applied Polymer Science
Biocomposite foams from poly(lactic acid) and rubber wood sawdust: Mechanical properties, cytotoxicity and in vitro degradation
 --Manuscript Draft--

Full Title:	Biocomposite foams from poly(lactic acid) and rubber wood sawdust: Mechanical properties, cytotoxicity and in vitro degradation
Manuscript Number:	app.20183073R2
Article Type:	Research Article
Order of Authors:	Varaporn Tanrattanakul, Prof. Pasuta Sungsee
Manuscript Classifications:	Biodegradable; Cellulose and Other Wood Products; Mechanical Properties
Additional Information:	
Question	Response
Please provide the principal investigator's name and affiliation. (Principal investigator MUST be listed as a co-author on the submission; please DO NOT list all other co-authors in this section.)	Varaporn Tanrattanakul Prince of Songkla University
Please submit a plain text version of your cover letter here. If you also wish to upload a file containing your cover letter, please note it here and upload the file when prompted to upload manuscript files. Please note, if you are submitting a revision of your manuscript, there is an opportunity for you to provide your responses to the reviewers later; please do not add them to the cover letter.	See attached file.

1 **Biocomposite foams from poly(lactic acid) and rubber wood sawdust:**

2 **Mechanical properties, cytotoxicity and *in vitro* degradation**

3 Pasuta Sungsee, Varaporn Tanrattanakul*

4 Department of Materials Science and Technology, Faculty of Science

5 Prince of Songkla University, Hatyai, Songkhla, Thailand 90110

6 Correspondence to V. Tanrattanakul (E-mail: varaporn.t@psu.ac.th)

7
8 **ABSTRACT**

9 Using a typical blowing agent and compression molding, biocomposite foams were
10 successfully prepared from a poly(lactic acid)/rubber wood sawdust blend (PLA/RWS).
11 Selection of RWS for the biocomposites was based on particle size. RWS particles in two size
12 ranges were used: 212-600 μm and $\leq 75 \mu\text{m}$. Alkaline and silane treatments were applied to the
13 RWS before blending with PLA. The tensile properties, Izod impact strength, foam
14 morphology and thermal degradation of the biocomposite foams were evaluated. Cytotoxicity
15 and in-vitro degradation were tested to determine the potential of the biocomposite foam for
16 use as a scaffold in tissue engineering. Silane treatment improved mechanical properties by
17 increasing the interfacial adhesion between PLA and RWS. The density and void fraction of
18 the foam samples had a greater effect on mechanical properties than pore size. Proliferation of
19 MG-63 cells increased with culture time, indicating that the foam samples were not cytotoxic.
20 Promising samples were tested for degradation in a lysozyme/PBS and showed a slow rate of
21 in-vitro degradation.

22 **Keywords:** Biocomposite, poly(lactic acid), sawdust, scaffold

1 INTRODUCTION

2 Poly(lactic acid) (PLA) is a well-known biodegradable, aliphatic thermoplastic polyester
3 widely used in medical applications such as drug delivery, implants and tissue engineering
4 scaffolds. A scaffold is an artificial, porous structural biomaterial. Scaffolds can be suitably
5 cultured with many kinds of cells to induce cell adhesion, proliferation, differentiation and
6 tissue formation both *in vivo* and *in vitro*.¹ Desirable properties of PLA for scaffold
7 applications, especially for bone tissue engineering, are its interconnected porous structure,
8 biocompatibility, biodegradability, certain mechanical properties, and processability. PLA
9 scaffolds have been prepared by various techniques. These techniques have included solvent
10 casting followed by porogen leaching, thermal phase separation (TIPS), 3D printing,²
11 electrospinning,³ melting processes, microcellular injection molding, and microcellular
12 extrusion using supercritical CO₂ as a physical blowing agent.^{4,5} Preparation of PLA foam
13 using a more typical blowing agent and compression molding is an alternative choice that
14 combines an easy process with low cost and simple equipment. Furthermore, this method of
15 preparing PLA foam for scaffold applications has not been reported.

16 PLA and certain bioactive compounds have been used in the fabrication of biocomposite
17 scaffolds to improve mechanical properties, biocompatibility, cell proliferation and
18 osteoconductivity. Biocomposites included PLA mixed with calcium phosphate (CaP),⁶
19 bioactive glass,⁷ and silk fiber.⁸ Among potential bioactive reinforcing materials for PLA in
20 scaffolds, wood sawdust is an interesting candidate. Before being blended with polymer, wood
21 sawdust is normally subjected to alkaline and/or silane treatment to increase interfacial
22 adhesion with the polymer matrix.⁹ The presence of wood sawdust in a PLA/tricosan blend
23 increased the antibacterial performance of the blend.¹⁰ Wood sawdust increased the anti-listeria
24 activity of PLA containing pediocin.¹¹ Rubber wood sawdust (RWS) was used as a reinforcing
25 agent in rubber composites for anti-stab body armour¹² and as the raw material for activated

1 carbon which acted as a microwave absorber in a polyurethane composite.¹³ RWS is a
2 promising material because it is very cheap, bioactive, and can act as a reinforcing agent. To
3 our knowledge, the use of PLA foam reinforced with RWS has not been reported in a tissue
4 engineering application. The objectives of this work were to prepare biocomposite foam from
5 PLA and RWS using a typical blowing agent and compression molding, and to establish the
6 feasibility of using this foam in tissue scaffold applications. Mechanical and morphological
7 properties of the developed biocomposite foam were described. Preliminary studies of
8 cytotoxicity and biodegradation were carried out to confirm the safety of the biocomposite
9 foam in the intended applications.

11 **EXPERIMENTAL**

12 **Materials**

13 Poly(lactic acid) (4042D grade) was produced by NatureWorks LLC, USA. Sodium hydroxide
14 (NaOH) and 3-glycidyloxypropyl trimethoxysilane (GPMS) were purchased from Sigma-
15 Aldrich (Thailand) Co., Ltd. Natural rubber wood sawdust (RWS) was kindly supplied by
16 Khoamahachai Parawood Co., Ltd., Thailand. The general chemical composition of the RWS
17 was cellulose (39 %), hemicellulose and cell wall (29 %), lignin (28 %) and ash (4 %).¹⁴ Two
18 particle size ranges of RWS were used: 212-600 μm and $\leq 75\mu\text{m}$. The smaller sizes ($\leq 75\mu\text{m}$)
19 were obtained by grinding the larger particles (212- 600 μm) in liquid nitrogen using a
20 NanoTech[®] NT-500D grinder at a speed of 25,000 rpm. The ground product was sieved.
21 Azodicarbonamide (AZDC) was purchased from Greatchem and Supply Pty., Ltd (Shandong,
22 China). Zinc Oxide (ZnO) was purchased from Kit Phaibun Chemistry Ltd., Part. (Bangkok,
23 Thailand). GPMS was used as a silane coupling agent. AZDC and ZnO were respectively used
24 as a blowing agent and an accelerator in the foaming process. Osteogenic medium (OS) was

1 purchased from Sigma Aldrich. It consisted of 10 mM of β -glycerophosphate, 50 mg/ml of
2 ascorbic acid, and 100 nM of dexamethasone.

3

4 **Surface Treatments of Rubber Wood Sawdust**

5 RWS underwent alkaline (NaOH) treatment followed by silane (GPMS) treatment.⁹ In the
6 alkaline treatment RWS was added to 5% (w/v) NaOH solution. The mixture was continuously
7 stirred for 1 h at room temperature and then washed with water until the pH was neutral. The
8 treatment was completed with drying in a rotary evaporator at 80°C for 1 h and then in a
9 vacuum oven at 70°C until a constant weight was obtained. Before GPMS treatment, the
10 coupling agent was hydrolyzed in 60% (v/v) ethanol solution with continuous stirring for 1 h
11 at room temperature. The solution was then adjusted to pH 5 with acetic acid. The NaOH-
12 treated RWS was added to the hydrolyzed GPMS solution and the mixture was heated at 70 °C
13 with continuous stirring for 1 h. The treated RWS was washed with water until pH was neutral.
14 It was then dried in a rotary evaporator at 80°C for 1 h, dried again for 2 h in a vacuum oven
15 at 150°C before being vacuum dried at 70°C until a constant weight was obtained. The optimal
16 GPMS concentration was determined in the preliminary study, which evaluated the effects of
17 concentrations of 1, 3 and 5 wt% GPMS based on RWS on the mechanical properties of PLA
18 composites (unfoamed samples). GPMS concentration of 1 wt% produced the highest impact
19 resistance and tensile strength (Table S1) and this concentration was determined to be optimal
20 for the present study.

21

22 **Characterization of Rubber Wood Sawdust**

23 After treatment with NaOH and GPMS, the surfaces of the RWS were characterized using
24 Fourier Transform Infrared spectroscopy and scanning electron microscopy (FEI® Quanta
25 400). FTIR spectra were recorded with a Bruker® TENSOR 27 spectrometer in ATR mode.

1 The crystallinity of RWS was examined using an X' Pert MPD[®] PHILIPS X-ray
2 diffractometer. The samples were scanned at a speed of 1 sec per step over a 2 θ range from 3.5
3 to 63.5°. The amorphous contribution in the RWS was subtracted from the XRD pattern. The
4 crystallinity Index (I_c) was calculated from equation (1),¹⁵

$$I_c = \frac{(I_{(002)} - I_{(am)})}{I_{(002)}} \times 100 \quad (1),$$

5 where $I_{(002)}$ was the peak intensity at 2 θ equal to 22.72° and attributed to a specific characteristic
6 of crystalline cellulose and $I_{(am)}$ was the intensity at 2 θ equal to 18.01°, which corresponded to
7 the amorphous portion of the cellulose material. Thermal degradation of RWS was determined
8 under nitrogen atmosphere using a thermal gravimetric analyzer (TGA), STA 449 F3 Jupiter[®]
9 NETZSCH. The temperature range was 30 to 500°C and the heating rate was 5°C/min.

12 **Preparation of PLA Biocomposite Foams**

13 PLA compounds were prepared by extrusion and PLA biocomposite foams were prepared by
14 compression molding. PLA and RWS at a weight ratio of 95:5 were melt-blended in a co-
15 rotating screw extruder (Prism[®] TSE16TC) with an L:D ratio of 15:1. Due to the short length
16 of the screws, the materials were extruded twice to obtain a homogeneous blend. The first
17 extrusion was carried out at temperatures of 140, 165, and 165°C in the feed, middle and die
18 zones, respectively. The screw speed was 100 rpm. In the present study, the formation of foam
19 by decomposition of AZDC must take place only in the compression molding machine, not in
20 the extruder. Therefore, when the extrudate was pelletized and extruded again, this time with
21 AZDC and ZnO in the blend, a lower temperature profile was used (130, 150 and 150°C, in
22 feed, middle and die, respectively) to prevent decomposition of AZDC in the extruder.
23 Degradation of PLA was minimized by using a higher screw speed (150 rpm) to reduce
24 residence time in the extruder. AZDC and ZnO content were 1.94 wt% and 0.06 wt%,

1 respectively. Specimens of the prepared biocomposites were compression molded at 145°C for
2 10 min under a pressure of 150 kg/cm² in a closed mold (130 x 130 x 2 mm³).

3 4 **Physical Properties Testing of Biocomposite Foams**

5 The density of the foams was determined by the buoyancy method (ASTM D792). Three
6 specimens of every sample were measured and the average value was reported. Specimen width
7 and length were 25 mm, and specimen thickness was 2.5 to 3.0 mm. Specimens were weighed
8 on an analytical balance in air and n-hexane (density 0.6954 g/cm³). The void fraction (VF)
9 was calculated from equation (2),¹⁶

$$10 \quad VF = 1 - \frac{\rho_1}{\rho_2} \quad (2),$$

11 where ρ_1 and ρ_2 were the density of foamed and unfoamed PLA samples, respectively. The
12 freeze-fracture surfaces of foam samples were investigated by scanning electron microscopy
13 (FEI® Quanta 400). All specimens were immersed in liquid nitrogen and then immediately
14 fractured. The specimens were coated with gold prior to observation. Pore size was measured
15 from SEM micrographs. Pore size calculation involved a total of 150 to 200 pores for each
16 specimen. The pores were oval in shape and only the longer diameter was determined. Dynamic
17 mechanical thermal analysis (DMTA) of the foam samples was conducted in single cantilever
18 mode using the METTLER Toledo® STARe system DMA1 Module. The specimen dimensions
19 were 25 x 6 x 2.5-3.0 mm. The testing temperature range was 10 to 140 °C with a heating rate
20 of 3°C/min, and the frequency was set at 1 Hz.

21

22 **Mechanical Properties Testing of Biocomposite Foams**

23 The Izod impact strength was determined in accordance with ASTM 256 using a Zwick® 5102
24 apparatus. The tensile properties were tested in accordance with ASTM D412 using die C. The

1 specimens were tested at room temperature using INSTRON®5569 equipment. The crosshead
 2 speed was 5 mm/min. At least 6 specimens were tested for every sample. An average value
 3 with standard deviations was reported.

4 5 ***In vitro* Degradation Testing of Biocomposite Foams**

6 The *in-vitro* degradation of PLA foam and biocomposite foam samples was evaluated by
 7 adding a dry foam sample (1 x 1 cm²) to 500 µl of lysozyme solution (4 mg of lysozyme in 1
 8 mL of phosphate buffer solution (PBS) with pH 7.4). The sample was then incubated in the
 9 solution at 37°C for 8 weeks.¹⁷ The lysozyme solution was replaced every week with fresh
 10 solution. At determined time intervals, the foam samples were removed from the solution,
 11 washed with distilled water and dried in a freeze dryer. The % weight loss was calculated from
 12 equation (3),¹⁸ where W_0 was the initial weight and W_d was the dried weight after degradation:

$$13 \quad \%Weight\ loss = \left[\frac{W_0 - W_d}{W_0} \right] \times 100 \quad (3).$$

14 **Cytotoxicity Assay of Biocomposite Foams**

15 MG-63 cells were cultured in alpha-MEM medium (Gibco™, Invitrogen, Carlsbad, CA, USA)
 16 with the addition of 1% penicillin/streptomycin, 0.1% fungizone, and 10% fetal bovine serum.
 17 Incubation took place at 37°C in a fully humidified atmosphere at 5% CO₂. MG-63 cells (5 x
 18 10⁴ cells) were seeded onto the surface of foam samples. The medium was changed every 3
 19 days during culture. Osteogenic medium (OS) was used for osteoblast differentiation of the
 20 MG-63 cells.¹⁹ MG-63 cells were cultured in a culture plate for 1, 3, 5 and 7 days. MG-63 cell
 21 proliferation was measured by WST-1 assay and cell proliferation was quantified according to
 22 the manufacturer's instructions.²⁰ The absorbance of each sample was recorded at 420 nm using
 23 a Multiskan™ GO Microplate Spectrophotometer.

1 The morphology of cells that adhered to the foam sample was investigated by scanning
2 electron microscope (FEI® Quanta 400). The seeded foam samples were washed with PBS and
3 fixed with 10% neutral formalin buffer for 5 h at 4°C. The samples were dried in a freeze dryer
4 and coated with gold prior to investigation.

6 **Statistical Analysis of Data**

7 One-way analysis of variance (one-way ANOVA) was performed using SPSS software
8 (version 20.0) at 0.05 significance level ($p < 0.05$). Significant differences among samples were
9 analyzed using Tukey's honestly significant difference (HSD) test. When the average values
10 were significantly different at $p < 0.05$, samples were identified by letters, e.g. A, B, C, D, AB
11 and CD.

13 **RESULTS AND DISCUSSION**

14 **Characterization of Rubber Wood Sawdust**

15 Since the RWS, supplied by a furniture manufacture, comprised particles of various sizes, it
16 was necessary to grade the particles by size using a series of sieves. The smallest particles
17 obtained (212-600 μm) were used in the study. Some of these particles were cryogenically
18 ground using a high speed grinder to obtain particles smaller than or equal to 75 μm . This size
19 was decided on the basis of the preliminary experiment. The aim of the present study was to
20 obtain PLA biocomposite with optimal properties. To determine the optimal conditions of
21 affecting parameters, four significant factors were selected: the particle size, surface treatment
22 (NaOH- and GPMS-treatment), concentration of silane and concentration of RWS. The criteria
23 that determined the optimal conditions of the significant factors were the Izod impact strength
24 and tensile properties of PLA biocomposites foam produced at each condition. Results of the
25 preliminary study of unfoamed PLA biocomposites are shown in Table S1 and Table S2. PLA

1 blended with untreated larger RWS particles (212-600 μm) exhibited slightly better mechanical
2 properties than PLA with untreated smaller particles ($\leq 75 \mu\text{m}$) and PLA blended with the
3 smaller particles of NaOH-treated RWS showed better mechanical properties than PLA with
4 the larger NaOH-treated particles. However, after silane treatment, blends containing both
5 particle sizes exhibited similar mechanical properties. The results of the silane treatment
6 indicated that 1 wt% GPMS concentration was the optimal concentration out of a range of 1, 3
7 and 5 wt% GPMS (Table S1). The blend with higher RWS content showed lower mechanical
8 properties (Table S2). The composites containing 15 wt% RWS showed poorest mechanical
9 properties. PLA containing 15 wt% of smaller particle RWS ($\leq 75 \mu\text{m}$) was so brittle that the
10 compression molded samples could not be cut into specimens to test mechanical properties.
11 PLA containing 15 wt% of large particle RWS (212-600 μm) showed the lowest impact
12 strength for both unnotched and notched specimens: 5.2 ± 1.3 and $0.5 \pm 0.03 \text{ kJ/m}^2$,
13 respectively. We concluded that 5 wt% RWS was the optimal condition for the present study.
14 The most appropriate RSW samples for the present study were those listed in Table 1. It was
15 not essential to use the NaOH-treated large particle RWS (212-600 μm) because it showed
16 poor mechanical properties in the PLA composite.

17 RWS is a lignocellulose consisting of cellulose, hemicellulose, lignin, pectin and non-
18 essential parts of lipid and waxes. The alkaline treatment generally applied to cellulosic
19 materials uses NaOH to reduce its hydrophilicity and to remove partial of hemicellulose and
20 impurities such as waxes and oils on the surface.^{10,15,21} Silanes are recognized as efficient
21 coupling agents and are widely used to improve interfacial adhesion in composites through
22 hydrolyzing and organofunctional reactions.^{10,22,23} After NaOH and silane treatment, the
23 surface of RWS was characterized by FTIR. The treatment removed a certain proportion
24 hemicellulose. Reducing the hydrophilicity of RWS before blending with PLA enhanced
25 compatibility in this biocomposite. Although PLA contains some hydroxyl and carboxylic end

1 groups, its polarity is much lower than that of RWS. This may cause poor interfacial adhesion
2 between PLA and RWS, resulting in poor mechanical properties. FTIR assignments are listed
3 in Table 2.^{21,24,25} In the FTIR spectra of RWS samples before and after treatment (Figure 1),
4 the peak in T0L at 1735 cm⁻¹ was assigned to C=O of hemicellulose. This peak was not
5 observed in the spectra of T1S and T2L, indicating the absence of hemicellulose after treatment
6 with NaOH.²¹ The peak in T0L at 1230 cm⁻¹, assigned to an acetyl group of xylan²⁶⁻²⁸ appears
7 as a new double peak in T1S and T2L at 1227 cm⁻¹ and 1267 cm⁻¹. The first and second split
8 peak were due to the vibration of the syringyl structure and guaiacyl structure of lignin,
9 respectively.^{26,28} The band split has been found in alkaline treatment of lignocellulosic
10 materials.²⁶⁻²⁸ After NaOH treatment, the average mass yield of T1S was 37.12 %.

11 The proposed interaction mechanism of GPMS with RWS and PLA is illustrated in
12 Scheme 1.²² Hydrolyzation transforms GPMS to silanols (hydrolyzed GPMS) containing a
13 large number of reactive hydroxyl groups (Scheme 1a). During this process, the Si-O-Si groups
14 formed concomitantly through self-condensation (Scheme 1b). When RWS was introduced
15 into the hydrolyzed GPMS solution, a linked -Si-O-Si- network structure formed to give
16 GPMS-treated RWS (Scheme 1c). During melt blending, the GPMS-treated RWS could graft
17 with PLA via epoxide ring opening (Scheme 1d). The spectra of GPMS and hydrolyzed GPMS
18 (Figure 1) show that after hydrolysis, the epoxide ring vibrations, apparent in GPMS at 1255
19 cm⁻¹ and 909 cm⁻¹, shifted to 903 cm⁻¹ and 844 cm⁻¹ in hydrolyzed GPMS and the Si-O bond
20 in Si-O-CH₃, detected at 1087 cm⁻¹ in GPMS, was a Si-O bond in Si-O-H at 1102 cm⁻¹ (Figure
21 1). This results are in accordance with a previous study.²⁴ T2L represented a product of Scheme
22 1c. The hydrolyzed GPMS on the surface of T2L was not clearly observed in the FTIR
23 spectrum. This might be due to the small concentration of GPMS (1%) and overlapped peaks.
24 The peaks of hydrolyzed GPMS at 2927 and 2861 cm⁻¹ overlapped with the broad peak of all
25 RWS samples at 2900 cm⁻¹. Likewise, peaks of the epoxide ring of hydrolyzed GPMS (903

1 cm⁻¹ and 844 cm⁻¹) overlapped with C-H bending of RWS (~ 900 cm⁻¹) and the peak of Si-O
2 in a linked -Si-O-Si- network structure or Si-O-RWS bond overlapped with the peak of C-O
3 stretching of RWS in the range of 1000-1110 cm⁻¹.²⁹ Effects of alkali and silane treatments on
4 the surface of 212- 600 μm RWS particles are shown in Figure 2. **The elimination of**
5 **hemicellulose and non-essential parts produced a cleaner surface with a grooved profile.**

6 XRD diffractograms of untreated, alkaline-treated and alkaline- and silane-treated
7 RWS (Figure S1) show the characteristic peaks of RWS at 2θ = 17°, 22.5° and 35° which
8 correspond respectively to the crystal plane diffraction peaks of (1 0 1), (0 0 2) and (0 4 0) in
9 cellulose.³⁰ The position of the XRD peaks did not change after NaOH and GPMS treatment,
10 indicating no change occurred in the crystal structure. This results at the low alkaline
11 concentration (5% NaOH) used is in accordance with a previous work, which found that the
12 crystal structure of cellulose did not change until the NaOH content of alkaline treatment
13 reached 17.5%.¹⁵ The crystallinity index (CI) of RWS slightly increased after silane treatment
14 (Table 3). The CI of T1S was significantly lower than that of T0L. T1S was prepared from
15 T0L under severe grinding. We concluded that the lower CI was due to the high speed grinding
16 (25,000 rpm) in liquid nitrogen because this process produced a very high shear rate which
17 could destroy some of the crystal structure of RWS (T0L).

18 DTG and TGA thermograms of RWS are shown in Figure 3 and the onset temperatures
19 ($T_{d\text{ onset}}$) and the thermal degradation temperatures (T_d) of different samples of RWS are listed
20 in Table 3. T_d was the temperature at the peak of the DTG curve and $T_{d\text{ onset}}$ was the temperature
21 of degradation at the initial weight loss, obtained from the TGA curve. The degradation
22 temperature of T2S was higher than that of T1S (Table 3). The increased degradation
23 temperature of RWS after surface treatment with GPMS might be due to the elimination of
24 impurities. The higher T_d of RWS after silane treatment could also be related to the presence
25 of Si on the surface of RWS. However, the increase of T_d in T2S was not great because of the

1 low concentration of GPMS in the treatment (1 wt% of RWS) and the low concentration of
2 RWS in the biocomposite (5 wt% RWS).

3 **These results indicated that surface treatment eliminated hemicellulose and impurities**
4 **such as waxes and oil and were in agreement with FTIR and SEM results.** Furthermore,
5 eliminating impurities and hemicellulose, which are amorphous parts, increased the
6 crystallinity index (CI), and, hence, increased the thermal stability of RWS.^{15, 29}

8 **Morphology of PLA Biocomposite Foams**

9 PLA and biocomposites foams containing 5 wt% RWS presented oval-shaped pores
10 and closed-cell morphology (Figure 4). The cellular structure of PLA foam without RWS
11 (Figure 4a) looks similar to the structure of the other biocomposite foams, except the T0L-PLA
12 foam. The T0L-PLA foam showed a very large variation in pore size (Figure 4b). Pores with
13 very large and very small diameters were found in this sample, resulting in the largest average
14 pore diameter and standard deviation (Table 4). Changes to the cellular structure caused by
15 surface treatment are apparent in the SEM micrograph of T2L-PLA foam (Figure 4e). A smaller
16 average pore diameter, narrower pore size distribution and more regular cell shape were
17 obtained. Surface treatment increased interfacial adhesion between PLA and RWS,
18 contributing to a finer cellular structure.³¹ The effect of RWS particle size is clearly seen in the
19 SEM micrograph. The biocomposite foams containing 75 μm -RWS, T1S-PLA and T2S-PLA
20 (Figure 4c and Figure 4d, respectively), show smaller pore sizes than the foam containing larger
21 RWS particles, T2L-PLA (Figure 4e).

22 The density of the foams was strongly dependent on void fraction (Table 4): the higher
23 the void fraction (%VF), the lower the density and both values could be ranked in the same
24 order. T1S-PLA foam showed the highest void fraction and lowest density, whereas T0L-PLA
25 foam showed the lowest void fraction and highest density. The average pore diameter could

1 not be ranked in the same order but the largest pore size was found in T0L-PLA and the smallest
2 in T1S- PLA foam. The addition of RWS slightly decreased the thermal degradation
3 temperature of PLA but there was no significant effect on the degradation temperature caused
4 by either surface treatment or the particle size of RWS (Table 4).

6 **Mechanical and Thermal Properties of PLA Biocomposite Foams**

7 When the Izod impact strength and tensile properties of foams containing 5 wt%RWS were
8 tested, the addition of RWS both increased and decreased the mechanical properties of PLA
9 foam. T1S-PLA foam showed the worst mechanical properties and T2L-PLA foam showed the
10 best (Table 5). The T1S-PLA foam also showed the lowest storage modulus (E') and T2L-PLA
11 foam showed the highest storage modulus (Figure 5a). Surface treatment proved to be essential.
12 T2L-PLA foam showed better mechanical properties than T0L-PLA foam, and the necessity
13 of silane treatment became obvious when the mechanical properties of T1S-PLA foam were
14 compared with those of T2S-PLA foam. Regarding the particle size of RWS, the larger
15 particles (200-600 μm) produced foam with better mechanical properties than the smaller
16 particles ($\leq 75 \mu\text{m}$). T1S-PLA foam had the smallest average pore size but produced the worst
17 mechanical properties. T1S-PLA foam did not undergo silane treatment and had the lowest
18 density and highest void fraction of the foam samples. The relatively better mechanical
19 properties of untreated T0L-PLA foam could not be due to the effect of surface treatment but
20 must, instead, have been due to the higher density and lower void fraction of T0L-PLA foam.
21 The experimental results in this section indicated that many factors controlled the mechanical
22 properties of these biocomposite foams and any one particular factor may not play a major role
23 in all samples.

24 The maximum $\tan \delta$ peak (the α -relaxation temperature) of PLA and biocomposite
25 foams appeared in the range of 61.4 to 63.6°C (Figure 5b). The higher relaxation temperature

1 at 85 to 105°C arose from cold crystallization of PLA. No significant changes due to RWS
2 were observed in either relaxation temperature range of PLA. The thermal degradation
3 temperatures of all the biocomposite foams were slightly lower than that of neat PLA foam
4 (Table 4).

6 **Cytotoxicity of PLA Biocomposite Foams**

7 The cytotoxicity and biodegradation of the developed foams were evaluated to determine their
8 safety in tissue engineering applications. Cytotoxicity was determined by evaluation of cell
9 proliferation using the WST-1 assay and MG-63 (osteoblast-like cell) cell culture. The WST-
10 1 assay is a colorimetric method using water soluble tetrazolium salt (WST-1) for
11 quantification of viable cells.²⁰ When added to the sample, WST-1 is reduced by living cells to
12 water soluble formazan through cellular dehydrogenase. The dark yellow water soluble
13 formazan can be measured from absorbance at 420 nm.³²⁻³³ The degree of conversion, indicated
14 by the intensity of color, is directly correlated with the amount of metabolic activity in viable
15 cells. An increase of viable cells with increasing culture time indicates increased cell
16 proliferation.³³ The 7-day duration of cell culture was referenced from previous studies.³⁴⁻³⁶
17 The data were statistically analyzed. Different letters were used to identify the samples when
18 the average values were significantly different at $p < 0.05$. PLA foam was used as a control
19 sample. Cell proliferation increased with cell culture time (Figure 6), indicating the non-
20 cytotoxicity of samples. MG-63 cell proliferation on the surface of the foam samples could be
21 ranked in the following order: PLA > T0L-PLA > T2S-PLA > T2L-PLA > T1S-PLA. The
22 extent of cell proliferation on T0L-PLA was unpredictable. The relatively large pore sizes in
23 this foam might have contributed to this result. In contrast, T1S-PLA foam, which had the
24 highest void fraction, did not promote cell proliferation so much, perhaps due to its smaller
25 pore size. PLA is a polymer of low hydrophilicity, therefore, large pores may be beneficial for

1 cell proliferation. Cell adhesion to the surface of foam samples was observed by SEM. Figure
2 7a displays the surface of PLA foam without cell culture and was referred to as a blank. Figures
3 7b to 7f show the surface of the foam samples after cell culture for 7 days. Cells of various
4 shapes were observed and are indicated by white arrows in the figures. Spindle-shaped cells
5 were present on the surface of PLA foam (Figure 7b). The presence of cells on the surfaces of
6 foam samples also indicated non-cytotoxic reactivity. As this experiment was a preliminary
7 study to verify the potential of these biocomposite foams as a scaffold and the experimental
8 results showed positive data, cell proliferation testing will be carried out over a longer time in
9 future study.

11 ***In Vitro* Degradation of PLA Biocomposite Foams**

12 The degree of degradation *in vitro* was determined by %weight loss observed. After incubation
13 for 8 weeks, the %weight loss data of the foam samples (Figure 8) were statistically analyzed.
14 Different letters were used to identify the samples when the average values were significantly
15 different at $p < 0.05$. The weight loss of all samples increased with increasing incubation time.
16 Neat PLA foam showed a rapid weight loss at 2 weeks and then the weight loss remained
17 constant at 5% until the end of testing. All biocomposite foam samples, except T0L-PLA foam,
18 showed a similar change of weight loss. A rapid change occurred in the first week, and then
19 the rate of weight loss decreased and became constant after 2 weeks. The T0L-PLA foam
20 showed a much slower rate of weight loss and remained constant at 2% after 6 weeks. After 3
21 weeks, the rates of weight loss of T1S-PLA and T2S-PLA foam were similar and higher than
22 that of T2L-PLA foam. The weight loss of the samples at the end of the experiment could be
23 ranked in the following order: T0L-PLA < T2L-PLA < PLA < T2S-PLA < T1S-PLA. A higher
24 weight loss indicates more degradation. Although RWS of larger particles reduced the weight
25 loss of PLA foam and RWS of smaller particles increased the weight loss, it should be

1 remembered that surface treatment, cellular morphology, density and void fraction have to be
2 considered as well. The very low weight loss of T0L-PLA foam came from the relatively high
3 density and low void fraction. The degradation resistance of T2L-PLA was higher than that of
4 PLA foam, implying a high interfacial adhesion between PLA and RWS that could correspond
5 to the good mechanical properties of this sample. Two factors were presumed to be involved
6 in the low degradation resistance of T1S-PLA foam: the high void fraction and low interfacial
7 adhesion. Both factors also affected the mechanical properties of T1S-PLA.

8 In the present study, the % VF and average pore size of the obtained foams were in the
9 range of 17.2 to 51.9% and 336 to 1022 μm , respectively (Table 4). The porosity of cancellous
10 bone is in the range of 30 to 90%.⁶ The optimal pore sizes for bone regeneration and collateral
11 bone ingrowth were in the range of 50-710 μm and 100-1000 μm , respectively.³⁷⁻³⁸ In addition,
12 bone fixations must have a slow rate of degradation and both PLA foam and the biocomposite
13 foams showed slow rates of degradation (< 6% after 8 weeks in T2L-PLA foam).

15 CONCLUSIONS

16 PLA foam and PLA/rubber wood sawdust (RWS) biocomposite foams were successfully
17 prepared by compression molding. Azodicarbonamide and zinc oxide were used as a chemical
18 blowing agent and accelerator, respectively. Alkaline and silane treatments were applied to
19 RWS and the surface modification was characterized by FTIR, XRD and SEM analysis. The
20 surface treatments did not change the crystal structure or degree of crystallinity of RWS,
21 whereas thermal degradation temperatures increased after surface treatment. Foam density
22 showed a direct relationship with void fraction (% VF); the higher the density, the lower the
23 % VF. Foam density of the samples was ranked in the following order: T1S-PLA < PLA <
24 T2L-PLA < T2S-PLA < T0L-PLA, and vice versa for the ranking of % VF. All foam samples
25 showed closed-cell structures and average pore diameters in the range of 336 to 608 μm , except

1 T0L-PLA foam, which showed a very large average pore diameter (1022 μm) and very wide
2 size distribution. Factors controlling the mechanical properties of the foam samples included
3 surface treatment, particle size of RWS and density and %VF. The addition of RWS improved
4 or degraded the mechanical properties of PLA foam depending on the above factors. T2L-PLA
5 foam exhibited the best mechanical properties whereas T1S-PLA foam exhibited the poorest
6 mechanical properties. Preliminary studies of non-cytotoxicity and biodegradation confirmed
7 the suitability of these foam materials for use in bone scaffolds. All the foams tested proved to
8 be non-cytotoxic based on increased cell proliferation observed throughout the duration of the
9 cell culture. In the in-vitro degradation test, T2L-PLA and T2S-PLA foams displayed a slow
10 rate of degradation. All experimental results, including pore size, void fraction, mechanical
11 properties, cytotoxicity and in-vitro degradation, indicate the potential of neat PLA, T2S-PLA
12 and T2L-PLA foam composites as scaffold in bone tissue engineering applications.

13

14 **ACKNOWLEDGEMENTS**

15 This work was financially supported by Prince of Songkla University, grant number
16 SCIS901465.

17

18 **REFERENCES**

- 19 1. Chen, B.-Y.; Jing, X.; Mi, H.-Y.; Zhao, H.; Zhang, W.-H.; Peng, X.-F.; Turng, L.-S. *Polym.*
20 *Eng. Sci.* **2015**, 1339-1348.
- 21 2. Rezwan, K.; Chen, Q.Z.; Blaker, J.J.; Boccaccini, A.R. *Biomater.* **2006**, 27, 3413-3431.
- 22 3. Zhang, C.; Salick, M.R.; Cordie, T.M.; Ellingham, T.; Yi Dan, Y.; Turng, L.-S. *Mater.*
23 *Sci. Eng. C.* **2015**, 49, 463-471.
- 24 4. Mi, H.-Y.; Salick, M.R.; Jing, X.; Jacques, B.R.; Crone, W.C. Peng, X.-P.; Turng, L.-S.
25 *Mater. Sci. Eng. C.* **2013**, 33, 4767-4776.

60
61
62
63
64
65

- 1 5. Matuana, L.M; Carlos A. Diaz, C.A. *Ind. Eng. Chem. Res.* **2010**, 49, 2186-2193.
- 2 6. Zhou, H.; Lawrence, J.G.; Bhaduri, S.B. *Acta. Biometer.* **2012**, 8, 1999-2016.
- 3 7. Habraken, W.J.E.M.; Wolke, J.G.C.; Jansen, J.A. *Adv. Drug. Deliv. Rev.* **2007**, 59, 234-
- 4 248.
- 5 8. Cheung, H-Y.; Lau, K-T.; Pow, Y-F.; Zhao, Y-Q.; Hui, D. *Composites Part B.* **2010**, 41,
- 6 223-228.
- 7 9. Moigne, N.L.; Longerey, M.; Taulemesse, J-M.; Bènezet, J-C.; Bergeret, A. *Ind. Crops.*
- 8 *Prod.* **2014**, 52, 481-494.
- 9 10. Praprudivongs, C.; Sombatsompop, N. *Composites Part B.* **2012**, 43, 2730-2737.
- 10 11. Woraprayote, W.; Kingcha, Y.; Amonphanpokin, P.; Krueante, J.; Zendo, T.; Sonomoto,
- 11 K.; Benjakul, S.; Visessanguan, W. *Int. J. Food. Microbiol.* **2013**, 167, 229-235.
- 12 12. Yong, K.C. *Polym. Polym. Compos.* **2014**, 22(4), 375-380.
- 13 13. Shaaban, A.; Se, S-M.; Ibrahim, I.M.; Ahsan, Q. *New Carbon Mater.* **2015**, 30(2), 167-
- 14 175.
- 15 14. Ali, N.; Tabi, A.N.M.; Zakil, F.A.; Fauzai, W.N.F.; Hassan, O. *J. Technol. Sci. Eng.*
- 16 **2013**, 64(1), 93-99.
- 17 15. Kamphunthong, W.; Hornsby, P.; Sirisinha, K. *J. Appl. Polym. Sci.* **2012**, 125, 1642-
- 18 1651.
- 19 16. Luo, Y.; Zhang, R.; Qi, R.; Lu, J.; Hu, X.; Jiang, P. *J. Appl. Polym. Sci.* **2013**, 330-337.
- 20 17. Zhang, Z.; Cui, H. *Molecules.* **2012**, 17, 3243-3258.
- 21 18. Rakmea, S.; Ruksakulpiwat, Y.; Sutapan, W.; Suoakarn, N. *Meter. Sci. Eng. C.* **2012**,
- 22 32, 1428-1436.
- 23 19. Sangkert, S.; Kamonmattayakul, S.; Chai, W.L.; Meesane, J. *Mater. Lett.* **2016**, 166, 30-
- 24 34.

- 1 20. Hsueh, Y-S.; Savitha, S.; Sadhasivam, S.; Lin, F-H.; Shieh, M-J. *Mater. Sci. Eng. C.*
2 **2014**, *38*, 119-126.
3
4
5 21. Zhou, F.; Cheng, G.; Jiang, B. *Appl. Surf. Sci.* **2014**, *292*, 806-812.
6
7 22. Lv, S.; Tan, H.; Gu, J; Zhang, Y. *BioResour.* **2015**, *10(3)*, 5426-5439.
8
9 23. Xie, Y.; Hill, C.A.S.; Xiao, Z; Militz, H.; Mai, C. *Composites Part A.* **2010**, *41*, 806-819.
10
11 24. Shukla, D.K.; Kasisomayajula, S.V.; Parameswaran, V. *Compos. Sci. Technol.* **2008**, *68*,
12 3055-3063.
13
14
15
16
17 25. Wahab M.A.; Jellali, S.; Jedidi, N. *Bioresour. Technol.* **2010**, *101*, 5070-5075.
18
19 26. Jaya, H.; Omar, M.F.; Akil, H.M.; Ahmad, Z.A.; Zulkepli, N.N.; Abdullah, M.M.A.B.;
20 Sandu, I.G.; Vizureanu, P. *Mater. Plast.* **2016**, *53(1)*, 85-90.
21
22 27. Reddy, S.S.; Bhaduri, S. K.; Sen, S.K. *J. Appl. Polym. Sci.* **1990**, *41(1-2)*, 329-336.
23
24 28. Roy, A.K.; Sen, S.K.; Bag, S.C.; Pandey, S.N. *J. Appl. Polym. Sci.* **1991**, *42 (11)*, 2943-
25 2950.
26
27
28 29. Tee Y.B.; Talib, R.A.; Abdan, K; Chin, N.L.; Basha, R.K.; Yunos, K.F.M. *BioResour.*
29
30 **2013**, *8(3)*, 4468-4483.
31
32
33 30. Liu, R.; Luo, S.; Cao, J.; Peng, Y. *Composites Part A.* **2013**, *51*, 33-42.
34
35
36 31. Mihai, M.; Huneault, M.A.; Favis, B.D.; Li, H. *Macromol. Biosci.* **2007**, *7*, 907-920.
37
38 32. Santiago, L. A. Cellular viability-WST-1 assay.
39
40 [https://www.nanopartikel.info/files/projekte/nanOxiMet/SOP/nanOxiMet_SOP_WST-1-](https://www.nanopartikel.info/files/projekte/nanOxiMet/SOP/nanOxiMet_SOP_WST-1-assay_V2.pdf?fbclid=IwAR3EYHICufnbbQ_eS7zzE3iwr7bxRPWPPCt4gddmd5plx0lf4L3Iu1JwFYw)
41 [assay_V2.pdf?fbclid=IwAR3EYHICufnbbQ_eS7zzE3iwr7bxRPWPPCt4gddmd5plx0lf4](https://www.nanopartikel.info/files/projekte/nanOxiMet/SOP/nanOxiMet_SOP_WST-1-assay_V2.pdf?fbclid=IwAR3EYHICufnbbQ_eS7zzE3iwr7bxRPWPPCt4gddmd5plx0lf4L3Iu1JwFYw)
42 [L3Iu1JwFYw](https://www.nanopartikel.info/files/projekte/nanOxiMet/SOP/nanOxiMet_SOP_WST-1-assay_V2.pdf?fbclid=IwAR3EYHICufnbbQ_eS7zzE3iwr7bxRPWPPCt4gddmd5plx0lf4L3Iu1JwFYw) (accessed Jan 31, 2019).
43
44
45
46
47
48 33. Wood, K.; Szewczuk, M.R; Rousseau, D.; Neufeld, R.J. *Oncotarget.* **2018**, *9(16)*, 12754-
49 12768.
50
51
52 34. Grèmare, A.; Guduric, V.; Bareille, R.; Heroguez, V.; Latour, S.; Heures, N.L.; Fricain,
53 J-C.; Catros, Q.; Mo, A.; Nie, J.; Liu, W.; Ye, C.; Chen, X. *Int. J. NanoMed.* **2011**, *6*,
54 1853-1861.
55
56
57
58
59
60
61
62
63
64
65

- 1 35. Ye, J.; Yao, Y.; Wang, Y.; Xu, Y-D.; Yang, Y-Q. *Int. J. Med. Sci.* **2013**, *3(1)*, 68-72.
- 2 36. Yan, L.; Jiang, D-M. *Drug. Des. Dev. Ther.* **2015**, *9*, 6497-6508.
- 3 37. Kramschuster, A.; Turng, L-S. *Handbook of Biopolymer and Biodegradable Plastics*,
- 4 **2013**; Chapter 17, pp 427-446.
- 5 38. Dutta, R.C.; Dey, M.; Dutta, A.K.; Basu, B. *Biotechnol. Adv.* **2017**, *35*, 240-250.
- 6
- 7
- 8
- 9
- 10
- 11
- 12
- 13
- 14
- 15
- 16
- 17
- 18
- 19
- 20
- 21
- 22
- 23
- 24
- 25
- 26
- 27
- 28
- 29
- 30
- 31
- 32
- 33
- 34
- 35
- 36
- 37
- 38
- 39
- 40
- 41
- 42
- 43
- 44
- 45
- 46
- 47
- 48
- 49
- 50
- 51
- 52
- 53
- 54
- 55
- 56
- 57
- 58
- 59
- 60
- 61
- 62
- 63
- 64
- 65

1 Table 1. Nomenclature of RWS

Type of RWS	Type of treatment			Particle size (μm)
	None (T0)	NaOH (T1)	GPMS (T2)	
T0L	✓	-	-	212-600 (L)
T1S	-	✓	-	≤ 75 (S)
T2S	-	✓	✓	≤ 75 (S)
T2L	-	✓	✓	212-600 (L)

4 Table 2. FTIR Assignment of RWS and GPMS ^{21, 24-28}

Peak (cm^{-1})	Untreated rubber wood sawdust (T0L)	GPMS
3339	OH stretching vibration	-
2943, 2842	-	C-H stretching vibration
2900	C-H stretching vibration	-
1735	C=O stretching vibration of hemicellulose ²¹	-
1643, 1597, 1505	Carboxylic groups	-
1456, 1149	Symmetric bending of CH_3	-
1370, 1324	C-O stretching vibration of carboxylic group	-
1255, 909	-	Epoxide ring vibration
1230	Acetyl group of xylan ²⁶	-
1195	-	C-O stretching vibration
1087	-	Si-O stretching vibration
1027	C-C-O or C-O-C stretching vibration	-
899	C-H bending of carboxylic	-
822	-	Si-O- CH_3 deformation

1 **Table 3. Crystallinity Index (CI) and Degradation Temperature of RWS**

Type of RWS	Crystallinity index (%)	Degradation temperature	
		T _{d onset} (°C)	T _d (°C)
T0L	91.7	293.4	331.5
T0S	61.7	265.1	341.8
T1S	87.7	311.4	354.5
T2S	93.1	318.5	357.7
T2L	94.4	311.2	353.2

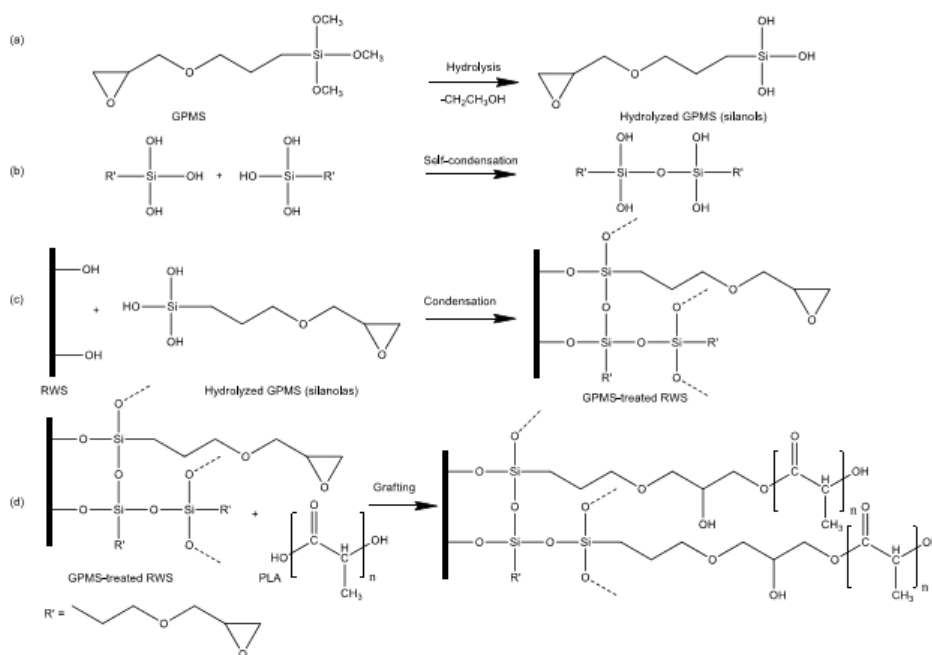
2
3
4 **Table 4. Effect of RWS on Morphology and Degradation Temperatures of PLA Foams**

Foam sample	Density (g/cm ³)	Void fraction (%)	Average pore diameter (μm)	Degradation temperature	
				T _{d onset} (°C)	T _d (°C)
PLA	0.746 ± 0.007	39.0 ± 0.5	495 ± 200	332.0	356.2
T0L-PLA	1.018 ± 0.012	16.7 ± 0.9	1022 ± 651	318.8	346.9
T1S-PLA	0.593 ± 0.014	51.5 ± 1.1	336 ± 111	302.0	336.8
T2S-PLA	0.932 ± 0.012	23.8 ± 1.0	466 ± 196	311.6	343.4
T2L-PLA	0.790 ± 0.003	35.4 ± 0.3	608 ± 235	310.0	343.6

5
6
7 **Table 5. Effect of RWS on the Mechanical Properties of PLA Foams**

Foam sample	Impact strength (kJ/cm ²)		Tensile properties		
	Unnotched	Notched	E (MPa)	σ _b (MPa)	ε _b (%)
PLA	4.9 ± 1.0 ^A	1.6 ± 0.2 ^{AB}	366 ± 20 ^A	18.4 ± 2.1 ^A	8.3 ± 1.3 ^B
T0L-PLA	4.5 ± 1.0 ^A	2.0 ± 0.4 ^A	349 ± 73 ^A	11.1 ± 2.7 ^B	4.3 ± 1.2 ^C
T1S-PLA	1.3 ± 1.0 ^C	1.1 ± 1.0 ^C	206 ± 20 ^B	5.4 ± 1.1 ^C	3.9 ± 0.7 ^C
T2S-PLA	3.1 ± 0.5 ^B	1.4 ± 1.0 ^{BC}	341 ± 30 ^A	17.1 ± 0.2 ^A	7.5 ± 0.5 ^B
T2L-PLA	5.2 ± 0.5 ^A	1.8 ± 1.0 ^{AB}	370 ± 28 ^A	20.1 ± 1.6 ^A	10.4 ± 1.6 ^A

8 Footnotes: Average values with different letters in the same column are significantly different
9 at p<0.05.



1
2
3
4
5
6
7
8
9
10
11
12
13
14
15
16
17
18
19
20
21
22
23
24
25
26
27
28
29
30
31
32
33
34
35
36
37
38
39
40
41
42
43
44
45
46
47
48
49
50
51
52
53
54
55
56
57
58
59
60
61
62
63
64
65

Scheme 1 Proposed interaction mechanism of GPMS with RWS and PLA.²²

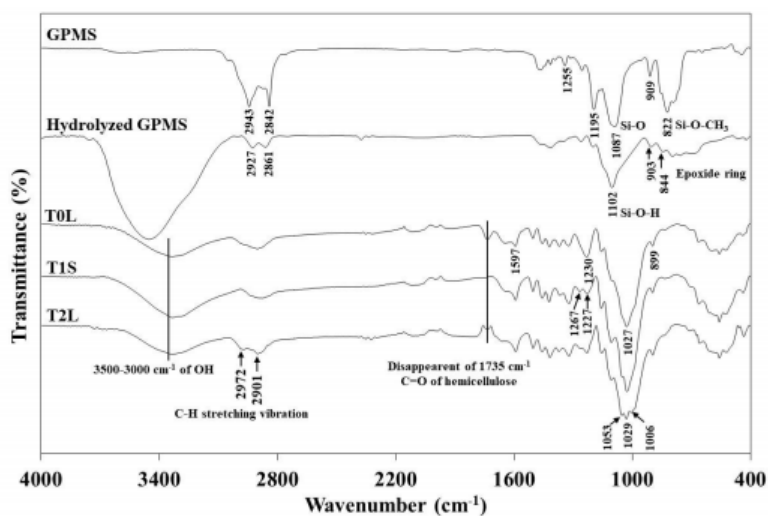


Figure 1 FTIR spectra of GPMS, T0L, T1S, and T2L.

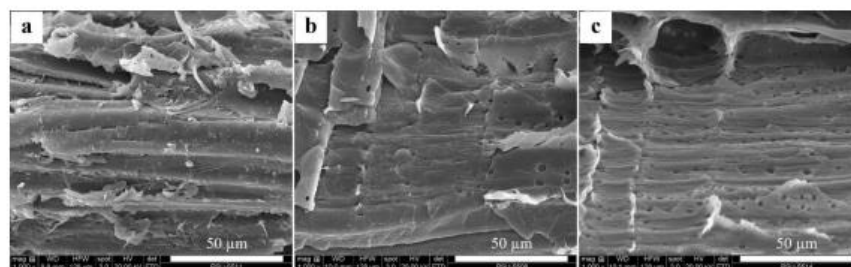


Figure 2 SEM micrographs of 212-600 μm -RWS particles: (a) untreated RWS (T0L), (b) NaOH-treated RWS, and (c) GPMS-treated RWS (T2L).

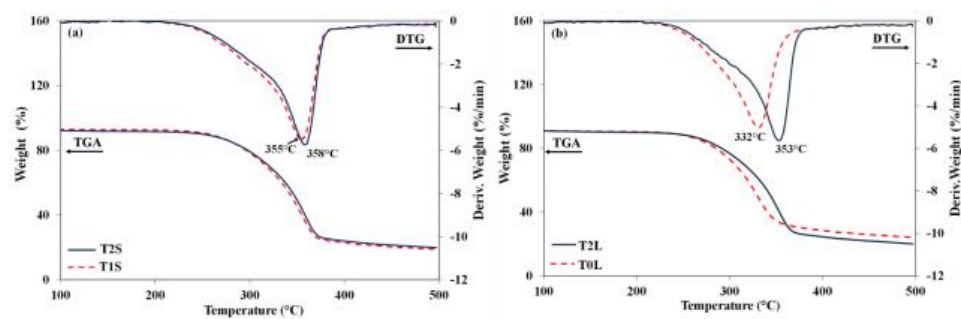


Figure 3 TGA and DTG thermograms of RWS: (a) T1S and T2S, and (b) T0L and T2L.

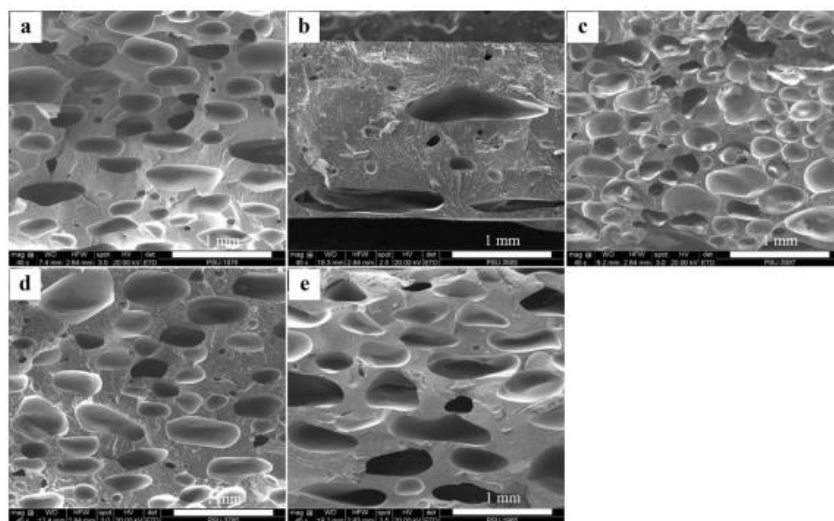


Figure 4 SEM micrographs of foam samples: (a) PLA, (b) T0L-PLA, (c) T1S-PLA, (d) T2S-PLA and (e) T2L-PLA.

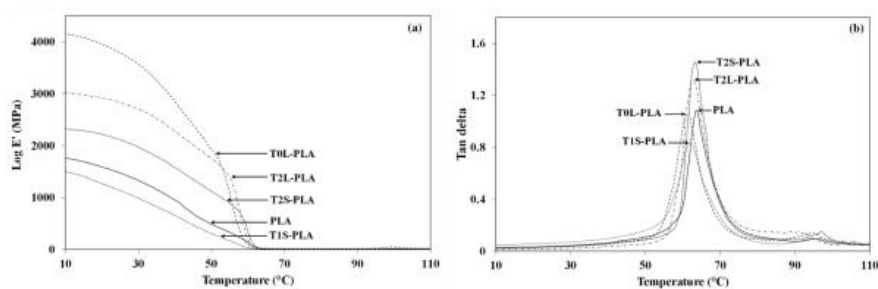


Figure 5 DMTA results of PLA foam and biocomposite foams: (a) Storage modulus and (b) tan delta.

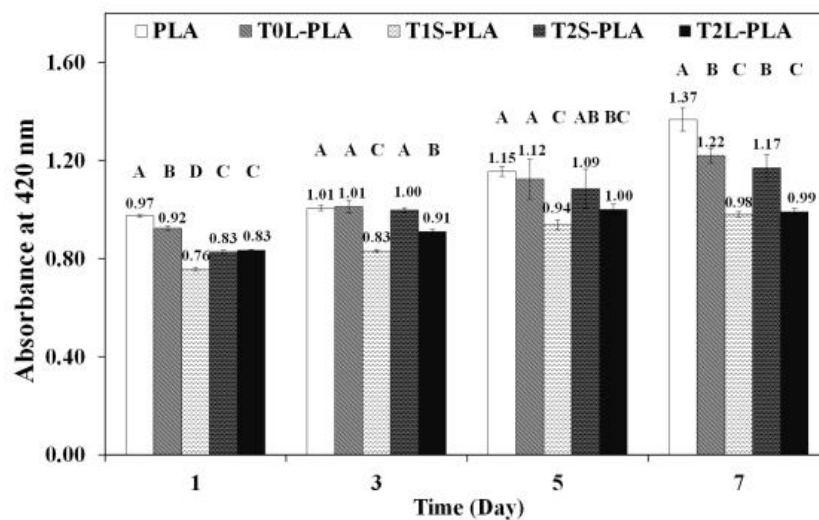


Figure 6 MG-63 cell proliferation on the polished surface of foam samples at 1, 3, 5 and 7 days, average values with different letters in the same day are significantly different at $p < 0.05$.

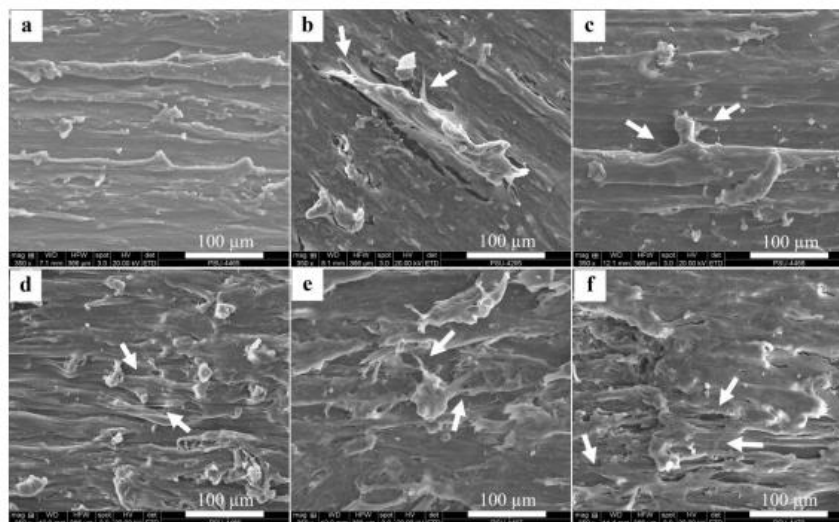
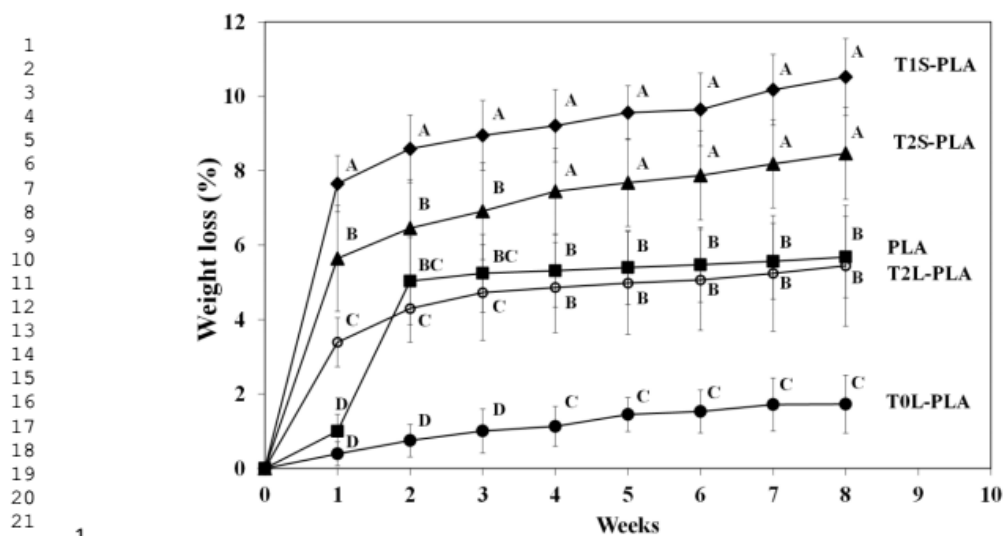


Figure 7 SEM micrographs of freeze-fractured surfaces of foam samples showing cell adhesion after 7 days: (a) blank, (b) PLA, (c) T0L-PLA, (d) T1S-PLA, (e) T2S-PLA and (f) T2L-PLA.



1
2
3
4
5
6
7
8
9
10
11
12
13
14
15
16
17
18
19
20
21
22
23
24
25
26
27
28
29
30
31
32
33
34
35
36
37
38
39
40
41
42
43
44
45
46
47
48
49
50
51
52
53
54
55
56
57
58
59
60
61
62
63
64
65

1
2
3

Figure 8 Weight loss as a function of incubation time of foam samples, average values with different letters in the same week are significantly different at $p < 0.05$.

APPENDIX F

(Original Article)

Topic: Poly(lactic acid)/chitosan foams prepared by conventional method: Mechanical properties, cytotoxicity and in-vitro degradation

Journal: Songklanakarin Journal of Science and Technology

Songklanakarín Journal of Science and Technology draft Tanrattanakul



Poly(lactic acid)/chitosan foams prepared by conventional method: Mechanical properties, cytotoxicity and in-vitro degradation

Journal:	<i>Songklanakarín Journal of Science and Technology</i>
Manuscript ID	Draft
Manuscript Type:	Original Article
Date Submitted by the Author:	n/a
Complete List of Authors:	Tanrattanakul, Varaporn; Prince of Songkla University, Department of Materials Science and Technology, Faculty of Science Sungsri, Pasuta; Materials Science and Technology
Keyword:	Chemistry and Pharmaceutical Sciences, Engineering and Industrial Research

SCHOLARONE™
Manuscripts

1
2
3
4
5
6
7
8
9
10
11
12
13
14
15
16
17
18
19
20
21
22
23
24
25
26
27
28
29
30
31
32
33
34
35
36
37
38
39
40
41
42
43
44
45
46
47
48
49
50
51
52
53
54
55
56
57
58
59
60

1 **Original Article**

2
3 **Poly(lactic acid)/chitosan foams prepared by conventional method:**

4 **Mechanical properties, cytotoxicity and *in-vitro* degradation**

5 Pasuta Sungsee, Varaporn Tanrattanakul*

6 Department of Materials Science and Technology, Faculty of Science,

7 Prince of Songkla University, Hadyai, Songkhla, Thailand 90110

8 * **Corresponding author, Email address: varaporn.t@psu.ac.th**

9
10 **Abstract**

11 The present study evaluated the feasibility of using a conventionally prepared
12 PLA foam for tissue scaffold applications. A simple PLA foam was successfully
13 prepared by compression molding. Azodicarbonamide was used as a chemical blowing
14 agent. Chitosan and poly(ethylene glycol) (PEG) were added. Chitosan promoted the
15 plasticization effect of PEG. The combination of chitosan and PEG contributed the
16 lowest T_g and T_{cc} of PLA. Only the plasticized PLA without PEG showed greater
17 impact strength than PLA. All foams showed closed-cell morphologies with relatively
18 large pores. Chitosan and PEG reduced pore size and the reduction in pore size was
19 greater when both additives were combined. Cytotoxicity was determined from cell
20 proliferation on samples. All foams showed non-cytotoxicity. The addition of chitosan
21 and/or PEG decreased weight loss of PLA in *in-vitro* degradation tests.

22
23 **Keywords:** Poly(lactic acid), chitosan, foam, tissue scaffold, cytotoxicity

1
2
3
4
5
6
7
8
9
10
11
12
13
14
15
16
17
18
19
20
21
22
23
24
25
26
27
28
29
30
31
32
33
34
35
36
37
38
39
40
41
42
43
44
45
46
47
48
49
50
51
52
53
54
55
56
57
58
59
60

1. Introduction

Tissue scaffolds are three-dimensional, artificial, porous biomaterials used in tissue culturing and are designed to induce cell adhesion, cell differentiation, cell proliferation and tissue formation both *in-vitro* and *in-vivo* (Chen-Turng et al., 2015). Tissue scaffolds have been prepared from poly(lactic acid) (PLA) by several techniques. These techniques included 3D printing (Serra, Planell, & Navarro, 2013), solid freeform fabrication (Tanodekaew, Channasanon, Kaewkong, & Uppanan, 2013), solvent casting with particle leaching (Huang, Zhu, Zhao, & Wan, 2014), thermally induced phase separation (La Carrubba, Carfi Pavia, Brucato, & Piccarolo, 2008), batch foaming with supercritical CO₂ (Chen-Wen et al., 2014) and a combination of batch foaming with supercritical CO₂ and particle leaching (Chen-Turng et al., 2015). Supercritical CO₂ has been used as a physical blowing agent for PLA foam prepared by extrusion (Pilla, Kim, Auer, Gong, & Park, 2009) or injection molding (Zafar-Ghosh et al., 2016). All these techniques require expensive specialized equipment.

PLA foam can be produced by a foaming process that uses a chemical blowing agent in the melt state. An interesting chemical blowing agent is azodicarbonamide (AZDC). It is cheap and foam can be produced using a very simple compression molding technique with inexpensive equipment. Using thermal compression followed by foam expansion without pressure in an electric oven, Zimmermann, Brambilla, Brandalise, and Zattera (2013) prepared PLA foam using AZDC with zinc oxide (ZnO). Luo-Jian et al. (2013) successfully prepared PLA foam by a chemical compression molding process, also using AZDC and ZnO. PLA foam has been produced by extrusion using a commercial blowing agent, BIH40 (Matuana, Faruk, & Diaz, 2009), citric acid and baking soda (Kmetty, Litauszki, & Rèti, 2018). However, to the best of our

1
2
3
4
5
6
7
8
9
10
11
12
13
14
15
16
17
18
19
20
21
22
23
24
25
26
27
28
29
30
31
32
33
34
35
36
37
38
39
40
41
42
43
44
45
46
47
48
49
50
51
52
53
54
55
56
57
58
59
60

1 knowledge, a PLA foam prepared using typical compression molding and AZDC has
2 not been used in a tissue scaffold application.

3 PLA has several advantages but one of its disadvantages is brittleness; therefore
4 plasticizer is usually added to PLA. Poly(ethylene glycol) (PEG) is one of the common
5 plasticizers of PLA. Tissue scaffold material has included chitosan for its
6 biodegradability, biocompatibility, non-toxicity and antimicrobial activity (Bonilla,
7 Fortunati, Vargas, Chiralt, & Kenny, 2013, Rodríguez-Vázquez, Vega-Ruiz, Ramos-
8 Zúñiga, Saldaña-Koppel, & Quiñones-Olvera, 2015 and Cai, Li, Weihs, & Wang,
9 2017).

10 The present study evaluates the preparation of PLA foam by a chemical melting
11 process that occurs in the compression mold using AZDC as a blowing agent. Chitosan
12 and PEG were used as a bioactive material and plasticizer, respectively. To assess the
13 viability of the obtained PLA foam in scaffold application, we determined foam
14 characteristics, mechanical properties, *in-vitro* degradation and cytotoxicity.

15 2. Materials and methods

16 2.1 Materials

17 Poly(lactic acid) (PLA 4042D) was produced by NatureWorks LLC USA.
18 Chitosan (94.69% degree of deacetylation) from Thai food and Chemical Co., Ltd. was
19 extracted from shrimp shells and had a particle size of ~ 100 mesh (~ 149 μm).
20 Poly(ethylene glycol) (PEG) with an average number molecular weight (M_n) of 6000
21 g/mol was supplied by Sigma-Aldrich Co., Ltd. Azodicarbonamide (AZDC), a blowing
22 agent, was purchased from Greatchem and Supply Pty., Ltd. Zinc Oxide (ZnO), used as
23 an accelerator of AZDC, was purchased from Kit Phaibun Chemistry Ltd., Part.

1
2
3
4
5
6
7
8
9
10
11
12
13
14
15
16
17
18
19
20
21
22
23
24
25
26
27
28
29
30
31
32
33
34
35
36
37
38
39
40
41
42
43
44
45
46
47
48
49
50
51
52
53
54
55
56
57
58
59
60

1 2.2 Preparation of PLA/chitosan foams

2 PLA and chitosan were dried in an oven for 12 h before use: PLA at 105°C and
3 chitosan at 50°C. PLA compounds were prepared in 2 steps. In the first step, PLA, PEG
4 and chitosan were blended in a twin screw extruder (Prism®TSE16TC) at a screw speed
5 of 80 rpm. Screw temperatures were 140, 165, and 165°C in the feed, middle and die
6 zones, respectively. In the second step, the compounds were mixed again in the extruder
7 with AZDC (1.94 wt%) and ZnO (0.06 wt%). Since it was necessary to prevent foam
8 formation in the extruder, the screw temperatures in the feed, middle and die zones were
9 lowered to 130, 150 and 150°C, respectively, and the screw speed was increased to 150
10 rpm. In this condition, an unfoamed extrudate could be obtained. A foam sheet was
11 produced by compression molding for 10 min in a closed mold (130 x 130 x 2 mm³) at a
12 temperature of 145°C under a pressure of 150 kg/cm². The compositions of the prepared
13 PLA compounds are listed in Table 1. The nomenclature of the PLA compounds was
14 based on concentrations of chitosan and PEG.

16 2.3 Foam characterization

17 The glass transition temperature (T_g), cold crystallization temperature (T_{cc}),
18 melting temperature (T_m) and degree of crystallization of all foam samples were
19 determined by DSC analyzer (NETZSCH® DSC200F3), using a scanning temperature
20 range from 20°C to 200°C and a heating rate of 10°C/min under nitrogen atmosphere.
21 The degree of crystallization was determined in terms of X_{c1} and X_{c2} from equations (1)
22 and (2), respectively, in which ΔH_{PLA} is the heat of fusion of 100% crystalline PLA (93
23 J/g) (Jaratrotkamjorn, R., Khaokong, C., & Tanrattanakul, V., 2012), ΔH_m is the melting
24 enthalpy, and ΔH_{cc} is the cold crystallization enthalpy.

1
2
3
4
5
6
7
8
9
10
11
12
13
14
15
16
17
18
19
20
21
22
23
24
25
26
27
28
29
30
31
32
33
34
35
36
37
38
39
40
41
42
43
44
45
46
47
48
49
50
51
52
53
54
55
56
57
58
59
60

$$X_{c1} = \left[\frac{\Delta H_m - \Delta H_{cc}}{\Delta H_{PLA}} \right] \times 100 \quad (1)$$

$$X_{c2} = \frac{\Delta H_m}{\Delta H_{PLA}} \times 100 \quad (2)$$

The thermal stability of all foam samples was determined by thermogravimetric analysis (NETZSCH® TGA/DSC STA 449 F3 Jupiter). Samples were heated at a rate of 5°C/min from 30°C to 500°C under nitrogen atmosphere.

Freeze-fractured foam surfaces were investigated using the scanning electron microscope (FEI® Quanta 400). Pore size was measured from SEM micrographs and approximately 150 to 200 pores were investigated for each specimen. The pores were oval, so only the wider diameter was determined.

2.4 Physical and mechanical properties tests

Foam density was measured by the buoyancy method described in ASTM standard D792. Three specimens of every sample were measured and the average value was reported. Specimen width and length were 25 mm, and specimen thickness was 2.5 to 3.0 mm. Specimens were weighed on an analytical balance in air and in n-hexane with a density of 0.6954 g/cm³. Void fraction (VF) was calculated from equation (3), according to Luo-Jiang et al. (2013), where ρ_1 and ρ_2 are the density of foam and unfoamed PLA samples, respectively:

$$\%VF = 1 - \left(\frac{\rho_1}{\rho_2} \right) \times 100 \quad (3).$$

The Izod impact strength was determined using Zwick® 5102 apparatus in accordance with ASTM standard 256. The tensile properties were analyzed in accordance with ASTM standard D412 die C. The specimens were tested at room

1
2
3
4
5
6
7
8
9
10
11
12
13
14
15
16
17
18
19
20
21
22
23
24
25
26
27
28
29
30
31
32
33
34
35
36
37
38
39
40
41
42
43
44
45
46
47
48
49
50
51
52
53
54
55
56
57
58
59
60

1 temperature using LLOYD® LR10K equipment. The crosshead speed was 5 mm/min.
2 At least 6 specimens were tested from every sample. An average value with standard
3 deviations was reported.

4 5 **2.5 *In-vitro* degradation test**

6 The *in-vitro* degradation of foam samples was evaluated by adding a dry foam
7 sample (1 x 1 cm²) to 500 µl of lysozyme solution (4 mg of lysozyme in 1 mL of
8 phosphate buffer solution (PBS) with pH 7.4). The sample was then incubated in the
9 solution at 37°C for 8 weeks (Zhang & Cui, 2012). The lysozyme solution was replaced
10 every week with fresh solution. At determined time intervals, the samples were removed
11 from the solution, washed with distilled water and dried in a freeze dryer. The % weight
12 loss was calculated from equation (4) (Rakmae, Ruksakulpiwat, Sutapun, & Suppakarn,
13 2012), where W_0 was the initial weight and W_d was the dried weight after degradation:

$$14 \quad \%Weight\ loss = \left[\frac{W_0 - W_d}{W_0} \right] \times 100 \quad (4).$$

15 16 **2.6 Cytotoxicity test**

17 MG-63 cells were cultured in alpha-MEM medium (Gibco™, Invitrogen,
18 Carlsbad, CA, USA) with the addition of 1% penicillin/streptomycin, 0.1% fungizone,
19 and 10% fetal bovine serum. Incubation took place at 37°C in a fully humidified
20 atmosphere at 5% CO₂. MG-63 cells (5 x 10⁴ cells) were seeded onto the surface of
21 foam samples. The medium was changed every 3 days during culture. Osteogenic
22 medium (OS) was used for osteoblast differentiation of the MG-63 cells (Sangkert,
23 Kamonmattayakul, Chai, & Meesane, 2016). MG-63 cells were cultured in a culture

1
2
3
4
5 1 plate for 1, 3, 5 and 7 days. MG-63 cell proliferation was measured by WST-1 assay
6
7 2 and cell proliferation was quantified according to the manufacturer's instructions
8
9 3 (Hsueh, Savitha, Sadhasivam, Lin, & Shieh, 2014). The absorbance of each sample was
10
11 4 recorded at 420 nm using a Multiskan™GO Microplate Spectrophotometer.
12
13 5 The morphology of cells that adhered to the foam sample was investigated by
14
15 6 scanning electron microscope (FEI® Quanta 400). The seeded foam samples were
16
17 7 washed with PBS and fixed with 10% neutral formalin buffer for 5 h at 4°C. The
18
19 8 samples were dried in a freeze dryer and coated with gold prior to investigation.
20
21
22
23 9
24
25 10 **2.7 Statistical analysis**
26
27 11 One-way analysis of variance (one-way ANOVA) was performed using SPSS
28
29 12 software (version 20.0) at 0.05 significance level ($p < 0.05$). Significant differences
30
31 13 among samples were analyzed using Tukey's honestly significant difference (HSD) test.
32
33 14 When the average values were significantly different at $p < 0.05$, samples were
34
35 15 identified by letters, e.g. A, B, C, D, AB and CD.
36
37
38
39 16
40
41 17 **3. Results and Discussion**
42
43 18 **3.1 Foam characterization**
44
45 19 In the DSC thermograms of samples obtained from the first heating scan, all
46
47 20 foams showed a cold crystallization temperature (T_{cc}), attributed to the double melting
48
49 21 peak typical of PLA and other polyesters (Figure 1). Transition temperatures (T_g , T_{cc}
50
51 22 and T_m) and degrees of crystallinity are listed in Table 2. PEG acted as an effective
52
53 23 plasticizer of PLA because the T_g of PLA significantly decreased after the addition of ~
54
55 24 5 wt% of PEG to the blend. Chitosan also acted as a plasticizer of PLA and promoted
56
57
58
59
60

1
2
3
4
5
6
7
8
9
10
11
12
13
14
15
16
17
18
19
20
21
22
23
24
25
26
27
28
29
30
31
32
33
34
35
36
37
38
39
40
41
42
43
44
45
46
47
48
49
50
51
52
53
54
55
56
57
58
59
60

1 the plasticization effect of PEG. This synergy was observed in the 3C5P sample, which
2 showed the lowest T_g . Both PEG and chitosan acted as nucleating agents, reducing T_{cc}
3 of PLA, and a mixture of PEG and chitosan produced the lowest T_{cc} . The occurrence of
4 cold crystallization affected the melting enthalpy of PLA. In this case, ΔH_m in the DSC
5 thermogram was a result of the initial crystallinity of PLA and the crystallinity during
6 heating in DSC analysis (ΔH_{cc}). By excluding ΔH_{cc} , X_{c1} represented the original degree
7 of crystallization of samples. Without PEG, chitosan did not affect the degree of
8 crystallinity of PLA. In contrast, PEG significantly increased the degree of crystallinity
9 of PLA. However, PEG and chitosan produced only slight changes to the overall degree
10 of crystallinity (X_{c2}) of samples.

11 SEM micrographs of samples show closed-cell morphologies with oval pores
12 (Figure 2). This cellular structure was also found in polyethylene foam (Almeida,
13 Demori, Zattera, & Zeni, 2007 and Sun-Qi et al., 2018) and PLA foam (Zimmermann et
14 al., 2013) prepared by compression molding using AZDC. The addition of chitosan and
15 PEG decreased pore size and pore size distribution (Table 3). Our results support
16 previous findings that chitosan and PEG acted as a nucleating agent for foam
17 nucleation. In polystyrene and polypropylene foams prepared by extrusion with AZDC
18 as a blowing agent, chitosan acted as a nucleating agent by reducing the size of cells
19 (Vázquez-González-Núñez et al., 2009). Chen-Turng et al. (2015) found that the
20 addition of 10 wt% of PEG decreased the pore size in a PLA scaffold.

21 Foam density was strongly influenced by void fraction (%VF). The foams with
22 higher void fractions had lower densities (Table 3). There was no correlation between
23 foam density and pore size. It seemed that foam density was related to the degree of
24 crystallinity, except in the 3C0P sample. Thermal degradation temperatures of samples

1
2
3
4
5
6
7
8
9
10
11
12
13
14
15
16
17
18
19
20
21
22
23
24
25
26
27
28
29
30
31
32
33
34
35
36
37
38
39
40
41
42
43
44
45
46
47
48
49
50
51
52
53
54
55
56
57
58
59
60

1 are listed in Table 3 in terms of $T_{d\text{ onset}}$ and T_d . Obtained from DTG curves from
2 thermogravimetric analysis, the onset temperature ($T_{d\text{ onset}}$) was the temperature at the
3 initial weight loss and T_d was the temperature at the peak of a DTG curve. The addition
4 of chitosan and PEG slightly affected the thermal stability of PLA.

6 **3.2 Mechanical properties**

7 The purpose of using chitosan in the present study was to evaluate the putative
8 bioactivity of chitosan in PLA foam for tissue regeneration. We did not expect
9 reinforcing behavior from chitosan. The addition of chitosan reduced the Izod impact
10 strength and tensile properties of PLA (Table 4). The incompatibility between PLA and
11 chitosan might have been due to the relatively large particle size of the chitosan (~ 149
12 μm). Reduced tensile properties were previously reported for PLA/chitosan blend.
13 (Răpă-Vasile et al., 2016). Likewise, chitosan decreased the tensile strength of LLDPE
14 (Isa & Mohammed, 2015). The plasticized PLA without chitosan (0C5P) showed
15 increased Izod impact strength and was the toughest of all the samples tested. The
16 impact strength of the plasticized PLA foams decreased with increasing chitosan
17 content (3C5P<1C5P<0C5P). All the plasticized PLA foams, with and without chitosan,
18 showed poorer tensile properties than PLA foam. Impact strength might be more
19 affected by chitosan than by the degree of crystallinity, foam density or pore size.
20 Notably, 1C5P, having higher density, the highest degree of crystallinity and the lowest
21 average pore size, showed lower impact strength, modulus and tensile strength than
22 0C5P. The data presented in Figure 3 confirmed that, as with impact strength, density
23 did not have a significant effect on the modulus and tensile strength.

24 **3.3 *In-vitro* degradation**

1
2
3
4
5
6
7
8
9
10
11
12
13
14
15
16
17
18
19
20
21
22
23
24
25
26
27
28
29
30
31
32
33
34
35
36
37
38
39
40
41
42
43
44
45
46
47
48
49
50
51
52
53
54
55
56
57
58
59
60

Data of the %weight loss of samples after incubation were statistically analyzed and the average values were significantly different at $p < 0.05$. PLA was used as a control sample. The weight loss of all samples increased with increasing incubation time and PLA showed the highest weight loss (Figure 4). At the end of the 2nd week, PLA showed a 5% weight loss while the weight loss of the other samples ranged from 0.5% to 1.3%. After 2 weeks, the weight loss of PLA was almost constant, whereas the other samples showed a constant weight loss from the 6th week. At the end of the experiment, the samples could be ranked by weight loss in the following order: 3C0P<0C5P<1C0P<3C5P<1C5P<PLA. PLA showed a 5.7% weight loss while the weight lost by of the other samples ranged from 1.4% to 3.0%. The addition of chitosan to PLA significantly reduced weight loss. Chitosan reduced %weight loss by neutralizing the acid product of the degradation of PLA and restraining self-catalysis in the PLA degradation process (Li, Ding & Zhou, 2004). Paradoxically, 0C5P showed relatively little weight loss. This sample will be investigated more deeply in future study.

3.4 Cytotoxicity

The WST-1 assay used in the cytotoxicity evaluation is a colorimetric assay using tetrazolium salt (WST-1) for the quantitation of viable cells. The occurrence of formazan dye from the cleavage of WST-1 is related to the number of viable cells in the cell culture and can be detected by absorption at suitable wavelengths. Increased absorbance is the result of an increase in the number of viable cells present in the culture (Hsueh et al., 2014). The data were statistically analyzed in a similar way to the data from the *in-vitro* degradation test. The proliferation of MG-63 cells increased with

1
2
3
4 1 cell culture time (Figure 5). This result demonstrated the non-cytotoxicity of all the
5
6 2 foam samples. The addition of 1 wt% chitosan (1C0P) slightly changed cell
7
8 3 proliferation on PLA whereas 3 wt% chitosan (3C0P) reduced proliferation more
9
10 4 significantly. The addition of PEG (0C5P) did not inhibit cell proliferation on PLA. The
11
12 5 addition of chitosan in conjunction with PEG inhibited cell proliferation on PLA. This
13
14 6 result was similar to the result from the *in-vitro* degradation test. MG-63 cells on the
15
16 7 surface of samples are shown in SEM micrographs (Figure 6). The white arrows
17
18 8 indicate areas covered by spreading cells (Balu, Sampath Kumar, Ramalingam, &
19
20 9 Ramakrishna, 2011). Cell adhesion is visible in the white circles. The appearance of
21
22 10 cells on the surfaces of all samples verified the non-cytotoxic reactivity of the samples.
23
24 11 Scaffold for bone tissue engineering requires relatively low weight loss and high cell
25
26 12 proliferation. In the present study, 1C0P and 0C5P were better in regard to these
27
28 13 properties than PLA.
29
30
31
32
33
34
35

36 15 4. Conclusions

37
38
39 16 PLA foam with and without chitosan and/or poly(ethylene glycol) was
40
41 17 successfully prepared by compression molding using azodicarbonamide as a chemical
42
43 18 blowing agent. Chitosan was used as a bioactive component and poly(ethylene glycol)
44
45 19 was used as a plasticizer. The PLA foam samples containing chitosan and poly(ethylene
46
47 20 glycol) showed the lowest T_g , T_{cc} and T_m and contributed the highest ΔH_{cc} . A closed-
48
49 21 cell morphology was obtained, which is common in plastic foam prepared with AZDC
50
51 22 in the melt condition. Chitosan and poly(ethylene glycol) decreased pore size and the
52
53 23 pore size distribution of PLA foam. The foam samples 0C5P and 1C5P showed higher
54
55 24 impact strength than PLA while the other samples showed lower impact strength. The
56
57
58
59
60

1
2
3
4
5
6
7
8
9
10
11
12
13
14
15
16
17
18
19
20
21
22
23
24
25
26
27
28
29
30
31
32
33
34
35
36
37
38
39
40
41
42
43
44
45
46
47
48
49
50
51
52
53
54
55
56
57
58
59
60

1 addition of chitosan and poly(ethylene glycol) impaired the tensile properties of PLA. In
2 the cytotoxicity test, cell proliferation on samples 1C0P and 0C5P, though slightly
3 lower than on PLA, indicated their potential for tissue scaffold application. But in the
4 *in-vitro* degradation test, both samples showed much lower weight loss than PLA. The
5 present study demonstrated that PLA foam prepared by a simple method could be used
6 in scaffold applications. The positive effect of chitosan and poly(ethylene glycol) on
7 PLA foam for tissue scaffold was also demonstrated.

9 **Acknowledgments**

10 The authors would like to acknowledge the financial support from Prince of
11 Songkla University, the grant number SCI5901465.

13 **References**

- 14 Almeida, M.G., Demori, R., Zattera, A.J., & Zeni, M. (2007). Morphological analysis of
15 polyethylene foams with post-use material incorporated. *Polymer Bulletin*, 59,
16 83-90. doi: 10.1007/s00289-007-0745-1
- 17 Balu, R., Sampath Kumar, T.S., Ramalingam, M., & Ramakrishna, S. (2011).
18 Electrospun polycaprolactone/poly(1,4-butylene adipate-co-polycaprolactone)
19 blends: potential biodegradable scaffold for bone tissue regeneration. *Journal*
20 *of Biomaterials and Tissue Engineering*, 1, 30-39. doi:10.1166/jbt.2011.1004
- 21 Bonilla, J., Fortunati, E., Vargas, M., Chiralt, A., & Kenny, J.M. (2013). Effects of
22 chitosan on the physicochemical and antimicrobial properties of PLA films.
23 *Journal of Food Engineering*, 119, 236-243. doi:10.1016/j.jfoodeng.2013.05.
24 026

- 1
2
3
4
5 1 Cai, S.-J., Li, C.-W., Weihs, D. & Wang, G.-J. (2017). Control of cell proliferation by a
6
7 2 porous chitosan scaffold with multiple releasing capabilities. *Science and*
8
9 3 *Technology of Advanced Materials*, 18(1), 987-996. doi: 10.1080/14686996.
10
11 4 2017.1406287
12
13 5 Chen, B.-Y., Jing, X., Mi, H.-Y., Zhao, H., Zhang, W.-H., Peng, X.-F., & Turng, L.-S.
14
15 6 (2015). Fabrication of polylactic acid/polyethylene glycol (PLA/PEG) porous
16
17 7 scaffold by supercritical CO₂ foaming and particle leaching. *Polymer*
18
19 8 *Engineering and Science*, 1339-1348. doi:10.1002/pen.24073
20
21 9 Chen, B.-Y., Wang, Y.-S., Mi, H.-Y., Yu, P., Kuang, T.-R., Peng, X.-F. & Wen, J.-S.
22
23 10 (2014). Effect of poly(ethylene glycol) on the properties and foaming behavior
24
25 11 of macroporous poly(lactic acid)/sodium chloride scaffold. *Journal of Applied*
26
27 12 *Polymer Science*, 1-10. doi: 10.1002/APP.41181
28
29 13 Hsueh, Y.-S., Savitha, S., Sadhasivam, S., Lin, F.-H., & Shieh, M.-J. (2014). Design
30
31 14 and synthesis of elastin-like polypeptides for an ideal nerve conduit in
32
33 15 peripheral nerve regeneration. *Materials Science and Engineering C*, 38, 119-
34
35 16 126. doi: 10.1016/j.msec.2014.01.058
36
37 17 Huang, R., Zhu, X., Zhao, T. & Wan, A. (2014). Preparation of tissue engineering
38
39 18 porous scaffold with poly(lactic acid) and polyethylene glycol solution blend
40
41 19 by solvent-casting/particulate-leaching. *Materials Research Express*, 1, 1-10.
42
43 20 doi: 10.1088/2053-1591/1/4/045403
44
45 21 Isa, S.A.B.M., & Mohammed, R. (2015). Physical and mechanical properties of
46
47 22 chitosan and polyethylene blend for food packaging film. *International Journal*
48
49 23 *of Mechanical and Production Engineering*, 3(10), 51-55.
50
51
52
53
54
55
56
57
58
59
60

- 1
2
3
4
5
6
7
8
9
10
11
12
13
14
15
16
17
18
19
20
21
22
23
24
25
26
27
28
29
30
31
32
33
34
35
36
37
38
39
40
41
42
43
44
45
46
47
48
49
50
51
52
53
54
55
56
57
58
59
60
- 1 Kmetty, Á., Litauszki, K., & Réti, D. (2018). Characterization of different chemical
2 blowing agents and their applicability to produce poly(lactic acid) foams by
3 extrusion. *Applied Science*, 8, 1-17. doi: 10.3390/app8101960
- 4 La Carrubba, V., Carfi Pavia, F., Brucato, V. & Piccarolo, S. (2008). PLLA/PLA
5 scaffolds prepared via Thermally Induced Phase Separation (TIPS): tuning of
6 properties and biodegradability. *International Journal of Material Forming*, 1-
7 5. doi: 10.1007/ s12289-008-0332-5
- 8 Li, L., Ding, S., & Zhou, C. (2004). Preparation and degradation of PLA/chitosan
9 composite materials. *Journal of Applied Polymer Science*, 91, 274-277. doi:
10 10.1002/ app.12954
- 11 Luo, Y., Zhang, J., Qi, R., Lu, J., Hu, X., & Jiang, P. (2013). Polylactide foams
12 prepared by a traditional chemical compression molding method. *Journal of*
13 *Applied Polymer Science*, 330-337. doi:10.1002/APP.39023
- 14 Matuana, L.M., Faruk, O., & Diaz, C.A. (2009). Cell morphology of extrusion foamed
15 poly(lactic acid) using endothermic chemical foaming agent. *Bioresource*
16 *Technology*, 100, 5947-5954. doi: 10.1016/j.biortech.2009.06.063
- 17 Jaratrotkamjorn, R., Khaokong, C., & Tanrattanakul, V. (2012). Toughness
18 Enhancement of Poly(lactic acid) by Melt Blending with Natural Rubber,
19 *Journal of Applied Polymer Science*, 124, 5027-5036.
20 doi:.org/10.1002/app.35617
- 21 Pilla, S., Kim, S.G., Auer, G.K., Gong, S. & Park, C.B. (2009). Microcellular extrusion-
22 foaming of polylactide with chain-extender. *Polymer Engineering and Science*,
23 1653-1660. doi:10.1002/pen.21385

- 1
2
3
4
5 1 Rakmae, S., Ruksakulpiwat, Y., Sutapun, W., & Suppakarn, N. (2012). Effect of silane
6
7 2 coupling agent treated bovine bone based carbonated hydroxyapatite on in-
8
9 3 vitro degradation behavior and bioactivity of PLA composites. *Materials*
10
11 4 *Science and Engineering, C 32*, 1428-1436. doi:10.1016/j.msec.2012.04.022
12
13 5 Râpă, M., Mitelut, A.C., Tanase, E.K., Grosu, E., Popescu, P., Popa, M.E., Resnes, J.T.,
14
15 6 Sivertsvik, M., Darie-Niță, R.N. & Vasile, C. (2016). Influence of chitosan on
16
17 7 mechanical, thermal, barrier and antimicrobial properties of PLA-
18
19 8 biocomposites for food packaging. *Composites Part C, 102*, 112-121. doi:
20
21 9 10.1016/j.compositesb. 2016.07.016
22
23 10 Rodríguez-Vázquez, M., Vega-Ruiz, B., Ramos-Zúñiga, R., Saldaña-Koppel, D.A. &
24
25 11 Quiñones-Olvera, L.F. (2015). Chitosan and its potential use as a scaffold for
26
27 12 tissue engineering in regenerative medicine. *BioMed Research International*, 1-
28
29 13 15. doi: 10.1155/ 2015/821279
30
31 14 Sangkert, S., Kamonmattayakul, S., Chai, W.L., & Meesane, J. (2016) A biofunctional-
32
33 15 modified silk fibroin scaffold with mimic reconstructed extracellular matrix of
34
35 16 decellularized pulp/collagen/fibronectin for bone tissue engineering in alveolar
36
37 17 boneresorption. *Materials Letter, 166*, 30-34. doi:10.1016/j.matlet.2015.12.032
38
39 18 Serra, T., Planell, J.A. & Navarro, M. (2013). High-resolution PLA-based composite
40
41 19 scaffolds via 3-D printing technology. *Acta Biomaterialia, 9*, 5521-5530. doi:
42
43 20 10.1016/j.actbio.2012.10.041
44
45 21 Sun, P., Quian, T.Y., Ji, X.Y., Wu, C., Yan, Y.S., & Qi, R.R. (2018). HDPE/UHMWPE
46
47 22 composite foams prepared by compression molding with optimized foaming
48
49 23 capacity and mechanical properties. *Journal of Applied Polymer Science*, 1-12.
50
51 24 doi: 10.1002/APP.46768
52
53
54
55
56
57
58
59
60

1
2
3
4
5
6
7
8
9
10
11
12
13
14
15
16
17
18
19
20
21
22
23
24
25
26
27
28
29
30
31
32
33
34
35
36
37
38
39
40
41
42
43
44
45
46
47
48
49
50
51
52
53
54
55
56
57
58
59
60

- 1 Tanodekaew, S., Channasanon, S., Kaewkong, P. & Uppanan, P. (2013). PLA-HA
2 scaffolds: preparation and bioactivity. *Procedia Engineering*, 59, 144-149. doi:
3 10.1016/j.proeng.2013.05.104
- 4 Vázquez, M.O., Ramírez-Arreola, D.E., Bernache, J., Gómez, C., Robledo-Ortiz, J.R.,
5 Rodrigue, D., & González-Núñez, R. (2009). Using chitosan as a nucleation
6 agent in thermoplastic foams for heavy metal adsorption. *Mecromolecular*
7 *Symposia*, 283-284, 152-158. doi: 10.1002/masy.200950920
- 8 Zafar, M.T, Zarrinbakhsh, N., Mohanty, A.K., Misra, M., Maiti, S.N., & Ghosh, A.K.
9 (2016). Biocomposites based on poly(lactic acid)/willow-fiber and their
10 injection moulded microcellular foams. *eXPRESS Polymer Letters*, 10(2), 176-
11 186. doi: 10.3144/express polymlett.2016.16
- 12 Zhang, Z., & Cui, H. (2012). Biodegradability and biocompatibility study of
13 poly(chitosan-g-lactic acid) scaffolds. *Molecules*, 17, 3243-3258. doi: 10.3390/
14 molecules17033243
- 15 Zimmermann, M.V.G., Brambilla, V.C., Brandalise, R.N., & Zattera, A.J. (2013).
16 Observations of the effects of different chemical blowing agents on the
17 degradation of poly(lactic acid) foams in simulated soil. *Materials Research*,
18 16(6), 1266-1273. doi: 10.1590/S1516-14392013005000133

1
2
3
4
5 1
6
7
8
9
10
11
12
13
14
15
16
17
18
19
20
21
22 2
23
24 3
25
26 4
27
28
29 5
30
31
32
33
34
35
36
37
38
39
40
41
42
43
44
45 6
46
47 7
48
49 8
50
51
52
53
54
55
56
57
58
59
60

Sample Code	Composition (wt%)		
	PLA	PEG	Chitosan
PLA	100.0	-	-
1C0P	99.0	-	1.0
3C0P	97.0	-	3.0
0C5P	95.0	5.0	0.0
1C5P	94.1	4.9	1.0
3C5P	92.2	4.8	3.0

Table 1 Blend composition of PLA compounds.

Foam sample	T _g (°C)	T _{cc} (°C)	T _{m1} (°C)	T _{m2} (°C)	X _{c1} (%)	X _{c2} (%)
PLA	59.6	101.0	144.8	155.3	9	43
1C0P	60.5	102.4	145.2	155.2	8	42
3C0P	57.4	97.6	141.9	152.1	7	41
0C5P	51.8	85.8	138.6	150.8	24	44
1C5P	50.3	82.4	132.4	147.2	44	49
3C5P	49.7	82.0	134.3	146.7	36	44

Table 2 Thermal properties of samples.

1

Foam sample	Density (g/cm ³)	VF (%)	Average pore diameter (μm)	Degradation temperature (°C)	
				T _{d onset}	T _d
PLA	0.746 ± 0.007	39.0 ± 0.5	495 ± 200	332	356
1C0P	0.723 ± 0.002	40.9 ± 0.2	450 ± 175	326	354
3C0P	0.819 ± 0.009	33.0 ± 0.7	316 ± 60	327	356
0C5P	0.760 ± 0.003	37.8 ± 0.2	355 ± 157	314	340
1C5P	0.816 ± 0.004	33.3 ± 0.3	282 ± 107	326	354
3C5P	0.759 ± 0.014	37.9 ± 1.1	300 ± 77	323	354

2

Table 3 Physical properties and average pore diameters of samples.

3

4

5

Foam sample	Izod impact strength (kJ/m ²)		Tensile properties		
	Unnotched	Notched	E (MPa)	σ _b (MPa)	ε _b (%)
PLA	4.9 ± 1.0 ^B	1.6 ± 0.2 ^{AB}	366 ± 20 ^A	18.4 ± 2.1 ^A	8.3 ± 1.3 ^B
1C0P	3.4 ± 0.4 ^C	1.3 ± 0.3 ^B	216 ± 12 ^{DE}	7.5 ± 1.4 ^C	5.6 ± 1.2 ^{CD}
3C0P	4.8 ± 0.5 ^B	1.5 ± 0.1 ^{AB}	275 ± 40 ^{BC}	10.8 ± 1.8 ^B	6.6 ± 1.6 ^{BC}
0C5P	7.3 ± 0.8 ^A	2.0 ± 0.3 ^A	319 ± 30 ^B	16.6 ± 0.6 ^A	7.8 ± 0.5 ^{BC}
1C5P	5.0 ± 1.0 ^B	1.7 ± 0.4 ^{AB}	258 ± 27 ^{CD}	10.6 ± 0.5 ^B	10.7 ± 2.1 ^A
3C5P	3.7 ± 0.8 ^{BC}	1.5 ± 0.3 ^{AB}	194 ± 24 ^E	5.0 ± 0.8 ^D	3.7 ± 0.5 ^D

6

Footnotes: Average values with different letters in the same column are significantly

7

different at p<0.05.

8

9

10

11

12

13

14

15

16

17

18

19

20

21

22

23

24

25

26

27

28

29

30

31

32

33

34

35

36

37

38

39

40

41

42

43

44

45

46

47

48

49

50

51

52

53

54

55

56

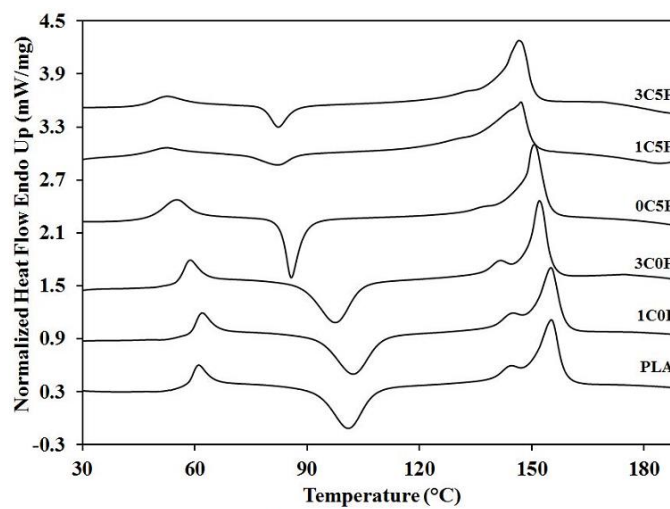
57

58

59

60

Table 4 Impact strength and tensile properties of samples.



27
28
29
30
31
32
33
34
35
36
37
38
39
40
41
42
43
44
45
46
47
48
49
50
51
52
53
54
55
56
57
58
59
60

1
2
3

Figure 1 DSC thermograms of samples.

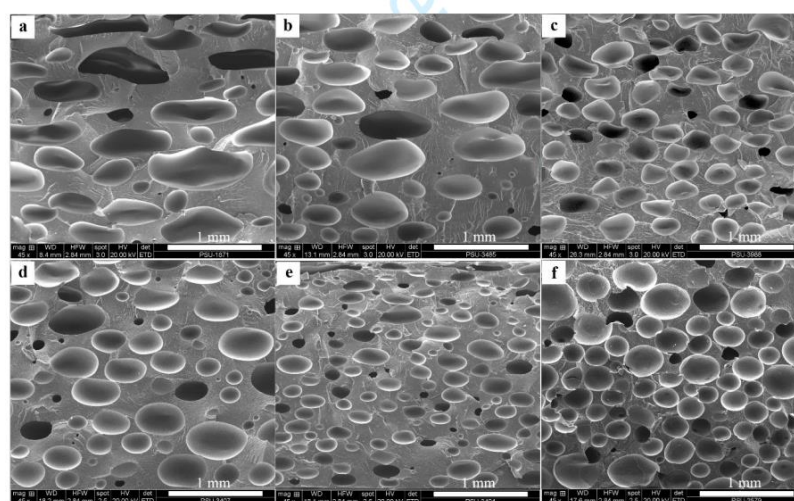


Figure 2 SEM micrographs of samples: (a) PLA, (b) 1C0P, (c) 3C0P, (d) 0C5P, (e) 1C5P, and (f) 3C5P.

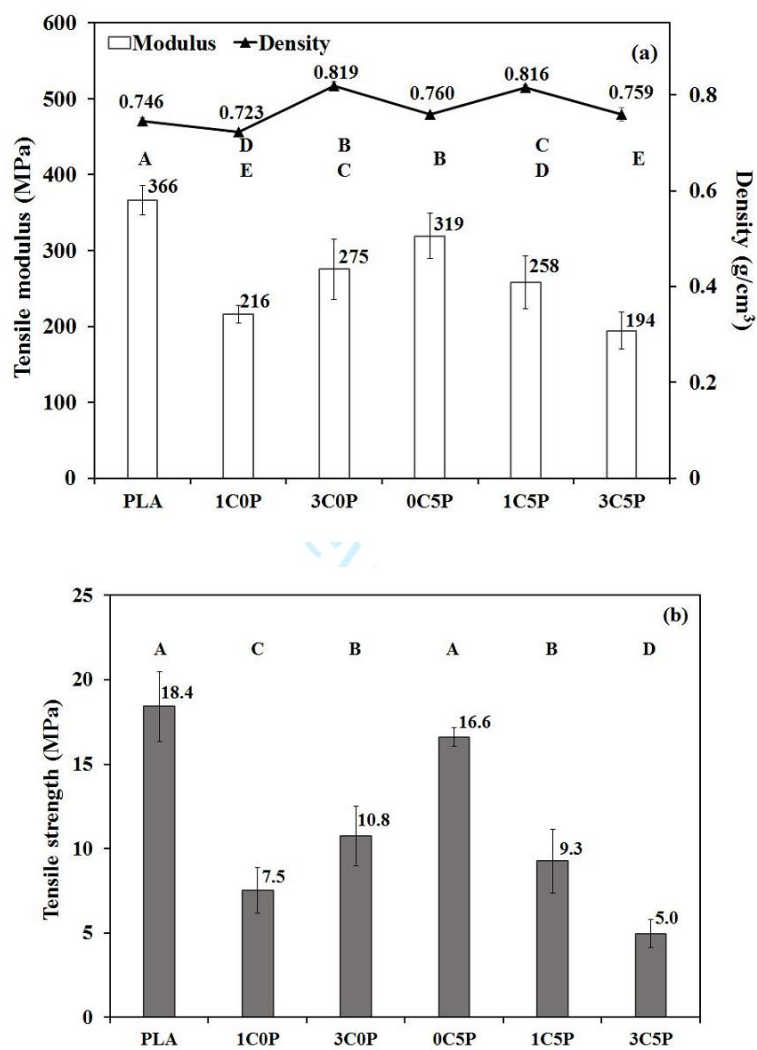


Figure 3 Tensile properties of samples: (a) tensile modulus and (b) tensile strength, average values with different letters are significantly different at $p < 0.05$.

1
2
3
4
5
6
7
8
9
10
11
12
13
14
15
16
17
18
19
20
21
22
23
24
25
26
27
28
29
30
31
32
33
34
35
36
37
38
39
40
41
42
43
44
45
46
47
48
49
50
51
52
53
54
55
56
57
58
59
60

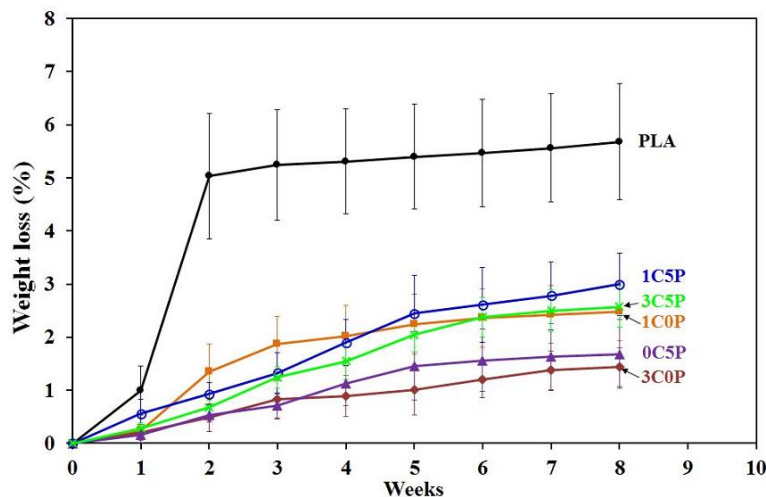


Figure 4 Weight loss as a function of incubation time of samples.

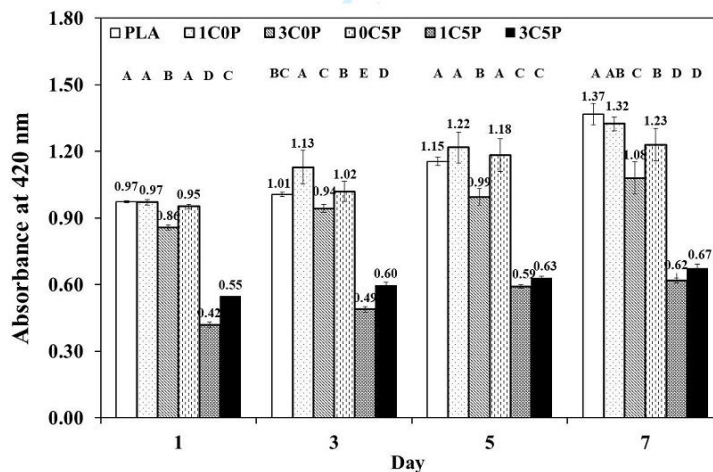
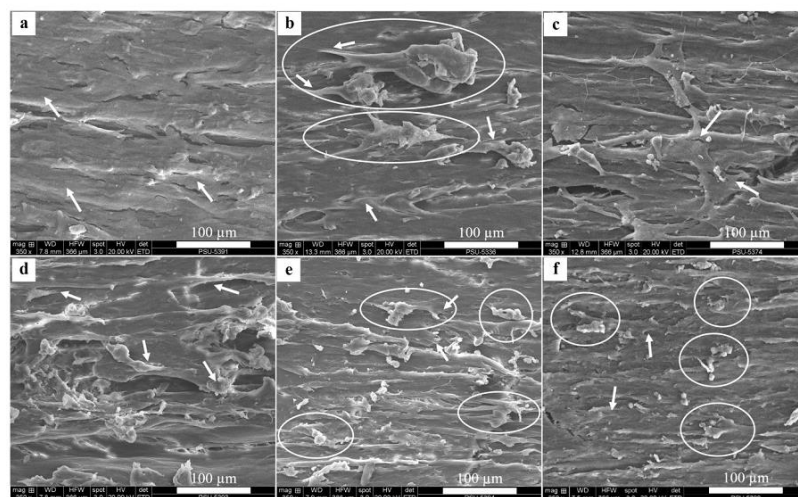


Figure 5 MG-63 cell proliferation on the polished surface of samples at 1, 3, 5 and 7 days, average values with different letters on the same day are significantly different at $p < 0.05$.

1



2

3

Figure 6 SEM micrographs of cell adhesion on the polished surface of samples after 7 days of cell culture: (a) PLA, (b) 1C0P, (c) 3C0P, (d) 0C5P, (e) 1C5P, and (f) 3C5P

6

1
2
3
4
5
6
7
8
9
10
11
12
13
14
15
16
17
18
19
20
21
22
23
24
25
26
27
28
29
30
31
32
33
34
35
36
37
38
39
40
41
42
43
44
45
46
47
48
49
50
51
52
53
54
55
56
57
58
59
60

VITAE

Name Miss Pasuta Sungsee

Student ID 5710230014

Educational Attainment

Degree	Name of Institution	Year of Graduation
Bachelor of Science (Polymer Science)	Prince of Songkla University	2005
Master of Science (Polymer Science)	Petroleum and Petrochemical College Chulalongkorn University	2009

Scholarship Award during Enrolment

Grant of Graduate School, Prince of Songkla University

Grant of Nakhon Si Thammarat Rajabhat University

Work-Position and Address

Lecturer at Department of Production Technology, Faculty of Industrial
Technology, Nakhon Si Thammarat Rajabhat University.

List of Publications and Communications

Pasuta Sungsee and Varaporn Tanrattanakul. 2014. PLA foams for scaffold application.

Proceedings in Pure and Applied Chemistry International Conference 2018
(PACON2018). Songkhla, Thailand, February 7-9, 2018. pp. PO13-PO18.

Pasuta Sungsee and Varaporn Tanrattanakul. Biocomposite foams from poly(lactic acid) and rubber wood sawdust: Mechanical, properties, cytotoxicity and in vitro degradation. Journal of Applied Polymer Science, Accepted.

Pasuta Sungsee and Varaporn Tanrattanakul. Poly(lactic acid)/chitosan foams prepared by conventional method: Mechanical properties, cytotoxicity and in-vitro degradation. Songklanakarin Journal of Science and Technology, Submitted.

- Pasuta Sungsee and Varaporn Tanrattanakul. 2016. Effect of zinc oxide content on morphology and tensile properties of PLA foam prepared by compression molding. The 11th SPSJ International Polymer Conference (IPC 2016), Fukuoka International Congress Center, Fukuoka, Japan, December 13-16, 2016. (Poster)
- Pasuta Sungsee and Varaporn Tanrattanakul. 2018. PLA foams for scaffold application. Pure and Applied Chemistry International Conference 2018 (PACON2018), The Throne International Convention Center, Hat Yai, Songkhla, Thailand, February 7-9, 2018. (Poster)
- Pasuta Sungsee and Varaporn Tanrattanakul. 2018. Effects of Chitosan and poly(ethylene glycol) on mechanical and thermal properties of poly(lactic acid). The 47th World Polymer Congress (MACRO 2018), Cairns Convention Center, Queensland, Australia, July 1-5, 2018. (Poster)